1976

Laboratory simulation of a tornado-like vortex boundary layer interaction

Behrooz Fattahi
Iowa State University

INFORMATION TO USERS

This material was produced from a microfilm copy of the original document. While the most advanced technological means to photograph and reproduce this document have been used, the quality is heavily dependent upon the quality of the original submitted.

The following explanation of techniques is provided to help you understand markings or patterns which may appear on this reproduction.

1. The sign or "target" for pages apparently lacking from the document photographed is "Missing Page(s)". If it was possible to obtain the missing page(s) or section, they are spliced into the film along with adjacent pages. This may have necessitated cutting thru an image and duplicating adjacent pages to insure you complete continuity.

2. When an image on the film is obliterated with a large round black mark, it is an indication that the photographer suspected that the copy may have moved during exposure and thus cause a blurred image. You will find a good image of the page in the adjacent frame.

3. When a map, drawing or chart, etc., was part of the material being photographed the photographer followed a definite method in "sectioning" the material. It is customary to begin photoing at the upper left hand corner of a large sheet and to continue photoing from left to right in equal sections with a small overlap. If necessary, sectioning is continued again — beginning below the first row and continuing on until complete.

4. The majority of users indicate that the textual content is of greatest value, however, a somewhat higher quality reproduction could be made from "photographs" if essential to the understanding of the dissertation. Silver prints of "photographs" may be ordered at additional charge by writing the Order Department, giving the catalog number, title, author and specific pages you wish reproduced.

5. PLEASE NOTE: Some pages may have indistinct print. Filmed as received.

University Microfilms International
300 North Zeeb Road
Ann Arbor, Michigan 48106 USA
St. John's Road, Tyler's Green
High Wycombe, Bucks, England HP10 8HR

Laboratory simulation of a tornado-like vortex boundary layer interaction

by

Behrooz Fattahi

A Dissertation Submitted to the

Graduate Faculty in Partial Fulfillment of

The Requirements for the Degree of

DOCTOR OF PHILOSOPHY

Co-majors: Aerospace Engineering
Mechanical Engineering

Approved:

Signature was redacted for privacy.

In Charge of Major Work

Signature was redacted for privacy.

For the Major Departments

Signature was redacted for privacy.

For the Graduate College

Iowa State University
Ames, Iowa

1976

TABLE OF CONTENTS

		Page
	LIST OF SYMBOLS AND ABBREVIATIONS	v
	FOREWORD	vii
I.	INTRODUCTION	1
	A. Review of Previous Research	3
	1. Laboratory simulation	3
	2. Direct observation	7
	3. Theoretical investigations	9
	B. Statement of the Problem	11
II.	TORNADO CYCLONES	13
	A. Experimental Modeling	16
	B. Vortex Generator	16
III.	FLOW VISUALIZATION	22
	A. Flow Similarities	22
	1. Dust cloud similarity	23
	2. Tornado funnel similarity	25
	B. Structure of Tornado Vortices	26
	1. Dust clouds	27
	2. Inner vortical tube	28
	3. The tornado funnel	29
	4. The center jet	31
	5. The outer vertical tube	33
	C. Other Important Observations	36
	1. Vortex formation	36
	2. Surface roughness effect	37
	3. Ground plane effect	39
	4. Multiple tornado funnels and multiple vortex tornadoes	43

IV. WIND SPEED AND AIR FLOW PATTERNS IN THE SIMULATED LABORATORY TORNADO 47

A. Time Averaged Velocity Measurement 47

1. Thermo Systems 1080 anemometer 48
2. Time averaging technique 49
3. Data acquisition 50

B. High Speed Motion Picture Measurement 53

1. Measurement of velocity components 54
2. Speed distribution near the ground surface 56
3. Radial inflow near the ground 58
4. Tangential velocity variation near the ground 59
5. Speed distribution above the ground surface 61
6. Tangential speed distribution at H^* = 1 in. 62
7. Tangential speed distribution at H^* = 2 in. 63
8. Tangential speed distribution at H^* = 3 in. 64
9. Tangential speed distribution at H^* = 6 in. 64
10. Tangential speed distribution at H^* = 9 in. 65
11. Tangential speed distribution at H^* = 12 in. 65
12. Tangential speed distribution at H^* = 15 in. 66
13. Tangential speed distribution at H^* = 18 in. 66
14. Tangential wind speed measurement in tornado, waterspout and dust devil 66
15. Axial speed distribution 70

C. Other Observations 72

V. WIND LOADING ON STRUCTURES 74

A. Mode (A). The Direct Pushing Force of the Wind 74

B. Mode (B). The Outward Forces due to Pressure Differentials Resulting from the Atmospheric Pressure Drop 75

1. The derived pressure distribution 78
2. Pressure measurements in natural tornadoes 83
3. Pressure deficit effect on buildings 88

C. Mode (C). The Inward Forces due to Pressure Differentials Resulting from the Atmospheric Pressure Recovery 93

D. Mode (D). Forces Transmitted through Flying Missiles 94

VI. MECHANISM OF A TORNADO VORTEX FORMATION 95

A. Formation of Tornadic Vortices 95

B. Concluding Comments 101

C. Recommendation for Further Research 103

VII. REFERENCES 107

VIII. ACKNOWLEDGMENTS 114

IX. APPENDIX A 116

X. APPENDIX B 118

XI. APPENDIX C 123

XII. APPENDIX D 126a

LIST OF SYMBOLS AND ABBREVIATIONS[1]

C_R	Rankine combined vortex distribution constant
F_r	speed of motion picture photography in frames per second
g^*	gravitational acceleration
h	dimensionless height from the ground plane
H^*	distance from the ground plane
H^*_{cr}	critical distance from the rotating tornado cyclone to the ground surface at which a tornado forms
J_o	Bessel function of the first kind
n	stream tube contraction ratio
n_f	number of frames of the motion picture in a certain time interval
P^*	static pressure
P^*_∞	static pressure measured far from the vortex core
q^*	dynamic pressure
Q^*	sink strength
r	dimensionless radius
r^*	radial distance of a particle from the vortex center
r^*_{cl}	radius of rigid body rotation at station 1
r^*_m	radius of maximum tangential velocity
R_o	Rossby number
t^*	time
T	Temperature
u^*	radial velocity

[1] Symbols and abbreviations not found in this list are defined and used locally within.

v^* tangential velocity

v_m dimensionless maximum tangential velocity at a given height

v_m^* maximum tangential velocity at a given height

V^* total velocity

w^* axial velocity

w_1^* axial velocity at station 1

w_2^* axial velocity at station 2

z^* axial distance

α swirl intensity

Γ^* circulation

ΔP^* pressure deficit

ΔP_c^* cyclostrophic maximum pressure deficit

ΔP_m^* measured maximum pressure deficit

θ total rotation angle for a particle around the vortex center

μ^* viscosity coefficient

ρ^* density

ω^* angular speed

FOREWORD

"It often happens that when one wind meets another at an obtuse angle, these same winds circle round together and twine themselves together into the shape of a huge column, ..." (MacCurdy, 1958).

"I have seen motions of the air so furious that they have carried, mixed up in their course, the largest trees of the forest and whole roofs of great palaces, and I have seen the same fury bore a hole with a whirling movement, digging out a gravel-pit, and carrying gravel, sand, and water more than half a mile through the air" (Richter, 1970).

Leonardo da Vinci (1452-1519),
Manuscripts

I. INTRODUCTION

Among the many natural phenomena, tornadoes are the most violent disturbances of the atmosphere, yet they are relatively small in their horizontal extent. Because of their highly localized nature, extreme wind speeds and associated rapid pressure drop and recovery, destruction is instantaneous and frequently complete.

Scientific observation of tornadoes is extremely difficult, due to their violence, elusive nature, random occurrence, short life time and relatively small size. Therefore, very little is known about their characteristics. The total pressure drop, maximum wind speed and the complicated flow pattern of tornadic flow fields are of great importance to engineers designing vital structures such as nuclear reactor housings, to architects designing buildings and finally to every citizen who may be directly or indirectly affected by such violent storms. The average losses attributed to tornadoes for the period of 1955 to 1969 have been 125 lives and 75,000,000 dollars in property damage annually (Kessler, 1970). On March 18, 1925, the famous Tri-State tornado spawned by a single storm cell travelled through the states of Missouri, Illinois and Indiana, killing 689 people, injuring 1980 in a period of just three hours. The estimated property damage was 16,500,000 dollars (U. S. Department of Commerce, 1952).

Many scientists and engineers have been engaged in active research with the hope of improving the present state of the knowledge of the mechanics of tornadic flows. Although significant progress has been made,

yet a reliable estimate of the maximum wind speeds or the pressure deficit is to be made in the future, as is an accurate definition of the tornado flow structure itself. Research efforts in tornadic storms are currently supported by the following organizations:

a. United States Nuclear Regulatory Commission

b. National Oceanic and Atmospheric Administration

c. National Science Foundation

d. Insurance companies, private aerospace corporations, etc.

e. University Research Foundations

These efforts may be subdivided into the following classification:

a. Direct Measurements of the Vortex Parameters

    1. Doppler Radar

    2. Doppler Lidar

    3. Direct Penetration

    4. Photogrammetry

b. Indirect Measurements of the Vortex Parameters

    1. Engineering Assessment of Damage

    2. Analysis of Characteristic of Ground Marks

    3. Electrical Activity

c. Laboratory Simulation of Tornado-Like Vortices

d. Numerical Modeling and Theoretical Analysis

The aim of the present research is to study the mechanics of formation and interaction of tornado flow fields with the ground boundary layer and the resulting phenomena through experimental modeling. A new approach for simulation of these flow fields is employed and its

utilization will be justified in Chapter II of this dissertation. Although the results are significant in terms of their resemblance to their natural counterparts, no attempt is made to claim that all tornadoes in nature have the same structure, and that this investigator's findings are universal. However, a majority of tornadoes are thought to be structured as will be proposed.

A. Review of Previous Research

The interests in understanding the atmospheric vortices is not new. Leonardo da Vinci in his famous Manuscripts described his personal observation of a seemingly violent vortex. Benjamin Franklin (Ludlum, 1970) observing many waterspouts and tornadoes also described the violent interaction of these phenomena and stressed the importance of the vacuum inside such vortices in damaging structures. But only in the latter part of the 19th century, did the real interest in some form of investigation of these phenomena arise.

1. Laboratory simulation

Probably the first attempt to simulate atmospheric vortices was that of Dines (1896) in 1895. The apparatus he used was made of six pieces of window glass, arranged such as shown in Fig. 1. On the top a wooden panel with a hole 7 in. in diameter was placed. A hand-driven ventilating fan maintained the motion of the air in the system by sucking the air through the sidewall openings and then upward through the hole, combining rotational and axial motion thus creating a vortex. The resulting vortex core in Dines' simulation was visualized by introducing water vapor into

the system. No measurements were taken, however, Dines recognized that the key to successful simulation was a good updraft plus rotation. He proposed that the twisting motion in the natural vortices was the result of the rotation of earth. Miller (1955) modified Dines' model by using a round chamber shown in Fig. 2 but basically forming a vortex just like the older model.

Chang (1969) introduced a new simulator, which consisted of a rotating cylindrical screen, a ground plate and a top plate with an opening at the center through which the air in the chamber was sucked out by a ventilating fan as shown in Fig. 3. The sink strength and circulation were controlled independently. Ying and Chang (1970) and later Wan and Chang (1972) found, despite the axisymmetricity of their simulator and strong suction produced by the fan at the top, which forced the vortex to remain at the center of the simulator, some unavoidable instabilities of the vortex motion occurred. They concluded that the instability of the vortex core was an inherent characteristic of the tornado even over smooth terrain.

Figure 4 shows Ward's (1972) entry into the field of atmospheric vortices simulation. His apparatus was assembled to produce a flow system in which both the diameter of the rising air column and the depth of the inflow layer could be varied. The simulator produces a convergent airflow through a fine mesh cylindrical wire screen, eight feet in diameter, which regulates the angular momentum by its rotation. The updraft is created by a variable speed exhaust fan. The inflow angle, relative to a radial can be measured by a wind vane. Pressure measurement at the

ground surface were achieved although apparently no attempt was made to measure velocity magnitudes. Ward's contribution was the simulation of multiple vortices. A pair of vortices may be produced when the inflow angle is greater than an experimentally found critical angle. Also, the ratio of the updraft diameter to the inflow depth (configuration ratio) should be greater than unity. After a pair is formed, a third vortex will form, and then a fourth as the inflow angle is further increased. Ward also found that the critical inflow angle inversely depended on the value of configuration ratio.

Muirhead and Eagleman (1971) developed a laboratory vortex generator as shown in Fig. 5. The rotation of an eighteen inch diameter wire cage provides the circulation at a height above the ground simulation level. Inside the cage, a two-inch diameter hole connected to a pressure reservoir provides a variable strength sink. Different flow visualization techniques were applied to investigate the flow pattern. Also, pressure measurements were performed at the ground level which were used to calculate velocity magnitudes by applying proper equations derived from compressible vortex theory. This model revealed that the supply of a small pressure over atmospheric into the core at the upper plate disintegrates an existing vortex immediately confirming the fact that a sink at the upper levels is necessary to initiate a vortical flow and maintain it. It was also shown that if a below atmospheric pressure was applied at the cage hole without the cage rotation, no vortex resulted. However, if the vortex was established and then the cage rotation stopped, the vortex continued, although weaker in strength. This clearly indicates the

requirement of a rotating system plus a sink in atmosphere for tornadic flow production. However, the induced vortex does not have to stay with mother vortex and separation occurs after which time the vortex dissipates. This phenomenon, along with an alternate source of vorticity will be discussed in more detail in Chapters II and VI.

Fujita (Roberts, 1972), also attempted to simulate atmospheric vortices. His model employs overlapping series of rotating cups turning slowly at the outside but more rapidly toward the center in an attempt to produce a tangential velocity profile close to that of a Rankine-combined vortex. The sink is provided by an exhaust fan. Fig. 6 shows the layout of Fujita's simulator. However, due to Fujita's interest in ground mark analysis and photogrammetric analysis of tornadoes, he apparently made no attempt to perform any kind of measurement utilizing his simulator. Fujita's contribution to the field of atmospheric vortices is outstanding and his observations and theories of tornado genesis and multiple vortex flow fields are valuable and will be discussed from time to time in this paper. A number of other attempts to simulate tornado-like vortices have been made, mostly generating vortices in liquids, however, due to their relative insignificance they are not mentioned here (e.g. Maxworthy, 1973).

A review of the important simulations of the tornado-like vortices mentioned above reveals that they have all combined the required ingredients for the vortex production namely the axial flow and angular motion. Dines, Miller, Chang and Ward introduced the tangential motion from the outer sidewalls relying on the theory that the background

rotation is the main source of the vorticity in generation and maintaining tornado vortices. On the other hand Muirhead, Eagleman and Fujita designed their simulator such that a downward development of the rotation from the cyclonic system at upper levels is responsible for generation of the required vorticity. In all of the cases mentioned, the low pressure system introducing the updraft is simulated by a suction or ventilating fan. This approach although resulting in a vortical flow lacks the basic dependence of the tangential motion and the consequent pressure drop at the center of rotation. In such simulations the angular speed of the rotating system may be arbitrarily set independent of the sink strength and vice versa, resulting in unrealistic information (i.e. Muirhead and Eagleman, 1971). The pressure deficit near the ground in the simulated vortex is severely affected by the upper suction pressure. Therefore, it is desirable to design a system for generation of vortices such that the pressure deficit is a fluid mechanics consequence of the swirling motion.

2. Direct observation

Brooks (1949), on the basis of his observations and investigation of St. Louis tornadoes of 1948, introduced and stressed the importance of the phenomenon that he called the tornado cyclone in relation to tornadoes. Also Fujita (1958), after extensive study of the Illinois tornadoes of 9 April 1953 showed that these tornadoes were associated with a tornado cyclone resembling a miniature hurricane in many respects. The tornado cyclone was only 30 miles in diameter and was characterized by an eye at its center. Radar observations in the echo movement inside the tornado

cyclone indicated that air converged at low levels then rose following the boundary of the eye. He concluded that a tornado is a secondary circulation imbedded in a much larger mother circulation or a tornado cyclone. In 1965, Fujita (1965) explained the formation and steering mechanisms of tornado cyclones and associated hook echoes. Using kinematics diagrams with coordinates of absolute tangential speed vs. cyclone radius he identified and related the different classes of macro-, and micro-circulations, where tornado cyclones are considered to be mesocyclones and tornadoes are classified as micro-circulations.

Doppler radar and recently improved doppler lidar available to researchers have produced significant volumes of information concerning the development of these circulations. Their use has been instrumental in understanding the structure and formation of the large-scale vortices, however, tornadoes have to date remained mysterious and unknown. Direct measurement of these micro-circulations is difficult. Most of the available data are those obtained outside the concentrated vortices or those extracted from the still pictures and movies of tornadoes by photogrammetric techniques.

The Dallas Tornado of April 2, 1957, is probably the best documented and the most thoroughly investigated tornado in history using techniques of extracting information from 450 black and white photos, 250 color transparencies and nearly 2000 feet of movie film, taken by some 125 photographers (Hoecker et al. 1960). In addition to these detailed photographic records this tornado occurred in an area where complete upper air observations, radar data and surface observations and many eyewitness

accounts were available. From all these sources Hoecker (1960) determined a composite distribution of tangential and upward components of air flow by tracing particles, debris and cloud tags. Although certain amount of error exists in these types of analyses, the approximate results not only shed some light on behavior of the tornado vortices but for the lack of a better method of measurement have remained valuable.

Many other tornadoes have also been photographed and investigated. Fargo tornadoes of June 20, 1957, and Palm Sunday tornadoes of April 11, 1965 are examples, thoroughly investigated by Fujita (1960) and Fujita et al. (1970). Although extracted quantitative information is sparse qualitative data obtained from the analyses of such tornadoes are significant.

Another approach to understand the structure of concentrated vortices is by direct probing. Due to extreme violence of tornadoes, approach and occasional penetrations have been limited to weak waterspouts and dust devils (Colden, 1969, Leverson et al. 1975, Sinclair 1973). The accuracy of these measurements is, of course, subject to the amount of unstable oscillations encountered during penetration. However, it is believed that gathering such information is useful for possible penetration into a tornado vortex using instrumented, remotely guided projectiles (Agee, 1969, 1970, 1971), armored vehicles (Morgan, 1972) or self-inflating constant volume balloons (Grant, 1971).

3. Theoretical investigations

Theoretical investigation of vortical flows have also failed to this date to reveal the true structure of the tornado flow fields although a

number of extensive research efforts have produced significant progress in this direction. The basic difficulties in theoretical analysis of such flow fields lie in non-linearity of the flow equations and the lack of a good understanding of the role of turbulence.

Early theoretical work have all assumed a constant turbulent viscosity to reduce the difficulty of solving the flow equations. These equations then were solved by similar solutions or by momentum integral techniques (Stewartson, 1957, Rott and Lewellen, 1964). Kuo (1971) first considered a real vortex of nearly solid body rotation in the inner core and potential vortex in the outer portion and solved the two non-linear boundary layer equations for the vertical and radial distributions of the velocities employing a momentum-integral technique. He pointed out the importance of variable turbulent viscosity by considering this variation in a small sublayer near the ground but assuming constant values above this layer. Chi and Jih (1974) solved the Navier-Stokes equations for a real vortex by numerical techniques, however, they also considered a constant viscosity coefficient.

With improvement of numerical techniques and employment of high speed digital computers, variable turbulence viscosity problems were considered. Smith (1967) solving the Navier-Stokes equations with variable turbulence viscosity for a narrow strip of the boundary layer, showed the downward motion of the air in the center portion of a two-cell vortex. Later Chi and Glowacki (1974), applying the mixing length theory, solved the boundary layer equations outside the vortex core. Chi (1975) extended his work by considering a one-equation model of turbulence in solving the Navier-Stokes equations for the entire flow region beneath a real vortex.

Results indicated the existence of a two-cell vortex in the upper portion of the boundary layer along with prediction of a downward converging vortex core. Hsu and Tesfamariam (1975), considering both the transport processes of the turbulent energy and a length scale, employed a two-equation model of turbulence together with the conventional boundary layer equations. Using numerical techniques, solutions were obtained predicting a complicated flow pattern in the boundary layer with four circulating regions. Additional effort is underway to solve the Navier-Stokes equations for the boundary layer region. The agreement of these results with that of the following simulation is significant and will be discussed later.

B. Statement of the Problem

As previously mentioned, man's knowledge of tornadoes is not well developed after many decades of research and interest in understanding this phenomenon. In view of the failure of other attempts to provide correct laboratory models of tornadoes, the thrust of this research is:

a. To produce laboratory vortices in the same manner that a tornado vortex is produced in nature.

b. To show the importance of the parent rotation and the ground surface interaction in forming the concentrated tornado vortices.

c. To investigate and explain the formation of tornado funnels.

d. To investigate the structure of their flow fields.

e. To provide initiatives in terms of flow visualization, measurement of velocity and pressure field, and observational techniques for further research.

II. TORNADO CYCLONES

Although the intent of this dissertation is to provide some explanations for the mechanism of formation, structure of tornado-like vortices and their interactions with the ground boundary layer (layer of significant inflow), because of a different and new approach in generating these vortices in the laboratory, some discussion of the tornado cyclones seems to be necessary to indicate the merits of this unique approach.

Researchers are not in complete agreement as to the structure of the formation of atmospheric micro vortices, however, the majority of them agree that instabilities in the atmospheric layer of our planet is responsible for vortical flow formation in this layer. These instabilities are of common occurrence in the central United States where usually tornadoes are the end results, however, they may occur in many parts of the world, mainly in the north and south temperate zones (Flora, 1953).

The region east of the Rockies in the United States has a very favorable topography for creation of the atmospheric instabilities. Cold, dry air, moving from a westerly direction, overruns warm, moist air moving from the gulf region inducing cyclogenesis. Figure 7 shows schematic features of such mechanism (Newton, 1967). Since the warm air is lighter, due to its buoyancy, has a tendency to rise through the cooler and heavier air. As it rises it cools, resulting in condensation of part of its water vapor, which releases latent heat producing enormous amount of energy. The combination of uprush and rotation in the two air masses, in addition to the passage of the turbulence generating jet stream at

high levels along with tremendous amount of generated energy are ingredients of formation of giant rotational systems or cyclones. These systems are usually several hundred miles in diameter and compose a general environmental background for the formation of smaller mesoscale circulations within the large system. A satellite view of the sequence of formation and dissipation of a macro-circulation is shown in Fig. 70. The mesoscale circulations or tornado cyclones generated within the larger macro-circulation systems are at least one order of magnitude smaller in size, usually between 5 to 30 miles in diameter and are characterized by an eye at the center and spiral echo bands on radar screens (Fujita, 1958).

Brooks (1949), recognizing the difference between the mentioned circulations stated that there exists a cyclone, intermediate in size between a regular cyclone and a tornado vortex, in which tornadoes formed. These tornado cyclones or rotating cumulonimbi are nature's tornado vortex generators. Fujita (1965), studying the formation and steering mechanism of tornado cyclones postulated that the source of angular momentum necessary to initiate these rotating clouds is found along mesohigh boundaries existing within the field of macroscale cyclonic circulation where pronounced low-level circulation exists. These systems, cylindrical in shape, extend vertically from a few thousand feet to as high as 60,000 feet above the ground.

Fankhauser (1971) constructed a three-dimensional model of the airflow within and around a cumulonimbus system based on earlier models (Browning, 1964, Goldman, 1968) and his own radar observation of two Great Plains

cumulominbi, shown in Fig. 8. The internal circulation is found to consist of essentially independent rising and descending branches. Of the total air influx, Newton (1966) estimated that about 60 percent ascends from the potentially warm and moist subcloud layer, while the remaining 40 percent is drawn from the cold and dry levels aloft which is the source of the downdraft. In Fig. 8, the thin, solid inflowing and ascending streamlines represent the history of moist air originating in the subcloud layer, while the heavy dashed lines trace the entry and descent of the cold and dry air, producing downwashing and diverging downdraft. The internal circular bands signify net updraft rotation. The entrainment of the environmental air through the vertical cloud walls of such a system produces some mixing, however, confined to a sheath surrounding the updraft core. Photograph of Fig. 71 shows a meso-circulation over the state of Kansas. These systems have a lifetime of the order of an hour and may spawn several tornadoes beneath them. Figure 9 shows the approximate relationship between such atmospheric vortices and tornadoes.

The preceding discussion points out that a sequence of events is needed to result in an occurrence of a tornado vortex. A macro-scale circulation to be followed by small mesoscale circulations within it are prerequisites to such tornado vortices. It is important to note that vortices of magnitudes comparable to tornadic circulations may be produced in other ways (e.g. severe thunderstorms), however, tornado cyclones such as ones discussed above have been observed to be responsible for most of the tornadic storms in the mid-west.

A. Experimental Modeling

As discussed in this Chapter, a rotating cumulonimbus acting as a natural tornado generator is responsible for most of the Great Plains tornadoes, however, the exact mechanism of the formation of a tornado funnel from these meso circulations is not yet explained. Since such storms occur locally, have a very short life time and are associated with violent winds, it has been extremely difficult to observe and investigate the formation mechanism and structural definition of any one of these natural phenomena. Therefore, great insight and understanding of the physical flow can be ascertained by experimental modeling of tornado-like vortices in the laboratory. Although many factors such as temperature, density, pressure and moisture variations play important parts in the formation of larger cyclones, it is believed and will be shown later that the fluid mechanics nature of the cyclone, if not the only cause, but by far is the most important agent in creation of a tornado vortex. The simulation of a tornado-like vortex, discussed hereafter in the present research is based only on this latter factor with no attempt to simulate the temperature, density and moisture variation at this preliminary stage of the research.

B. Vortex Generator

The vortex generator used for the present investigation was first proposed by Hsu (1972, 1973). The new design is different from the conventional approach such as those discussed in Chapter I. The research objective is not merely to study a simply structured vortex but to investigate the complicated structure of a tornado-like vortex and more

importantly its interaction with a ground boundary layer.

To simulate a tornado cyclone (cumulonimbus), a honeycomb disk of 17" in diameter is rotated inside a Plexiglas cylindrical tube shown in Fig. 72. The schematic layout of the simulator is shown in Fig. 10. The Plexiglas section simply simulates the vertical cloud walls of a cumulonimbus system. The honeycomb rotation creates the angular momentum needed to form one of such meso-circulations. Although the rotating disk is made of a 2" thick honeycomb material, the upflow air into the Plexiglas section does not pass through the honeycomb completely and some of the flow approaches the walls just below the honeycomb and returns along the walls downward. This part simulates the downrush of the cooler air in a cumulonimbus, however, its interaction with the upmoving air must be prevented. To achieve this, an air deflector is added to divert the return flow and prevent any interference of such a downrush with the sequence of the generation of a tornado-like vortex. No exhaust fan or blower is used in this facility and the upflow is generated due to the horizontal convergence motion of air towards the instantaneous center of the rotation.

The rate of rotation of the honeycomb disk is regulated by a speed control system with variation of zero to about 1700 rpm. Utilizing this facility then it is possible to form a typical tangential velocity profile for atmospheric vortices below the vortex generator. The earth surface is simulated by a 10' x 10' ground plane capable of changing its distance from the vortex generator, using hydraulic jacks. The plane simulates the ground surface at various distances from the cloud base. A 4' x 4' square opening in the center of the plane permits installation of a

water tank or different plates for various research purposes. The 6" deep water tank, when filled with water, simulates the sea surface and with dry ice in the water the resulting vapor permits visualization of the entire flow region from the surface to the simulated cloud base. The distance from the plane to the air deflector may be varied from 2' to 7' although mostly the distance was kept at 31" for the present investigation. The interaction of the generated vortex (simulated tornado cyclone) at the exit of the simulator with the ground plane (simulated earth surface), then forms the complicated flow structure of a tornado-like vortex which will be discussed in detail in a later chapter.

As mentioned previously, the objective of this research is to obtain the information which has otherwise been impossible to ascertain from natural tornadic storms, namely the structure of the vortex flow field in contact with a solid ground boundary layer, flow pattern and velocity distribution, pressure variation and some damage observations. The similarities between the present simulator and natural vortex generators or rotating cumulonimbi have been discussed and the new approach in simulation has been justified. Although it is not believed that the mechanism discussed here is responsible for the generation of all tornadoes, it is thought that the present simulation is the most correct method of generating such laboratory vortices. The conventional method of vortex production adopted by Dines, Miller, Chang and Ward is fine as long as the study of a vortex is concerned. However, a tornado vortex is simply more than a vortex, one which is interacting with a ground boundary. Following such methods angular momentum is

generated at the outside vertical boundaries of the region then is transferred inward due to low pressure at the center of rotation and also due to the convection enforced by the suction at upper boundary. In such modeling, because of generation of rotation at all levels, there is no interaction with the ground boundary other than the fact that the ground level serves as a constraint and introduces frictional effects into the flow field. Such flow fields do exist in nature. Dust devils, for example, are such vortices. In hot, and flat desert regions with extremely high lapse rates above the surface, the buoyancy effects become large, introducing constant ascending motion of the low level hot air. When environmental surface winds below certain critical velocities meet or when rotation is introduced in the wake of an obstacle, a simply structured vortex forms. Sinclair (1973) investigated the structure of such vortices by direct penetration into their flow fields. On the basis of his observations along with velocity and pressure measurements of Arizona dust devils, he established the existence of a low-pressure core and a downcurrent along the axis. Immediately outside the downcurrent, upward velocities were measured which decreased rapidly with increasing radius. Dust devils do not become violently strong because their supply of vorticity is limited to what they acquire from their immediate environment. The conventional approach in producing tornado-like vortices adopted by Dines, Chang and Ward contrary to the claim of their designers, only results in non-violent small scale vortices, such as dust devils. The suction fan in these vortex generators simulates the desert upflow due to extreme lapse rates. The generation of angular momentum from

surrounding walls also simulates such generations in the deserts due to different surface wind directions caused, for example, by topography of these areas. Therefore, the results are very similar. At times dust devils have been observed (Fujita, 1971) to contain smaller vortices travelling around the core of the mother vortex. Ward has produced such multiple vortices rotating around a central core which exhibits a downflow just as natural dust devils have been found to do. The extreme violence of the tornadic flow field is absent in the photograph or any of the movies of his simulation. Ward can only produce such multiple vortices when the ratio of the updraft diameter to the inflow depth is greater than unity, and the inflow angle with respect to radial is larger than about 30°. This is certainly a common possibility in vast, hot deserts where the upflow exists everywhere in a large area but surface winds and inflow exist in a relatively thin layer with a wide variety of inflow angles due to topographical effects. Chang's simulation also exhibits similarities to the natural dust devils. With small fan suction, streamline pattern in the flow indicates downward motion at the center However, when suction is increased by a factor of almost 10, then upflow is indicated at the center, mainly due to unnecessary interference of the large suction with the vortex formation at lower levels. The preceding discussion points out the shortcomings of the previous attempt in a true simulation of tornadoes. Tornado flow fields are much more complicated than the flow of dust devils mainly because of their different source of formation. However, before closing out this section, the following possibilities are proposed to explain the downflow occurrence

in dust devils.

1. The phenomenon of the reverse flow in a swirling environment is a well-established fluid dynamic occurrence. Weske (1955) obtained numerical solutions and Burgers (1956) obtained analytical solutions of this problem, which will be discussed later. Other observations of this phenomenon have been made by Lewellen et al. (1969) and So (1967) for flow in nozzles or diffusers. Therefore, inside the core of dust devils surrounded by upmoving swirling flow a downflow may be a fluid dynamic possibility.

2. Dust devils, as mentioned previously, are small scale vortices and their total vertical extent seldom exceeds a few hundred feet from the ground surface. As an example, assume a height H_d^* for a typical dust devil. Throughout this height and inside the core region, below environmental pressure exists due to swirling flow of the dust devil. However, such a vortex terminates in a non-rotating environment at height H_d^* where a uniform pressure region exists with a pressure equal to that of the environment. Therefore, a constant downward motion of upper air level into the lower pressure tube of the vortex becomes a possibility and extends all the way to the ground surface. Fig. 11 illustrates such a mechanism.

III. FLOW VISUALIZATION

A. Flow Similarities

Research in aerodynamics, hydrodynamics, and related fields often involves the use of tracers to delineate flow patterns in the fluid. Photographic methods then are employed to make a permanent record from which flow direction and velocity may be determined.

Such techniques may be used to not only reveal the detailed structure of the flow but also to investigate the degree of similarity between the natural flow field and its laboratory counterpart. Of course, correct modeling of atmospheric vortices requires approximate selection of non-dimensional ratios involving rotation, inertia, diffusion and length scale. Similarity is achieved when these ratios are the same for different scale flows. For example, the Rossby number, or the ratio of inertial to Coriolis forces is a significant characteristic of the rotational flows as is the Reynolds number in non-rotating flow fields. However, these non-dimensional ratios are not easily achieved even in less structurally complicated flows in the wind tunnel simulation experiments, let alone in simulation of complicated atmospheric vortices. Additionally, due to the lack of any reliable information and measurements of such natural vortices, it has not been possible to determine the magnitude of the similarity ratios specially in the case of tornadic storms, although very rough estimates of some parameters have been made under simplifying assumption for different tornadoes. Adding to the existing problems of studying tornadoes, Morton (1966) notes that there is no reason why tornado vortices should all be dynamically similar. Brooks

(1951) also gives evidence that the ratio of inflow to tangential speeds near the ground may vary appreciably between different tornadoes or during the life of a single tornado. However, the large number of still photographs and some motion pictures of tornadoes in action may help to simulate these vortices such that a similarity between the flow appearance in nature and laboratory is achieved. This will include the shape of the tornado funnels and dust clouds and flow pattern of the visible portion of such vortices. Once such a similarity is attained, then invisible part of tornadoes may be investigated in the laboratory. The accuracy of such findings may be checked from time to time by rare photos of some tornadoes revealing more than merely the usual outside appearance of these storms or from the accounts given by people sometimes trapped inside of such flow fields. Some other findings may be compared with theoretical determinations while some may be new and yet to be measured or investigated in the tornadic flow fields in the future. In the present investigation, a variety of mediums such as smoke, dry ice, saw dust, flour, and instant tea were employed for the purpose of visualizing the flow field under study.

1. Dust cloud similarity

Gaseous mediums reveal the flow pattern of the vortical flow while those with heavier particle size simulate the dust cloud formation due to flying debris. Such dust clouds are usually observed in association with tornadic storms, however, their shape is varied according to the general quality of the flying debris and topography of the ground environment.

Figures 73, 74, 75 and 76 show dust clouds of the Dallas tornado of 1957. The first two photographs were taken while the tornado was travelling over the city where flying debris were made of lumber, plywood sections and household equipments. In neither one of these photos a funnel is observed despite the fact that the tornado was violently damaging at the ground level. The photo of Fig. 75 was taken where the vortex was almost in the open country while photo of Fig. 76 shows the dust cloud formed in the open country where flying debris are relatively small dust particles. Such small particles due to their small mass are not readily ejected from the orbit around the vortex core thus forming cylindrical dust clouds. Dust clouds of this kind may become dense and cover the entire height of the subcloud portion of the vortex. Figure 77 is an example of such dust clouds. More massive debris, due to their mass and size, suffer a higher drag force thus leave the orbit and fall back to the ground following a curved path. Many of these larger particles do not even complete a single turn around the core when they are picked up and ejected outward. Such particles, on the other hand, truly exhibit the explosive power of tornadoes. Saw dust simulates these large particles in the laboratory while flour or instant tea simulates sand and gravel in the open country. Figures 78, 79, 80 and 81 depict the basic similarity of the laboratory dust clouds to those of natural tornadoes shown previously. Saw dust is used in the first two photos while glass particles and flour were used in the photos of Figs. 80 and 81, respectively. The proper distance between the air deflector and the ground plate was determined to be 31" as this resulted in the best dust cloud shapes.

By watching the dust clouds in the laboratory, it was found that the vortex, produced in the present simulation, travelled at random speeds around the centerline of the simulator. Its path covered a circular region of approximately 6" in diameter, standing still at a point, then moving away, however, generally in a counter-clockwise direction. The maximum translational speed was observed to be about 1 fps. Such random motions of the lower end of the vortex is, of course, a familiar characteristic of atmospheric vortices although such vortical flows generally follow their mother cyclone for the reasons discussed later in this chapter.

2. Tornado funnel similarity

Another characteristic appearance of a tornado is a usually narrow, pendant cloud extending from a cumulunimbus cloud base, nearly to the ground. Such funnel clouds may have different appearances. Some may be short and relatively wide, some long and small in diameter, and some may not appear at all while the ground surface is experiencing damage. Tornado funnels originate from the cloud base and approach the ground surface, making use of the clouds as a flow visualizing medium. Photos of Figs. 75 and 76 show such funnel clouds. Due to the random motion of the vortex core in the laboratory, it is not possible to show such downflow regions at all times, however, when smoke is fed into the vortex core at some height, a funnel appears with a downward motion. Near the upper end of the flow and close to the generators exit no such downflow could be observed. In this latter region upward axial velocities are large at the center compared to the tangential speeds. Remarkable

similarity between these laboratory produced funnel clouds and those of natural tornadoes are clearly shown in Figs. 82 through 87. Tornado funnels do not necessarily decrease their diameter with decreasing height. The Kingfisher tornado shown in Fig. 88 is an example of such cases. Figure 89 shows a simulated constant diameter funnel cloud in the laboratory. The difference between these funnels and sharp end funnels is thought to be due to the flow visualization effect and the characceristics of the inflow at lower layers.

Similarities between the dust clouds and tornado funnels and their simulated counterparts once again point out the superiority of the present simulation over any previous attempt and signifies the correctness of the theory of tornado vortex formation from tornado cyclones based on which the present simulator is designed.

Armed with such excellent agreements, the research was continued to investigate the detailed structure of the tornadic flows in the laboratory. Most of the findings will be supported with rare photographs or eyewitness accounts of natural tornadoes or will provide some explanations for them. Other findings, however, may not be substantiated at present due to lack of methods of direct observation of these phenomena in natural cases.

B. Structure of Tornado Vortices

In the previous discussion, dust clouds and tornado funnels were mentioned for the purpose of flow similarity investigation. Although these are the commonly visible portions of tornadoes, they are only

a part of a more complex flow field. In the following discussion each part of the flow is investigated and explained employing slow motion pictures and still photography techniques, and will be finally combined to explain the structural formation of tornadic flows.

1. Dust clouds

As mentioned previously, dust clouds are the end result of interaction of tornadoes with the ground surface. Such clouds are formed from the debris accumulated at the root of the vortex core from the damaged structures, trees, etc., and in the case of tornadoes over water (waterspouts) from water spray. Such accumulation takes place because of the inflow towards the instantaneous center of rotation. Figure 90 shows the typical path of two groups of particles on the surface as they were attracted inward. The photo is taken through a Plexiglas plane looking up into the simulator. The Plexiglas was covered with a shallow layer of flour. The dark spot in the center of the rotation indicates the existence of an upward suction region and will be discussed in the following sections. When debris particles arrive at this circular region of approximately 1" in diameter, they sharply turn upward (upmoving dust cloud jet). Then, depending on their size and mass, they are either ejected immediately after leaving the surface (large particles) or remain in an orbit forming a cylinder around the main core but with relatively large diameter (smaller particles). Figures 73, 74, 78 and 79 are examples of dust clouds with large debris while Figs. 75, 76, 77, 80 and 81 are those with smaller particles. Of interest is the upward jet trajectory shown at the center of rotation in the photo

of Fig. 80. Small particles finally leave the orbit in a less noticeable manner. The inflow path of particles in the boundary layer will be analyzed in Chapter IV in an attempt to measure radial and tangential wind speeds in this layer. Figure 12 shows the approximate path of particles in the meridional plane of a dust cloud.

2. Inner vortical tube

When smoke or dry ice gas with extremely small particle size is fed into the flow, a tube appears extending from the surface upward into the vortex generator, along which air spirals upward. Although similar tubes have been produced by most researchers, they have often been incorrectly interpreted as tornado funnels. Figure 91 shows a vortical tube visualized by generating dry ice gas at the ground surface. Swift axial and tangential motion is observed along such vortical tubes. Their diameter varies slightly with other fluctuations in the flow field, however, it remains larger than the dust cloud jet mentioned previously but smaller than the dust cloud cylinder diameter. It will be shown that tornado funnels drop into these tubular structures. Such vortical tubes are usually invisible in natural tornadoes since they only contain clear air. However, when dust or other very fine materials enter the flow field, working as a visualizing medium, show the tube often partially. Figure 84 shows the vortical tube around the funnel of Peshawar Tornado of 1933. Figure 13 illustrates the approximate path of the particles in the meridional plane of such vortical tubes.

3. The tornado funnel

As discussed previously, tornado funnels are the downward extension of the clouds, thus usually visible. These funnels, although have been observed to have dropped downward from the cloud base, have been of some controversy as to the direction of motion of air along them. Hoecker's (1960) impression, for example, of the motion of air along the Dallas Tornado funnel was that only tangential speed existed with no axial motion. However, experiments conducted in the present laboratory simulation pointed to a definite downward motion. Such funnels were observed to be the downward extension of the clouds into the upmoving vortical tube. Their downward motion is thought to be the result of the well-established fluid dynamic occurrence of axially reversed flow in a swirling environment which will be the subject of a later discussion. Figure 92 shows the downward spiral of the smoke funnel into the upmoving vortical tube visualized by dry ice gas generated at the surface. The photo of Fig. 82 specially indicates the downward spiralling motion of clouds along the tornado funnel while Fig. 84 shows the Peshawar tornado of 1933 to be enclosed by the partially visible vortical tube. Figure 14 illustrates the tornado funnel relative to the other portions of the flow discussed so far. It should be noted that the region immediately outside such down flow regions is also affected by the upmoving vortical tube and therefore the particles or clouds existing in this region are trapped in a state of rotation with no or small net axial flow. Such an occurrence was probably observed by Hoecker (1960) which led him to believe that funnel flows lacked any axial motion. Similar cases were

observed when slow motion pictures of the funnel flows were analyzed in an attempt to measure axial and tangential speeds of the flow in this region, and will be discussed in more detail in Chapter IV. Tornado funnels simulated in the laboratory do not touch the ground surface although they do approach it. It is thought that such a downflow region adjusts itself with respect to the surface such that there remains enough space for the upturn of the downcoming flow. An upward jet at the root of the vortex which will be discussed in the next section, is also responsible for keeping the funnel off the ground surface. However, tornado funnel, pressing down on the inflow layer, probably modifies it in the manner shown in the sketch of Fig. 14. Again, photographs of Figs. 82 and 84 are excellent examples showing the funnel off the ground. Usually the dust clouds covering the lower portion of the vortex gives an impression of the funnel touching the surface. The simulated funnel, when observed from its bottom side through the Plexiglas plate was found to be hollow. Figure 93 shows the bottom view of the funnel while photo of Fig. 94 is a side view of the smoke funnel, again exhibiting a hollow structure. Both photographs were taken when smoke was fed into the vortical tube to visualize the downmoving funnel. The diameter of the hole is approximately 0.5 in., however, varies slightly with height and other flow fluctuations. Such finding indicates that a downflow cannot exist at the center, otherwise the funnel would be filled up by smoke. The observations of the hollow funnel with no central downflow has been reported in some rare occasions where people trapped in a tornado vortex overhead could look into such funnel clouds. Flora (1953) and Flora (1949) report accounts of such experiences by the editor of the Topeka

Daily News on March 23, 1913 and a farmer residing near Greenburg, Kansas. A similar incident is also reported by Hall (1951) describing his personal experience. All of the above mentioned people reported hollow funnels, circular in cross section with the end off the ground surface. Hoecker et al. (1960) also analyzing the photographs and movies of the Dallas tornado report the existence of the definite hollow structure of the tornado funnel.

4. The center jet

An extremely difficult portion of a tornado vortex to observe is the flow at its very center. Motion and still pictures fail in most instances to show the central portion of the vortex due to the fact that it is usually enveloped with the funnel or dust clouds. However, in the laboratory such observations may be readily made with proper flow visualization techniques. Any medium fed into the flow field for this purpose mostly fails to enter the innermost circular region of the vortex core, discussed previously. Therefore, only smoke or dry ice gas generated inside this region can be of any help in visualizing the nature of the flow field in this portion of the vortex. Dry ice gas generated at the surface of a water tank probably gives the best visualizing effect. When the vortex core passes directly over a piece of dry ice the generated gas shows a definite upflow jet in the center of the core. Photographs of Figs. 95 and 96 were taken in such instances exhibiting a needle-like swift, upward motion exactly at the center of the core. Photo of Fig. 96, however, is of particular interest due to its coverage of an explosion type phenomenon in a region just above the

ground surface. Analysis of the slow motion movies of the present laboratory simulation also supports the existence of such a phenomenon, in a region connecting the lower dust cloud jet to the upper jet just discussed. A gas parcel lifted from the surface through the swift upflow of the lower dust cloud jet suddenly decelerates almost to a zero axial speed at a height of approximately 2-4 inches above the surface. Such a hesitation in upward motion is thought to be due to a head-on encounter of the upmoving lower jet with the downflow of the tornado funnel. The result is an explosion-type effect such as shown in Figs. 96 and 97. This phenomenon will be called the "Jet breakdown" from now on. From the center portions of the flow of this region then a sharp upmoving jet separates, which swiftly moves into the hollow funnel and continues upward. Figure 82 is a very rare photograph of such an upmoving jet, while photo of Fig. 98 may be an example of the jet breakdown phenomenon near the surface of a tornado. Sketch of Fig. 15 illustrates the center jet and its associated phenomenon relative to the outer portions of the flow described up to this point. Hudson (1958), who flew his Beechcraft Bonanza 225 aircraft at a height of 200 ft. from the ground and within 800 ft. of the Dallas Tornado also reports the sudden disappearance of the water in a 175 ft. diameter round pond into the mouth of the funnel as the tornado moved directly over it. The funnel grew dark throughout and there was no sign of the water being thrown out. It is suspected that the upmoving jet is directly connected to the upflow region of the cumulonimbus system. Therefore, the debris picked up by this jet may be carried to altitudes as high as 60,000 ft.

where they are then transported by the cold jet aloft to far distances from the storm site. Stanford (1976) gives an account of the Ryan tornado (Iowa) which carried papers and cancelled checks of some local residents into Illinois to towns 55 and 75 miles downwind. Flora (1956) reports the existence of foreign matter such as pebbles, leaves, twigs, nuts and insects in hailstones. Such extraneous material have probably been carried up by tornadic storms to great altitudes where they were trapped inside rapidly forming hailstones usually accompanying tornadoes.

5. The outer vortical tube

Another observable portion of the flow in the present laboratory simulation is a third upflow region enclosing the entire structure discussed up to this point. Photograph of Fig. 99 shows the inner and outer vortical tubes when smoke is fed into the flow for flow visualization. The diameter of this shell is approximately 3 to 4 times the diameter of the inner tube, however, the flow tangential and upward axial velocities are noticeably smaller in this region than the speeds in the inner vortical tube. This region starts just above the ground inflow layer and usually is formed by fine particles that are ejected from the dust cloud jet region. The flow in this shell seems to be more turbulent than probably any other part of the flow field. Photograph of Fig. 100 shows the smoke funnel dipping down into such a vortical tube formed by flour particles. Note also the small circular region on the surface which is cleared off of flour by the vortex. Figure 77 shows this third upflow region covering the entire Great Bend Tornado.

Photograph of Fig. 101 again shows the two upmoving vortical tubes formed by instant tea where the dust cloud jet is also shown. However, a dark region between the two upflow shell is also indicated. No definite information concerning the direction of motion of air in this dark region could be obtained although it has been thoroughly examined through slow motion picture studies of this region. It is, however, proposed here that a very low speed downflow of air should exist in this region, much weaker than the downflow of the funnel. Obviously, an upflow would fill up this dark region with flow visualizing medium, introduced from lower levels. It is also suggested that extremely wide funnels observed to have dropped from very low clouds may only be this second downward flow enveloping the much faster motions of the inner vortical tube, tornado funnel and central jet. Photograph of Fig. 102 shows such a possibility while the sketch of Fig. 16 illustrates the outer upmoving vortical tube and the second downflow region in the meridional plane relative to the other portions of the flow discussed up to this point. Outside of the third upflow shell generally no definite direction of the air motion is observed with some tendency of downflow at lower levels. Small tangential speeds are observed in this region decaying rapidly with increasing distance from the vortex core. Table 3.1 summarizes the structural characteristics of the simulated tornado flow of the present research.

Table 3.1. Summary of the structural characteristics of the simulated flow of the present research.

Portion of Structure	General Flow Direction in the Meridional Plane	Approximate Distance from Centerline (in)
Center Jet		
Lower dust cloud jet	Upflow	0.00 - 0.25
Jet breakdown	Upflow and outflow	0.00 - 3.00
Upper jet	Upflow	0.00 - 0.25
Funnel	Downflow	0.50 - 1.20
Inner Vortical Tube	Upflow	1.30 - 2.80
Second Downflow	Downflow	3.00 - 4.50
Outer Vortical Tube	Upflow	4.50 - 6.00
Dust Cloud (massive particles)	Upflow and outflow	0.00 - 6.00
Surface Layer Motion	Inflow	30.00 - 0.00

Numerical solution of the conventional boundary layer equations of a vortex along with a two equation model of turbulence obtained by Hsu and Tesfamariam (1975) revealed a complicated flow pattern in the meridional plane of the boundary layer as shown in Fig. 17. Note specially the similarity of the numerically predicted flow regions to those of the present simulation. Excellent qualitative agreement of this result with the flow pattern observed in the laboratory stresses again the accuracy of the theory based on which the present simulation is being conducted.

C. Other Important Observations

The preceeding analysis reveals the excellent qualitative agreement between the present simulation and natural tornado flow fields. As mentioned previously, tornadic storms do not seem to be dynamically similar, however, the large amount of visual information such as those discussed in this chapter point out the structural similarity of most of such storms. It is also very possible that some tornadoes not produced under circumstances described in Chapter II may exhibit different flow structure characteristics. Such tornadoes are unusually strengthened dust devils or fire tornadoes (Idso, 1974) formed by buoyancy effects of the heated surface environment in large scale forest fires or near volcanoes.

To further examine and explain the other phenomena, the following experiments were conducted.

1. Vortex formation

The sequence leading to the formation of a vortex in contact with a ground boundary layer was recorded employing high speed photography. When viewed in slow motion such photographical technique can yield valuable information otherwise extremely difficult to obtain in this field.

Dry ice pieces were set in the water tank where they provided a layer of gas covering the ground plane. Then, while high speed photography was in progress, the vortex generator was turned on, and the sequence of the vortex formation was recorded on film.

The initial effect was a noticable inflow with the central portion of the gas layer below the generator rising slowly. The rotation seemed to start shortly after, at a radius of approximately equal to that of the generator while the inflow and upflow still in the process of strengthening. The rotation was then transferred inward presumably by the inflow and finally a vortical tube appeared with inflow only near the surface. Such mechanism will be discussed in more detail in Chapter VI of this dissertation.

2. Surface roughness effect

In the preceding experiments, the simulation was performed over smooth surfaces such as the Plexiglas and sheet metal plates or over relatively smooth surface of the water in the water tank of the ground plate. With no exceptions vortical tube, funnel, and associated flow structure were simulated. However, it was observed that although the vortical tube had a smooth surface with swift flow throughout, when it encountered an obstacle on the ground plate, the flow became disturbed and such disturbance was rapidly transmitted upward throughout the tube. Figure 103 shows the vortical tube seconds after passing over a 3/8" x 5/8" x 5/8" model of a house. Note no characteristic double wall is observed. With increasing number of obstacles on the ground, the tube became more turbulent and its swift upmoving flow disturbed and finally no tube with a definite tubular shape was formed when the surface became very rough. Figure 104 shows the disrupted vortical tube as the vortex is passing over a model of a city. Small scale houses are only 0.5 in.

while larger buildings are about 2 inches high. Since it was shown that the funnel had to dip down into such a vortical tube, the same experiment was repeated this time for observation of the funnel. Again, it was found that the funnel was also disturbed and finally did not form with the surface being very rough. When the same experiment was repeated with instant tea particles covering the plane of obstacles the formation of the dust cloud jet was found to be little affected by such surface roughness. The above observation not only indicated that the funnel formation is dependent on the formation of the vortical tube but also revealed that they both depend on an undisturbed and strong inflow to concentrate the vorticity content of the flow at the center of rotation. The formation of the lower jet indicated that unless a drastic cut in the inflow takes place, the lower part of the vortex is not severely disrupted by the increasing roughness while the upper flow is more vulnerable to such disturbances.

These observations, of course, are consistent with those of tornadic vortices. While Fig. 76 shows the Dallas Tornado with its visible funnel over an open country, Figs. 73 and 74 do not show a funnel formation when the tornado is travelling over the rough ground surface of the city. Note that the lower portion of the storm is not seemingly affected by such roughness. The degree of disruption of the flow in tornadoes depends on the relative size of the tornado and its strength with respect to the size of obstacles and amount of roughness of the surface. For example, the extremely powerful and towering Union City Tornado funnel showed no observable sign of decay as it passed over the Union City, Oklahoma.

3. Ground plane effect

Observation of the vortical tube and the funnel were performed with changes in the distance from the generator's air deflector to the ground plate. The tube decreased its diameter with increasing distance between the vortex generator's exit and the plate. Also, the tube shape attained more curvature and the lower end of the tube travelled farther from the center, as far as 5' from it when the ground plate was lowered to a level of 75" from the air deflector. The tube had a tendency to dissipate at such long distances. A long and narrow funnel could still be observed from time to time, however, its flow visualization became more difficult due to its weakness. Inflow could definitely be detected although weaker, as was generally the entire flow field. Figure 105 shows the vortical tube with its characteristic double wall structure, while it is bending to connect itself to the source of rotation at upper levels. Figure 106 shows a funnel reaching near the ground. In both cases the distance from the ground plate to the air deflector was approximately 62 inches, or twice the regular distance used in the present simulation. Figure 107 shows the vortical tube of Fig. 105 as it is dissipating with characteristic snake-like motion. Such behaviors are often observed in nature. Figure 108 shows a photograph of the Jasper Tornado (Minnesota) in its dissipating, rope-like stages. Other interesting features shown in this photograph are the visible vortical tube with its double wall structure and the center jet flowing into the mouth of the funnel. Dissipation of tornadoes occur under the following circumstances:

a. Large distances between the rotation aloft and the ground surface weakens the tornado vortex as was shown in above experimentations.

b. Weakening or dissipation of the tornado cyclone naturally result in the loss of the ample vorticity supply to the tornadic vortex, disintegrating the vortex structure. Such observations may be readily made in the laboratory. When the rotational rate of the honeycomb disk inside the vortex generator was decreased, vortical tubes weakened and dissipated just as the same way as they did with increasing length of the vortex, even with small distances between the rotation source and the surface of the ground plane. However, in this latter case with small distance and small rotation, vortical tubes were formed with laminar lower structure and a turbulent upper portion, connected by an unstable, knot-like region with recirculating flow. Such phenomenon known as the "vortex breakdown" is shown in Fig. 109. This is usually encountered in swirling flows or trailing vortices of delta wings (Bossel, 1969). It is possible that a rope funnel may not appear and instead with decreasing intensity of the rotation the funnel may simply retract and disappear into the clouds.

c. Separation of tornadoes from their mother cyclone and consequent loss of the main supply of vorticity to such vortices results in rapid decay of tornadic storms. Such separations are very unusual and not well understood. Fujita (1975) reports the separation of the Saylor Park Tornado (Illinois) from its mother cyclone and moving practically under the blue sky just outside the storm system. The famous Xenia Tornado (Ohio) also separated from its generator and dissipated.

d. Another form of tornado dissipation occurs when the lower end of the vortex can not travel as fast as the mother cyclone is translating. With its dependence on the supply of the vorticity from tornado cyclones such tornadoes are forced to be connected to the fast moving source of rotation aloft to keep them alive and active while the lower end may be left behind for many miles due to frictional limitations of the rough ground surface. Therefore, the entire vortex elongates and with upper end in a more rapid translation it almost becomes horizontal. In such a process the rope-like vortex decays and usually is replaced by a newborn tornado if the mother cyclone maintains its intensity.

e. It is very possible that sudden changes in environmental characteristics such as rapid temperature changes and large lapse rates may interfere with the process of maintaining a tornado vortex. Although not a general rule, but, tornadoes are thought to avoid heat islands such as large cities. No tests were performed to investigate this, but Fujita (Roberts, 1972) reports the decay of his laboratory vortex under a condition of increased environmental temperature. However, lapse rate modeling or simulation of a heat island is difficult and with incorrect models, wrong information is obtained. As mentioned before, at least exceptions exist, the most notable of which are the famous Dallas Tornado and the recent Omaha Tornado both travelling over large cities with their full intensity.

The effect of the ground plane on formation of tornadic vortices was further examined by removing the plane. Although the rotation rate of

the generator was kept at its normal 1700 rpm, no concentrated vortex was formed. Upflow was observed everywhere with very small rotation near the vertical centerline of the vortex generator indicating the possible existence of a very weak vortex but definitely not a strongly concentrated one. Photograph of Fig. 110 illustrates the general trend of the flow. With no vortical tube formed no funnel did form either indicating the extreme importance of the existence of a ground surface to form a concentrated vortex. It is demonstrated by this simple experiment that formation of a tornado vortex is the end result of the interaction of a tornado cyclone (mesoscale circulation) with a solid ground surface. It is this interaction that creates the inflow towards the center of rotation, therefore concentrating the vorticity at the center where large amount of it is required to form a tornadic vortex.

From the observations made in this preceding discussion it is concluded that for a given strength of a tornado cyclone (which may be a function of rotational intensity plus the upward-downward motion in it) a critical height, H^*_{cr}, from the ground surface, exists for the rotating system aloft at or below which ($H^* \leq H^*_{cr}$), a concentrated tornado vortex may be formed definitely, but at any other height ($H^* > H^*_{cr}$) no, or a very weak vortex (depending on H^*) is produced with no intensified core. This may be an explanation for the failure of some tornado cyclones to produce tornadoes even when favorable conditions are observed by forcasting meteorologists. If this is proved true, a drastic reduction in the number of tornado watches released by weather bureaus may be made, in addition to predicting the possible sites of tornado production in the path of a

storm system aloft. It should be noted that the critical height H^*_{cr} is only discussed with respect to the formation but not maintaining the concentrated vortices. It is observed by Fujita (1974) that once a tornado vortex is formed it can travel over mountains or valleys and still remain intense. However, such observations have been limited in number and probably no reliable final conclusion may be made at the present.

Finally, a simple experiment was performed to investigate the Helmholz theory, that a vortex in a perfect fluid flow can end at a solid boundary surface perpendicular to the vortex filament. With surface inclination changed, the vortical tube and consequently, the funnel bent to end normal to the solid surface. Such behavior is always observed in tornadic vortex flows. Photographs of Figs. 111 and 112 are laboratory examples while all tornado photographs included in this dissertation are proofs for the naturally produced vortices.

4. Multiple tornado funnels and multiple vortex tornadoes

Multiple tornadoes have been observed to occur under the same cumulonimbus system. Photograph of Fig. 113 is an example of such phenomena, showing twin tornadoes of Wamego, Kansas. Simultaneous observation of tornado and waterspout was reported by Maier and Brandli (1973). Both of these vortices occurred under a single cumulonimbus towering to a height of 43,000 ft. Such a finding indicates that waterspouts and tornadoes should be very similar and at least those formed under the same convective cell should have identical structures.

Snow and Agee (1975) hypothesized that tornado families are generated by interacting multiple small tornado cyclones rotating about a common center and embedded within a larger mesoscale circulation.

Brown et al. (1973) analyzing the data, obtained by single Doppler radar showed that two tornado cyclones were present aloft at the time two tornadoes were on the ground. These cyclones appeared to be rotating around each other but embedded within a thunderstorm cell. Fujita (1974) also found such tornado cyclone "brothers" while investigating the tornado outbreak of April 1974 by examining radar pictures. All the evidence presented here indicates that simultaneously more than one vortical flow may be formed in a parent vortex. In Chapter II, it was explained that many mesoscale circulations may be embedded in a larger macro-circulation. The preceeding discussion shows that multiple tornadoes (micro-circulation) may exist in any meso-circulation. Therefore, one may expect that still smaller vortices do form in a single tornado vortex. Observation of such secondary vortices in dust devils have been made as early as 1948 (Williams, 1948), and Ward (1972) simulated these smaller vortices in the laboratory. However, Fujita (1971) publicized such observations based on which he proposed that such secondary vortices or suction spots exist at least in some tornadoes. Figure 18 illustrates Fujita's proposed model of multi-suction tornadoes. Observation of the path of Anchor Tornado, and Palm Sunday Tornado leaving cycloidal marks on the ground surface and finally recording on film of suction spots in Muncie (Fujita, 1971), Parker (Agee et al. 1975) and Oshkosh tornadoes (Blechman, 1975) have confirmed Fujita's hypothesis. Photograph of Fig. 114 is taken from a

film of Oshkosh multi-suction tornado clearly showing three visible vortices rotating on the rim of the larger vortex of the mother tornado.

Such multiple vortices were produced by the present vortex generator under a condition of small inflow towards the center of rotation. Proper small inflow was produced when the rotation of the honeycomb disk decreased to only 20% of the normal rotation rate. Turbulent vortical tubes were formed to approximately rotate around a common center, however, it was observed that such vortices had a tendency to join and form a stronger vortex. Photograph of Fig. 115 shows a pair of such laboratory vortices, with striking similarity to their natural counterpart, shown in Fig. 114. With any increase in upper rotation such vortices rapidly joined to form a single vortex indicating their vulnerability to increased inflow rate. During the experimentation, a maximum of three such vortices were observed at one time, however, with better flow visualization techniques, possibly more vortices may be observed. Ward (1972) defining:

$$\text{Inflow Angle} = \theta_i = \tan^{-1} \frac{\text{tangential velocity}}{\text{radial velocity}}$$

$$\text{Configuration Ratio} = \text{C.R.} = \frac{\text{updraft diameter}}{\text{inflow layer thickness}}$$

showed in his laboratory, that for the range of

$\theta_i \geq 30°$ C.R. = 4

$\theta_i \geq 75°$ C.R. = 1

multiple vortices could be generated.

As discussed in Chapter II, this is a common possibility for dust devils, however, for tornadoes, such conditions may be provided by

relatively small upper rotation rates as shown by the preceeding experiment or by topographical limitations imposed on the inflow layer of the tornado vortex. It is not known yet whether a multi-vortex tornado evolves from a single vortex with increasing turbulence or if created as a multi-vortex tornado, remains the same throughout its lifetime. Extensive research is needed in this area, however, a simple explanation is added here for the formation of such vortices to be justified with more extensive observations.

As described in this chapter, a tornado vortex contains many vertical layers of upflow and downflow. Such sleeve-like structures due to their varied distance from the center of rotation, also enjoy varied tangential speeds. Near the radius of maximum tangential velocity, r_m^*, the gradient of tangential speed becomes large. Thus, velocity magnitude differentials between vertical layers of this region may result in formation of secondary vortices. Figure 19 illustrates such a mechanism. Clockwise vortices to the right of the peak tangential velocity region, possibly do not form due to appreciable inflow, while inflow decreases near the center, as will be discussed in more detail in Chapter IV of this dissertation.

IV. WIND SPEED AND AIR FLOW PATTERNS IN THE SIMULATED LABORATORY TORNADO

A. Time Averaged Velocity Measurement

The three-dimensional velocity measurement of a flow field is a challenge to any investigator, however, with utilization of three-dimensional hot wire, hot film or laser anemometers, such measurements have become less tedious.

Hot films and hot wires generally cost much less than three-dimensional laser velocimeters, but their use requires their penetration into the flow field of interest resulting in interference of the anemometer probes with the flow of their environment. Hot wires are smaller than hot films but due to their extremely delicate structure are more vulnerable to damage. These instruments have been in use for some time, but laser velocimeters are relatively new arrivals in the area of three-dimensional anemometry. Since they are optical devices they may be set at a safe distance from the flow field eliminating any chance of interference with the flow. However, their use requires seeding of such flow fields with small particles, which, in turn, introduces inaccuracies in estimation of velocity magnitudes.

As mentioned in the last chapter, the observed simulated vortex is in constant random motion in the vicinity of the simulator's centerline. Any measurement of the instantaneous velocity magnitudes then requires constant observation of the vortex visually and recording the velocity information continuously in relation to the instantaneous location of the anemometer with respect to some reference point in the vortical flow such as its centerline. Such elaborate measurements then require employment

of sophisticated recording and digitizing instruments for the analog signals and optical systems for complete surveillance of the vortex in order to determine the location of the recorded data. Any medium for flow visualization purposes would contaminate the hot wire or film anemometers.

Due to such difficulties, an available three-dimensional hot film anemometer was chosen for the purpose of preliminary investigation and velocity measurement of the simulated tornado vortex, in association with a signal time averaging system with the intention to obtain a very rough estimate of the flow pattern.

1. Thermo Systems 1080 anemometer

A Thermo Systems, Inc. model 1080 total velocity vector anemometer and model 1126 calibration system were used to measure the tangential, axial and radial components of the velocity (Thermo Systems, 1970). This system may be used to measure the velocity vector in the total 360 degrees solid angle. It consists of three split-film sensors and a copper-constantan thermocouple for ambient temperature measurement. Each sensor is made of a 0.006 inch diameter quartz rod which is coated with a platinum film. The three split-film sensors are oriented orthogonally as shown in Fig. 20. These sensors are supported on only one end to minimize support interference.

It has been shown by experiment that the heat flux distribution around a constant-temperature cylinder in cross flow is non-uniform (Schmidt and Wenner, 1943). Anemometer sensors are such cylinders which are coated by thin metallic film and electrically heated to a constant temperature.

The non-uniformity in heat flux is detected by comparing the individual heat flux to each split-film. By the above comparison for any two split-films on a given sensor, quantitative information on the direction of the velocity component normal to the sensor is found. Advantages of this system, in addition to the capability of determining the direction of the velocity vector, are its fast response of up to about 1000 Hz., good low speed sensitivity and its relatively simple application and data reduction procedure. Six simultaneous velocity dependent analog voltages and a single analog temperature signal comprise the system's output. This output may be stored via magnetic tape recorder or oscillograph although a Fluke digital voltmeter was used in the experiment for this purpose. Figure 116 shows the control panel for the instrumentations.

2. Time averaging technique

The signals were first directed to six averaging circuits to obtain the mean velocity. This process was required due to the fact that the sensors were stationary while the vortex core was not, therefore creating a fluctuation, especially large in the vicinity of the simulator's centerline where the highly concentrated vortical tube travels in different directions at random. A time constant of 30 seconds was used for this purpose. Such averaging has a tendency to smooth out the fluctuations, however, large scale trends may be observed. A specially designed positioning system was used to enable the anemometer to measure the velocity vector at different points in the flow field and at different orientations. Figure 117 shows the positioning system in the test section.

3. Data acquisition

Velocity data were taken at different significant levels in the flow field. For each level, 31 points were measured on a radius from the centerline of the simulator, proceeding at every 0.5". For each point, six output voltages, flow temperature, atmospheric pressure and temperature, probe angle of attack as measured from the ground plane, probe yaw angle as measured from the reference vertical plane and distance from the simulator's centerline were recorded. These were then fed to an IBM 370 digital computer to be reduced to velocity magnitude. Figure 21 shows the block diagram of the data processing system. The data obtained were reduced to velocity components using the so-called "ϕ-method" described in Thermo Systems, Inc. (1970). A coordinate transformation as described in Appendix (A) was required to transform the velocity components along the sensor directions into radial, axial and tangential components along the XYZ directions of the reference ground plane (local horizon).

One set of "time-averaged" three-dimensional velocity measurements of the entire simulated flow field was obtained. Figure 22 shows the meridional flow pattern as deduced from combining the many measurements of different heights. Also, some tangential velocity profiles are shown at different levels. The peak tangential velocity approximately indicates the location of thepoint through which the high intensity core travelled most during the averaging time period. It should be noted that an application of averaging technique does only result in an approximate measurement from which a general flow pattern in the vicinity of an intense core is obtained. In such measurements extreme velocity magnitudes

are absent. Therefore, depending on the frequency of the vortex fluctuations, the velocity magnitudes in the vicinity of the simulator's centerline are underestimated while far from the centerline where generally the effect of the core fluctuations is small, such errors are reduced. However, despite the appreciable quantitative errors involved, some qualitative information may be derived.

The random, circling motion of the vortical core in a 6 inch diameter circular region is indicated in Fig. 22, where zero tangential velocity components do not occur at the simulator's centerline but at some distance from it. The double peak exhibited in tangential velocity profiles at higher levels is an indication of two different types of flows. The inner peak belongs to the upflowing core while the outer peak represents the rotational rate of the downflow region near the generator's walls. The latter dissipates when the flow is at some distance from the simulator's exit.

When the ground plate was removed, the disappearance of the concentrated vortical core was revealed again. The tangential velocity profiles at higher levels lost their inner peaks while at lower levels much smaller peaks were observed indicating the existence of an extremely weak core in contrast to the highly concentrated vortical core when the ground plane was in position. Figures 23, 24, and 25 show the ground effect on tangential, axial and radial velocity profiles. Positive quantities indicate cyclonic, upward and outward motion. Axial velocity profiles indicate strong upflow in the neighborhood of centerline. Near the exit of the simulator a 3-inch wide downflow region is indicated at 7 inches from

the centerline. This is, of course, due to the return flow along the simulator's walls. An axially stagnant region is also observed just below the air deflector. When the ground plane is removed, axial flow at lower levels decrease noticeably with little or no change at upper levels. This indicates the disappearance of the vortical core along with only small modification of the upper structure.

Radial velocity components in Fig. 22 reveal the inflow toward the time averaged center of rotation in layers near the ground. At midlevels in Fig. 25 very small radial velocities are indicated, while at upper levels generally inflow towards the center is detected, with outflow in the vicinity of the air deflector. Removal of the ground plate results in changes at all layers with more noticeable change at the simulator's centerline. The modification from outflow to inflow at the center of lower levels is due to the existence of an extremely weak vortex which lacks the violent fluctuations of the strong vortex. For this reason the center of rotation almost coincides with that of the simulator's, resulting in a more symmetric flow pattern with respect to the centerline. A more detailed discussion of three-dimensional anemometry is given in Fattahi and Hsu (1976).

The results presented above are only rough estimates of the flow pattern under investigation. Downflow in a narrow region such as funnel flow is not indicated by such approximate measurements. It should be noted that because of an inflow towards the center of rotation continuity demands a net upward flow. Therefore, the averaged results indicate the dominating upflow neglecting the relatively small downflow regions.

However, Fig. 22 shows a general inflow-upflow combination of a vortical flow field. Near the ground a layer of inflow originates far from the vortex core due to the existence of a radially inward pressure gradient in the boundary layer. Arriving at the location of the vortex core it forms an upflow buried within a complicated flow field as discussed in Chapter III. The removal of the ground plate resulted in the disappearance of the highly concentrated vortical core indicating again that such flows may only form when a vortex aloft interacts with a ground plane.

Due to the errors involved in such averaging measurements, no further examination of the results were made. In view of this an alternate and more reliable method of measurement was then employed.

B. High Speed Motion Picture Measurement

As discussed in Chapter I, great amount of information has so far been obtained from the analysis of movies showing natural tornadoes in action. In such cases, the science of photogrammetry has been utilized to extract valuable pieces of data such as velocity magnitudes, the size and structure of the shear flows in tornadic flow fields. However, employment of such methods have been forced upon investigators in view of the fact that these storms are highly localized, unpredictable and extremely violent in nature and may not be penetrated or even approached at least at present time.

Although laboratory simulation eliminates the problem of violence, the inherent instability of such vortical flows remain. Laboratory vortices like their counterparts in nature tend to roam all over making

investigation of their behavior difficult. Therefore, once again a suitable alternative is to observe them through the art of slow motion cinematography.

The objectives for such observations were to determine:

a. Tangential and axial velocity profiles above the boundary layer

b. Tangential and radial velocity profiles near the ground surface

c. Trajectories of particles in the boundary layer

A HyCam movie camera capable of frame speeds of up to 11,000 frames per second was utilized for recording the events on film. Also, a Lafayette stop action projector capable of frame-by-frame projection was used for the measurement of velocity components to be discussed in this chapter. Dry ice cloud was generated at the surface of the water tank which then automatically traced the entire flow field. Rotation of the honeycomb disk and the height from the air deflector to the ground surface were kept at the usual 1,700 rpm and 31 in., correspondingly.

1. Measurement of velocity components

Observation of the tornado vortex in the laboratory indicated that above the inflow layer near the ground surface generally no radial flow existed or it was so small that could not be observed in the motion pictures. The dominant flow in this region was axially and tangentially oriented. Therefore, at least for short time observation of cloud elements a constant radius of rotation was assumed for each element under observation. To measure the velocity components, the time rate of movement of cloud elements or roughness elements on the surface of funnel,

vortical tube, etc. were traced. It was assumed that such elements were moving at the actual speed of the air in which they were imbedded. The radii of the circular paths of these elements were measured at the extreme left or right hand projected distance, that such elements extended from the center of rotation. Figure 26 illustrates the motion of an element around a vortical tube. When r^* is determined, tangential and axial components of the total velocity may be computed from:

$$v^* = \frac{r^* \cdot \theta \cdot F_r}{n_f} \tag{4.1}$$

$$w^* = \frac{\Delta H^* \cdot F_r}{n_f} \tag{4.2}$$

where θ is the total rotation angle in n_f frames and is in radians and F_r is the speed of the photography in frames per second. The vertical displacement of ΔH^* is the change in vertical distance from initial to final positions. The resulting values of v^* and w^* were determined in feet per second. It should be mentioned here that the tangential and axial velocity components obtained by this method represent the mean values of such speeds for the measurement period, however, with short time intervals of typically around 0.05 second such averaging results in relatively accurate measurement of the true speed. The movies of the laboratory vortex were made at different times and the measurements were taken throughout the films. Therefore, it was assumed that as long as the generator was at its constant maximum rotational rate the vortex would exhibit the same dynamic behavior and aside from turbulence fluctuations the mean components of the wind speeds remained constant. From

the observation of the laboratory vortex and Hoecker's (1960) observation of the movies of the Dallas Tornado such an assumption is acceptable. However, in natural tornadoes with no guarantee that the tornado cyclone would retain its strength such assumption may not be valid for long time intervals. Measurements of wind speeds, then, must be taken while the tornado is in the same stage of development.

2. Speed distribution near the ground surface

The distribution of tangential and axial speeds may be determined as described above. However, near the surface where inflow towards the center exists equation (4.1) based on assumption of no radial displacement is not valid. To overcome this problem a Plexiglas ground plane was installed with a movie camera looking upward into the flow field from a point under the ground plane. With smoke cloud generated immediately above the surface and far from the center, the sequence of smoke particles approach to the instantaneous center of rotation was recorded on film. A typical path of such inflow particles is plotted in Fig. 27. Photograph of Fig. 90 also shows the inflow path of a group of flour particles as observed through the Plexiglas plane.

When the movie is viewed at slow speed, the radial displacement $(r_2^* - r_1^*)$ with respect to the instantaneous center and total displacement ΔS^* along the path could be measured for each frame. Far from the center with small inflow angle ΔS^* may not be approximated by $r^*\theta$, while in the vicinity of the center such approximation may involve less error. To eliminate errors, then the technique illustrated in Fig. 28 was employed.

It should be remembered that immediately above the surface the axial component of velocity is negligible outside the central upflow jet region. Therefore, the magnitudes of total velocity V^* and its radial and tangential components u^* and v^* may be determined from the equations below:

$$|V^*| = |\Delta S^* \cdot F_r| \tag{4.3}$$

$$|u^*| = |\Delta r^* \cdot F_r| \tag{4.4}$$

$$|v^*| = |\sqrt{V^{*2} - u^{*2}}| \tag{4.5}$$

The smoke particles were traced inward until they arrived at their surface departure point where inflow speeds became extremely small and negligible. The terminal path just before the surface departure was found to be almost circular and around the central upflow jet region. No smoke particles were observed to penetrate the jet region, however, with sudden upward jet motion introduced in this region any penetrating particle may leave the surface before its penetration is detected on film. Maximum frame speed of the camera was 400 frames per second for the surface wind speed measurement, however, with higher frame speeds the observation of particle penetration into the jet region may be possible. It should be noted that for the upflow jet to be maintained, air must penetrate this region near the surface to satisfy the continuity.

Employing the technique just described, total velocity and its tangential and radial components immediately above the surface were measured and plotted. Figure 29 is a plot of total velocity, V^* vs. radial distance while Figs. 30 and 31 show the distribution of radial

speed u^* and tangential speed v^* in the radial direction. The scatter of 276 data points is due to several factors:

a. Although smoke is generated immediately above the surface, the distance of smoke parcels used in tracing the flow from the surface varies slightly throughout its course of motion towards the instantaneous center of rotation. Due to this variation, although small, a change in velocity component magnitudes occurs with distance from the surface.

b. Small errors may be introduced in finding the exact center of rotation, specially affecting the accuracy of radial velocity determination. The motion of the center, however, was negligible.

c. It should be remembered that the flow under the investigation is a turbulent one and therefore some variation of velocities is expected.

d. Generally the flow of a vortex in interaction with a ground boundary layer is inherently unstable and fluctuating. Instabilities, therefore, introduce errors in measurement of the entire flow field. However, with sufficiently large number of data points such errors may be reduced and a general trend observed. Fluctuations described here appear as gusts in tornadic storms specially at some distance from the rotation center. The source of error just described is thought to be more important than other previous sources in creating scatter in measurements.

3. Radial inflow near the ground

The distribution of radial velocity shown in Fig. 30 is of interest since such measurement is not possible in tornadic storms. At some

distance from the center, particles are attracted towards the instantaneous center of rotation with increasing speed starting from rest. The magnitude of the radial speed in this outer region is comparable to that of the tangential component. Particles then enter a region where radial speed increases to a maximum before their departure from the boundary layer into the upflow jet, however, still remains comparable to tangential speed. Radial speed in this region increases less rapidly with decreasing radius. In some measurements particles exhibited a constant radial speed in this region. The third and final segment of the approach involves a sudden loss of the radial speed of the particles at which time or immediately after attaining a nearly constant radius orbit such particles leave the surface layer surging upward into the upmoving flow. The nearest approach to the center depends very much on the distance of the upmoving particle from the ground level. The sequence just described is shown in the sketch of Fig. 32. The top sketch explains the existence of positive or no radial velocity in the region of $0.5 < r^* < 2.25$ of Fig. 30. A typical radial velocity distribution for a particular smoke parcel is also plotted in Fig. 30. Negative values imply inflow. The path of the same is shown in Fig. 27.

4. Tangential velocity variation near the ground

The distribution of tangential speed near the ground surface shown in Fig. 31 is of importance to a researcher in determining design limits for structures which may be subjected to tornadic wind loading.

The tangential speed variation to the right of the maximum point exhibited a definite break in the slopes between the inner and outer portions. A comparison of this distribution with that of the so-called Rankine combined vortex described by

$$v^* r^{*n} = C_R , \qquad n = \begin{cases} +1 & r^* \geq r_m^* \\ -1 & r^* \leq r_m^* \end{cases}$$

r_m^* = radius of maximum tangential speed, v_m^*

C_R = a constant evaluated at (r_m^*, v_m^*)

reveals deviation, indicating that the observed speed distribution is not irrotational. However, the outer portion which is shallowly sloped and the inner portion with steeper slope were fitted with the curves

$$v^* r^{*0.8} = \text{constant}$$

and

$$v^* r^{*1.6} = \text{constant}$$

Agreements of the outer portion with the curve $v^* r^{*0.8} = \text{constant}$ indicates the effect of the surface friction on the normal rate of increase of tangential speed preventing the conservation of angular momentum. No information inside of the circular region of radius 0.59" could be obtained due to rapid departure of smoke parcels from the surface in this region.

Total velocity shown in Fig. 29 is generally dominated by the tangential speed specially in the vicinity of the center where radial speed becomes negligible compared to tangential component. No attempt was made to fit the total velocity distribution with a mathematical curve.

5. Speed distribution above the ground surface

The tangential components of wind around the simulated laboratory vortex may be determined by the method described earlier in this chapter. It should be remembered that the data points are located where by chance tracer cloud elements were recognizable and could have been followed at least for 1/4 of a full rotation around the vortex. Because of this random variation in position of the tracer elements, then constant tangential velocity contours had to be developed using the data points as a guide. Such data points are shwon in Fig. 33 on a graph of height versus radial distance from the center of rotation where tangential isotachs were smoothed to these points. The points represented by solid triangles are those taken from the ground surface tangential speed distribution previously discussed. The solid squares represent the data points on the downmoving funnel, while circles indicate data points taken at random throughout the flow field. No attempt was made to trace elements above 26 in. level where the flow may be modified to some extent because of contact with solid sections of the vortex generator. The latter region is, of course, far from the surface and may be compared to regions above the cloud base for a natural tornado. The tangential speed at the ground surface and along the centerline is required to be zero. Below the three inch level, the radial velocity becomes large enough to interfere with the assumption of Equation (4.1). Therefore, no data was taken in this region, relying mainly on information obtained from ground layer flow analysis discussed previously. The analysis presented in Fig. 33 shows a band of absolute maximum tangential speed (shaded area) starting at the surface

and extending upward into the upper layers. The mean distance of this band from the centerline varies from 0.6 in. at the surface to 1.6 in. at 4 inches above the surface. It then decreases its distance slightly to about 1.5 in. at 7 in. level and remains constant from then upward. Note that this high speed band is located just outside the lower upmoving jet near the surface and in the vicinity of the upmoving vortical tube at higher levels. The farthest distance of this band from the centerline occurs at a height of about 4 in. which coincides with the area of the "jet breakdown" previously discussed in Chapter III.

A tangential isotach graph enables one to plot the radial distribution of the tangential speed at any height. In the following tangential velocity distributions for a few representative levels are derived from the graph of Fig. 33 and discussed in more detail.

6. Tangential speed distribution at $H^* = 1$ in.

The radial distribution of tangential speed at this level is shown in Fig. 34. The maximum speed appears at a radius of 1 in. and is estimated to be equal to 31.5 fps at this level. Note the sharp drop in the absolute maximum speed compared to that of $H^* = 0.25$ in. which is also in qualitative agreement with analytical solution (Hsu and Tesfamariam, 1975) of the vortex-boundary layer interaction problem.

Interior to the point of maximum speed the curve is deviated to speeds less than that required for solid body rotation, however, this deviation is not great. Exterior to the point of maximum speed, the curve exhibited a break with a steeply sloped inner portion and

shallowly-sloped outer portion, which are approximated by the curves of $v^{*}r^{*1.6}$ = constant and $v^{*}r^{*0.8}$ = constant correspondingly. The region between these portions indicates a drop of the tangential speed at 2 in. radius with a recovery at about 2.8 in. radial distance. The second local maximum indicates the formation of another vortical tube structure outside of the inner vortical tube which was introduced as the "outer vortical tube" in Chapter III. Sketch of Fig. 16 and photograph of Fig. 99 show the tendency of this latter tube to form and increase its diameter immediately above the ground. The curve of Fig. 34 may then be thought of as the superposition of the tangential distribution of the concentric vortical tubes. The dashed line represents the Rankine combined vortex described by $v^{*}r^{*+1} = C_R$ which is also shown in the plots of tangential speed variation to be followed.

7. Tangential speed distribution at H^{*} = 2 in.

The radial distribution of tangential speed at this level is shown in Fig. 35. The location of the absolute and second maximum tangential velocities has now moved to the right indicating the effect of the jet breakdown and the growth of the outer vortical tube. The deviation from solid body rotation in the interior region is now more obvious which is thought to be caused by internal frictions in the core. Exterior to the point of absolute maximum slope of the inner portion is steeper, and is now approximated by $v^{*}r^{*3}$ = constant while the outer portion retains its slope and is approximated by $v^{*}r^{*0.8}$ = constant.

8. Tangential speed distribution at $H^* = 3$ in.

The radial distribution of tangential speed at this level is shown in Fig. 36. The outstanding feature of this curve is the appearance of a new local maximum between the two discussed previously. The significance of this is not well understood, however, it may be due to the jet breakdown phenomena indicating the possible expansion and continuation of the lower jet but with less intensity into the upper levels outside of the inner vortical tube.

The deviation of the inner curve from solid body rotation is appreciable due to increasing frictional effect of the jet breakdown. The maximum tangential velocity has now decreased slightly to 31 fps. and is located farther to the right at r_m^* equal to 1.55 in. The outer maximum has retained its magnitude while its location once again points out the growth of the outer vortical tube. Exterior to the absolute maximum the inner portion of the curve is approximated by the still steeper sloped $v^* r^{*4}$ = constant, while the outer portion closely follows the $v^* r^{*0.8}$ = constant curve.

9. Tangential speed distribution at $H^* = 6$ in.

The radial distribution of tangential speed at this level is shown in Fig. 37. While the absolute maximum has retained its previous magnitude and location, the other two local maximums have moved yet farther to the right while retaining their magnitudes. The growth of the outer vortical tube with translation of its peak to the right has intensified the neighboring region such that the tangential speed curve is located

slightly above the Rankine combined distribution, however, the curve is still approximated by $v^{*}r^{*0.8}$ = constant equation. The steeply-sloped inner portion to the right of the absolute maximum point is again described by $v^{*}r^{*3}$ = constant which is shallower compared to 3 in. level portion.

10. Tangential speed distribution at H^{*} = 9 in.

The radial distribution of tangential speed at this level is shown in Fig. 38. A slight decrease in both magnitude and radial distance of the absolute maximum is observed. The outer vortical tube has now grown to its equilibrium position, with the constant magnitude indicated. The middle local maximum has moved away from the vortical tube and shows sign of dissipation. Exterior to the absolute maximum the steep and shallow curves are again approximated by $v^{*}r^{*3}$ = constant and $v^{*}r^{*0.8}$ = constant. A new feature of this level is the inflection of the curve about the solid body rotation line interior to the maximum point.

11. Tangential speed distribution at H^{*} = 12 in.

The radial distribution of tangential speed at this level, is shown in Fig. 39. Basically, this distribution is very similar to the previous one with the exception of the strong indication of the dissipation of middle maximum. Such behavior supports the argument that the ground surface interaction may be responsible for the creation of this local maximum possibly through the actions of the jet breakdown phenomenon.

12. Tangential speed distribution at $H^* = 15$ in.

The radial distribution of tangential speed at this level is shown in Fig. 40. While the two peak tangential speeds for the two vortical tubes have basically remained the same, the middle one has now completely dissipated. Interior to the absolute maximum point solid body rotation prevails while exterior to this point the two portions of the curve are approximated by $v^* r^{*1.6}$ = constant and $v^* r^{*0.8}$ = constant. Note that these changes are occurring at a distance where the surface friction and jet breakdown effects are not influential.

13. Tangential speed distribution at $H^* = 18$ in.

The radial distribution of tangential speed at this level is shown in Fig. 41. Basically, the entire distribution may be approximated by a Rankine combined vortex equation in the form of $v^* r^{*+1} = C_R$, although far from the core $v^* r^{*0.8}$ = constant may still give a slightly better fit. Lack of the effect of surface friction at this height has permitted conservation of angular momentum.

No attempt was made to plot any tangential speed distribution above this height since no data points were available specially away from the vortex core. However, the flow is expected to remain similar to that of a Rankine combined vortex.

14. Tangential wind speed measurement in tornado, waterspout and dust devil

As has been mentioned, the measurements of air speed of atmospheric vortices have been very rare and those measurements available have not

been complete and reliable.

Dallas Tornado has remained the most documented tornado in the history even after 19 years of its occurrence and despite the increased accuracy in pinpointing the possible sites of tornado formation.

Hoecker (1960) determined a distribution of tangential speeds in the Dallas Tornado by tracing particles of debris and cloud tag movements in scaled movies of the tornado. The technique in reducing the data to tangential velocity distribution is exactly the same as that followed in the present investigation. Distribution of the derived tangential speed from the center of the tornado to a radius of 2,000 ft. and from near the ground to about 1800 ft. in elevation was plotted by Hoecker and is partially shown in Fig. 42. Like the tangential speed contours obtained in the present investigation, there are data points that do not fit the isotachs drawn, however, such tangential isotachs were drawn to fit most of the data points obtained in the movie analyses. Hoecker then plotted the variation of tangential speed with radius for elevations of 150, 300 and 1,000 ft. as deduced from the analysis of Fig. 42. These are shown in Fig. 43. For the 150 and 300 ft. level the break from a steeply-sloped variation to a shallowly sloped variation is apparent, however, it is even more interesting to note that these portions of the curves are nicely approximated by $v^{*}r^{*1.6}$ = constant and $v^{*}r^{*0.8}$ = constant relationships. A Rankine combined distribution is also plotted for comparison. Excellent agreement between these curves and those obtained for the present simulation immediately above the ground surface (H^{*} = 0.25 in.) and at

$H^* = 1.0$ in. is readily apparent. It should be noted that all of the four mentioned curves describe the radial distribution of tangential speed in the boundary layer of their respective flow fields. The distribution of tangential velocity at 1,000 ft. level for the Dallas Tornado is also shown in Fig. 43. For comparison $v^* r^{*+1} = \text{constant}$ is also plotted where its qualitative agreement with Hoecker's measurement is obvious. Since this measurement describes the trend of tangential speed variation far from the boundary layer then it may be compared to the laboratory measurement of $H^* = 18"$. Generally good agreement results, however, the laboratory results at this height, indicates an almost solid body rotation interior to the maximum point while Hoecker's results is slightly deviated from it. It should be mentioned that during Hoecker's measurement the funnel changed from wide to a tall and narrow one. Such changes, although may not have affected the entire flow field but definitely affects the core region to the left of the maximum tangential speed point. In fact, the core flow characteristics must have been changed to permit the downmoving funnel to extend to near the ground to form a tall and narrow structure. Therefore, Hoecker's results in this region may not be very accurate.

Although close agreements are observed at the mentioned levels, the Dallas Tornado measurements do not indicate the existence of the local maximum that appeared in the laboratory results between the height of $H^* = 3$ in. and $H^* = 15$ in. While the phenomenon just described may not exist in all tornadoes it must be kept in mind that portions of

Hoecker's measurements are based on the motion of solid debris such as 4' x 8' rectangular plywood sections which may not reveal the true air speed due to their drag and centrifugal forces and at the same time their poor response to sudden changes in the flow air speed. For the sake of comparison the tangential speed distribution for dust devils (Sinclair, 1973) and waterspouts (Golden, 1969) are plotted in Figs. 44 and 45 and are fitted with $v^* r^{*+1} = C_R$ curve. Golden's measurement were taken from the Lower Matecumbe Key film and is the vertically averaged tangential speed distribution across the uppermost layers of the spray vortex. Such a measurement is taken in a region which is away from the surface frictional effects, therefore nicely approximates the Rankine combined vortex profile. Sinclair's measurement of Arizona dust devil, approximated by $v^* r^{*+1} = C_R$ relationship, is also taken away from the ground surface. As mentioned in previous chapters, Hsu and Tesfamariam (1975) numerically predicted the flow pattern in the boundary layer of a tornado-like vortex. Tangential speed distribution for different levels in this layer are plotted in Fig. 46. The tangential velocity and the radial distance are normalized with respect to v_m^* and r_m^* which are the maximum tangential speed and its radial distance of the main vortex. At h = 1.0 which is the upper edge of the boundary layer region a tangential velocity distribution given by

$$v_\infty = a[1 - \exp(-br^2)]/r, \qquad a,b = \text{constant}$$

is imposed (Kuo, 1971). Also a Rankine combined vortex distribution is plotted for comparison. It should be noted that because of imposing such

a boundary condition which is somewhat different than the distribution obtained in the present simulation, then the radial variation of tangential speed in the boundary layer are also different, however, characteristically comparable. Note specially the second local maximum at h = 0.1, gradual outward motion of the absolute maximum with increasing height and the fact that v_m is larger at h = 0.1 compared to v_m at h = 1.0.

15. Axial speed distribution

While the tangential wind speeds were being obtained from the movie analysis, vertical components of motion were also observed. These data points are plotted in Fig. 47. An attempt to construct a meaningful graph of constant axial speed contours was not successful, possibly due to the complicated vertical flow structure. However, it may be possible to construct such a contour graph if relatively large number of data points are available. This, of course, was not possible in this preliminary investigation of the tornadoes due to limited footage of the movies of laboratory vortex available in addition to problems in visualizing the entire flow field. However, information obtained is still significant. It is obvious from the plotted data points that the center jet is definitely the axially dominant portion of the flow specially at higher levels where the magnitude of the axial wind speed is more than four times larger than that of the neighboring funnel. Of interest is the distribution of the axial velocity across the funnel wall thickness. It should be noted that the funnel is a down-moving flow which is surrounded

by two upmoving flows of the center jet and the inner vortical tube. Therefore, the funnel flow immediately next to these vertical layers exhibited a drop in the magnitude of the downflow and in some instances the downflow speed became zero while the flow in the middle was unaffected. As mentioned in Chapter III, then the outer layer of the tornado funnel structure which is the visible portion of it may be axially stagnant, as may have been observed by Hoecker (1960) in his investigation of the Dallas Tornado.

The inner vortical tube is shown to have an upflow speed of approximately equal to that of the downmoving funnel. Outside of this vertical layer between radii of 5" to 6" where the second upmoving vortical tube is located the upflow speeds are drastically smaller than those of the inner portions of the vortex core. Between the inner and outer vortical tubes no downflow is observed but some of the upflow speeds measured in the vicinity of this layer were even smaller than those of the either vortical tubes. As mentioned in Chapter III the lack of information about this region of the flow might be due to its weak flow and its consequent inability to make use of the smoke as a flow visualizing medium. Therefore, no conclusive explanation may be given at this time as to the nature of the flow in this region. It should be re-emphasized that the above portion of the flow appears as a dark region surrounded by two distinctly upmoving vortical tube layers when observed in the photographs or movies.

Hoecker (1960) constructed a contour plot of axial isotachs for the Dallas Tornado shown in Fig. 48, however, the contour plot does not

include the center jet and the funnel regions.

C. Other Observations

While the radial and tangential speeds near the surface were being measured the smoke parcel motions were also traced to construct the path taken by each parcel. A typical path is shown in Fig. 27C for which the radial velocity was shown in Fig. 30. In the particular path shown the inflow angle, with respect to the radial was measured to be around 55° at a radius of 4.5 in. while it increased to about 90 degrees at the radius of 1 inch when the smoke parcel went into the orbit around the center. Far from the center, however, the inflow angle is very small where the radial displacement is larger than the tangential motion. The numbers given above are typical, however, some variations were observed for different paths.

Also shown in Fig. 27 is a typical trajectory of a spherical glass particle (average diameter = 530×10^{-6} meters). Two movie cameras were positioned as shown in Fig. 49 to record the motion of such particles. The projection of the path of the above glass particle on the XY and YZ planes are plotted as they were traced on the film. Then for any particular height the X and Z coordinates of the points on the path were determined and plotted in the XZ plane. The result shown in Fig. 27A is the projection of the path of a particle on the horizontal XZ plane. Of interest is the inward motion of the particle in the terminal portion of the path when it entered the surface inflow layer. However, this was not a common occurrence. The low flying particles exhibited a more straight

outward motion of the XZ plane while the paths of the higher flying debris were of more curvature. The low flying objects flying at heights where tangential speeds are greater than higher altitudes attain a larger centrifugal momentum which carries them outward with such tremendous speeds that they become probably the most dangerous effect of a tornadic storm on the environment. The photograph of Fig. 118 shows the penetration of a piece of wood into a 1.5 in. steel fence pipe resulted from the "missile effect" of a tornado.

The results presented in this chapter once again point out the superiority of the present simulation. Although not enough information about natural tornadic storms exists, the characteristic similarities between the present laboratory vortex and that of the Dallas Tornado demonstrate the correctness of the simulation.

No attempt was made to non-dimensionalize the results in view of the fact that not enough information is yet available about the speed distribution and air flow pattern in different tornadoes. More analyses such as that of Dallas Tornado by Hoecker and more laboratory investigation with different size vortex generators are needed before a set of similarity parameters are derived based on which the results may be non-dimensionalized and generalized to all tornadic flow fields.

V. WIND LOADING ON STRUCTURES

An understanding of tornadic wind loading on structures is essential. Absolute fail-safe construction, such as is needed for nuclear reactor housing requires knowledge of extreme wind speeds and maximum pressure deficits, in a tornado. Severe shearing stresses due to large wind speed gradients and sudden atmospheric pressure drops in a tornado are responsible for structural damages, some of which are incredibly complete.

The forces of a tornado on a structure may be classified into four broad categories:

A. Mode (A). The Direct Pushing Force of the Wind

The pushing force of the wind or dynamic pressure on the surface of a structure is directly proportional to the square of the wind speed and is given by $q^*=\rho^* V^{*2}/2$ where V^* is the total wind speed and ρ^* is the air density. Rigid body motion in an overturning mode or a sliding mode may be induced by such wind pressures if the structure can withstand the initial impact of the sudden increase of the dynamic loading. Figure 119 shows the twisting motion of a house structure off of its concrete foundation. No other damage to the house is apparent. Similar motions were observed in the laboratory when a house model was set on the ground plane under the vortex simulator. From the measurements discussed in Chapter IV and observations of natural tornadoes by Hoecker and others the maximum dynamic pressure occurs near the ground and at a radial distance of r_m^* from the center of the vortex where the ring of maximum tangential speed is located. Studies of tornado damage by experts and observations of

tornado movies, indicates that the maximum wind speeds in such storms may not exceed 300 mph. (Defense Civil Preparedness Agency, 1974). Therefore, an estimate of the dynamic pressure becomes, $q^* = 1.51$ psi, where density is computed at T = 70F and $P_{atm} = 14.2$ psi. In the laboratory, the maximum wind speed near the ground surface was found to be about 43 fps at a height of 0.25 inches, which yields a dynamic pressure of $q^* = 0.014$ psi.

B. Mode (B). The Outward Forces due to Pressure Differentials Resulting from the Atmospheric Pressure Drop

It is generally agreed that the pressure differential produced by the mechanics of tornadoes is the major cause of damage when tornadic storms strike. A building enveloped by the core of the vortical flow experiences a drop in pressure whose magnitude depends on the prevailing wind speeds of the flow.

Equations of motion for a three-dimensional, incompressible flow in cylindrical coordinate may be written as follows:

Continuity

$$\frac{1}{r^*}\frac{\partial(r^* u^*)}{\partial r^*} + \frac{1}{r^*}\frac{\partial v^*}{\partial \theta^*} + \frac{\partial w^*}{\partial z^*} = 0 \qquad (5.1)$$

Radial Momentum

$$\rho^*\left[\frac{\partial u^*}{\partial t^*} + u^*\frac{\partial u^*}{\partial r^*} + \frac{v^*}{r^*}\frac{\partial u^*}{\partial \theta^*} + w^*\frac{\partial u^*}{\partial z^*} - \frac{v^{*2}}{r^*}\right] \qquad (5.2)$$

$$= F_R^* - \frac{\partial P^*}{\partial r^*} + \mu^*\left[\frac{\partial^2 u^*}{\partial r^{*2}} + \frac{1}{r^*}\frac{\partial u^*}{\partial r^*} + \frac{1}{r^{*2}}\frac{\partial^2 u^*}{\partial \theta^{*2}} + \frac{\partial^2 u^*}{\partial z^{*2}} - \frac{u^*}{r^{*2}} - \frac{2}{r^{*2}}\frac{\partial v^*}{\partial \theta^*}\right]$$

Tangential Momentum

$$\rho^*\left[\frac{\partial v^*}{\partial t^*} + u^*\frac{\partial v^*}{\partial r^*} + \frac{v^*}{r^*}\frac{\partial v^*}{\partial \theta^*} + w^*\frac{\partial v^*}{\partial z^*} + \frac{u^*v^*}{r^*}\right] \tag{5.3}$$

$$= F_\theta^* - \frac{1}{r^*}\frac{\partial P^*}{\partial \theta^*} + \mu^*\left[\frac{\partial^2 v^*}{\partial r^{*2}} + \frac{1}{r^*}\frac{\partial v^*}{\partial r^*} + \frac{1}{r^{*2}}\frac{\partial^2 v^*}{\partial \theta^{*2}} + \frac{\partial^2 v^*}{\partial z^{*2}} - \frac{v^*}{r^{*2}} + \frac{2}{r^{*2}}\frac{\partial u^*}{\partial \theta^*}\right]$$

Axial Momentum

$$\rho^*\left[\frac{\partial w^*}{\partial t^*} + u^*\frac{\partial w^*}{\partial r^*} + \frac{v^*}{r^*}\frac{\partial w^*}{\partial \theta^*} + w^*\frac{\partial w^*}{\partial z^*}\right] = F_Z^* - \frac{\partial P^*}{\partial z^*} + \tag{5.4}$$

$$\mu^*\left[\frac{\partial^2 w^*}{\partial r^{*2}} + \frac{1}{r^*}\frac{\partial w^*}{\partial r^*} + \frac{1}{r^{*2}}\frac{\partial^2 w^*}{\partial \theta^{*2}} + \frac{\partial^2 w^*}{\partial z^{*2}}\right]$$

Some simplifying assumptions have to be made at this time, otherwise the complicated equations may not be specialized to the flow of the simulated tornado vortex mainly because of lack of enough understanding of the flow field under study.

It is assumed that the vortical flow is steady, axisymmetric and of constant viscosity and density. Body forces are neglected except in the axial direction where hydrostatic variation is assumed. Then equations (5.1) through (5.4) may be written as:

$$\frac{u^*}{r^*} + \frac{\partial u^*}{\partial r^*} + \frac{\partial w^*}{\partial z^*} = 0 \tag{5.5}$$

$$\rho^*\left[u^*\frac{\partial u^*}{\partial r^*} + w^*\frac{\partial u^*}{\partial z^*} - \frac{v^{*2}}{r^*}\right] = -\frac{\partial P^*}{\partial r^*} + \mu^*\left[\frac{\partial^2 u^*}{\partial r^{*2}} + \frac{1}{r^*}\frac{\partial u^*}{\partial r^*} + \frac{\partial^2 u^*}{\partial z^{*2}} - \frac{u^*}{r^{*2}}\right] \tag{5.6}$$

$$\rho^* \left[u^* \frac{\partial v^*}{\partial r^*} + w^* \frac{\partial v^*}{\partial z^*} + \frac{u^* v^*}{r^*} \right] = \mu^* \left[\frac{\partial^2 v^*}{\partial r^{*2}} + \frac{1}{r^*} \frac{\partial v^*}{\partial r^*} + \frac{\partial^2 v^*}{\partial z^{*2}} - \frac{v^*}{r^{*2}} \right] \quad (5.7)$$

$$\rho^* \left[u^* \frac{\partial w^*}{\partial r^*} + w^* \frac{\partial w^*}{\partial z^*} \right] = - \rho^* g^* - \frac{\partial P^*}{\partial z^*} + \mu^* \left[\frac{\partial^2 w^*}{\partial r^{*2}} + \frac{1}{r^*} \frac{\partial w^*}{\partial r^*} + \frac{\partial^2 w^*}{\partial z^{*2}} \right] \quad (5.8)$$

Of initial interest is the radial momentum equation which under cyclostrophic assumption of no radial flow reduces to

$$\frac{\partial P^*}{\partial r^*} = \rho^* \frac{v^{*2}}{r^*} \quad (5.9)$$

Equation (5.9) is based on the balance of radial pressure gradient and the centrifugal force of the rotating air which is not true in the boundary layer where the above equilibrium is distorted due to frictional effects of the surface boundary on the centrifugal tendencies of the rotating air. However, above the boundary layer region where the flow is free of surface friction effect equation (5.9) may be integrated radially to provide a profile of pressure distribution at any height where the tangential speed variation with radius is given. It should be noted that above the inflow layer near the surface the radial velocity is generally small and negligible, therefore, the cyclostrophic assumption is expected to yield somewhat reasonable results. In the boundary layer, however, radial inflow may not be neglected where such inflow is produced due to the upset of balance between the inward pressure gradient and the centrifugal force. In such a layer, therefore, cyclostrophic assumption is not valid and the contribution of radial velocity terms must be included.

1. The derived pressure distribution

To determine the radial distribution of the pressure, equation (5.9) was applied to the tangential speed distributions obtained in Chapter IV. The tangential speed distributions were approximated by several functions relating v^* to radius, r^*. These functions and the process of integration of equation (5.9) are described in Appendix B.

At any height equation (5.9) becomes:

$$\frac{dP^*}{dr^*} = \rho^* \frac{v^{*2}}{r^*} \tag{5.10}$$

which then may be integrated radially from the core center to infinity where the local pressure becomes that of the atmospheric

$$P_\infty^* - P_C^* = \rho^* \int_o^\infty \frac{v^{*2}}{r^*} \, dr^* \tag{5.11}$$

The quantity $(P_\infty^* - P_C^*)$ is replaced by ΔP^* which is the core pressure deficit. The pressure distributions obtained from equation (5.11) are plotted for selected heights in Figs. 50 through 57. The pressure distribution at the surface was obtained experimentally using a Statham Differential Pressure Transducer, which measured the pressure at the ground surface as compared to that of the atmospheric. The signal was recorded on the scope of a Tektronix 5103N Oscilloscope capable of holding the signal until an erase command was given. The pressure port was located at 1.5 in. from the generator's center line where the vortex traffic was the highest. The registered signal was, of course, a plot of pressure deficit in the vortex versus time, t^*, which is a function

of both the translational speed of the vortex and time base of the scope. Figure 58 shows a block diagram of the experimental set-up. To plot the pressure deficit as a function of radial distance from the vortex center a separate experiment was performed. Smoke was fed into the flow to visualize the vortical tube. Then the vortex was followed through closed circuit television with calibrated screen to indicate the distance between the pressure port and the vortex center. Then pressure deficits at a few different radial distances were measured and recorded using a chart recorder. Finally, these points with known radial locations were plotted upon which the pressure distribution obtained from the oscilloscope measurement was smoothed. The resulting curve was then a distribution of pressure deficit as a function of radial distance from the vortex center, which is shown in Fig. 59. The pressure distributions presented in the present chapter all indicate that there exists a low pressure region at the center of rotation which is responsible for the explosive force of a tornado on structures.

It should be noted that the pressure distributions derived for levels above the ground surface are all based on the cyclostrophic assumption which its accuracy depends on the magnitude of the radial velocity and other terms that were neglected in equation (5.6). Sinclair (1973) showed by actual measurement of velocity and pressure distribution in dust devils, that the calculated values of pressure drop, utilizing cyclostrophic assumption, may generally be within 75% of the data obtained by actual measurements, however, near the ground the difference in the calculated and measured pressure deficits grew where at least in one

case the derived pressure deficit was only 47% of that of the measured value. Leverson et al. (1975) after penetration case studies of 16 waterspouts concluded that the simple cyclostrophic Rankine combined vortex model is capable of explaining approximately 74% of the total measured pressure deficit. Although this compares favorably with Sinclair's (1973) dust devil measurements, it should be kept in mind that such measurements were made relatively far from the surface layer and its effect on the immediate flow field, and where a Rankine combined tangential speed distribution prevails. However, in a tornado flow field, violent interaction near and with the ground surface such as the jet breakdown, with increased flow shear and turbulence levels disrupt the vortex structure in such a way that not only the tangential speed distribution is not that of a Rankine combined vortex but with large gradients of radial velocity and axial velocity immediately above the surface and in the area of the jet breakdown the cyclostrophic assumption is not valid and its agreement with the measured value should not be expected. In the above mentioned region of the flow then the remaining terms in equation (5.6) should be included in any theoretical computations of pressure distribution. To support the argument, measurement of pressure deficit at the vortex center was carried out from the surface to a height of 6.75 inches above the ground utilizing a differential pressure transducer and an oscilloscope to record the data. At each selected height a 30 minutes time period was allowed during which the vortex was expected to travel over the pressure port approximately 300 times. A constant pressure tube length of 7 in. was used for all heights to hold

any tube frictional or response effect the same throughout the experiment. No measurement above the 6.75 in. level was performed as it required a longer pressure tube length which in turn could introduce some errors in measurement. The results of this experiment are plotted in Fig. 60. Also plotted are the computed pressure deficits along the vortex centerline for different heights. While the solid line represent a simplotter smoothed curve fitted to experimental data the dashed line is the possible continuation of the same line at higher levels, however, based on the assumption that at the height of 18 in. where Rankine combined vortex exists the computed pressure drop may be 75% of the actual deficit. A comparison of the data plotted in Fig. 60 reveals that the cyclostrophic assumption fails to provide an accurate estimate of the pressure deficit specially in the region of the jet breakdown where the vortex becomes distorted and gradient of radial speeds becomes large in magnitude. The computed data immediately above the surface ($H^* = 0.25$ in.) is approximately 67% of the measured value. At this height, of course, axial speed is small or non-existent depending on the flow region and radial speed is to some extent retarded due to frictional effect of the surface. However, with increasing height, radial inflow attains a maximum value and then changes to outflow. Such sudden changes within a short distance above the ground and specially large near the center along with increase and decrease of upward axial velocity in the jet breakdown region all help to make the cyclostrophic assumption invalid in this region. At the height of $H^* = 3.0$ in. which is probably the most turbulent part of the flow

field the computed pressure deficit is only 26% of the measured drop. With more increase in height and away from the jet breakdown region the computed deficit and the measured pressure drop approach each other. At the height of 18 in. where Rankine combined vortex prevails the projected curve is drawn through a point such that the computed value is about 75% of the projected actual value. This, of course, is based on the findings of Leverson et al. (1975) and Sinclair (1973) for waterspouts and dust devils. The pressure drop is expected to remain constant above this height where the changes are small and a Rankine combined distribution of tangential speed exists. However, near the exit of the vortex generator possible changes in the flow characteristics may affect the amount of pressure deficit in this region. In natural tornadoes the flow is also affected by the flow of the tornado cyclone at higher levels, however, the exact nature of changes and distribution of wind speeds and pressure deficits in such cyclonic systems is not known up to date.

The foregoing discussion points out that a simple model such as cyclostrophic assumption should not be generalized to describe the pressure deficit distribution for the entire flow field. Near the ground where pressure deficits are of particular interest, the actual pressure drops may be as much as four times larger than the pressure deficits predicted by such simple models. The static pressure drops at all levels were greater than the maximum (tangential) dynamic pressure at the same levels, pointing out that the static pressure loading is quite significant in damaging structures especially near the ground level where it can be four to five times larger than the maximum dynamic pressure loading.

The results discussed in this section are tabulated in Table (5.1). The measured pressure distribution shown in column 3 is tabulated up to the height of 6.0 inches above the surface. Column seven shows the ratio of the measured static pressure drop to the maximum (tangential) dynamic pressure at each level.

The results presented here, therefore, confirm the common assumption that the pressure differential produced by the mechanics of tornadoes is an extremely important factor in damaging the building structures.

In a separate experiment the core pressure deficit at the surface, ΔP_m^*, was measured for various rotational speeds of the honeycomb disk ω_h^* inside the vortex generator. The results are shown in Figs. 61 and 62. Figure 62 indicates that the static pressure drop at the surface is approximately proportional to the square of the characteristic rotational speed of the flow field, which in the laboratory, is that of the honeycomb disk. In natural tornadoes the characteristic rotation maybe defined to be that of the tornado cyclone which can be estimated from radar observations. However, whether a universal proportionality constant exists is to be answered with numerous actual measurements of the core pressure deficits of the tornado vortices and radar observation of the rotational rate of the associated tornado cyclones.

2. Pressure measurements in natural tornadoes

The pressure data of real tornadoes available up to the present time are few and the degree of their dependability varies according to the instrument used in actual measurement and accuracy of the determination

Table 5.1. Summary of computed and measured pressure distribution at the center of the simulated tornado.

Height H^*(in.)	Pressure deficit (computed) ΔP_c^*, psi	Pressure deficit (measured) ΔP_m^*, psi	Maximum (tangential) dynamic pressure q^{*a}, psi	$\Delta P_c^*/\Delta P_m^*$	$\Delta P_c^*/q^*$	$\Delta P_m^*/q^*$
0.25	0.02345	0.0349	0.01409	0.672	1.664	2.477
1.0	0.01354	0.0344	0.00775	0.394	1.747	4.439
2.0	0.00885	0.0335	0.00751	0.264	1.178	4.461
3.0	0.00860	0.0325	0.00751	0.265	1.145	4.328
6.0	0.01034	0.0280	0.00751	0.369	1.377	3.728
9.0	0.01178		0.00703		1.675	
15.0	0.01260		0.00703		1.792	
18.0	0.01406		0.00703		2.000	

[a] q^* = (dynamic pressure based on maximum tangential velocity, v_m^*) = $\frac{1}{2}\rho^* v^{*2}$

of the radial distance from the point of measurement to the center of the tornado vortex.

Flora (1953) reports the maximum pressure deficit in the 1896 tornado of St. Louis to have been approximately 1.46 psi taken unofficially. In the Minneapolis Tornado of 1904 also an unofficial pressure drop measurement was taken to be approximately 2.8 psi. Both of these measurements were reported to have been taken exactly in the center of the path of the tornadoes. Morton (1966) estimated that pressures in the cores of violent tornadoes may fall by about 3 psi. Today for design purposes the generally accepted value for maximum pressure deficit for a tornado is also estimated to be about 3 psi (Defense Civil Preparedness Agency, 1974).

The only pressure distribution available obtained by direct measurement for a real tornado is that of Cleveland Tornado (Lewis and Perkins, 1953). The pressure deficits were measured by nine barographs located in a relatively small area close to the path of the tornado. However, all nine barographs were located in a range from 715 ft. to 2300 ft. from the path of the tornado center. The maximum deficit recorded by any of the barographs was approximately 0.096 psi at a distance of 715 ft. from the probable center. No information within the radius of 715 ft. is available. From the pattern of damage, Lewis and Perkins (1953) determined that the radius of the circle of maximum wind speed was much less than 715 feet, probably being of the order to 100 to 200 feet. Therefore, the pressure measurements obtained in Cleveland Tornado were taken far from the center and from the vortical core where the extreme pressure deficits exist.

Also shown by the same researchers was the agreement of the pressure variation with the simplified irrotational model of

$$V^* = \frac{C_R}{r^*} = \sqrt{v^{*2} + u^{*2}} \tag{5.12}$$

$$v^* = \frac{\Gamma^*}{2\pi r^*} \tag{5.13}$$

$$u^* = -\frac{Q^*}{2\pi r^*} \tag{5.14}$$

where Γ^* and Q^* represent the circulation and sink strength and v^* and u^* are tangential and radial velocities respectively. It should be noted that according to the findings of the present research and that of Dallas Tornado, etc., the flow far from the rotational core is irrotational or near irrotational. Therefore, the pressure distribution of Cleveland Tornado although realistic but is of little significance in estimating the maximum destructive power of tornadoes.

Hoecker (1961) obtained three dimensional pressure field of the Dallas Tornado of 1957, as integrated from a distribution of observed tangential wind speeds. Cyclostrophic wind equation was assumed for the entire flow field. According to the results and arguments presented in this chapter, therefore, Hoecker's pressure distribution of Dallas Tornado is questionable specially at low levels. The derived central pressure deficit at the ground was approximately 0.863 psi. This compares with a value of about 0.5 psi for the absolute maximum derived (tangential) dynamic pressure in the same tornado. The ratio of $\Delta P_C^*/q^*$ is then 1.73, a value comparable to those obtained in the present research and tabulated in column 6 of Table 5.1. Another reference to the pressure deficit of

Dallas Tornado is made, in an interview article with J. A. Hudson (1958), a pilot who flew his small aircraft within 800 ft. of the vortex center and 200 above the ground. In addition to his excellent observation of the jet flow into the mouth of the funnel from his vantage point, he also mentioned:

". . . It passed over two small ponds while we were following it. One of them was about 150' - 175' in diameter, almost round. The tornado covered the entire pond: suddenly the pond disappeared into the mouth of the funnel, which sucked it completely dry. . . It definitely went into the funnel. . . ."

He also mentioned that the pond could have been two to fifteen feet deep, but from the 800 ft. altitude that he was flying at the time he could not be exact. If one takes an average diameter of 162.5 ft. and average depth of 8.5 ft., a simple calculation results in the weight of the water to be approximately 11,000,000 lbs. A pressure deficit in excess of 3.7 psi is required to pick up the entire body of water at once. However, it should be remembered that the dimension estimates used above are not accurate and the weight of the water may have been more or less than the average value obtained. In any case the pressure deficit must have been appreciable and possibly a few times larger than Hoecker's computed pressure deficit, barring possible changes in flow characteristics from the time of Hoecker's measurement to the time of above observation.

The arguments and evidence presented above all indicate that the pressure deficits experienced in atmospheric vortices are larger than

those predicted by simple models. Simplified assumption of cyclostrophic flow fails to result in correct estimate of the pressure field, specially near the ground where pressure drop is of particular interest to designers. Finally, it was shown that at any level the actual pressure deficit can be two to five times larger than the maximum (tangential) dynamic pressure. If this is confirmed in future investigations, then with a commonly accepted maximum tangential wind speed of 300 mph, the static pressure drop associated with such a wind speed may be as large as half of an atmosphere. The explosive power associated with such large pressure deficits is responsible for the complete destruction of structures in the path of giant tornadoes.

3. Pressure deficit effect on buildings

One of the tornado safety instructions issued by Weather Service to the public is to leave the windows and doors on the north and east side open for a tornado approaching from the south-westerly direction. It is well-known that proper venting is required to prevent the structural explosion. However, designing adequate venting for balancing the pressure differential requires the knowledge of the following factors:

a. Maximum value of the pressure deficits
b. Time rate of change of pressure
c. Volume of the building under design consideration
d. Desired velocity of escaping air
e. Desired velocity of incoming air after pressure recovery

It was argued that the pressure drops in the core of tornadoes can be appreciable with a possible maximum of half of an atmosphere. Therefore,

there is no doubt that such outward loadings on the walls of the buildings is an important design consideration. The damaged garage of Fig. 119 is an excellent example showing the explosive effect of the low pressure core of tornadic flows.

To investigate the pressure drop effect on structures a series of experiments were conducted in the laboratory. A hard plastic hollow cube with base dimensions of 5/8" x 5/8" and height of 3/8 in. was used as the model of a house. The thickness of the walls and roof was 1/16 in. The model was glued to the ground surface and was air tight. Then a 1/8 in. hole was made on each side wall plus the roof, to simulate windows and a roof vent. The house was so located that the vortex always approached it from a south-westerly direction as shown in Fig. 63.

In part one of the experiment the maximum pressure deficit was measured at the floor surface of the house model when one or more windows were open with the remaining windows sealed so no air flow was permitted. In part two of the experiment the maximum pressure deficits were measured at the surface of each wall. The same series of experimentation was performed again with larger window size of 11/64 in. in diameter. The results are tabulated in Tables 5.2 and 5.3.

In Table 5.2 the columns 3 and 5 show the ratio of the pressure deficits of the inside to that of the vortex core outside of the house for different open window combinations. The higher percentage indicates a better depressurization of the house. It is seen from Table 5.2 that generally windows on the north and east side provided better ventilation,

Table 5.2. Maximum pressure deficit inside the house model (measured).

Open Window	(window size = 1/8 in. diam.) Pressure deficit inside the house, ΔP_i^* (psi)	Ratio of inside to outside pressure deficit $\Delta P_i^* / \Delta P_o^*$ (percent)
N	0.0273	80
N, E	0.0232	68
N, E, S	0.0219	64
N, E, S, W	0.0198	58
E	0.0280	82
E, S	0.0246	72
E, S, W	0.0239	70
S	0.0287	84
S, W	0.0253	74
S, W, N	0.0225	66
W	0.0273	80
W, N	0.0253	74
W, N, E	0.0219	64
N, S	0.0191	56
E, W	0.0205	60
T	0.0341	100

Table 5.2. (Continued)

Open Window	(window size = 11/64 in. diam.) Pressure deficit inside the house, ΔP_i^* (psi)	Ratio of inside to outside pressure deficit $\Delta P_i^*/\Delta P_o^*$ (percent)
N	0.0287	84
N, E	0.0233	68
N, E, S	0.0212	62
N, E, S, W	0.0192	56
E	0.0301	88
E, S	0.0246	72
E, S, W	0.0211	62
S	0.0281	82
S, W	0.0232	68
S, W, N	0.0212	62
W	0.0259	76
W, N	0.0232	68
W, N, E	0.0205	60
N, S	0.0184	54
E, W	0.0191	56
T	0.0340	99

Table 5.3. Maximum pressure deficit on the surface of the sidewalls and roof of the house model.

Surface	Pressure deficit, ΔP_m^* (psi)
Wall N	0.0300
Wall E	0.0300
Wall S	0.0273
Wall W	0.0273
Roof T	0.0342

however, the best ventilation was provided by an opening at the roof. Such a difference is due to the fact that side wall windows are under the influence of incoming air towards the house upon which the vortex is located. Such an inflow, therefore, prevents proper ventilation through the side openings. However, the top vent is free of the influence of any inflow, therefore perfect ventilation occurs. When more than one windows were opened the influence of the inflow became greater and less ventilation occurred.

Based on the results of this experiment, it is therefore suggested that a top vent to be considered in design of buildings where possible. In case of a tornado approach some but not all of the windows should be opened preferably on the opposite side of the approach direction. For each house the amount of the needed opening should be determined for optimum ventilation. Proper speed for escaping air should also be considered in vent design in order to limit the damage to household objects. The tornado resistant wood frame houses built along Harrison Street in

Kansas City fifty-five years ago, not only had reinforced frames but had two large chimneys that could equilibrate the pressure differential and at the same time act as an additional anchorage of the structure to the foundation (Flora, 1953).

Finally the results presented in Table 5.3 shows that the roof experiences a higher pressure deficit than the side walls do. This then explains the common occurrence of the roof lifting while side walls remain undamaged.

C. Mode (c). The Inward Forces due to Pressure Differentials Resulting from the Atmospheric Pressure Recovery

It was indicated in the previous discussion that when a building structure is enveloped in the tornado funnel it is surrounded by a pressure, lower than the atmospheric pressure which exists in the building. Due to such a pressure differential an outward loading results until proper ventilation through broken windows and other openings occurs. In case the structure is strong enough to survive the loading modes of (A) and (B), it is then subjected to another type of loading.

After ventilation, the inside pressure equalizes that of the low pressure core outside. However, when the funnel moves away, the outside pressure rises to its original point while inside the building structure the pressure is equal to the low vortex core pressure. At such an instance the walls experience a pressure loading directed inward. This reversed loading on the walls, seconds after they have experienced outward loading is more critical considering the fact that the structure has experienced mode (A) and (B) loadings and has weakened. The time rate of

pressure loss and recovery, of course is related to the translational speed of the vortex which varies considerably among tornadoes and even for the same tornado at different instants. Photograph of Fig. 120 shows the end result of the implosive force of the tornado.

D. Mode (D). Forces Transmitted through Flying Missiles

Objects picked up by tornadic winds attain speeds of tremendous magnitude which makes their penetration into even harder material possible. Photograph of Fig. 118 shows the penetration of a piece of wood into a 1.5 in. diameter steel pipe. Such objects are first lifted by the upmoving jet and thrown outward after they attain large tangential speeds in the jet breakdown region. However, forces due to missile penetration do not usually destroy the entire building structure but inflict damages locally.

The sequence of the pressure loading on a structure is summarized in Fig. 64. Sketch (a) represents the loading as the tornado vortex approaches the building structure, during which time modes (A) and (D) are important. As the vortex envelopes the house (sketch b) then mode (B) dominates while modes (A) and (D) also exist. When the tornado vortex leaves the structure, modes (A), (C) and (D) are effective (sketch c) with mode (C) to be the most damaging. As the vortex moves away (sketch d) mode (C) diminishes rapidly while modes (A) and (D) retain their effect until the tornado vortex is at some distance from the structure.

VI. MECHANISM OF A TORNADO VORTEX FORMATION

The arguments and evidence presented in the preceding chapters clearly indicate the superiority of the present approach in simulating tornadic vortices in the laboratory. The qualitative agreement of the observed structure, velocity and pressure field of the present laboratory vortex with natural tornado characteristics not only can be of help towards a better understanding of the tornado flow field but also a help in explaining the creation of such powerful and devastating natural phenomenon.

Based on such observations presented in this dissertation, the following mechanism for the formation of tornadic vortices is proposed.

A. Formation of Tornadic Vortices

It was suggested by Brooks (1949), based on his observation of the St. Louis Tornado of 1948 that a tornado cyclone was associated with a tornado vortex, however, the basic mechanism leading to the formation of such concentrated vortices was not explained. Even after almost three decades the exact mechanism of the downward transfer of rotational momentum from the tornado cyclone to the ground level is not known. However, the observation of tornadoes and their associated tornado cyclones and the results of present simulation shows that not only such downward rotational momentum transfer is possible but the tornado vortices feed from the supply of the vorticity available to them from such cyclones.

The vortical strength of the atmospheric vortices is usually defined as the ratio of their local vertical vorticity compared to the background vertical vorticity, 2Ω, due to the earth's rotation. This ratio is called the Rossby number, R_o, and by its definition is non-dimensional. Fujita (1965), after careful study of the Fargo Tornado and its tornado cyclone (Fujita, 1960) and based on the analysis of Scottsbluff Tornado (Van Tassel, 1955) and Dallas Tornado (Hoecker, 1960) concluded that the Rossby number for tornadoes is of the order of 10^4, and 10^2 for tornado cyclones. The Rossby number for macroscale cyclones is of the order of 1 which is therefore negligible compared to the vorticity required for the formation of tornadoes. Although such large-scale cyclones provide an environment of background vorticity, appreciably higher levels of vorticity is needed before concentrated vortices can form. Mesoscale cyclones with vorticity levels of 100 times greater, then provide the proper supply of vorticity for the formation of such tornadic vortices. Tornado cyclones, therefore, act as both a vorticity source and a source of vertical momentum by creating a sink at upper levels above the ground surface.

Observations by Fujita (1975) has shown that the tornadic vortices mainly depend on tornado cyclones for maintaining their strength. It is possible for a tornado to leave its mother cyclone upon maturity, however, such tornadoes dissipate soon after the separation occurs. This indicates that the vorticity supply of the ground boundary layer by itself is not enough to maintain a tornado. Maxworthy (1973) speculated that

for large dust-devils the source of vertical vorticity in the vortex comes from turning of the horizontal vorticity in the main boundary flow into the vertical direction. However, he also expressed an opinion that the greatly needed supply of vorticity for tornadoes must come from mesoscale cyclonic systems.

Based on the foregoing discussion then it is argued that tornadoes form under rotating cumulonimbus systems and as a necessity, stay with them. The initial rotation starts at high altitudes where an atmospheric vortex forms near squall lines or pressure jump lines. Necessary ingredients of axial flow plus rotation exists at these discontinuity lines where cold and warm masses of air collide and interact. Due to such rotations a low pressure region forms inside the cumulonimbus. The upflow and the low pressure are then maintained by the high altitude jet stream which shears off the top of the vortex and forms the anvil. The rotation is then transferred downward by the action of the downrushing cold air and probably by diffusion. Therefore, a relatively weak rotating cylinder with a diameter comparable to that of the parent tornado cyclone forms extending downward to the surface. Initially far from the ground surface, a possible solid body rotation exists and all vortical layers are in lateral equilibrium due to a balance between the centrifugal tendencies of the flow and the inward pressure gradient. However, near the ground the tangential wind speed is retarded due to frictional effect of the surface. The direct result is a decrease in centrifugal force which, in turn, distorts the equilibrium of the rotation. With the

loss of centrifugal force, the flow is attracted radially by the inward pressure gradient force. Numerous analytical works, e.g., Kuo (1971), have shown that the radial inflow is automatically induced in the boundary layer of an intense vortex when it interacts with a solid surface. Actual ground observation also shows that a radial inflow wind of 20 to 30 mph exists in an area of approximately 30 miles by 30 miles (Kessler, 1972). Such a horizontal convergence transports the ambient vorticity and that generated by viscous stresses at the ground to the center of the yet relatively weak vortex. Arriving at the center from all directions the flow then turns upward and forms a concentrated vortical tube (Hsu and Fattahi, 1975a, 1975b). Massive particles carried upward by such a mechanism continue upward motion to high altitudes by the jet flow in the center of the tube or leave it due to increased centrifugal acceleration just above the surface. The mode of the motion depends on the mass, size and the radial distance at which the particles commence their upward motion. The above sequence of events continues and as time passes, the vortical tube becomes more concentrated during which time the inflow wind speeds near the surface may become large enough to induce damage to surface environment. The vortical tube increases its diameter with height where the rate of increase could be zero or more depending on the nature of the inflow, surface roughness and possibly some as yet unknown factors.

Observation of tornado vortices and the tornado-like laboratory vortex under investigation shows that the vortical tube is only one part of

a very complicated flow pattern which includes upflow-downflow, the central jet and jet breakdown flow regions as discussed in detail in Chapter III. The formation of the funnel, however, has always been of interest and the direction of motion in the funnel region controversial. Hoecker (1960), for example, had the impression that the Dallas Tornado funnel flow was axially stagnant while present laboratory observations indicates a definite downward motion. The recent Ames Tornado of June 13, 1976 also showed downward motion in the funnel region[1]. Based on such observations it is then suggested that the downmoving funnel is an extension of the clouds which move into the vortical tube (Hsu and Fattahi, 1976) down to near the ground surface where its interaction with the lower jet, forms the jet breakdown flow pattern.

The possible mechanism of forcing the downflow funnel into the upflow vortical tube may be explained by Weske (1955) and Burgers (1956) theory of reverse flow in swirling converging or diverging vortex tubes. Weske and Burgers considered an incompressible, inviscid, swirling flow of rigid body rotation in the core region of radius r^*_{C1} and potential vortex flow for outer region between r^*_{C1} and R^*_1. Since the theory was to explain the reversed flow in nozzles or diffusers then the flow was considered to be enclosed by solid walls at R^*_1, and R^*_2 of station 2 where the reversed flow is to originate and proceed towards station 1. In Region 1, the swirling flow is assumed to originate with a uniform axial velocity w^*_1, as shown in Fig. 65. For simplification, only the flow in

[1]Paul J. Hermann. 1976. Department of Aerospace Engineering, Iowa State University, Ames, Iowa. Private communication.

Region 2 was investigated by above researchers since the radial velocity and its derivatives could be neglected.

Making use of the conservation of angular momentum, Burgers (1956) arrived at the following equation relating the flows between the two regions:

$$\frac{d^2 w_2^*}{dr_2^{*2}} + \frac{1}{r_2^*}\frac{dw_2^*}{dr_2^*} + \frac{4\omega^{*2}}{w_1^{*2}}(w_2^* - w_1^*) = 0 \qquad (6.1)$$

where w_2^*, r_2^* and ω^* denote the axial velocity component, the radial distance in Region 2, and the angular velocity of the rigid core in Region 1, respectively. The above equation is a Bessel equation of zero order and its solution is given as

$$w_2^* = w_1^* [1 + \beta^* J_o(2\omega^* r_2^*/w_1^*)] \qquad (6.2)$$

where J_o is the Bessel function of the first kind and β^* is a constant that may be determined from the conservation of mass. For the simple case of a solid body rotation for the entire region 1, $r_{C1}^* = R_1^*$ and $r_{C2}^* = R_2^*$ then

$$\beta^* = \frac{\alpha}{2J_1(n\alpha)}\left(\frac{1}{n} - n\right) \qquad (6.3)$$

where $n = R_2^*/R_1^*$ is the stream tube contraction ratio and $\alpha = 2\omega^* R_1^*/w_1^*$ is the initial swirl intensity. For this case also equation (6.2) may be simplified to:

$$w_2^* = w_1^* [1 + \beta^* J_o(n\alpha r_2)] \qquad (6.4)$$

where $r_2 = r_2^*/R_2^*$. It is obvious that J_o and J_1 have different negative and positive values depending on the parameters n, α and r_2. If in equation (6.4), β^* is negative and $[\beta^* J_o(n\alpha r_2)] < -1$, then w_2^* becomes negative indicating a reverse flow.

The reverse flow is a common occurrence in rocket engine and swirling pipe flow problems which has not only theoretically been proved but also experimentally observed. In tornadic flow fields, with the vortical tube forming a rotating structure apparently resistive to lateral motion of air particles the flow inside it is reversed downward. It is very likely that the simple equation (6.4) with the simplified assumptions of steady flow and no radial velocity components fails to describe the complicated, and turbulent flow of a tornado core. However, the emphasis here is on the fact that axially reversed flows exist in all swirling flow problems which the swirling vortical tube of the tornado vortex may be one of such problems. The equation describing the flow of the latter is expected to be more complicated than equation (6.4) to account for factors such as initial non-uniformity of the axial flow, turbulence, gradual change of the cross-sectional area, radial velocity and its related derivatives.

B. Concluding Comments

In 1970 a summary report published by the Conference on Wind Loads on Structures (National Science Foundation, 1971) sponsored by the National Science Foundation stated:

"It is felt that we have reached a plateau in tornado forecasting, are really forecasting only the intensity of a thunderstorm, and further

improvement in tornado forecasts can only be realized by additional work in this field."

Such a statement was issued at a time when the laboratory simulations of tornadic storms had failed to reveal significant results in terms of understanding the structure of such flow fields. The failure of such simulations was related to their incorrect approach in generating tornadic vortices in the laboratory. Therefore, a new vortex generator was proposed and funded by the National Science Foundation to truly simulate the vortex boundary layer interaction.

The thrust of the present investigation was to show the superiority of the new approach. With the lack of the needed amount of actual data from natural tornadoes it is very difficult to generalize the findings of this research. However, the similarities between real and laboratory vortices were pointed out and the significant improvement of the present simulation over all of the previous attempts were emphasized. Suggestions were made on the possible mechanism of the formation of tornadoes and its complicated structure and were supported by laboratory or field data to the extent that such information were available. Rough estimates of the velocity and pressure fields of tornadoes were given. However, the information obtained in this preliminary investigation should be treated only as estimate as contrasted to accurate data not only due to rough methods of measurement utilized but also due to our yet much needed improvement of understanding of tornadic flow fields.

C. Recommendation for Further Research

The preliminary study, results of which are presented in this dissertation, has provided some explanations for mechanism of formation, structure and characteristics of tornado vortices. However, unless further research along the same lines are conducted, the observations and explanations provided in this dissertation should be treated as preliminary and not universal. To substantiate the present findings the following recommendations for further research are made:

1. The vortex generated in the laboratory was small (approximate core diameter 1.0 in. near the ground and 3.0 in. away from it). Therefore, observations were difficult and fine measurements impossible. It is then necessary to install a larger vortex generator in an attempt to produce a larger vortex. Not only this provides an easier subject to study but also the dimensions of the new vortex as compared to the dimensions of the house models will be more realistic. The experimentations conducted in the present investigation should be repeated for the larger vortex to search for the possibility of providing scaling factors and non-dimensionalizing parameters in an attempt to generalize the present or improved findings.

2. Considering velocity and pressure field measurement, the obvious shortcoming of the present approach to simulate tornado vortices is its incapability to produce a stationary vortex. However, this problem also exists in all other simulation attempts. Realizing the fact that the translational motion of the vortex significantly limits the ease and

accuracy of the measurements it should be remembered that real tornado vortices are also non-stationary and any attempt to stabilize the laboratory vortex may modify its structure. It is then necessary to conduct experiments in a way to overcome the problem of vortex translation. In the case of wind speed measurement the only improvement possible is to optimize the definition of the motion pictures. The camera available for the present investigation was a Hycam high speed movie camera capable of shooting up to 11000 frames per second. Such a camera is not very well suited for frame by frame analysis since it does not provide optimum definitions in each frame of the motion picture. A preferable camera would be one which is designed for lower speeds of less than 1,000 frames per second with frame by frame exposure capability to optimize the image definition. Significant improvements in pressure measurement may be made. The pressure measurements conducted in the present research were performed with a single pressure transducer. Therefore, to construct a pressure distribution curve the location of data points were determined visually and the transducer's output was recorded utilizing an oscilloscope. To obtain an accurate distribution a number of transducers are needed with a tape recorder to record the analog signal of each transducer. This then would provide a number of data points all measured at an instant and at different radial locations. The above transducers should be of enough response to accurately react to the transient behavior of the vortex. Instrumentation for such an experiment should also include an analog to digital converter to digitize the transducer's signal. Such experimentation not only reveals a

radial distribution of the pressure, but also provides a history of the pressure drop and recovery as the tornado-like vortex approaches, crosses and leaves the region in which transducers are set to perform pressure measurement. This finding would be extremely important for design engineers who handle the design of nuclear reactor housing or vent design for residentials. It would be very important if velocity measurements through Plexiglas plate were also taken at the same time to provide a relationship between wind speeds near the surface and associated radial pressure variation.

3. The following observations may be easily made in the laboratory:

a. Effect of different surface roughness grades on the flow field in terms of funnel formation, static pressure drop at the surface, etc.

b. Skipping action of the vortex, always associated with all tornadic storms. A moving ground plane such as a conveyor belt is extremely helpful.

c. Behavior of the vortex under increased surface temperature (simulate a heat island).

d. Investigation of critical height, H^*_{cr}, and its dependence on the rotation rate of the honeycomb plate. This would explain the reason for absence of a tornado vortex when a tornado cyclone exists and other conditions are favorable. Such finding is also valuable in predicting the formation of the tornado funnel and possibly the point of formation when a tornado cyclone has already been under observation.

e. Observation of different portions of the flow field with improved flow

visualization techniques. This is specially important in view of the fact that better flow visualization results in more accurate wind speed measurement, in addition to better understanding of the flow structure.

VII. REFERENCES

Agee, E. M. 1969. Tornado project activities at Purdue University. Bulletin of the American Meteorological Society, 50(10):806-807.

Agee, E. M. 1970. Purdue tornado project activities--Part II. Bulletin of the American Meteorological Society, 51(10):951.

Agee, E. M. 1971. Purdue tornado project activities--Part III. Bulletin of the American Meteorological Society, 52(7):575.

Agee, E. M., C. Church, C. Morris, and J. Snow. 1975. Some synoptic aspects and dynamic features of vortices associated with the tornado outbreak of 3 April 1974. Monthly Weather Review, 103(4):318-333.

American Meteorological Society. 1975. Front cover photograph. Proceedings of the 9th Conference on Severe Local Storms, 9.

Blechman, J. B. 1975. The Wisconsin Tornado event of April 21, 1974: Observations and theory of secondary vortices. Proceedings of the 9th Conference on Severe Local Storms, 9:344-349.

Bossel, H. H. 1969. Vortex breakdown flowfield. The Physics of Fluids, 12(3):498-508.

Brooks, E. M. 1949. The tornado cyclone. Weatherwise, 2(2):32-33.

Brooks, E. M. 1951. Tornadoes and related phenomena. In Compendium of Meteorology, Pages 673-680, American Meteorological Society, Boston, Mass.

Brown, R. A., D. W. Burgess, and K. C. Crawford. 1973. Twin tornado cyclones within a severe thunderstorm: Single doppler radar observations. Weatherwise, 26(2):63-71.

Browning, K. S. 1964. Airflow and precipitation trajectories within severe local storms which travel to the right of the winds. Journal of Atmospheric Sciences, 21(6):634-639.

Burgers, J. M. 1956. The effect of stretching of a vortex core. University of Maryland, College Park, Maryland, Technical Note BN-80.

Byers, H. R. 1948. Probing the thunderstorm. Weatherwise, 1(3):47-50.

Chang, C. C. 1969. Recent laboratory model study of tornadoes. Proceedings of the 6th Conference on Severe Local Storms, 6:244-252.

Chi, S. W. 1975. Numerical modeling of ground turbulent boundary layers of intense atmospheric vortices. Proceedings of the 2nd U. S. National Conference on Wind Engineering Research, 2:II4(1-3).

Chi, S. W., and W. J. Glowacki. 1974. Applicability of mixing length theory to turbulent boundary layers beneath intense vortices. Journal of Applied Mechanics, 41(1):15-19.

Chi, S. W. and J. Jih. 1974. Numerical modeling of the three-dimensional flows in the ground boundary layer of a maintained axisymmetrical vortex. Tellus, 26(4):444-455.

Defense Civil Preparedness Agency. 1974. Multiprotection Design. TR-20-Vol. 6. Washington, D.C.

Dines, W. H. 1896. Experiment illustrating the formation of the tornado cloud. Quarterly Journal of the Royal Meteorological Society, 22: 71-74.

Fankhauser, J. C. 1971. Thunderstorm-environment interactions determined from aircraft and radar observations. Monthly Weather Review, 99(3):171-192.

Fattahi, B. and C. T. Hsu. 1976. Feasibility of the use of three dimensional anemometers in a simulated tornado flow measurement. Journal of Physics E: Scientific Instruments. (Accepted for publication.)

Flora, S. D. 1949. The nature of tornadoes. Weatherwise, 2(2):27-39.

Flora, S. D. 1953. Tornadoes of the United States, 1st Ed. The University of Oklahoma Press, Norman, Oklahoma, 221 pp.

Flora, S. D. 1956. Hailstorms of the United States, 1st Ed. The University of Oklahoma Press, Norman, Oklahoma, 201 pp.

Fujita, T. 1958. Mesoanalysis of the Illinois tornadoes of 9 April 1953. Journal of Meteorology, 15(3):288-296.

Fujita, T. 1960. A detailed analysis of the Fargo tornadoes of June 20, 1957. United States Department of Commerce Research Paper No. 42.

Fujita, T. 1965. Formation and steering mechanisms of tornado cyclones and associated hook echoes. Monthly Weather Review, 93(2):67-78.

Fujita, T. 1971. Proposed mechanism of suction spots accompanied by tornadoes. Proceedings of the 7th Conference on Severe Local Storms, 7:208-213.

Fujita, T. 1973. Proposed mechanism of tornado formation from rotating thunderstorm. Proceedings of the 8th Conference on Severe Local Storms, 8:191-196.

Fujita, T. 1974. Jumbo tornado outbreak of 3 April 1974. Weatherwise, 27(3):116-126.

Fujita, T. 1975. New evidence from April 3-4, 1974 tornadoes. Proceedings of the 9th Conference on Severe Local Storms, 9:248-255.

Fujita, T., D. L. Bradbury, and C. F. Van Thullenar. 1970. Palm Sunday tornadoes of April 11, 1965. Monthly Weather Review, 98(1):29-69.

Golden, J. H. 1969. The Lower Florida Keys waterspout project. Bulletin of the American Meteorological Soceity, 51(3):235-237.

Golden, J. H. 1971. Waterspouts and tornadoes over South Florida. Monthly Weather Review, 99(2):146-153.

Goldman, J. L. 1965. The Illinois tornadoes of 17 and 22 April 1963. Satellite and Mesometeorology Research Project, Department of the Geophysical Sciences, The University of Chicago, Chicago, Ill., Research Paper 39.

Goldman, J. L. 1968. The high speed updraft--the key to the severe thunderstorms. Journal of Atmospheric Sciences, 25(2):222-248.

Grant, F. C. 1971. Proposed technique for launching instrumented balloons into tornadoes. NASA TN D-6503.

Hall, R. S. 1951. Inside a Texas tornado. Weatherwise, 4(3):54-65.

Hoecker, W. H. 1960. Wind speed and air flow patterns in the Dallas Tornado of April 2, 1957. Monthly Weather Review, 88(5):167-180.

Hoecker, W. H. 1961. Three-dimensional pressure pattern of the Dallas Tornado and some resultant implications. Monthly Weather Review, 89(12):533-542.

Hoecker, W. H., R. G. Beebe, D. T. Williams, J. T. Lee, S. G. Bigler, and E. P. Segner. 1960. The tornadoes at Dallas, Texas, April 2, 1957. United States Department of Commerce Research Paper No. 41.

Hsu, C. T. 1972. Tornado modeling and its suction mechanism. Iowa State University Engineering Research Institute Report No. 62160.

Hsu, C. T. 1973. Laboratory modeling of the tornado suction mechansim. Proceedings of the 8th Conference on Severe Local Storms. 8:199-202.

Hsu, C. T. and B. Fattahi. 1975a. Laboratory simulation of tornadoes. Proceedings of the 2nd U. S. National Conference on Wind Engineering Research, 2:II.3.1-II.3.2.

Hsu, C. T. and B. Fattahi, 1975b. Tornado funnel formation from a tornado cyclone. Proceedings of the 9th Conference on Severe Local Storms, 9:358-363.

Hsu, C. T. and B. Fattahi. 1976. Mechanism of a tornado funnel formation. Physics of Fluids. (Accepted for publication.)

Hsu, C. T. and H. Tesfamariam. 1975. Turbulent modeling of a tornado boundary layer flow. Iowa State University Engineering Research Institute Report No. 76126.

Hudson, J. A. 1958. The pro's nest: Tornado. Flying, 63(2):47-75.

Idso, S. B. 1974. Tornadic vortices spawned by a desert brush fire. Weather, 29(8):280-283.

Journal of Physics E: Scientific Instruments. 1975. DISA advertisement photograph. Journal of Physics E: Scientific Instruments, 8(9):iii.

Kessler, E. 1970. Tornadoes. Bulletin of the American Metheorological Society, 51(10):926-936.

Kessler, E. 1972. On tornadoes and their modification. M.I.T. Technology Review, 74(6):48-55.

Kuo, H. L. 1971. Axisymmetric flows in the boundary layer of a maintained vortex. Journal of Atmospheric Sciences, 28(1):20-41.

Leverson, V. H., P. C. Sinclair, and J. H. Golden. 1975. Waterspout wind, temperature, and pressure structure deduced from aircraft measurements. Proceedings of the 9th Conference on Severe Local Storms, 9:350-357.

Lewellen, W. S., W. J. Burns, and H. J. Strickland. 1969. Transonic swirling flow. American Institute of Aeronautics and Astronautics Journal, 7(7):1290-1297.

Lewis, W., and P. J. Perkins. 1953. Recorded pressure distribution in the outer portion of a tornado vortex. Monthly Weather Review, 81(12):379-385.

Ludlum, D. M. 1970. Early American tornadoes. 1st Ed. Americal Meteorological Society, Boston, Mass., 219 pp.

MacCurdy, E. 1958. The notebooks of Leonardo da Vinci. Vol. 1, George Braziller, New York, New York.

Maier, M. W., and H. W. Brandli. 1973. Simultaneous observation of tornado, waterspout and funnel cloud. Weather, 28(8):322-327.

Maxworthy, T. 1973. A vorticity source for large-scale dust devils and other comments on naturally occurring columnar vortices. Journal of the Atmospheric Sciences, 30(8):1717-1722.

Miller, J. E. 1955. A tornado model and the fire whirlwind. Weatherwise, 8(4):88-91.

Morgan, B. J. 1972. Tornado detection, tracking and interception. University of Notre Dame, South Bend, Indiana, College of Engineering Report.

Morton, B. R. 1966. Geophysical vortices. Progress in Aeronautical Sciences, 7:145-193.

Muirhead, V. U., and J. R. Eagleman. 1971. Laboratory compressible flow tornado model. Proceedings of the 7th Conference on Severe Local Storms, 7:284-291.

National Science Foundation. 1971. Wind loads on structures. Summary Report. (California Institute of Technology, Pasadena, California.) National Science Foundation, Washington, D.C.

Newton, C. W. 1966. Circulations in large sheared cumulunimbus. Tellus, 18(4):699-713.

Newton, C. W. 1967. Severe convective storms. Advances in Geophysics, 12:257-308.

Pearson, A. D. and J. A. Miller. 1971. The tornado season of 1970. Weatherwise 24(1):12-17.

Richter, J. P. 1970. The literary works of Leonardo da Vinci. Vol. 2. Phaidon, New York, New York.

Roberts, W. O. 1972. We're doing something about the weather. National Geographic, 141(4):518-555.

Rott, N., and W. S. Lewellen. 1964. Boundary layer in a rotating flow. Aerospace Corporation (California) Report ATN-64(9227)-6.

Schmidt, E., and K. Wenner. 1943. Heat transfer over the circumference of a heated cylinder in transverse flow. N.A.C.A. TM-1050, 21 pp.

Serrin, J. 1972. The swirling vortex. Philosophical Transactions of the Royal Society of London, A, 271:325-360.

Sinclair, P. C. 1973. The lower structure of dust devits. Journal of the Atmospheric Sciences, 30(8):1599-1619.

Smith, R. C. 1967. Flow in the boundary layer beneath an intense vortex such as a tornado. National Center for Atmospheric Research Pre-publication Report. (National Center for Atmospheric Research, Boulder, Colorado.)

Snow, J. T. and E. M. Agee. 1975. Vortex splitting in the mesocyclone and the occurrence of tornado families. Proceedings of the 9th Conference on Severe Local Storms, 9:270-277.

So, K. L. 1967. Vortex phenomena in a conical diffuser. American Institute of Aeronautics and Astronautics Journal, 5(6):1072-1078.

Stanford, J. L. 1976. Tornado: An account of Iowa tornadoes. 1st Ed. The Iowa State University Press, Ames, Iowa. (In press)

Stewartson, K. 1957. On rotating laminar boundary layers. Proceedings of the Symposium on Boundary Layer Research, Berlin, 1957:59-71.

Thermo Systems, Inc. 1970. Instruction manual for 1080 total velocity vector anemometer. Thermo System, Inc., St. Paul, Minn.

United States Department of Commerce. 1952. Tornado occurrences in the United States. U. S. Department of Commerce Technical Paper No. 20.

Van Tassel, E. L. 1955. The North Platte Valley tornado outbreak of June 27, 1955. Monthly Weather Review, 83(11):255-264.

Wan, C. A. and C. C. Chang. 1972. Measurement of the velocity field in a simulated tornado-like vortex using a three-dimensional velocity probe. Journal of the Atmospheric Sicences, 29(1):116-127.

Ward, N. B. 1972. The exploration of certain features of tornado dynamics using a laboratory model. Journal of the Atmospheric Sciences, 29(6):1194-1204.

Weatherwise. 1973. Front cover photograph. Weatherwise, 26(2):53.

Weske, J. R. 1955. The effect of stretching of a vortex core. University of Maryland, College Park, Maryland, Technical Note BN-57.

Williams, N. R. 1948. Development of dust whirls and similar small scale vortices. Bulletin American Meteorological Society, 29(3): 106-117.

Ying, S. J. and C. C. Chang. 1970. Exploratory model study of tornado-like vortex dynamics. Journal of the Atmospheric Sciences, 27(1): 3-14.

VIII. ACKNOWLEDGMENTS

The persons who deserve acknowledgment for their aid, direct or indirect, in the completion of this study are too numerous to mention. However, several persons deserve special note.

Dr. C. T. Hsu has been a constant supporter and stabilizing factor during the author's graduate study, serving as major professor and the director of this research. His valuable advice, beyond merely the academic, has guaranteed continuity. His hours of consultation, his patience with my problems and his constant encouragement and trust may never be fully acknowledged, or properly repaid.

Appreciation is also extended to Dr. W. J. Cook, my co-major professor for his timely discussions and advice.

I must gratefully acknowledge the willingness of Dr. R. F. Brodsky, Dr. D. A. Anderson, Professor R. C. Fellinger and Dr. D. E. Sanderson to take time from their responsibilities to serve on the author's graduate committee.

I would like to acknowledge and greatly appreciate the support and encouragement of my parents throughout my years of education. They made my advancement possible with their many sacrifices. Reimbursement is not possible, however, I hope I can do the same for my children. I extend my special appreciation to my brothers who not only were supportive but also involved in actual preparation of the drawings presented in this dissertation.

I would like to thank Ms. Cecilia Byers for typing the rough draft and final version of this writing.

My wife Farzaneh and son Omid deserve a heart-felt thanks for enduring these years. I extend my thanks and apologies for having furthered my own career at the expense of the moments I could have spent with them.

This study was funded by the grant GK-43655 from the National Science Foundation and made available through the Engineering Research Institute of the Iowa State University. Partial funding was also provided by the Iowa State University Research Foundation.

Finally, I would like to thank the Department of Mathematics, Iowa State University Technical Institute, Department of Engineering Mechanics and Department of Aerospace Engineering who provided me teaching or research assistantships throughout my years of graduate study.

IX. APPENDIX A

Following the methods proposed by Thermo Systems, Inc. (Thermo Systems, Inc., 1970), velocity components along the 1080-3D anemometor sensors may be determined. However, in the present experimentations the components of the total velocity vector are sought in the XYZ directions of the reference ground plane (local horizon) as shown in Fig. 66. Therefore, a coordinate system transformation is required to compute radial, axial and tangential velocities.

A right-hand rectangular coordinate system is defined for any point in the flow field with positive X and Y directions representing radial inflow and axial upflow. Let s_1, s_2 and s_3 be the positive sensor directions as shown in Fig. 20. A complete three step coordinate transformation from positive sensor directions to positive XYZ coordinate system is shown in Fig. 67. Figure 68 shows the positive probe angle of attack, α and yaw angle β. The angle of inclination between each sensor and the plane normal to the probe, η is equal to 35°16'.

After each axis rotation one unit vector equality is obtained as follows:

$$\begin{bmatrix} i_1 \\ j_1 \\ k_1 \end{bmatrix} = \begin{bmatrix} 1 & 0 & 0 \\ 0 & \cos 45 & \sin 45 \\ 0 & -\sin 45 & \cos 45 \end{bmatrix} \begin{bmatrix} s_1 \\ s_2 \\ s_3 \end{bmatrix} \qquad (A.1)$$

$$\begin{bmatrix} i_2 \\ j_2 \\ k_2 \end{bmatrix} = \begin{bmatrix} \sin(\eta-\alpha) & \cos(\eta-\alpha) & 0 \\ -\cos(\eta-\alpha) & \sin(\eta-\alpha) & 0 \\ 0 & 0 & 1 \end{bmatrix} \begin{bmatrix} i_1 \\ j_1 \\ k_1 \end{bmatrix} \qquad (A.2)$$

$$\begin{bmatrix} i \\ j \\ k \end{bmatrix} = \begin{bmatrix} -\sin\beta & 0 & -\cos\beta \\ 0 & 1 & 0 \\ \cos\beta & 0 & -\sin\beta \end{bmatrix} \begin{bmatrix} i_2 \\ j_2 \\ k_2 \end{bmatrix} \qquad (A.3)$$

When the above unit vector equalities are combined then a total transformation from sensor velocities to radial, axial and tangential velocities may be obtained from:

$$u^* = [\sin\beta \sin(\eta-\alpha)]\, V_1^* - \frac{\sqrt{2}}{2}\,[\cos\beta - \sin\beta \cos(\eta-\alpha)]V_2^* + \frac{\sqrt{2}}{2}\,[\cos\beta + \sin\beta \cos(\eta-\alpha)]V_3^* \qquad (A.4)$$

$$w^* = -\,[\cos(\eta-\alpha)]\, V_1^* + \frac{\sqrt{2}}{2}\,[\sin(\eta-\alpha)]V_2^* + \frac{\sqrt{2}}{2}\,[\sin(\eta-\alpha)]V_3^* \qquad (A.5)$$

$$v^* = [\cos\beta \sin(\eta-\alpha)]\, V_1^* + \frac{\sqrt{2}}{2}\,[\sin\beta + \cos\beta \cos(\eta-\alpha)]V_2^* - \frac{\sqrt{2}}{2}\,[\sin\beta - \cos\beta \cos(\eta-\alpha)]V_3^* \qquad (A.6)$$

where u^*, w^* and v^* are radial outflow, axial upflow and cyclonic tangential velocities corresponding to positive X, Y and Z directions.

X. APPENDIX B

The following equations were used to plot, compare or approximate the radial distribution of the tangential velocity. All velocities are in inch per second and distances are in inch.

At $H^* = 0.25$ in.

$v_m^* = 509.64$ ips	$r_m^* = 0.59$ in.
$v^* = 863.8\ r^*$	$0 \leq r^* \leq 0.59$
$v^* r^{*1.6} = 219.09$	$0.59 \leq r^* \leq 1.4$
$v^* r^{*0.8} = 167.39$	$1.4 \leq r^* \leq \infty$

At $H^* = 1.0$ in.

$v_m^* = 378$ ips	$r_m^* = 1.0$ in.
$v^* = 378\ r^*$	$0 \leq r^* \leq 1.0$
$v^* r^{*1.6} = 378$	$1.0 \leq r^* \leq 2.2$
$v^* = 32.97\ r^* + 34.54$	$2.2 \leq r^* \leq 2.7$
$v^* r^{*0.8} = 273.47$	$2.7 \leq r^* \leq \infty$

At $H^* = 2.0$ in.

$v_m^* = 372$ ips	$r_m^* = 1.3$ in.
$v^* = 210\ r^*$	$0 \leq r^* \leq 1.0$
$v^* = 540\ r^* - 330$	$1.0 \leq r^* \leq 1.3$
$v^* r^{*3} = 817.28$	$1.3 \leq r^* \leq 2.2$

$v^* = 32.78\ r^* + 4.63$ $\quad 2.2 \leq r^* \leq 3.7$

$v^* r^{*0.8} = 358.67$ $\quad 3.7 \leq r^* \leq \infty$

At $H^* = 3.0$ in.

$v_m^* = 372$ ips $\quad r_m^* = 1.55$ in.

$v^* = 170\ r^*$ $\quad 0 \leq r^* \leq 1.2$

$v^* = 480\ r^* - 372$ $\quad 1.2 \leq r^* \leq 1.55$

$v^* r^{*4} = 2147.2$ $\quad 1.55 \leq r^* \leq 2.1$

$v^* = 228\ r^* - 368.4$ $\quad 2.1 \leq r^* \leq 2.5$

$v^* = -213.82\ r^* + 736.15$ $\quad 2.5 \leq r^* \leq 3.05$

$v^* = 23.75\ r^* + 11.56$ $\quad 3.05 \leq r^* \leq 4.5$

$v^* r^{*0.8} = 394.52$ $\quad 4.5 \leq r^* \leq \infty$

At $H^* = 6.0$

$v_m^* = 372$ ips $\quad r_m^* = 1.55$ in.

$v^* = 185.45\ r^*$ $\quad 0 \leq r^* \leq 1.1$

$v^* = 373.33\ r^* - 206.67$ $\quad 1.1 \leq r^* \leq 1.55$

$v^* r^{*3} = 1385.3$ $\quad 1.55 \leq r^* \leq 2.5$

$v^* = 427.76\ r^* - 980.74$ $\quad 2.5 \leq r^* \leq 2.75$

$v^* = 195.6$ $\quad 2.75 \leq r^* \leq 3.15$

$v^* = -138.35\ r^* + 631.41$ $\quad 3.15 \leq r^* \leq 4.0$

$v^* = 28.8\ r^* - 37.2$ $\quad 4.0 \leq r^* \leq 5.5$

$v^* r^{*0.8} = 474$ $\quad 5.5 \leq r^* \leq \infty$

At $H^* = 9.0$ in.

$v_m^* = 360$ ips $\quad r_m^* = 1.50$ in.

$v^* = 240\ r^*$ $\quad 0 \leq r^* \leq 1.5$

$v^* r^{*3} = 1215$ $\quad 1.5 \leq r^* \leq 2.4$

$v^* = 153.5\ r^* - 280.5$ $\quad 2.4 \leq r^* \leq 3.0$

$v^* = 180$ $\quad 3.0 \leq r^* \leq 3.4$

$v^* = -160\ r^* + 724$ $\quad 3.4 \leq r^* \leq 4.0$

$v^* = 24\ r^* - 12$ $\quad 4.0 \leq r^* \leq 5.5$

$v^* r^{*0.8} = 469.32$ $\quad 5.5 \leq r^* \leq \infty$

At $H^* = 12.0$

$v_m^* = 360$ ips $\quad r_m^* = 1.55$

$v^* = 232.26\ r^*$ $\quad 0 \leq r^* \leq 1.55$

$v^* r^{*3} = 1340.6$ $\quad 1.55 \leq r^* \leq 2.6$

$v^* = 60.18\ r^* - 72.60$ $\quad 2.6 \leq r^* \leq 3.4$

$v^* = -40.32\ r^* + 269.09$ $\quad 3.4 \leq r^* \leq 4.65$

$v^* = 40.74\ r^* - 107.83$ $\quad 4.65 \leq r^* \leq 5.7$

$v^* r^{*0.8} = 500.53$ $\quad 5.7 \leq r^* \leq \infty$

At $H^* = 15.0$ in.

$v_m^* = 360$ ips	$r_m^* = 1.60$ in.
$v^* = 225\ r^*$	$0 \leq r^* \leq 1.60$
$vr^{*1.6} = 763.65$	$1.60 \leq r^* \leq 4.2$
$v^* = 34.157\ r^* - 66.6$	$4.2 \leq r^* \leq 5.6$
$v^* r^{*0.8} = 494.63$	$5.6 \leq r^* \leq \infty$

At $H^* = 18.0$ in.

$v_m^* = 360$ ips	$r_m^* = 1.65$ in.
$v^* = 218.2\ r^*$	$0 \leq r^* \leq 1.65$
$v^* r^* = 594$	$1.65 \leq r^* \leq \infty$

A Rankine-combined tangential velocity distribution is also plotted for all derived distributions and is given by

$v^* = C_{1R} r^*$	$0 \leq r^* \leq r_m^*$
$v^* r^* = C_{2R}$	$r_m^* \leq r^* \leq \infty$

where C_{1R} and C_{2R} are constants and are evaluated at (v_m^*, r_m^*). To determine the pressure distribution the cyclostrophic expression of

$$dP^* = \rho^* \frac{v^{*2}}{r^*} dr^*$$

was integrated radially at a given height, H^*. Then

$$\Delta P^* = \int_{P_C^*}^{P_\infty^*} dP^* = \int_0^\infty \rho^* \frac{v^{*2}}{r^*} dr^*$$

or with assumed constant density

$$P_\infty^* - P_C^* = \rho^* \int_0^\infty \frac{v^{*2}}{r^*} dr^*$$

The above expression which describes the pressure difference between the environment atmospheric pressure and the vortex core pressure is generally referred to as the pressure deficit in the text of this dissertation.

XI. APPENDIX C

The following equipments were used in the present experimental investigation:

1. System 1080 Total Vector Anemometer--Thermo Systems, Inc.

   This system measures the velocity magnitude and direction over the full 360° solid angle in a three dimensional flow field. The probe features split-film sensors which allow the determination of magnitude and direction of the instantaneous velocity vector. The probe includes a built-in calibration feature (system 1126). Performance specifications:

   Usable range: 0-500 fps (Air, 1.0 atm.)

   Magnitude accuracy: $\pm$3% of reading and $\pm$1% of full scale, 0-150 fps

   Directional accuracy: Two independent directional angles are within 3° over the complete solid angle

   Response: DC-1 KHz.

2. Series 1126 Pneumatic Calibration System--Thermo Systems, Inc.

   This calibration system is used to operate the anemometer's pneumatic shield and calibrator. It consists of a pressure regulator, pressure gauge and solenoid valves and provides a specified air velocity magnitude through the anemometer's sensor arrangement for calibration purposes.

3. Averaging Circuit.

   This system is simply a low-pass filter to remove the fluctuations and provide a mean flow measurement. Specifications:

Input: Range 0-20 volts

Output: Range 0-20 volts

Time constant: 30 seconds

4. Model PM5TC Differential Pressure Transducer--Statham.

This is a bi-directional differential pressure transducer designed for general purpose applications requiring low ranges and high accuracy.

Specifications:

Full scale output: ± 0.3 psid range

Resolution: Infinitesimal

Combined non-linearity and hysteresis: Less than ± 0.5% FS output

Excitation: 10 VDC

Transduction: Resistive, balanced, fully active strain gage bridge

Frequency response: Up to 600 Hz.

Flat response: Up to 75 Hz.

This model is calibrated by the manufacturer, however, its accuracy was checked against a micromanometer in the steady flow of the low speed wind tunnel of the Aerospace Engineering Department at Iowa State University. Results are plotted in Fig. 69.

5. Model 5103N Oscilloscope--Tektronix.

Model 5A19N Differential Amplifier

Model 5B10N Time Base/Amplifier

6. Model 3520V-1 DC Amplifier--DANA Laboratories, Inc.

Gain: 20-1000

Bandwidth: 0.01-10 kilocycles and wide band

7. Model 110 Television--Sony.

   Closed circuit operation.

8. Model AVC-3200 Video Camera--Sony.

   Closed circuit operation.

9. Model 8000A Digital Multimeter--Fluke.

10. Model 400 High Speed Camera--Hycam, Redlake Laboratories.

    Range: 0-11000 frames/sec

11. Model AAP-300T--Lafayette Analyzer (16 mm.).

    This stop action projector is designed for time motion, high speed, standard film or whenever critical analysis of film is required. The above model was used for frame-by-frame projection of the motion pictures for the purpose of instantaneous velocity determination.

XII. APPENDIX D

Figure 1. The laboratory vortex generator proposed by Dines (1896).

Figure 2. The improved version of Dines' vortex generator by Miller (1955).

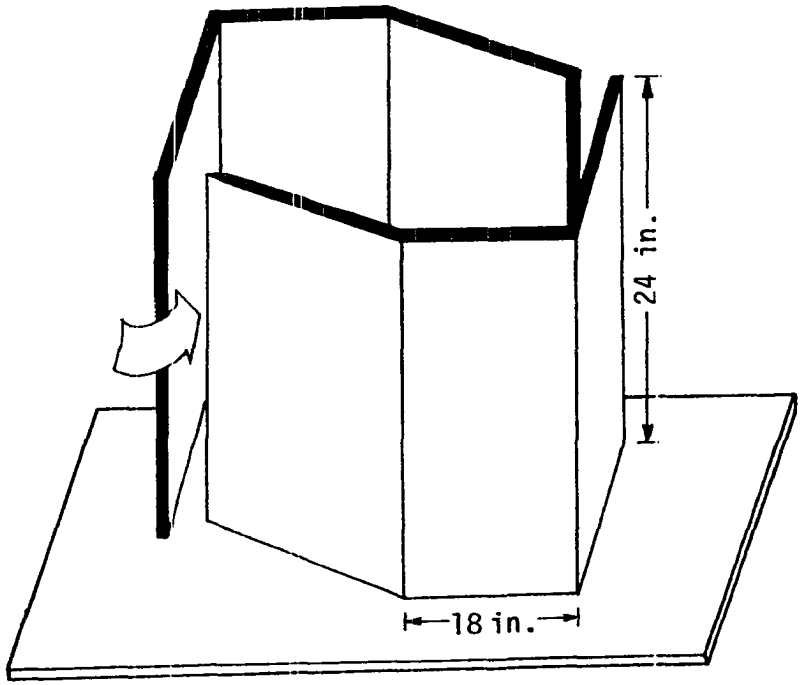
24 in.
18 in.

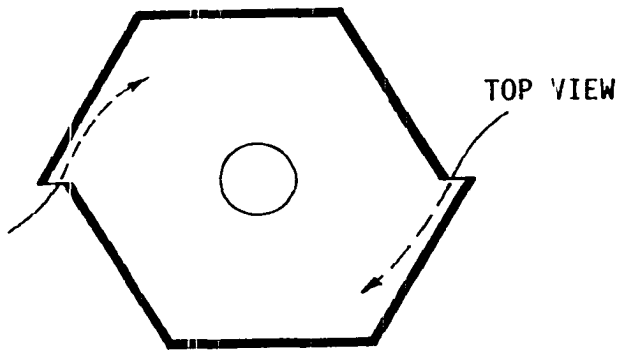
TOP VIEW

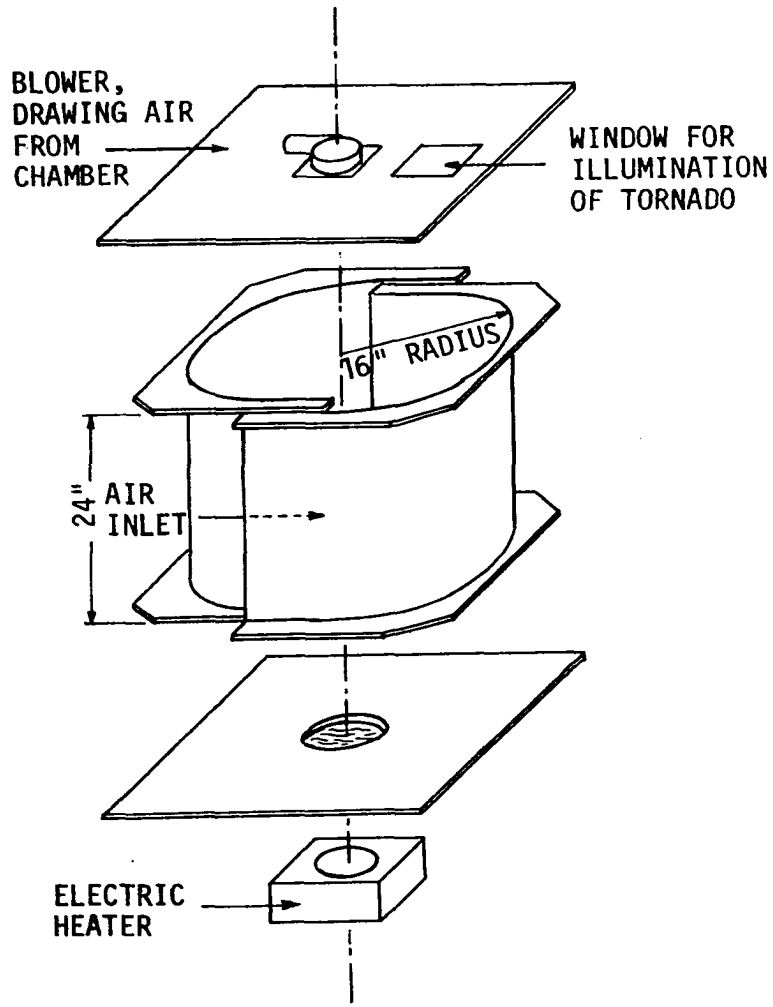
BLOWER, DRAWING AIR FROM CHAMBER
WINDOW FOR ILLUMINATION OF TORNADO
16" RADIUS
24"
AIR INLET
ELECTRIC HEATER

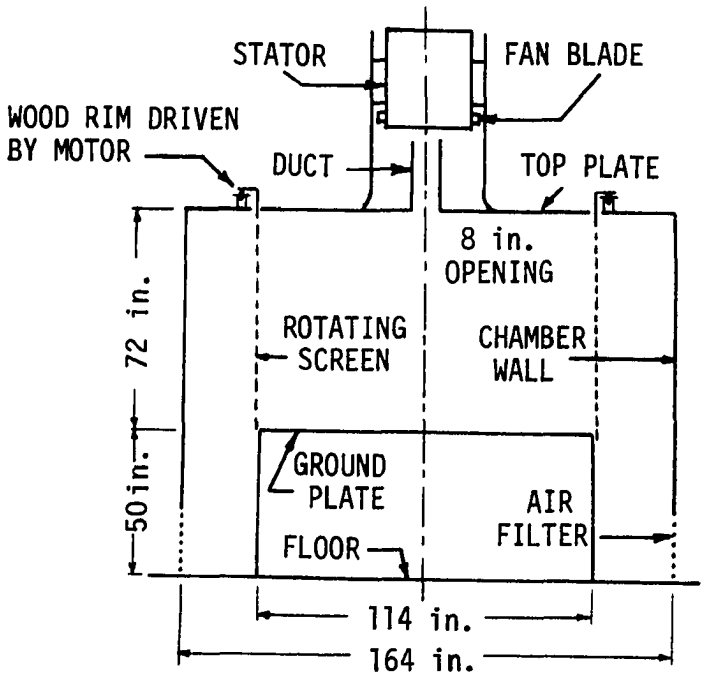

Figure 3. The laboratory vortex generator proposed by Chang (1969).

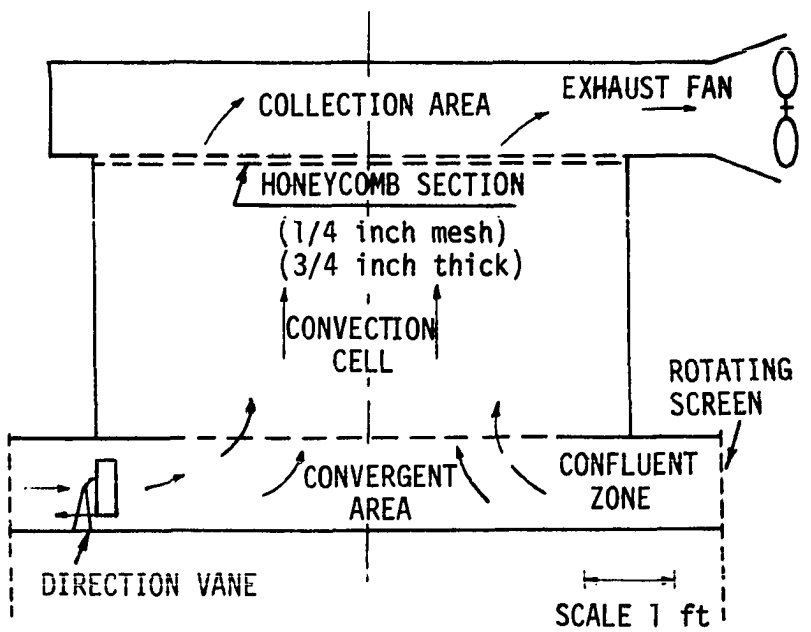

Figure 4. The laboratory vortex generator proposed by Ward (1972).

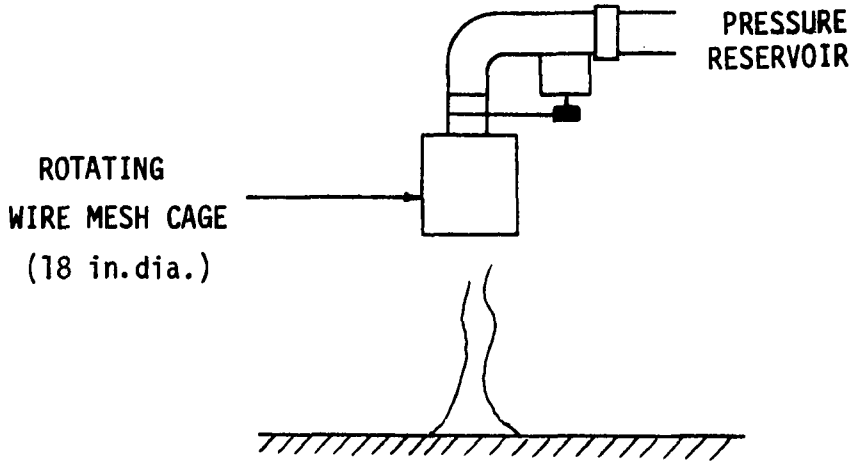

Figure 5. The laboratory vortex generator proposed by Muirhead and Eagleman (1971).

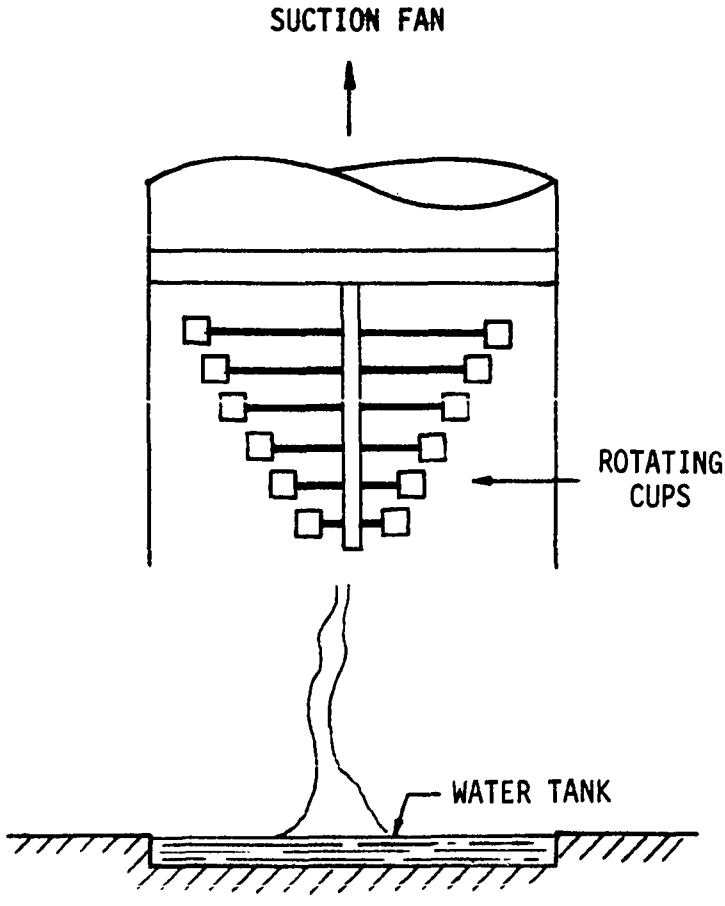

Figure 6. The laboratory vortex generator proposed by Fujita (Roberts, 1972).

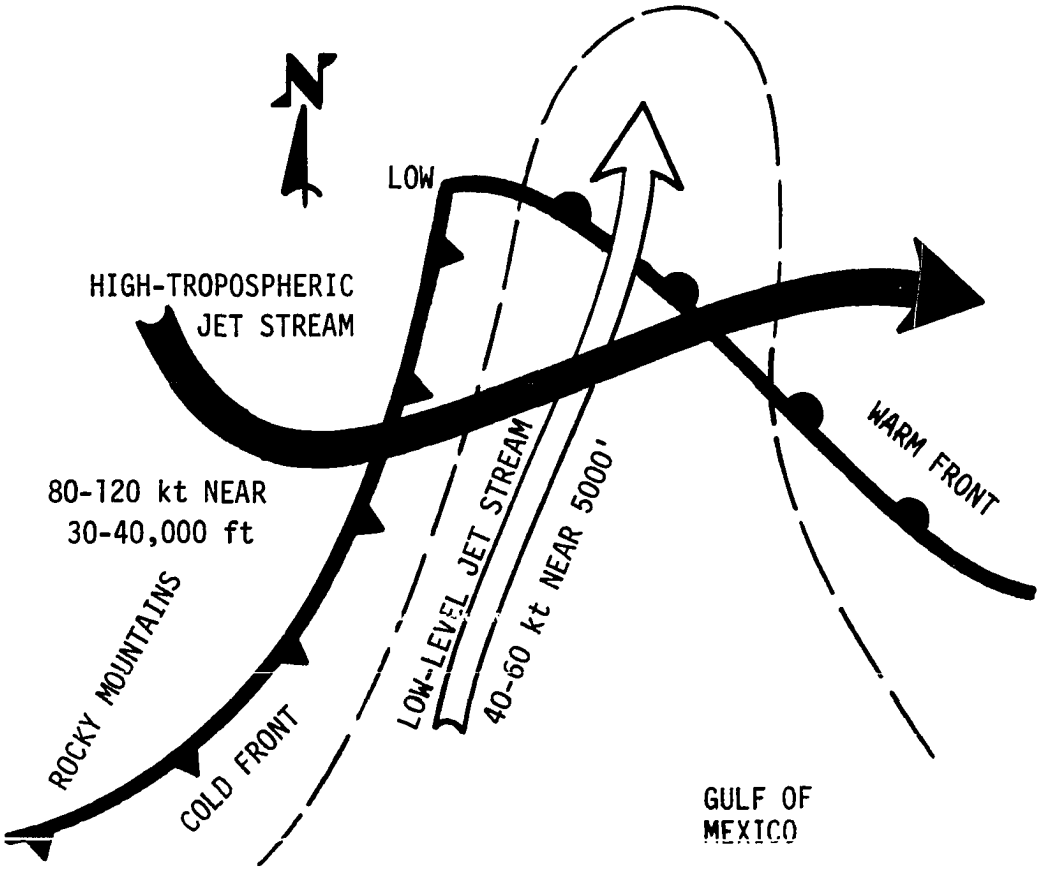

Figure 7. The schematic features of a midwestern macro-circulation.

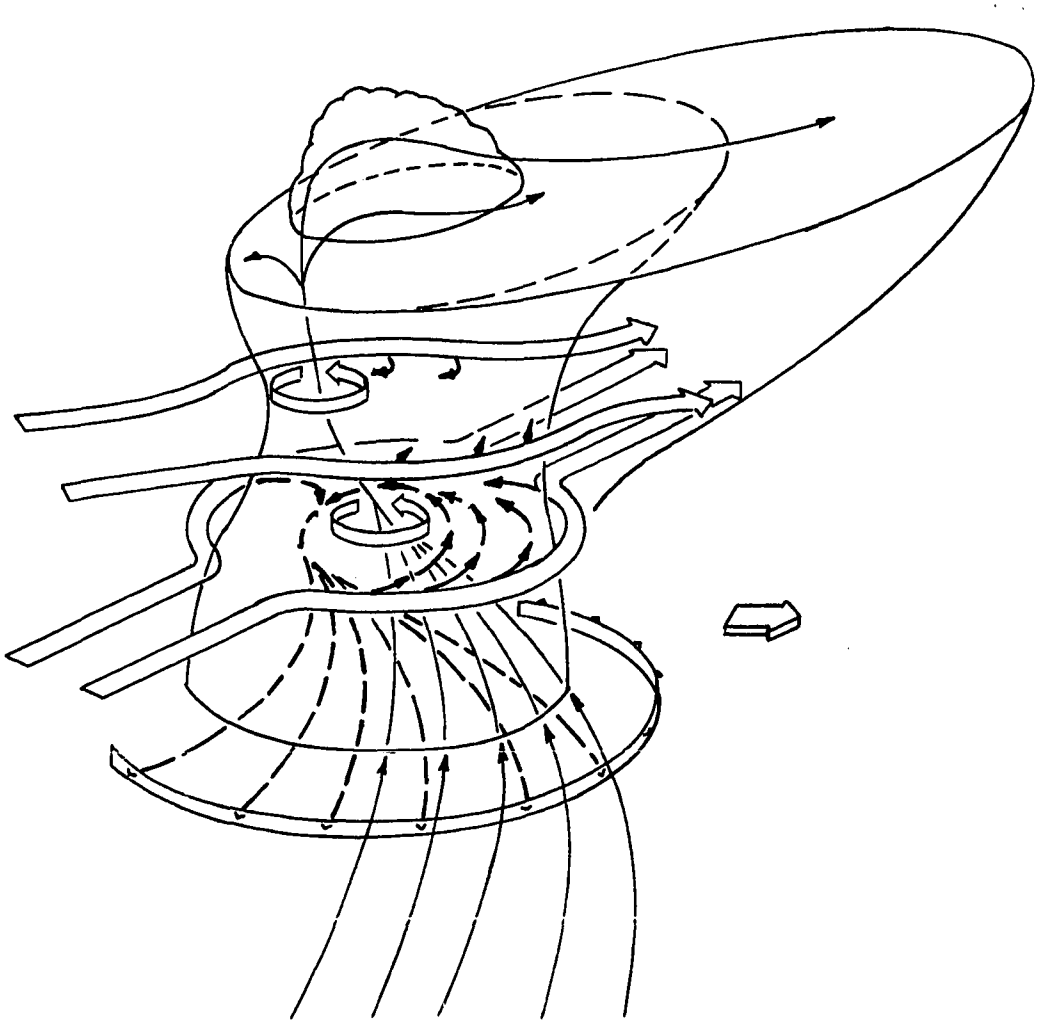

Figure 8. Three-dimensional model of the airflow within and around a cumulonimbus system. The thin, solid inflowing and ascending streamlines represent the history of moist air originating in the subcloud layer. The heavy dashed streamlines trace the entry and descent of potentially cold and dry middle-level air feeding downrushing and diverging downdraft. The internal circular bands signify net updraft rotation. (Fankhauser, 1971)

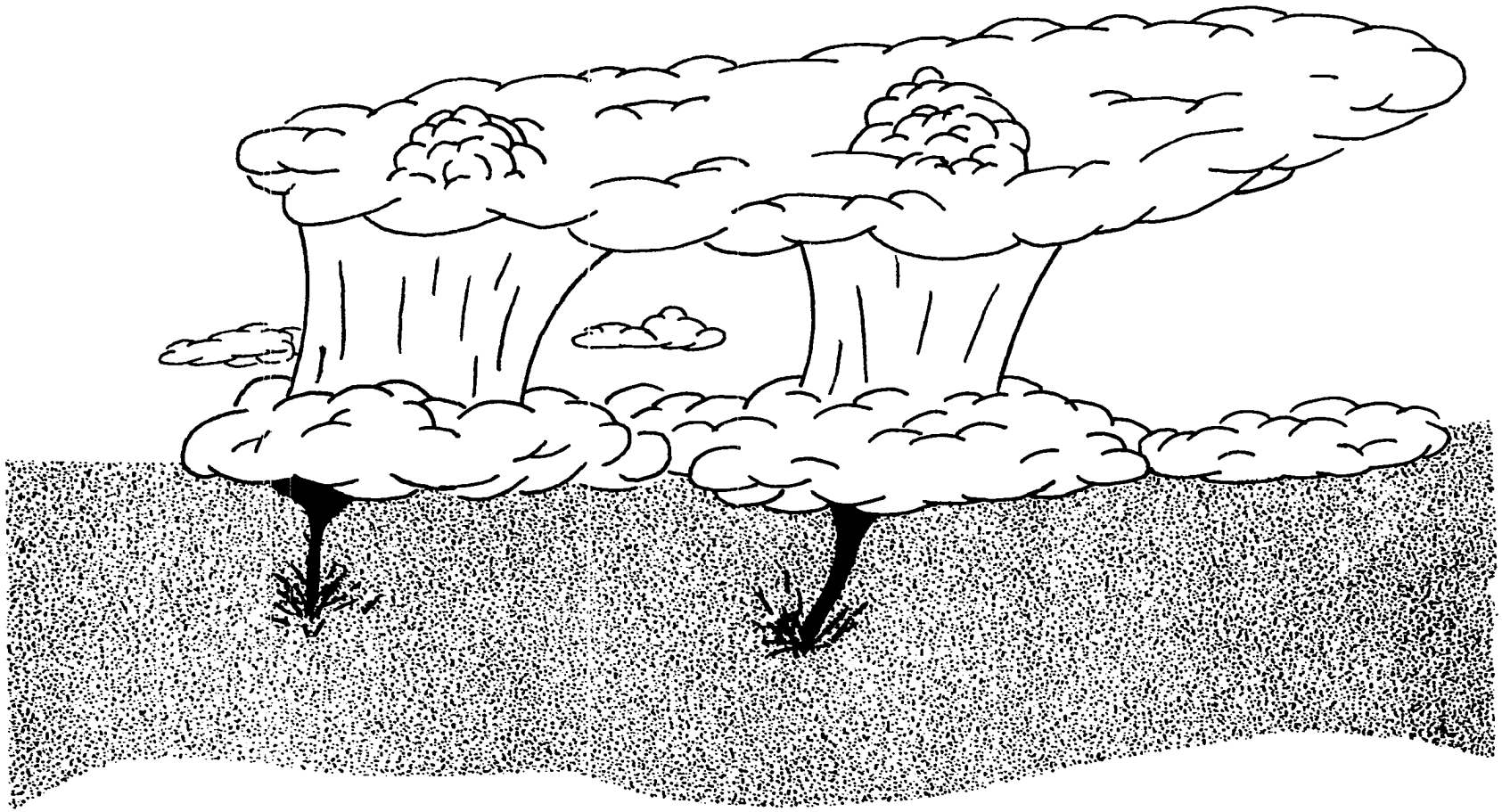

Figure 9. An approximate relationship between tornado cyclones and tornado vortices.

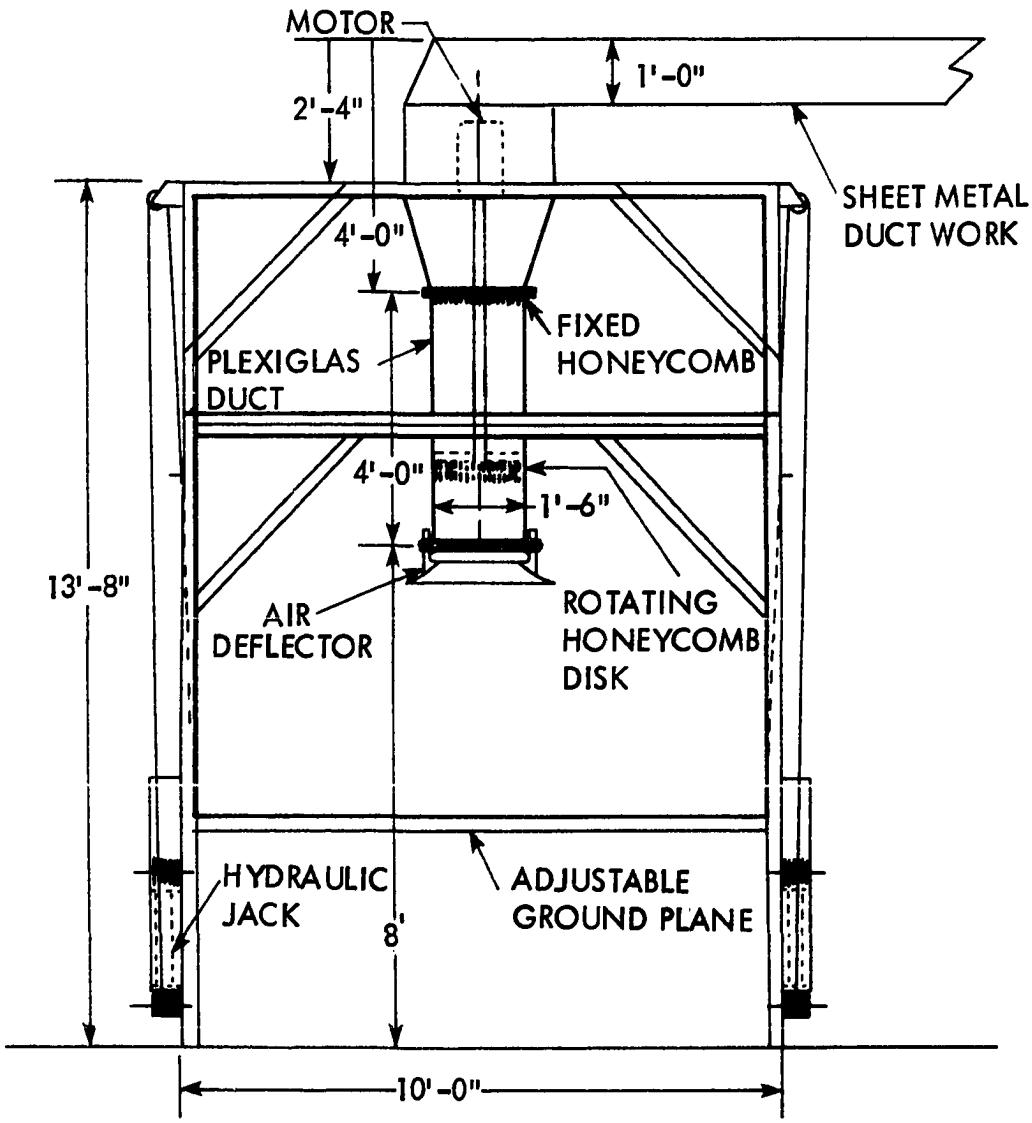

Figure 10. The schematic layout of the present tornado like vortex generator.

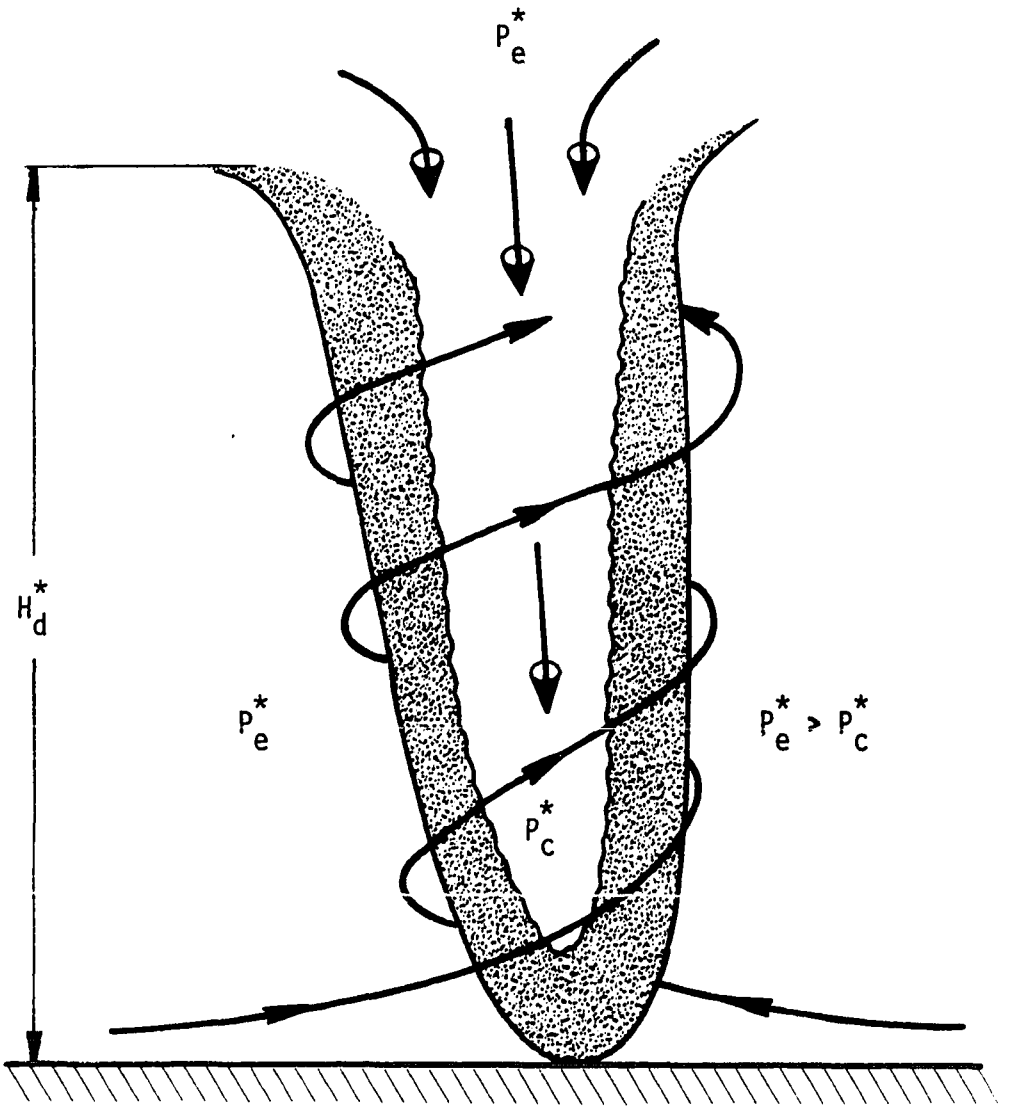

Figure 11. A possible explanation for the dust devil core downflow based on pressure differential.

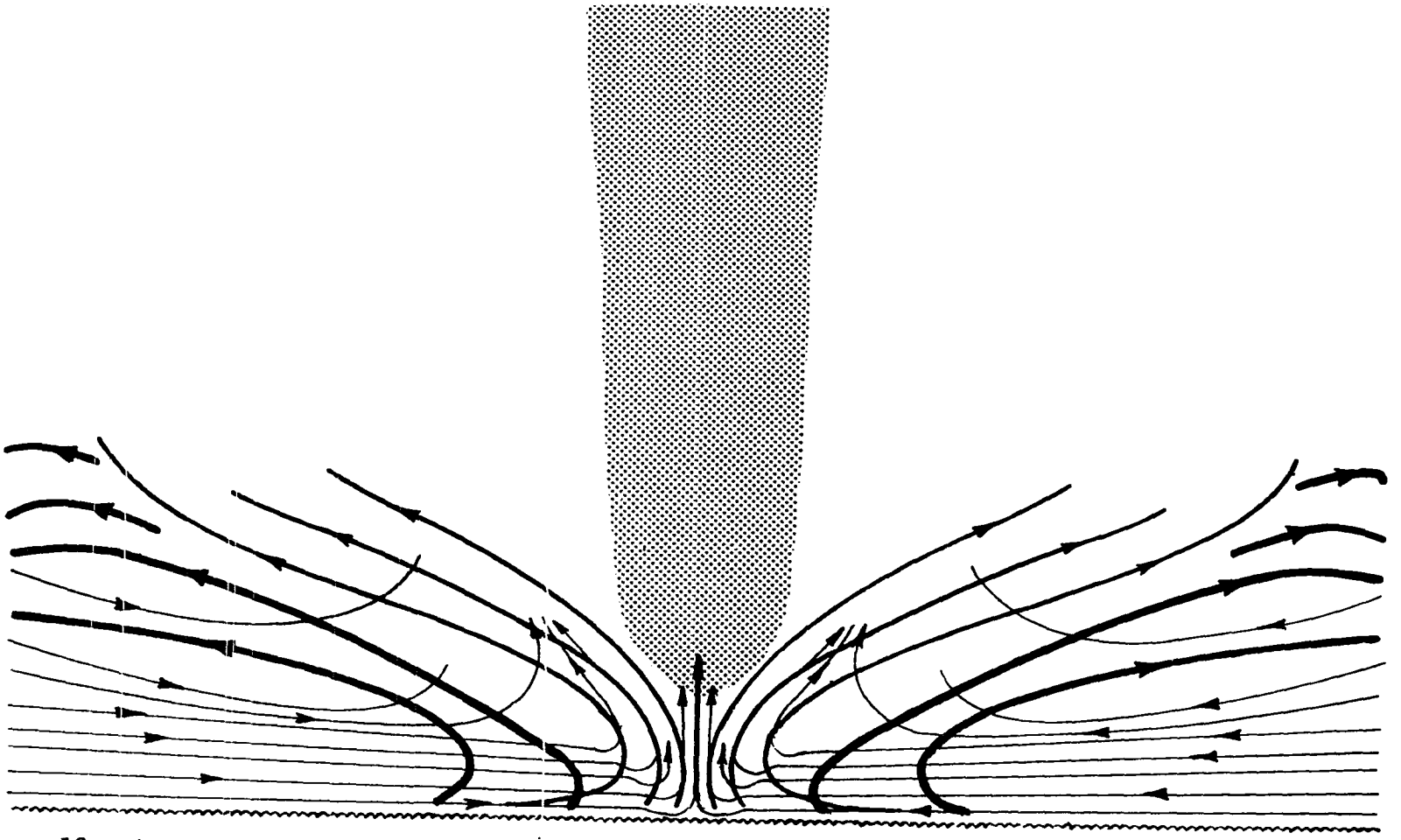

Figure 12. Approximate trajectory of inflowing particles in the meridional plane of the laboratory vortex flow. Thickest lines show the path of the larger and heavier debris, medium lines indicate the trajectory of smaller and lighter debris while thin lines represent the air flow pattern and the path of very fine particles. The shaded area indicates the funnel.

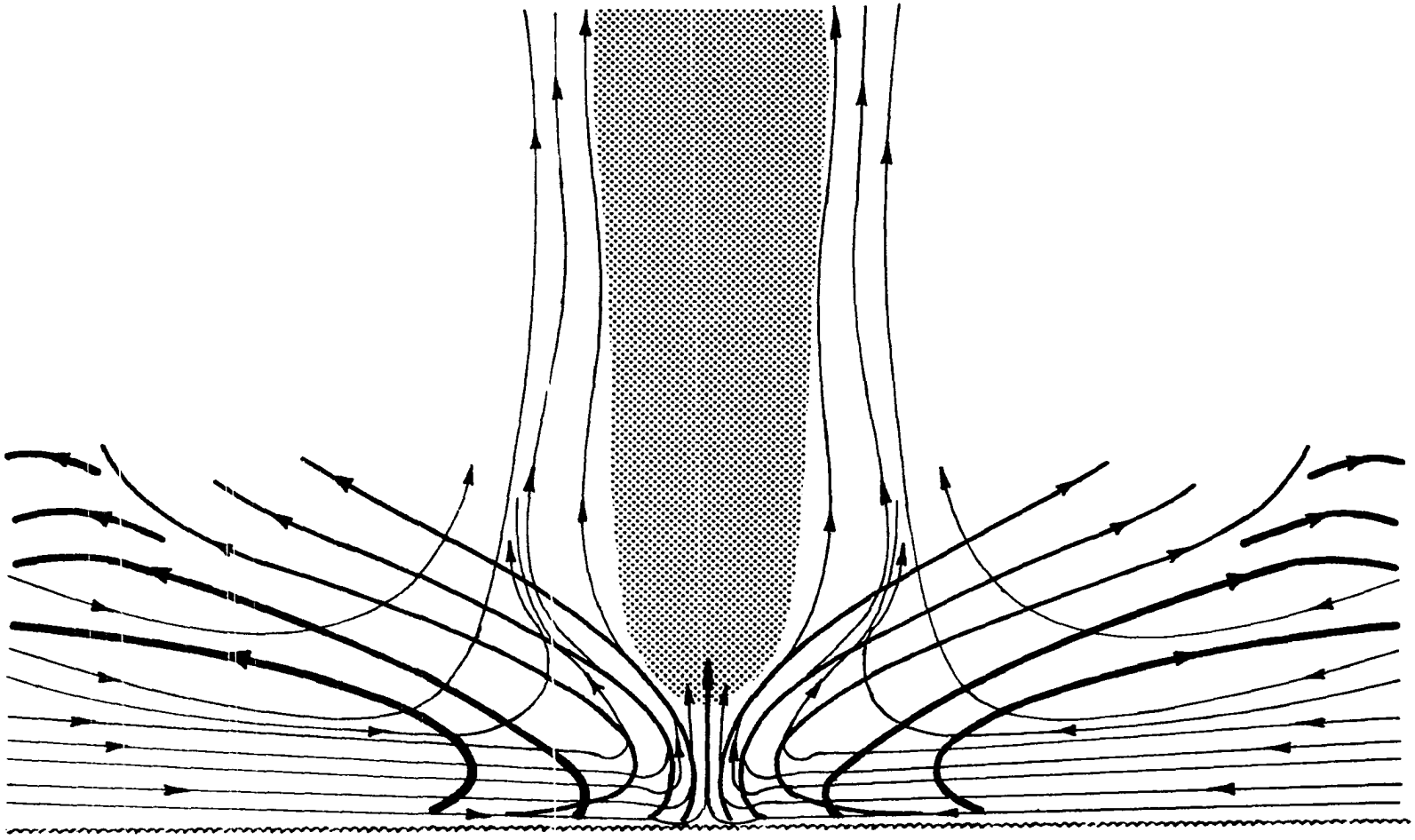

Figure 13. The airflow pattern in the meridional plane of the inner vortical tube, superimposed on the previous sketch.

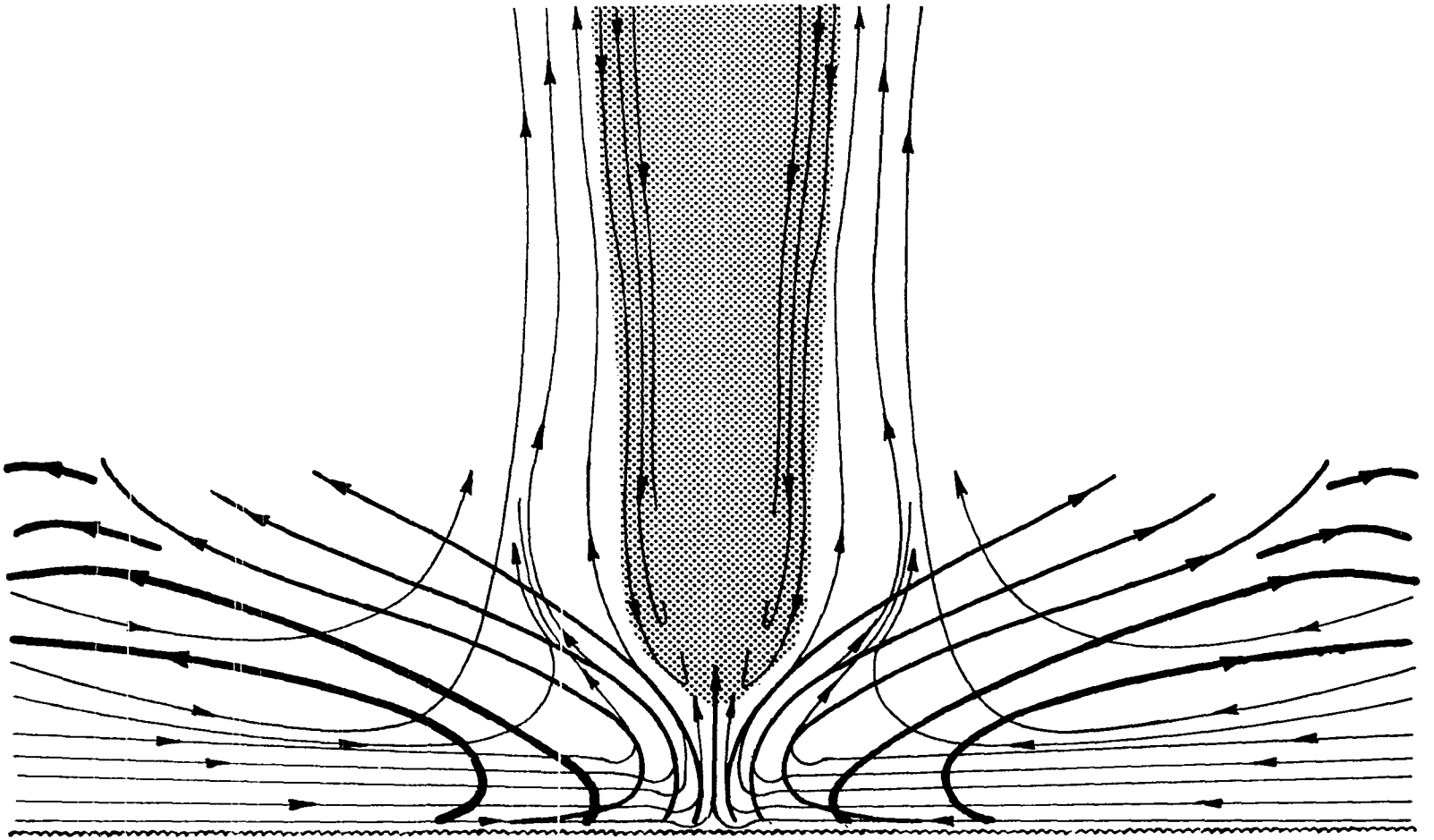

Figure 14. The airflow pattern in the meridional plane of the funnel, superimposed on the previous sketch.

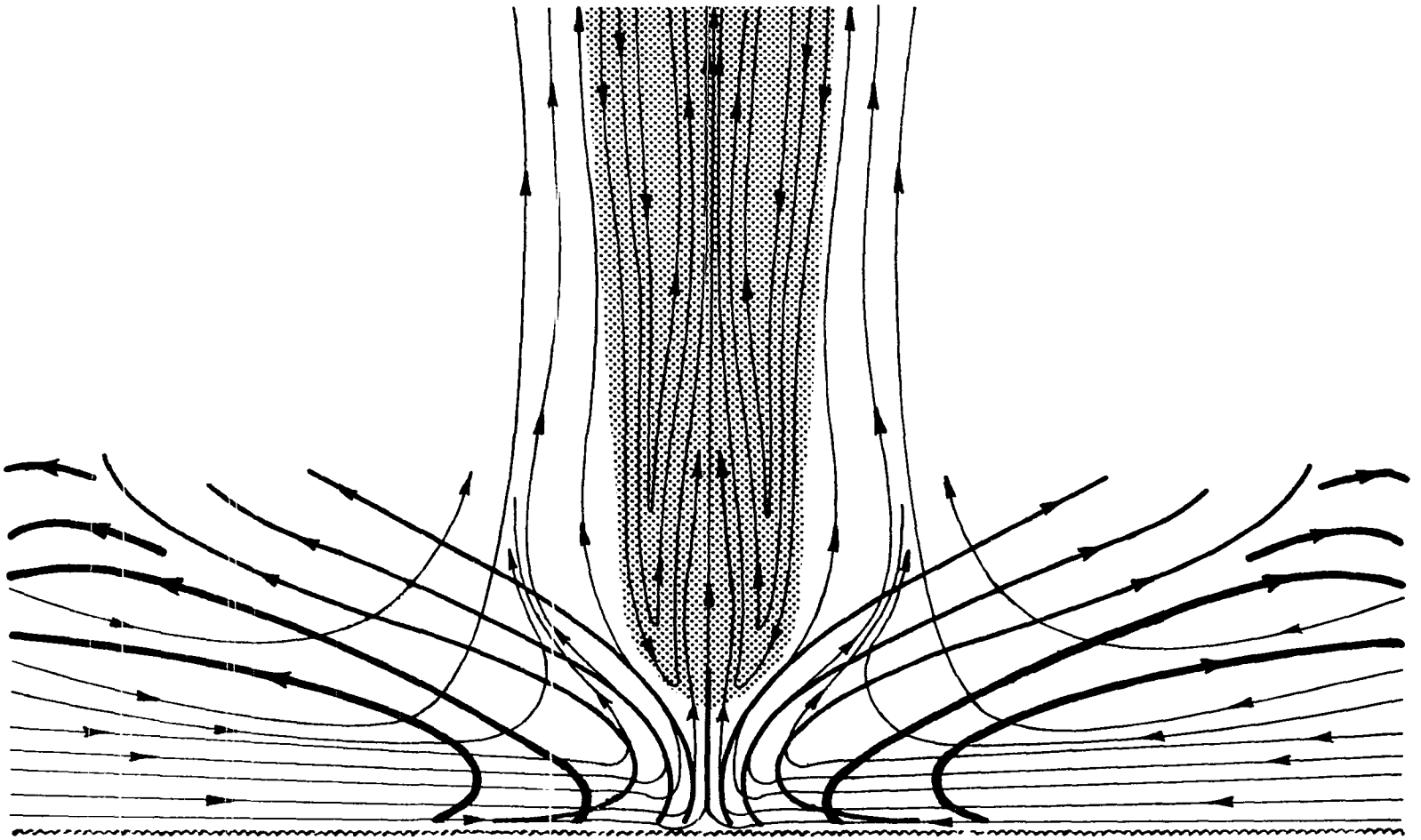

Figure 15. The airflow pattern in the meridional plane of the center jet, superimposed on the previous sketch.

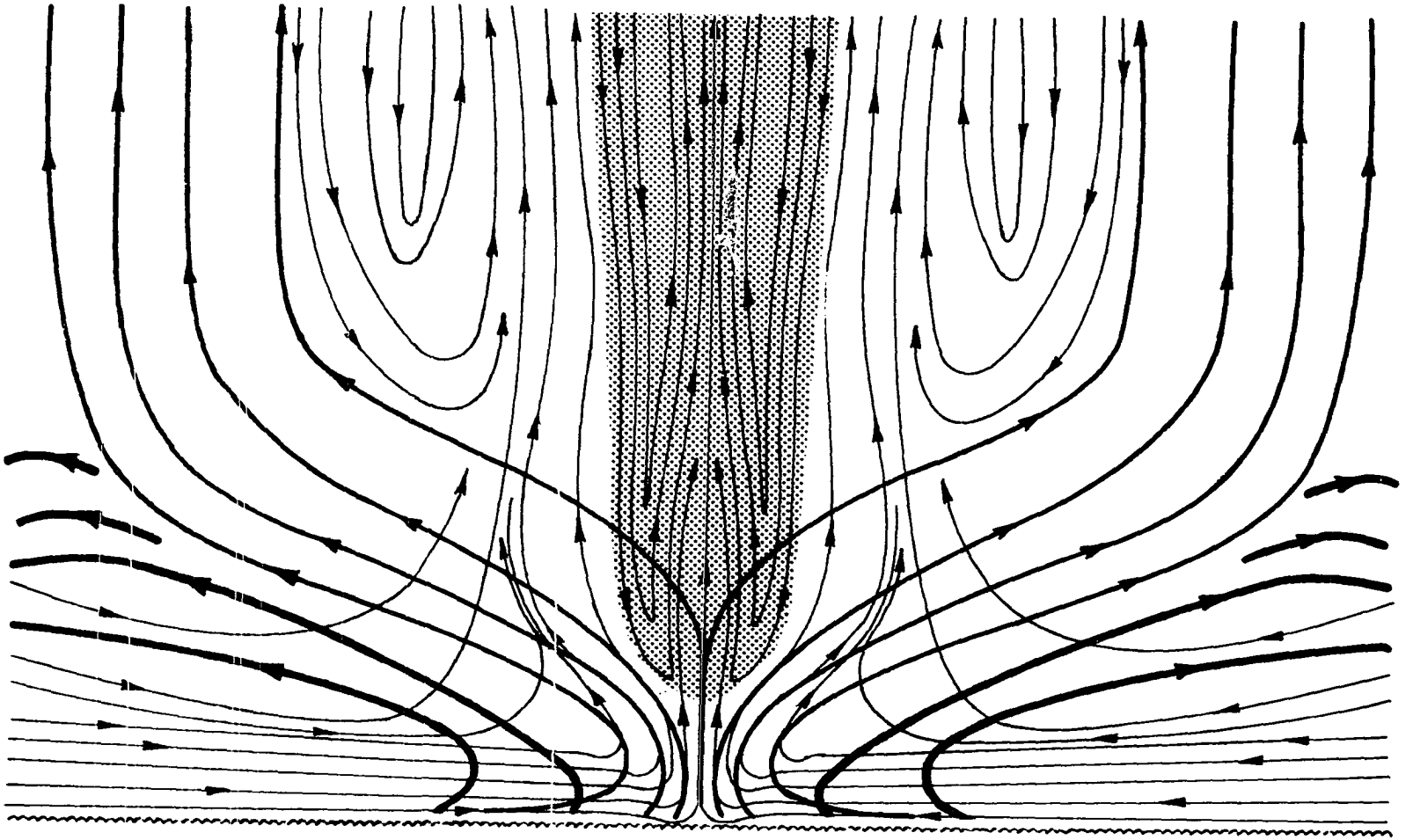

Figure 16. The airflow pattern in the meridional plane of the outer vortical tube and the possible second downflow region, superimposed on the previous sketch.

Figure 17. The flow pattern obtained by numerical techniques. All quantities shown are non-dimensionalized with respect to v_m^* (maximum tangential velocity outside of the boundary layer), r_m^* (radial position of v_m^*), and δ_o^* (reference boundary thickness at r = 0.2). (Hsu and Tesfamariam, 1975)

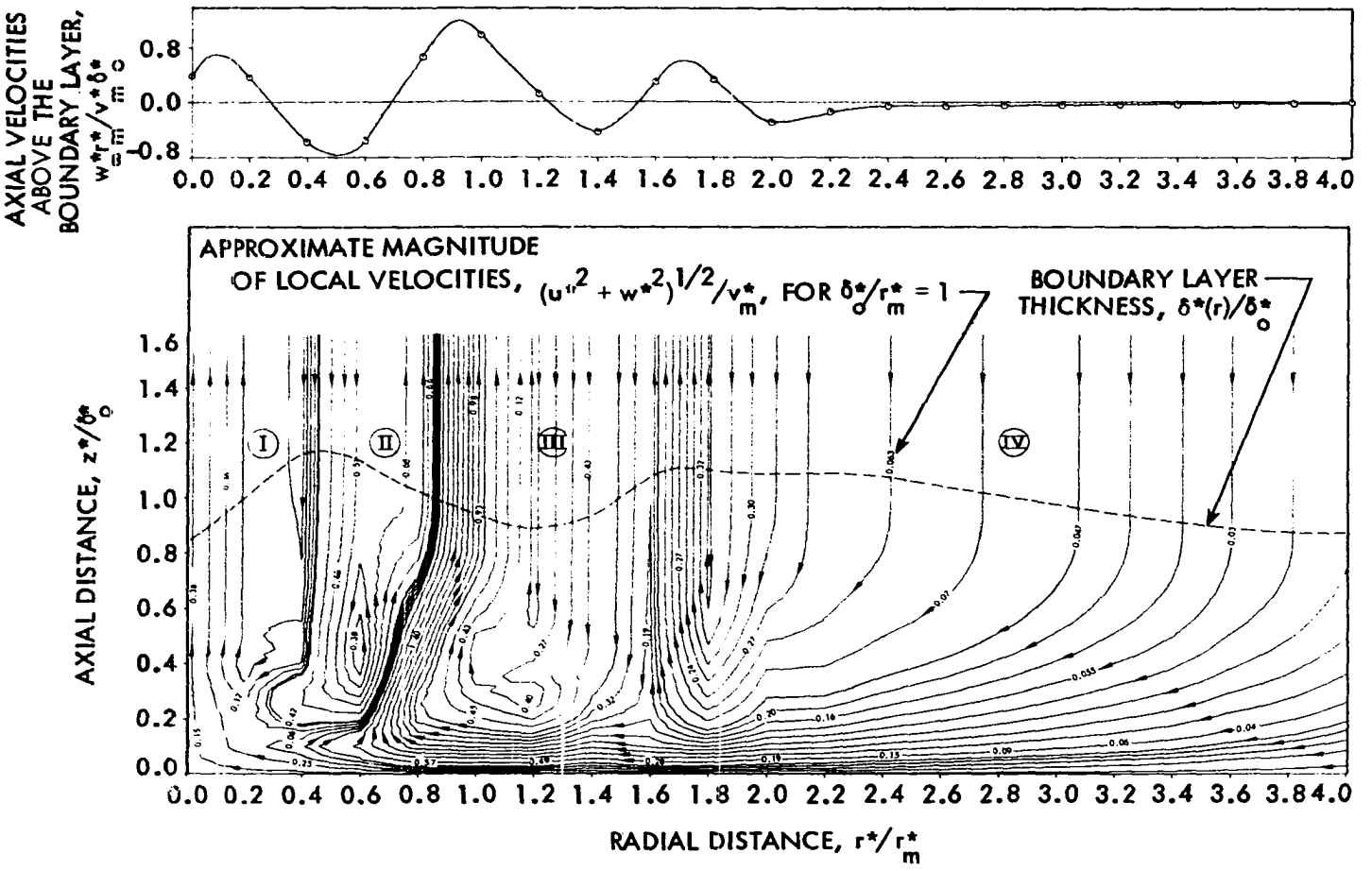
AXIAL VELOCITIES ABOVE THE BOUNDARY LAYER, $w^*r^*/v^*\delta^*_m$
0.8
0.0
-0.8
0.0 0.2 0.4 0.6 0.8 1.0 1.2 1.4 1.6 1.8 2.0 2.2 2.4 2.6 2.8 3.0 3.2 3.4 3.6 3.8 4.0
APPROXIMATE MAGNITUDE OF LOCAL VELOCITIES, $(u^{*2} + w^{*2})^{1/2}/v^*_m$, FOR $\delta^*_o/r^*_m = 1$
BOUNDARY LAYER THICKNESS, $\delta^*(r)/\delta^*_o$
I
II
III
IV
AXIAL DISTANCE, z^*/δ^*_o
1.6
1.4
1.2
1.0
0.8
0.6
0.4
0.2
0.0
0.0 0.2 0.4 0.6 0.8 1.0 1.2 1.4 1.6 1.8 2.0 2.2 2.4 2.6 2.8 3.0 3.2 3.4 3.6 3.8 4.0
RADIAL DISTANCE, r^*/r^*_m

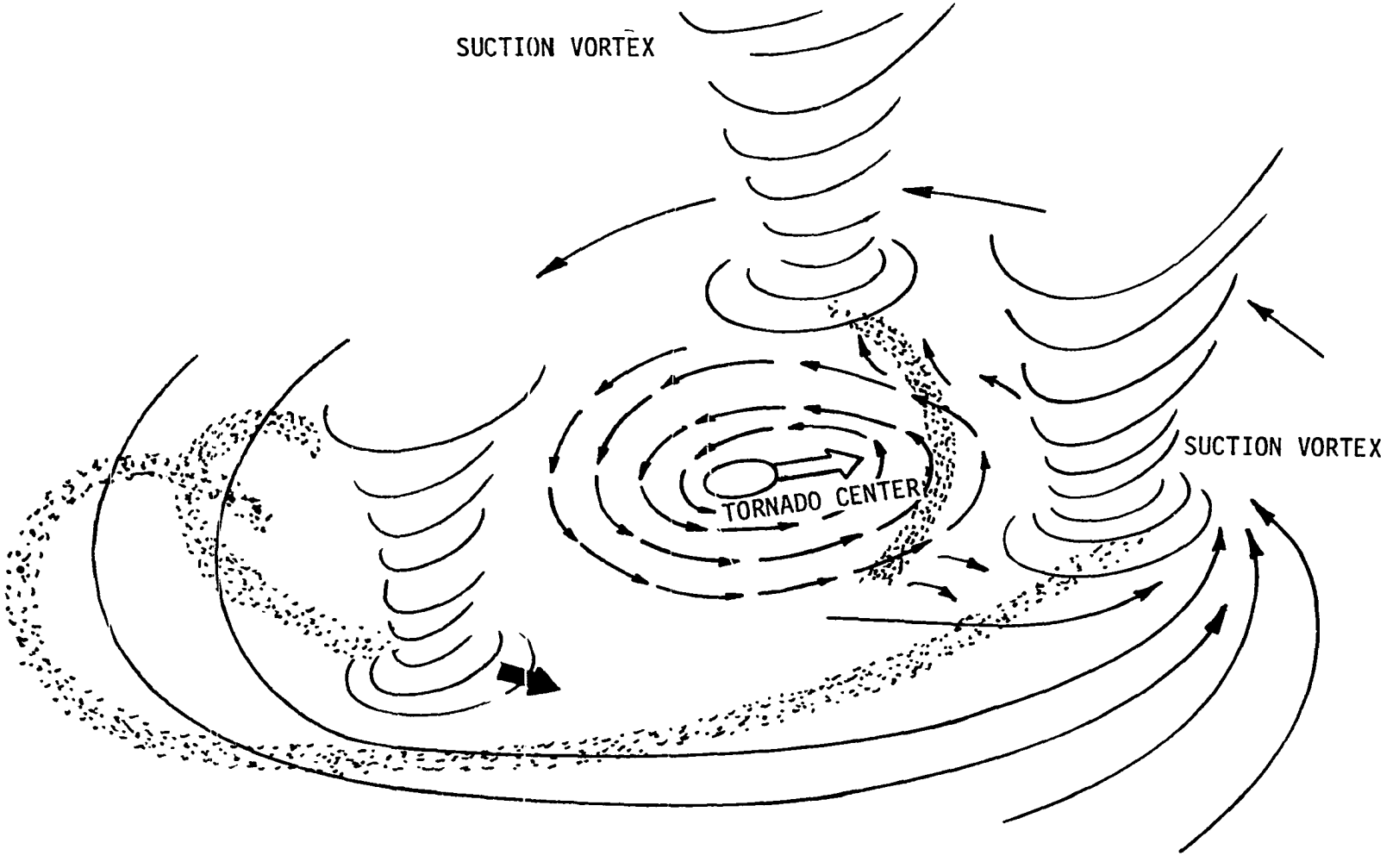

Figure 18. Model of multi-suction tornado proposed by Fujita (1971). Shaded areas show the paths of such suction vortices as they travel around the translating main core.

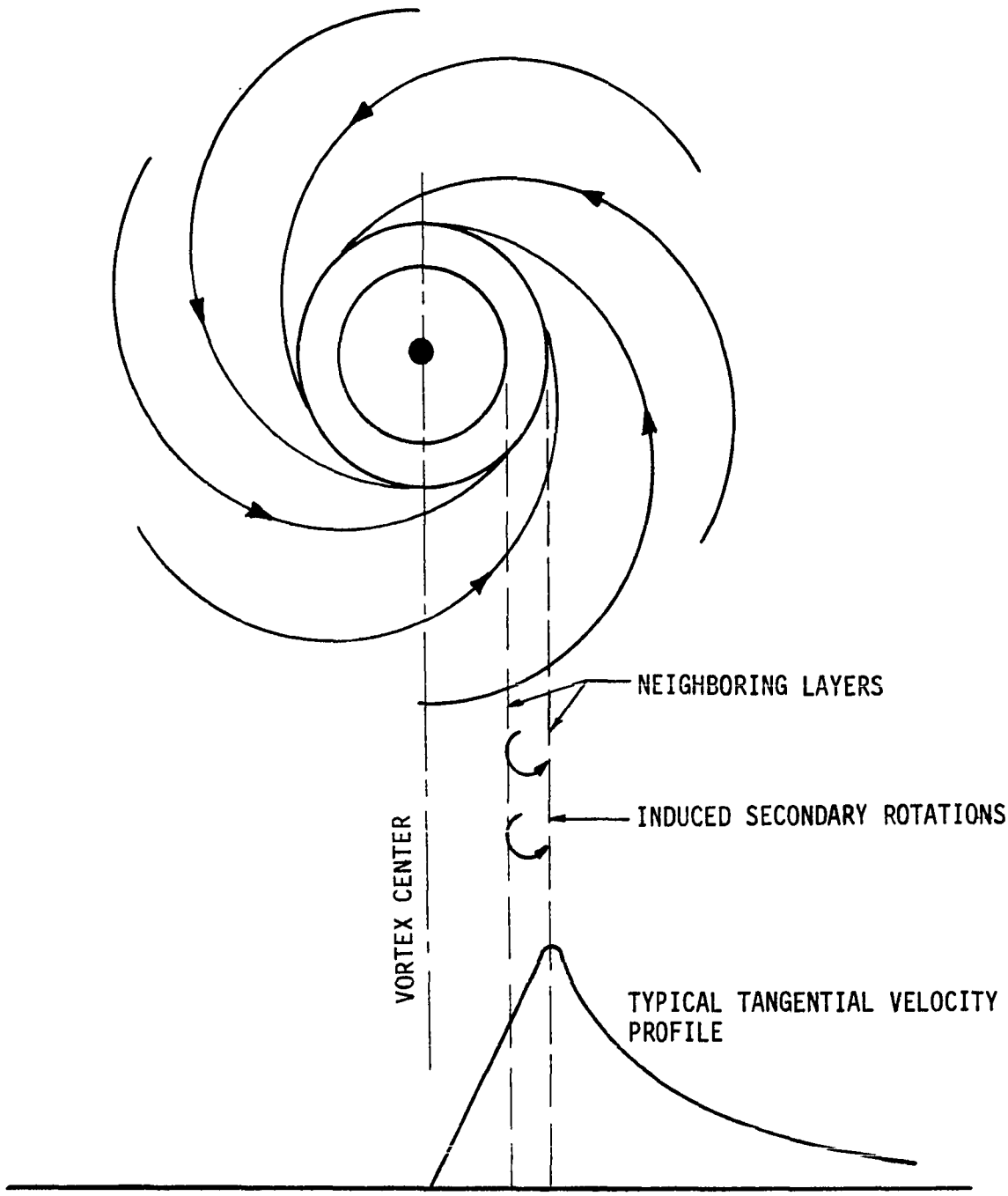

Figure 19. Possible mechanism of formation of secondary vortices.

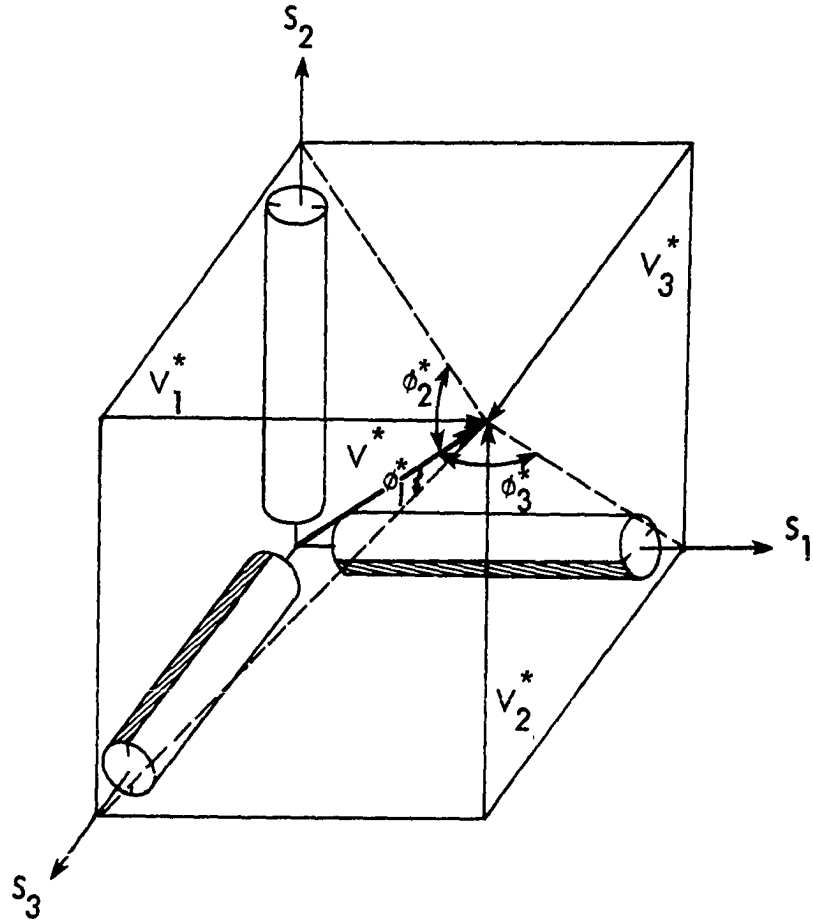

Figure 20. Three orthogonal split film sensors for total vector measurement.

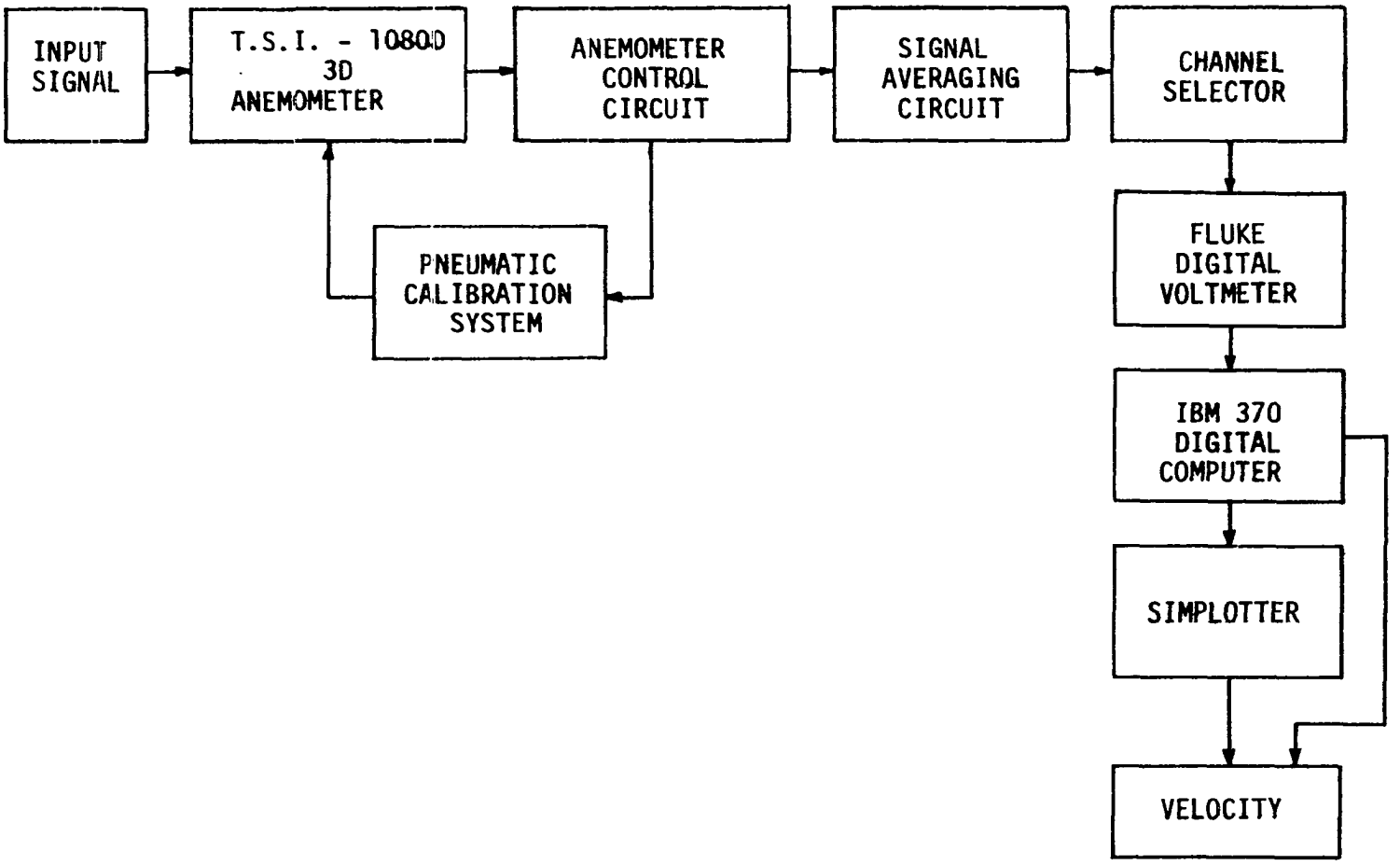

Figure 21. Schematic diagram of the data processing and handling system for 3-D measurement of velocity in a simulated tornado field.

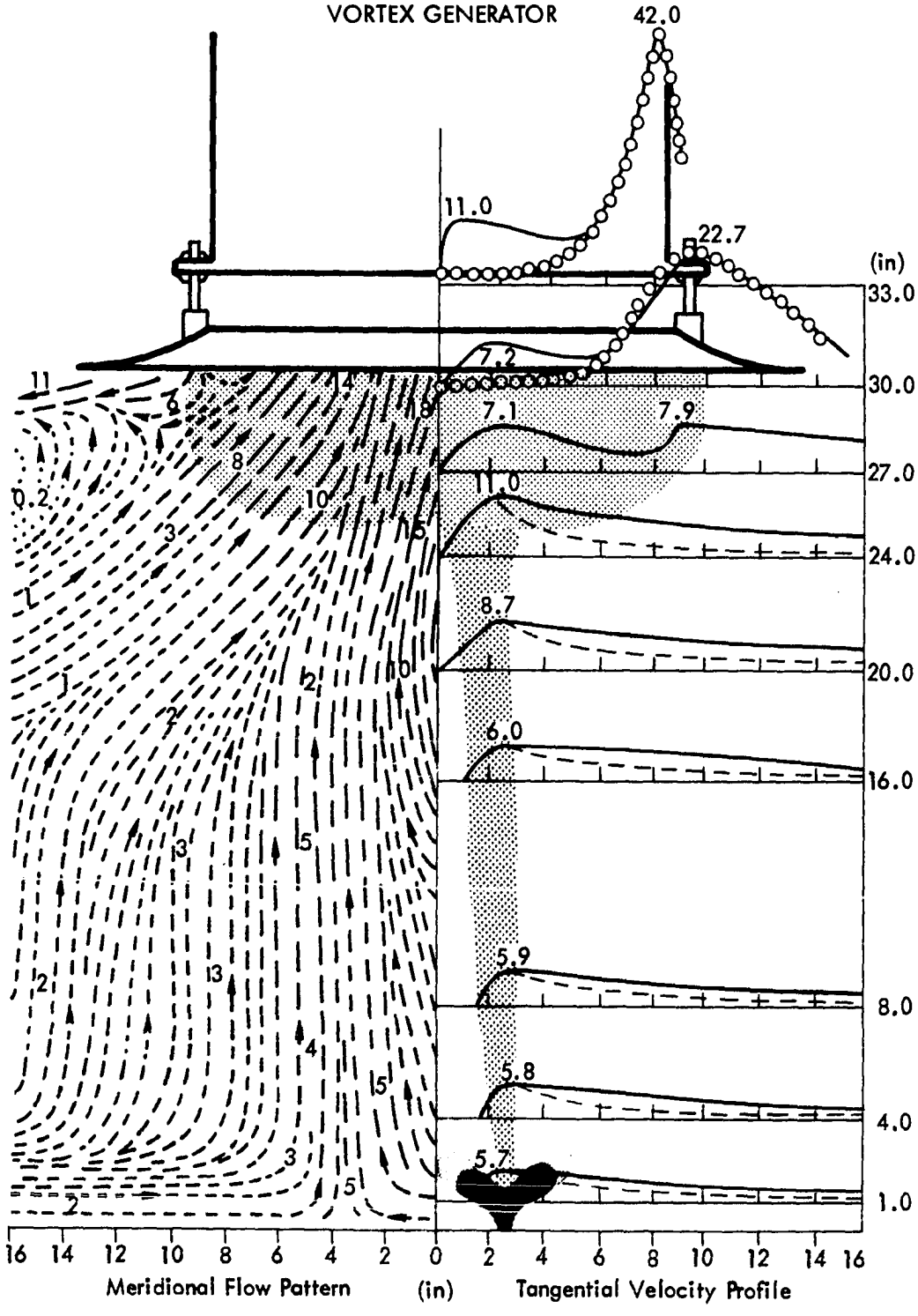

Figure 22. Time-averaged velocity measurement for meridional flow pattern and tangential velocity profiles. The circles indicate tangential velocity profiles for no ground plane condition.

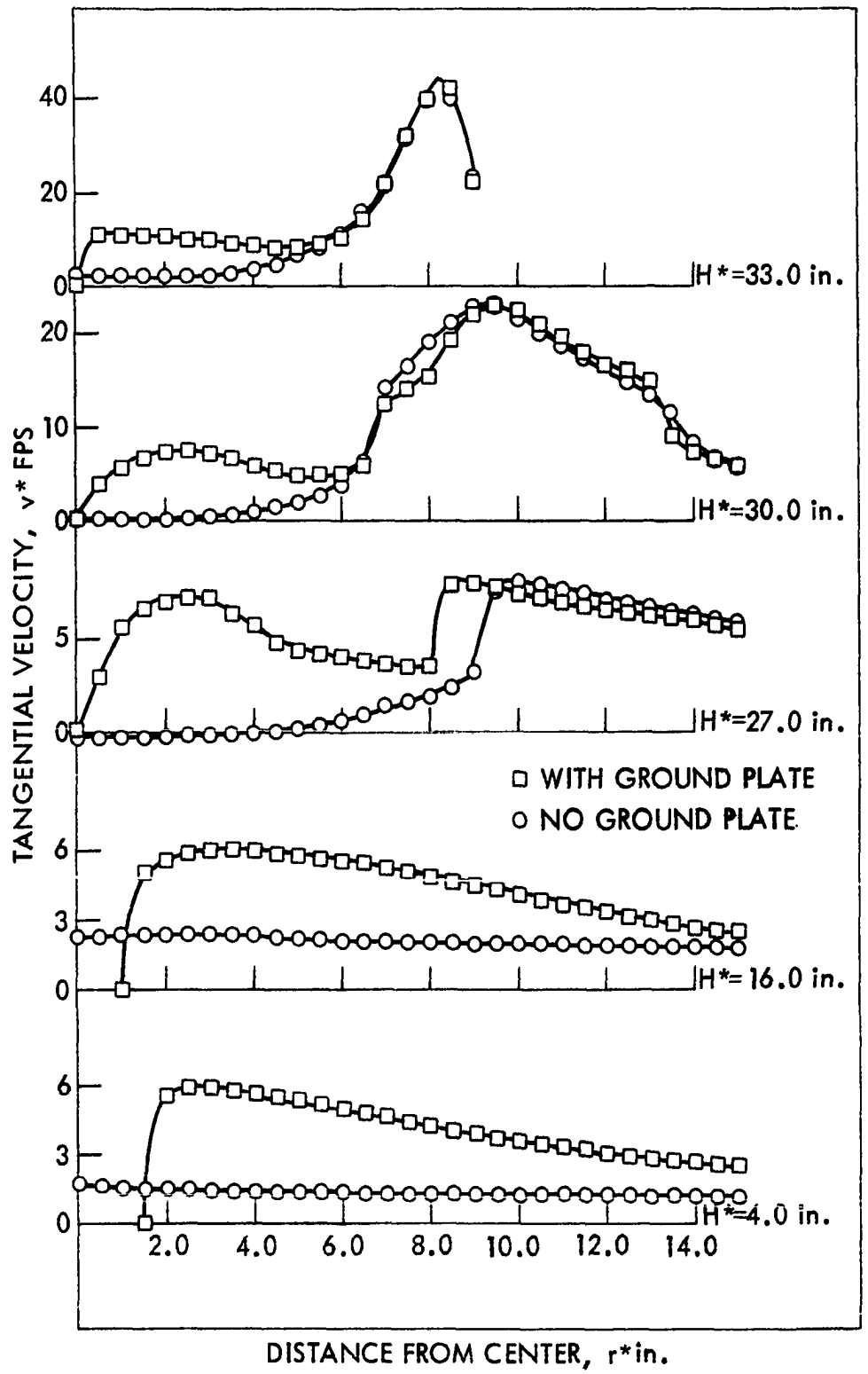

Figure 23. Ground effect on tangential velocity profiles of different heights, H*.

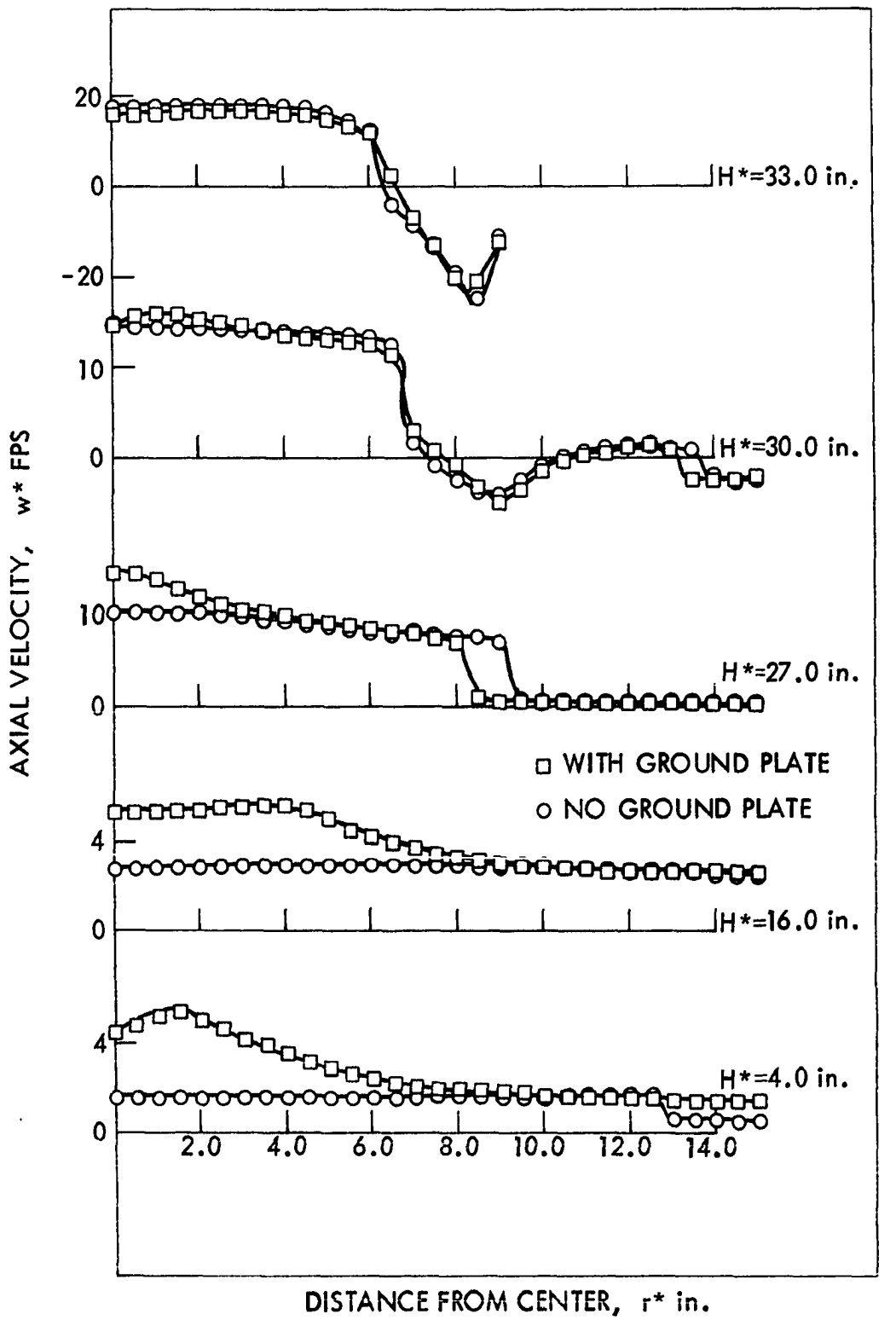

Figure 24. Ground effect on axial velocity profiles of different heights, H*.

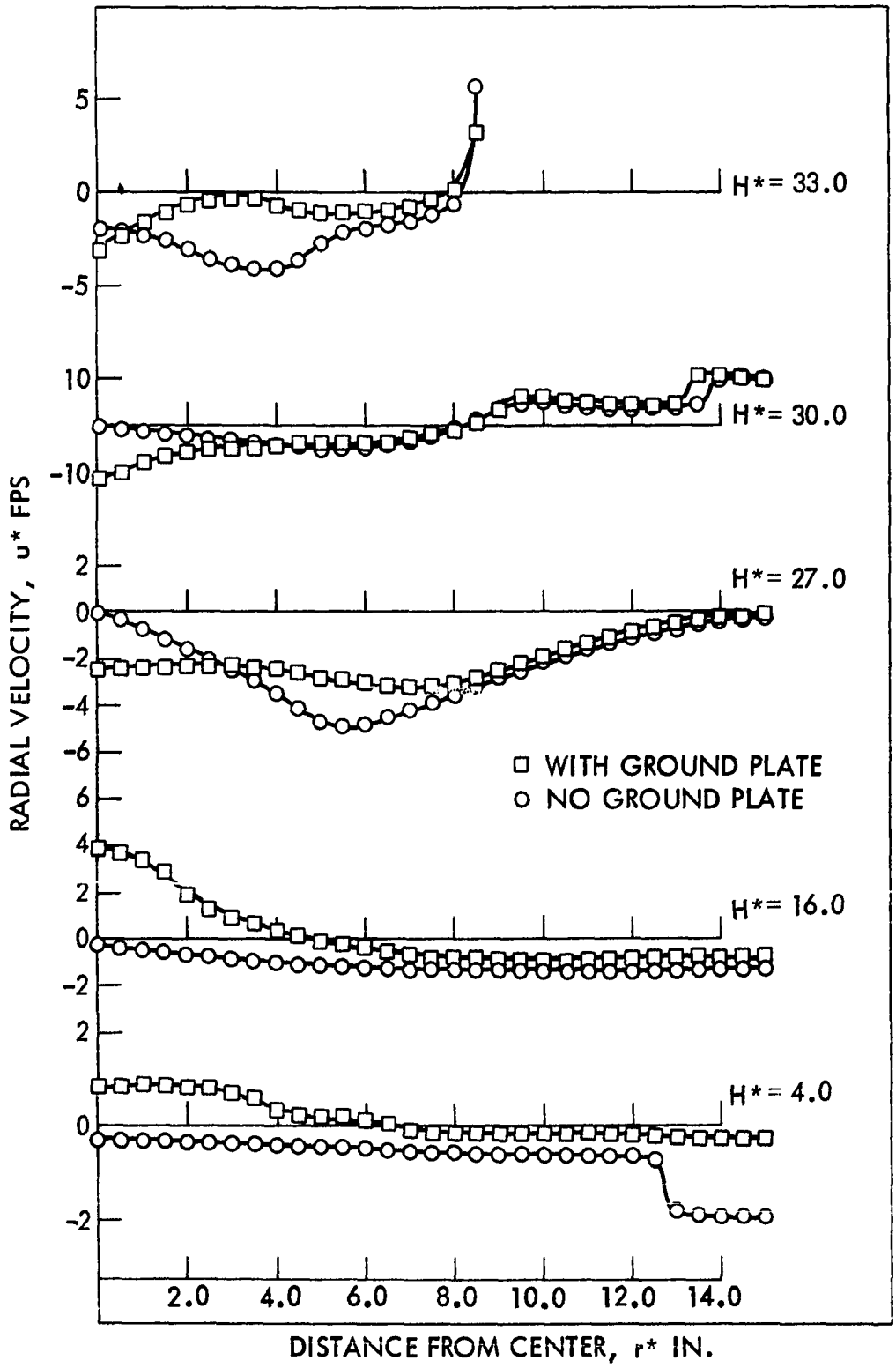

Figure 25. Ground effect on radial velocity profiles of different heights, H^*.

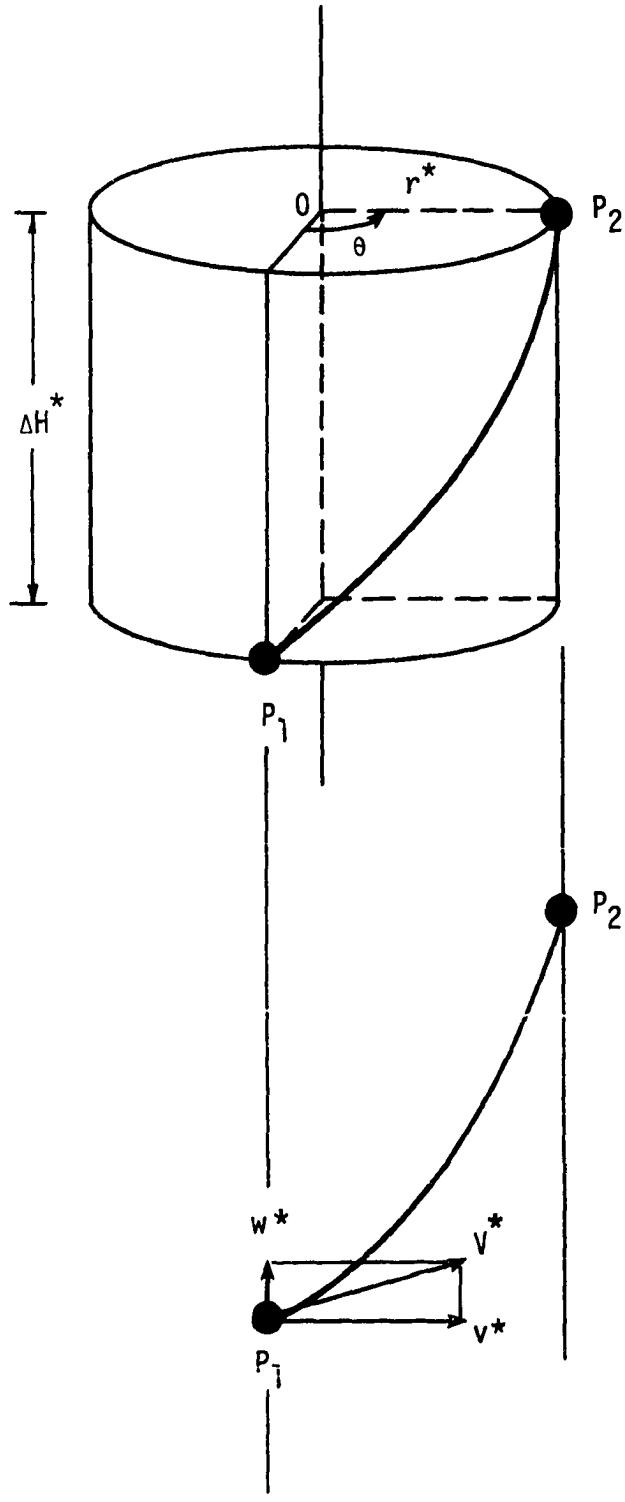

Figure 26. Sketch of the motion of a cloud element around the vortical tube of the laboratory vortex.

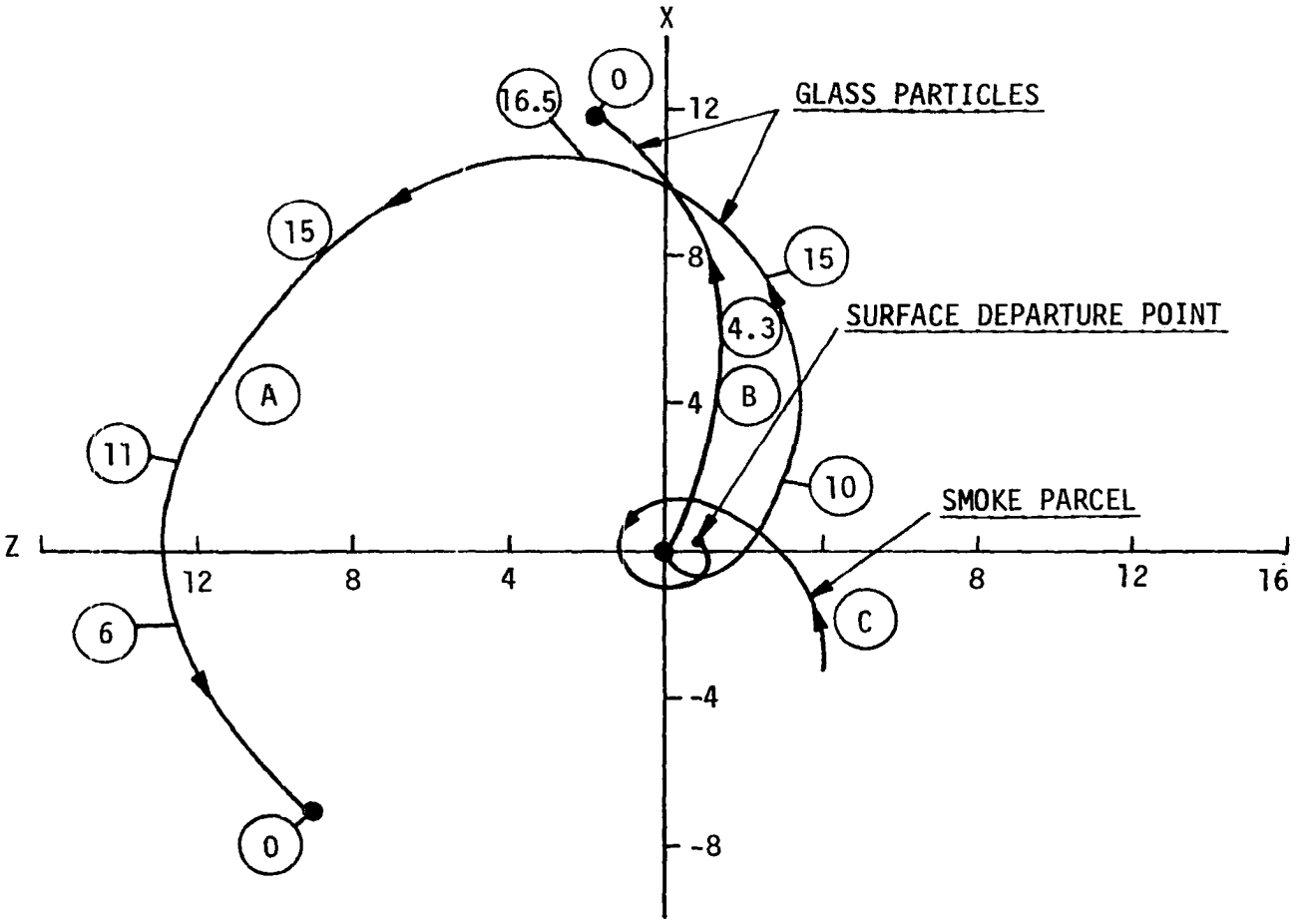

Figure 27. Typical projected trajectories of: (A) a high flying particle, (B) a low flying particle, and (C) an inflow particle on the horizontal plane XZ. Numbers in the circles indicate the distance from the ground plane in inches.

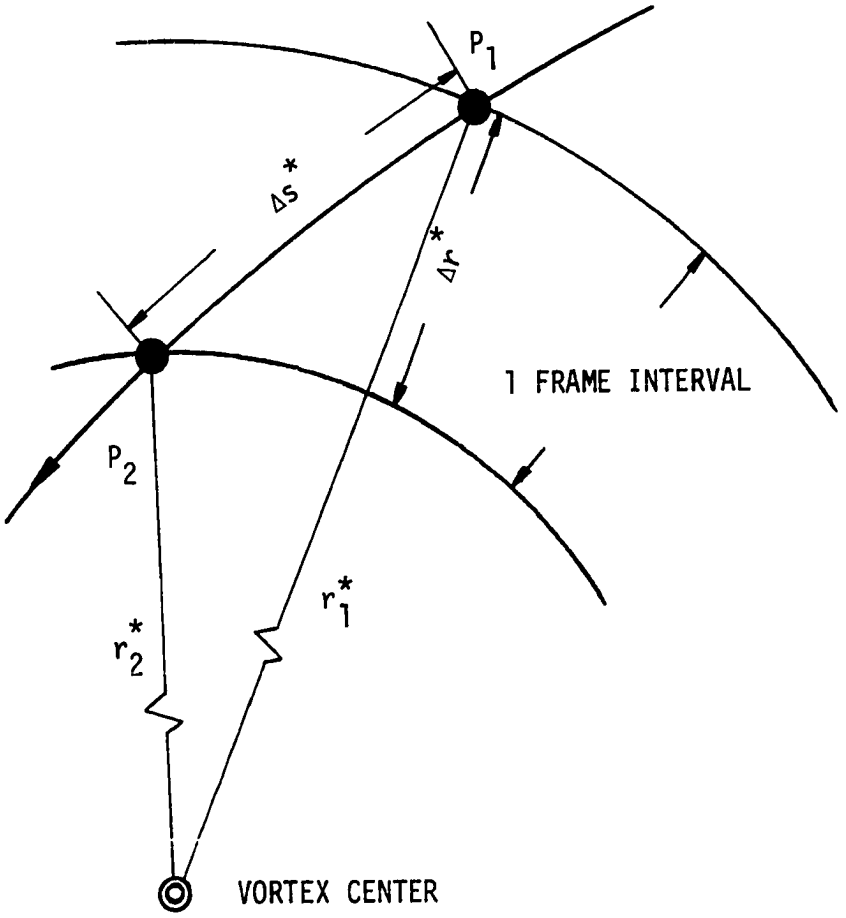

Figure 28. Sketch illustrating the technique used to measure total, tangential and radial speeds of an inflowing particle in the boundary layer of the laboratory vortex flow.

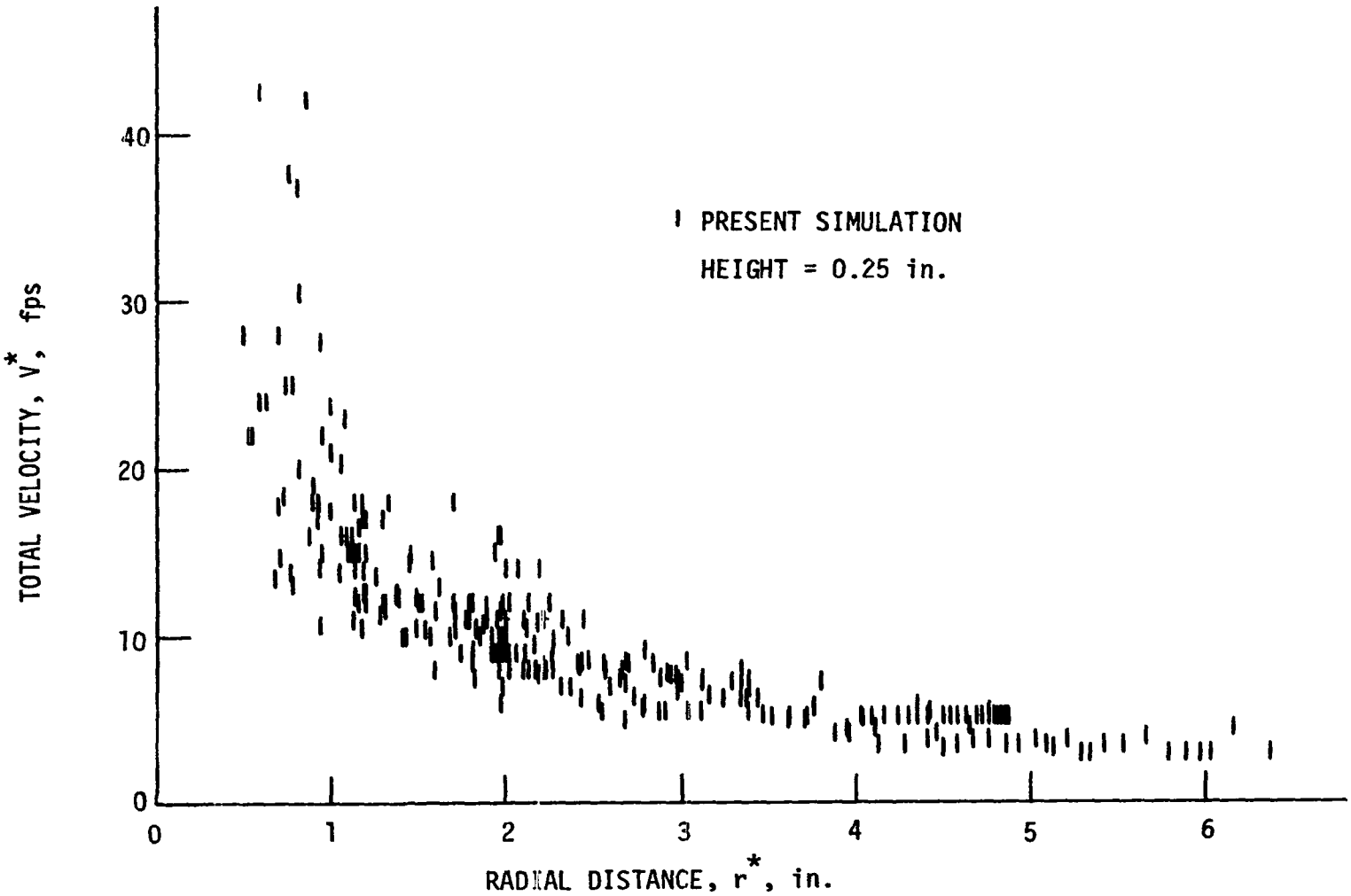

Figure 29. Total velocity of inflowing air as measured by the method shown in Fig. 28. A total of 276 data points are plotted.

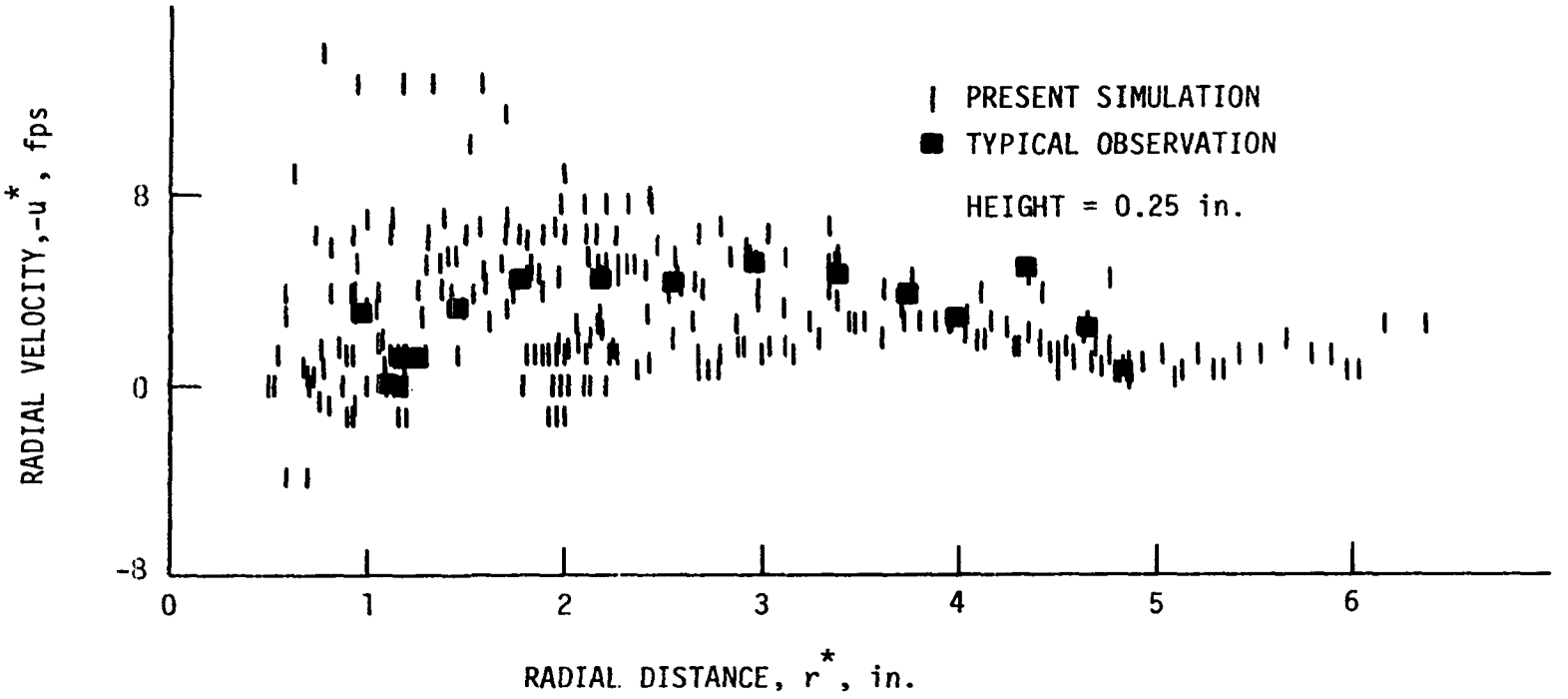

Figure 30. Radial velocity of inflowing air vs. radial distance from the center of the vortex. Solid squares indicate the radial speed of the particle of Fig. 27C.

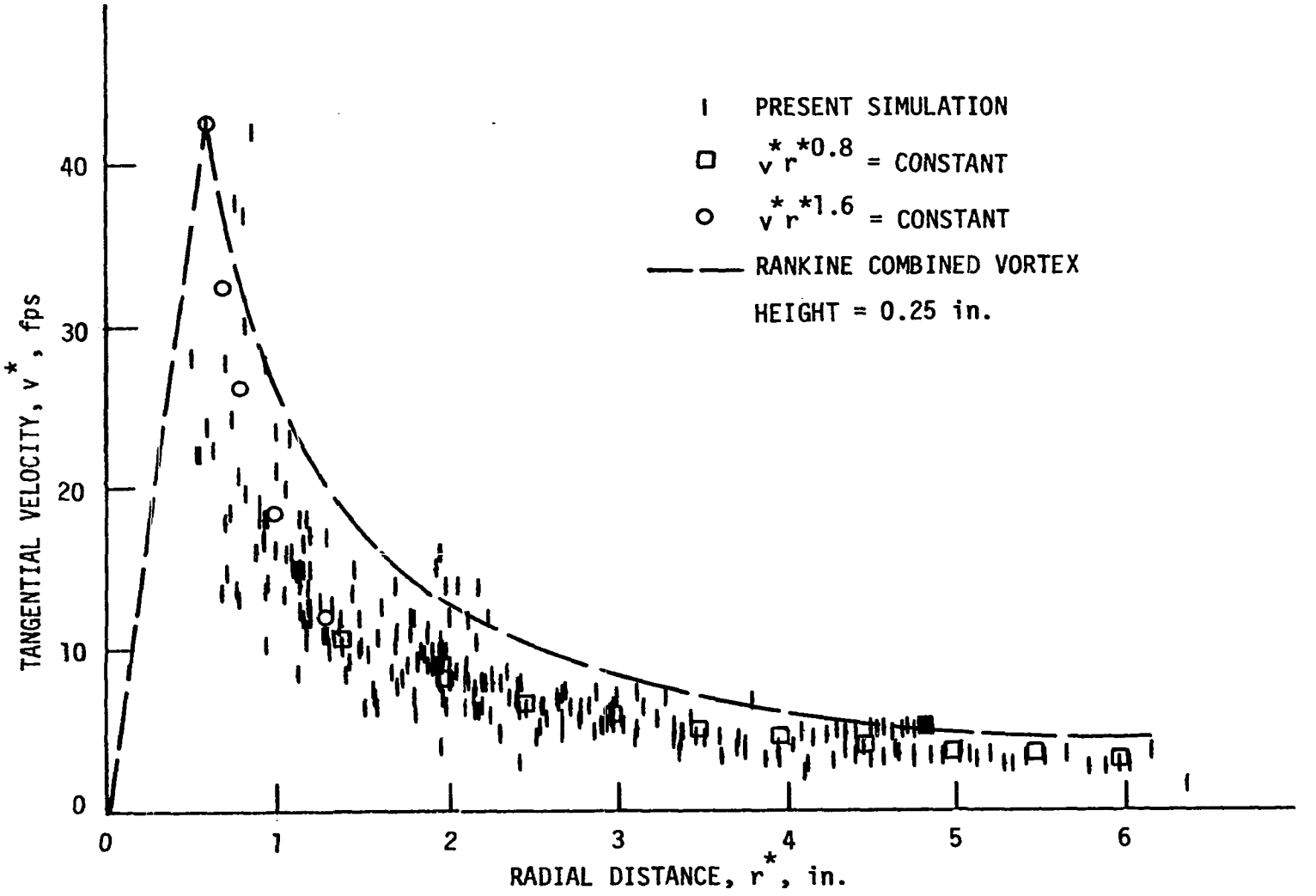

Figure 31. Tangential velocity of inflowing air vs. radial distance from the center of the vortex.

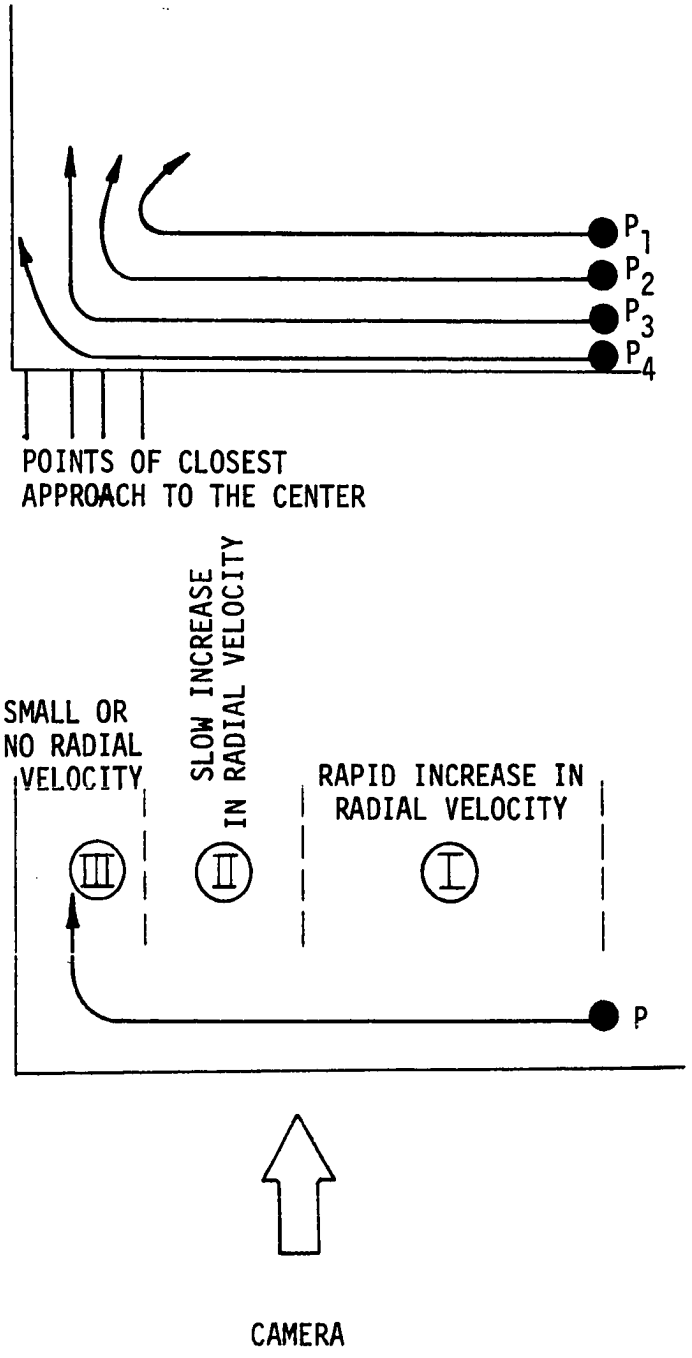

Figure 32. Typical paths of inflowing particles towards the instantaneous center of rotation.

Figure 33. Tangential isotachs in the laboratory vortex flow field. Numbers indicate the magnitude of the tangential wind speeds in feet per second. Data points shown with solid squares indicate the speeds in the downflowing funnel, while solid triangles are those data points obtained from Fig. 31. The shaded area indicates the band of maximum tangential velocity.

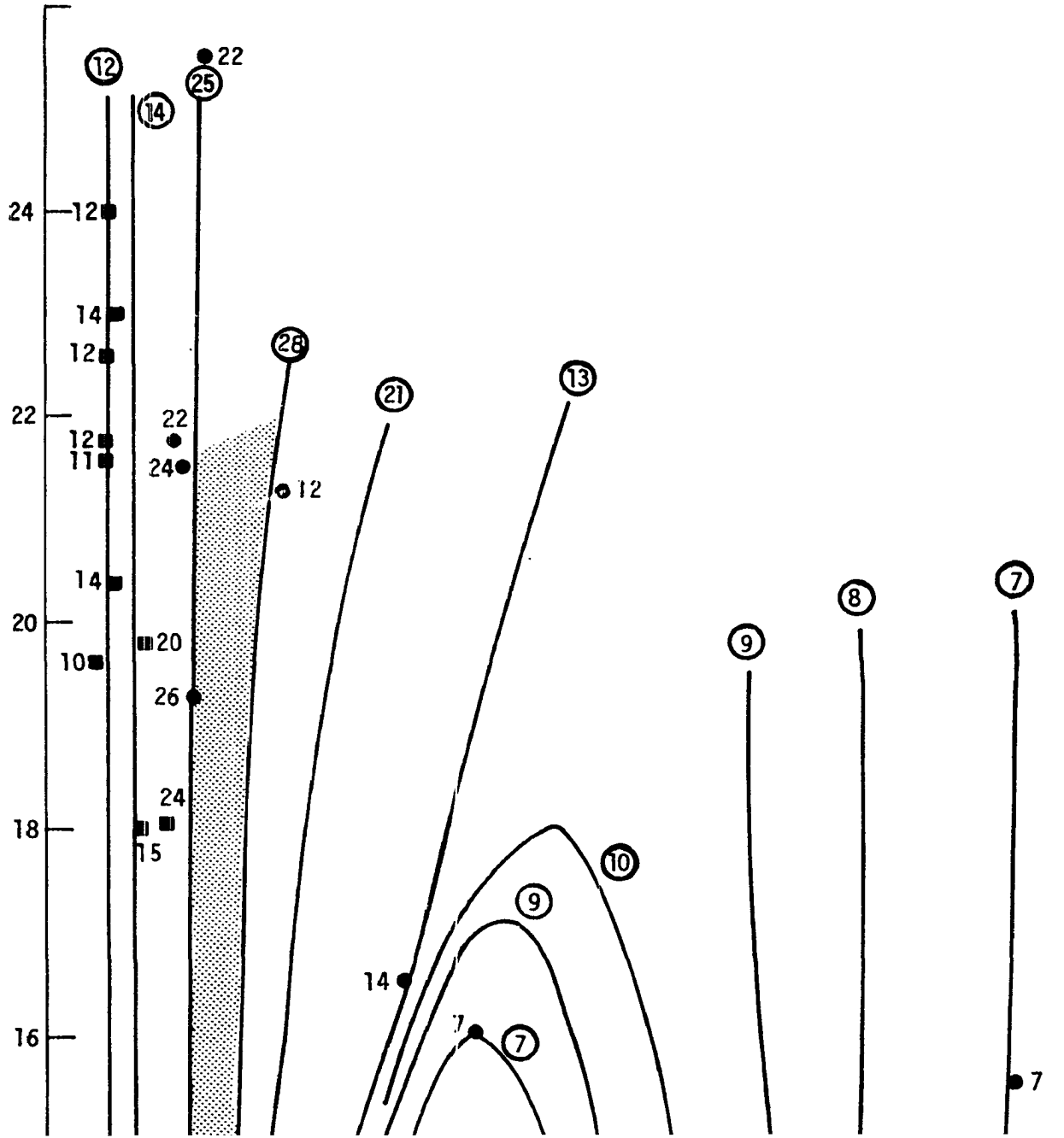
24
22
20
18
16
12
25
14
28
21
13
10
9
8
7
12
14
12
12
11
14
10
22
24
12
20
26
24
15
22
14
7
7
7

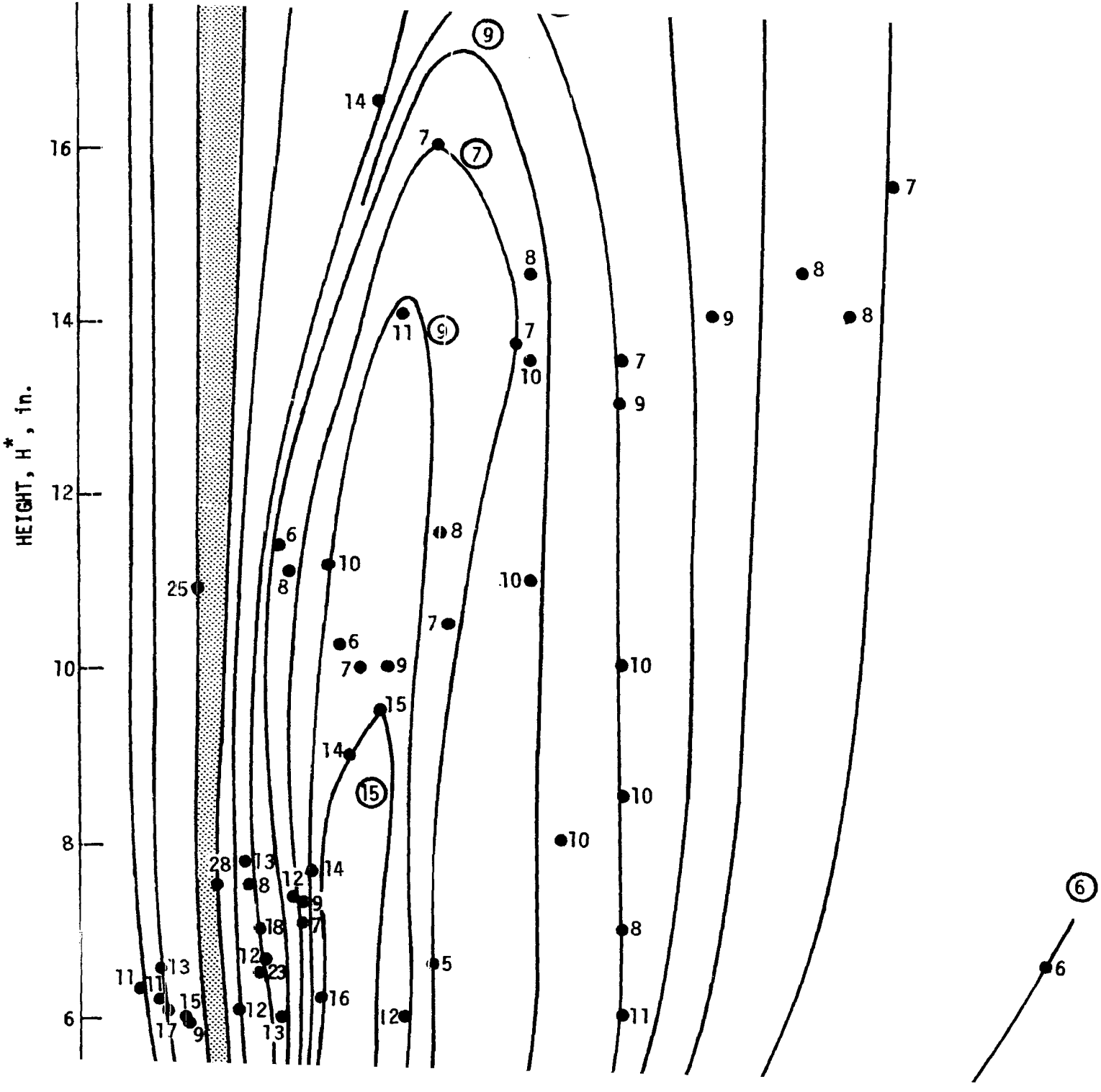
HEIGHT, H*, in.
16
14
12
10
8
6

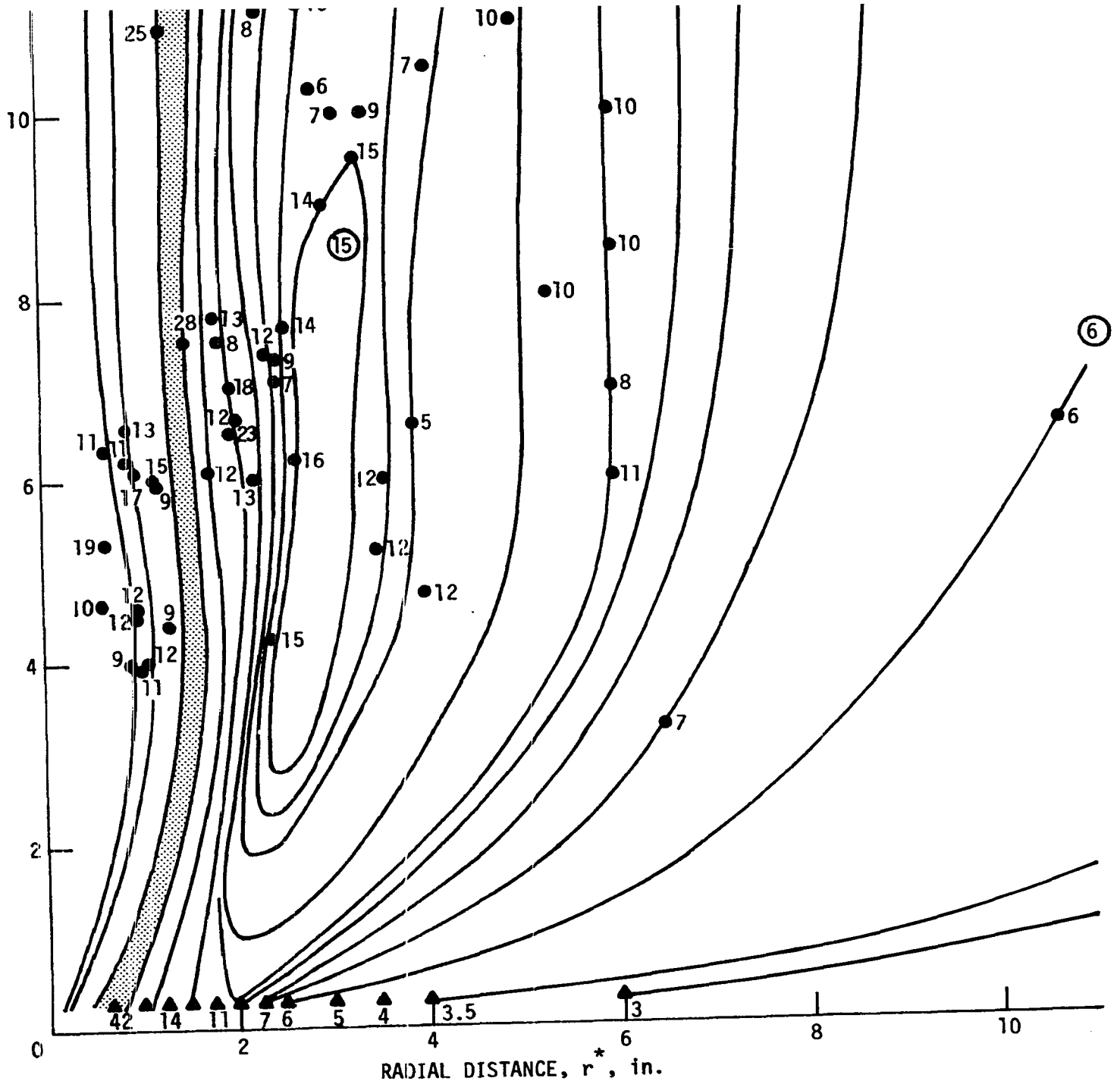
RADIAL DISTANCE, r*, in.
0
2
4
6
8
10
42
14
11
7
6
5
4
3.5
3
4
6
8
10
15
6

Figure 34. Tangential speed distribution at $H^* = 1$ in.

Figure 35. Tangential speed distribution at $H^* = 2$ in.

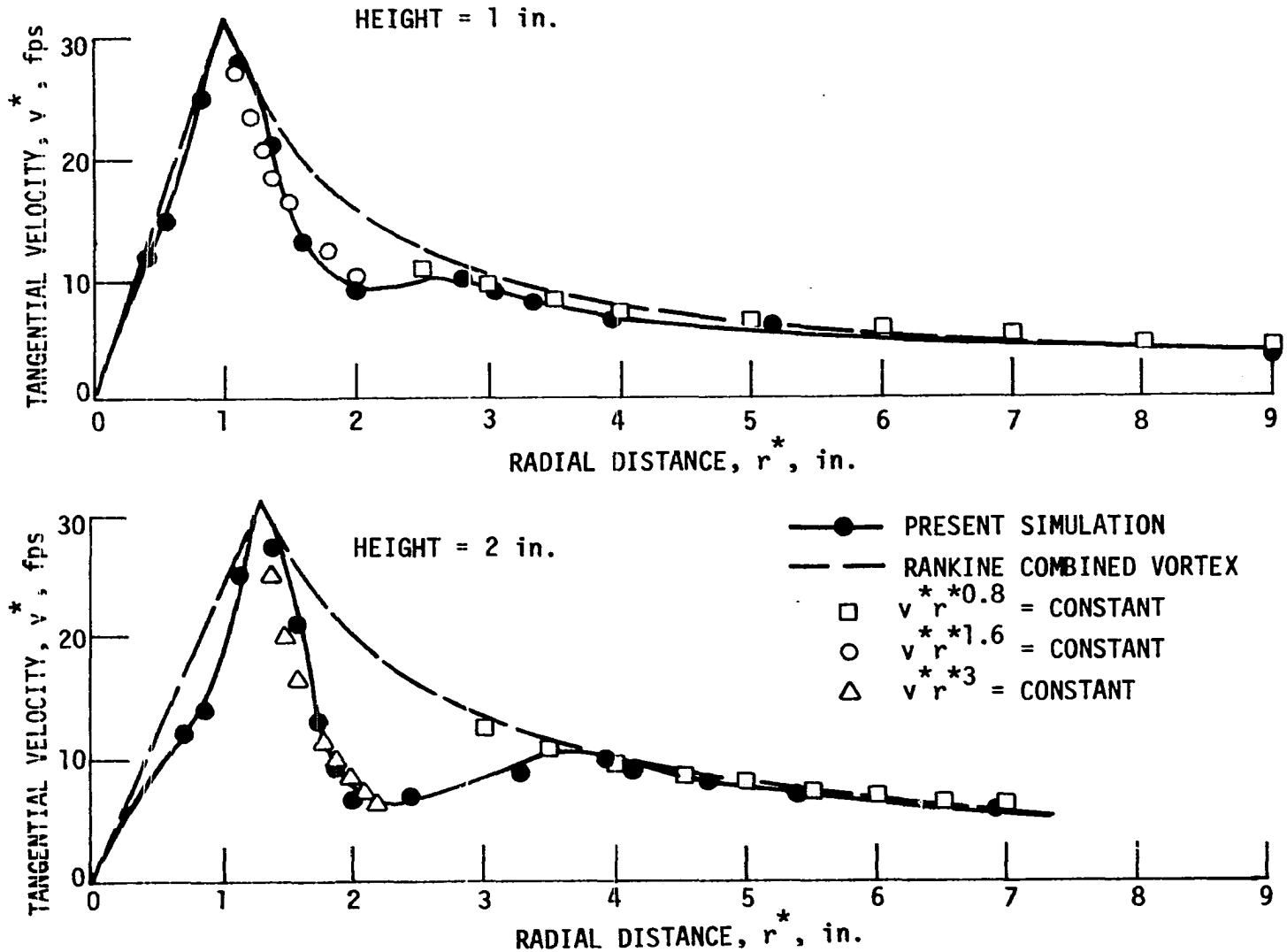
HEIGHT = 1 in.
HEIGHT = 2 in.
TANGENTIAL VELOCITY, v*, fps
RADIAL DISTANCE, r*, in.
0
10
20
30
0
1
2
3
4
5
6
7
8
9
PRESENT SIMULATION
RANKINE COMBINED VORTEX
v*r*0.8 = CONSTANT
v*r*1.6 = CONSTANT
v*r*3 = CONSTANT

Figure 36. Tangential speed distribution at $H^* = 3$ in. Note the appearance of a local maximum at $2 < r^* < 3$ in.

Figure 37. Tangential speed distribution at $H^* = 6$ in.

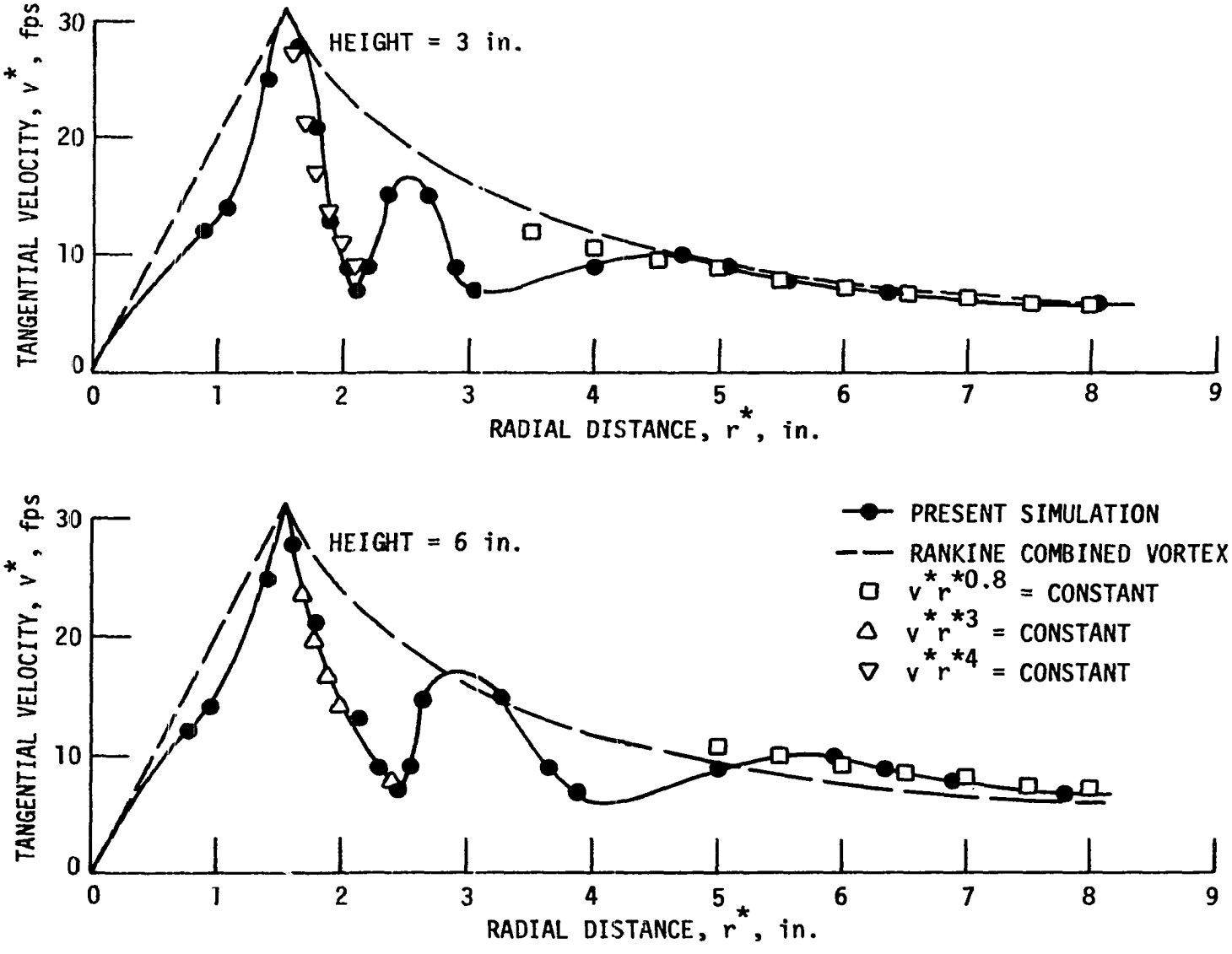
HEIGHT = 3 in.
TANGENTIAL VELOCITY, v*, fps
RADIAL DISTANCE, r*, in.
HEIGHT = 6 in.
PRESENT SIMULATION
RANKINE COMBINED VORTEX
v*r*0.8 = CONSTANT
v*r*3 = CONSTANT
v*r*4 = CONSTANT

Figure 38. Tangential speed distribution at $H^* = 9$ in.

Figure 39. Tangential speed distribution at $H^* = 12$ in. Note the decreasing magnitude of the local maximum at $2.5 < r^* < 4.5$ in.

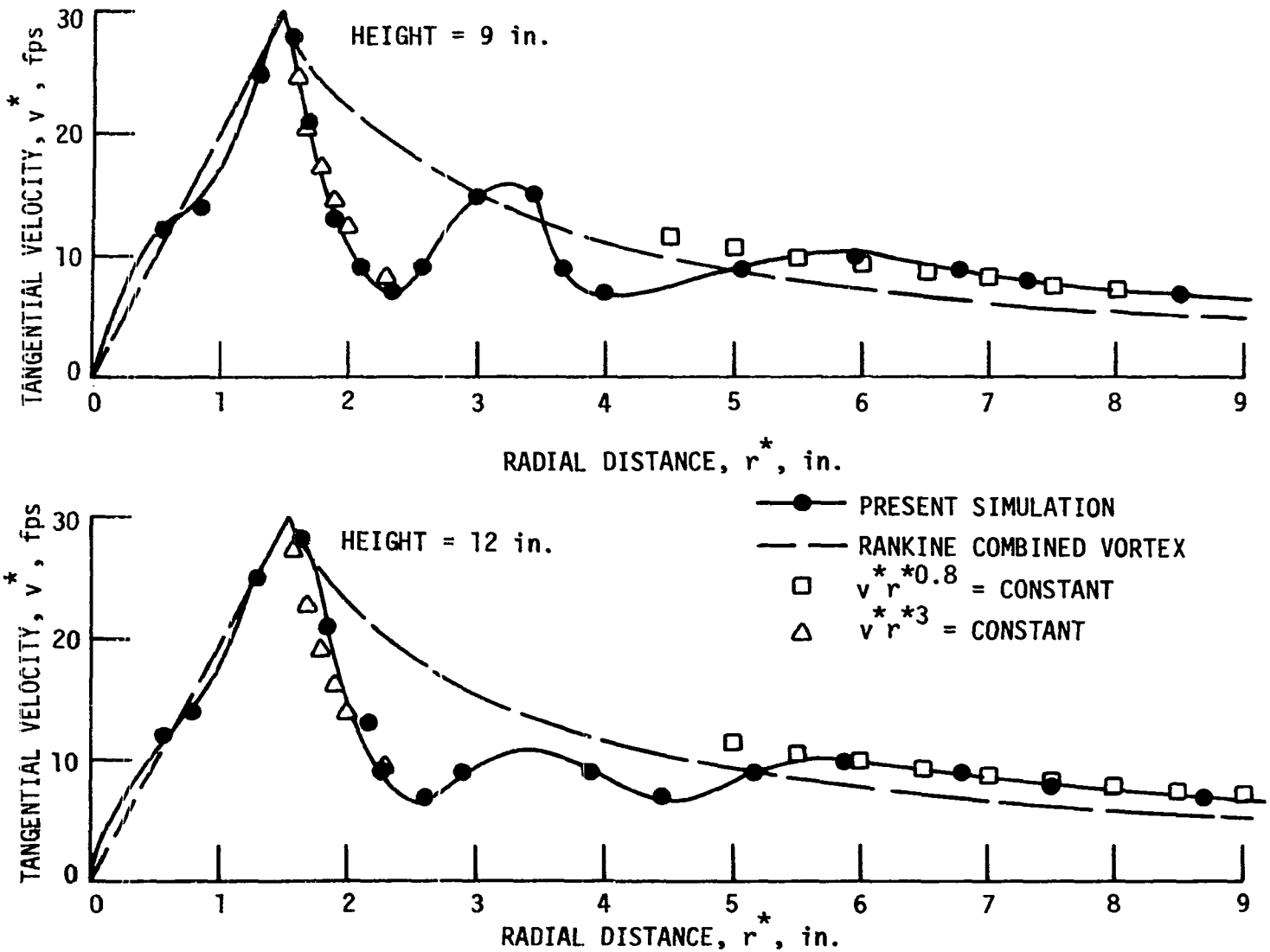
HEIGHT = 9 in.
TANGENTIAL VELOCITY, v*, fps
RADIAL DISTANCE, r*, in.
HEIGHT = 12 in.
PRESENT SIMULATION
RANKINE COMBINED VORTEX
v*r*0.8 = CONSTANT
v*r*3 = CONSTANT

Figure 40. Tangential speed distribution at $H^* = 15$ in. Note the disappearance of the local maximum at $2.5 < r^* < 4.5$ in.

Figure 41. Tangential speed distribution at $H^* = 18$ in. Away from the frictional effects of the ground surface the distribution of tangential speed is in remarkable agreement with that of a Rankine combined vortex.

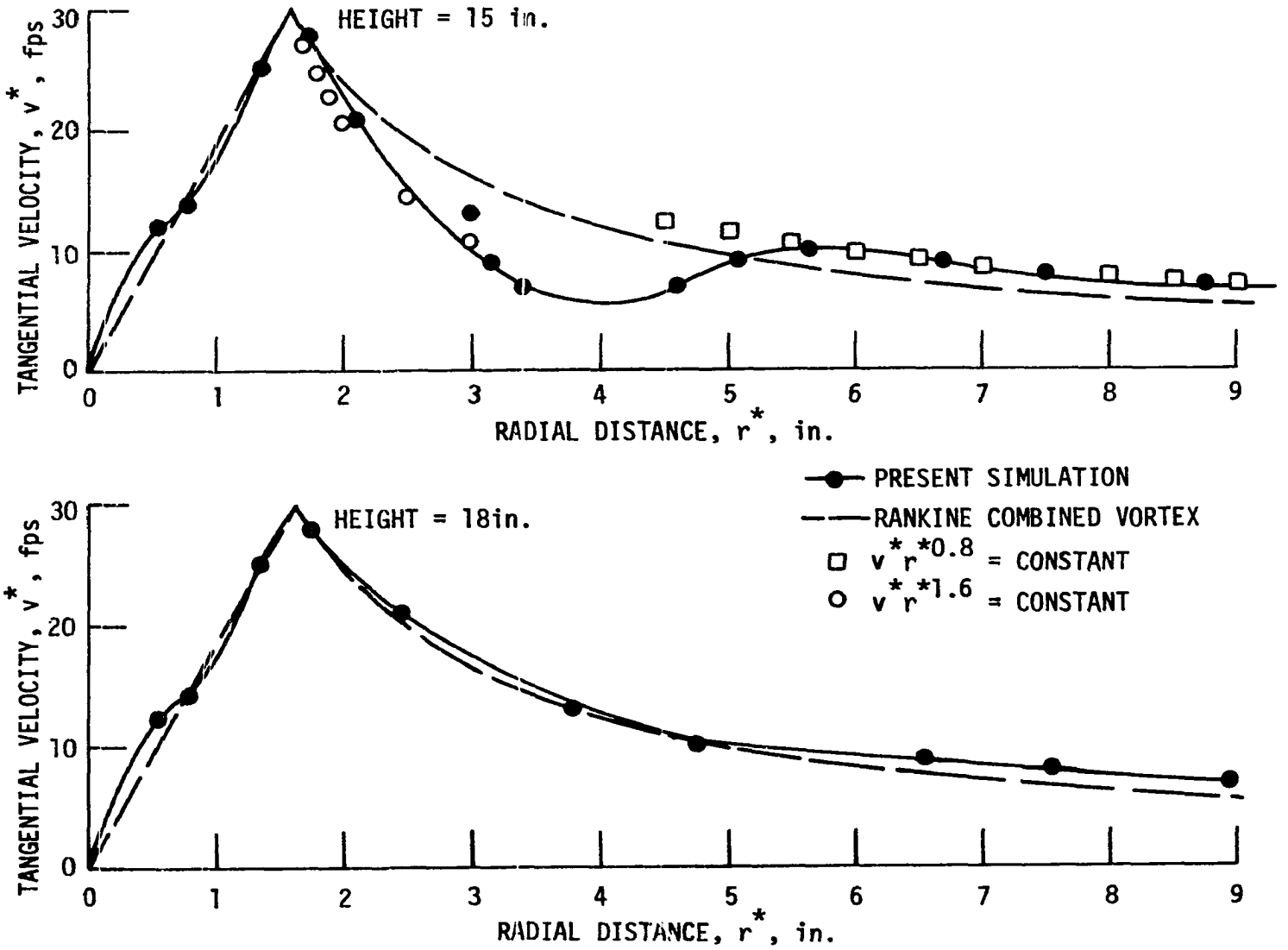
HEIGHT = 15 in.
TANGENTIAL VELOCITY, v*, fps
RADIAL DISTANCE, r*, in.
HEIGHT = 18in.
TANGENTIAL VELOCITY, v*, fps
RADIAL DISTANCE, r*, in.
PRESENT SIMULATION
RANKINE COMBINED VORTEX
v*r*0.8 = CONSTANT
v*r*1.6 = CONSTANT

Figure 42. Tangential isotachs in the Dallas Tornado of April 2, 1957. Numbers indicate the magnitude of the tangential wind speeds in miles per hour. The dashed line shows the boundaries of the tornado funnel. (Hoecker, 1960)

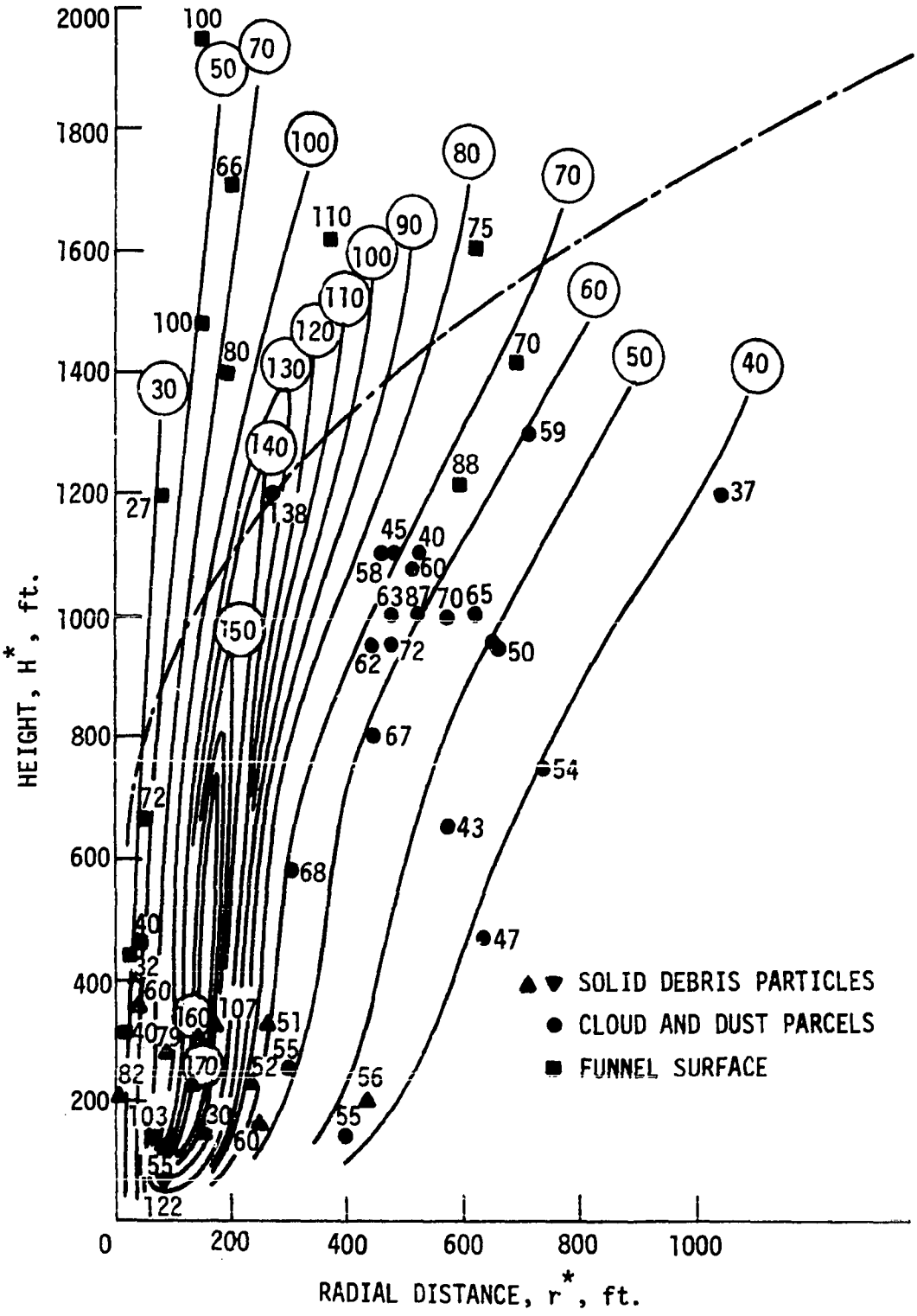
HEIGHT, H*, ft.
RADIAL DISTANCE, r*, ft.
SOLID DEBRIS PARTICLES
CLOUD AND DUST PARCELS
FUNNEL SURFACE

Figure 43. The derived distribution of tangential wind speeds at selected heights in the flow field of the Dallas Tornado of April 2, 1957. (Hoecker, 1960)

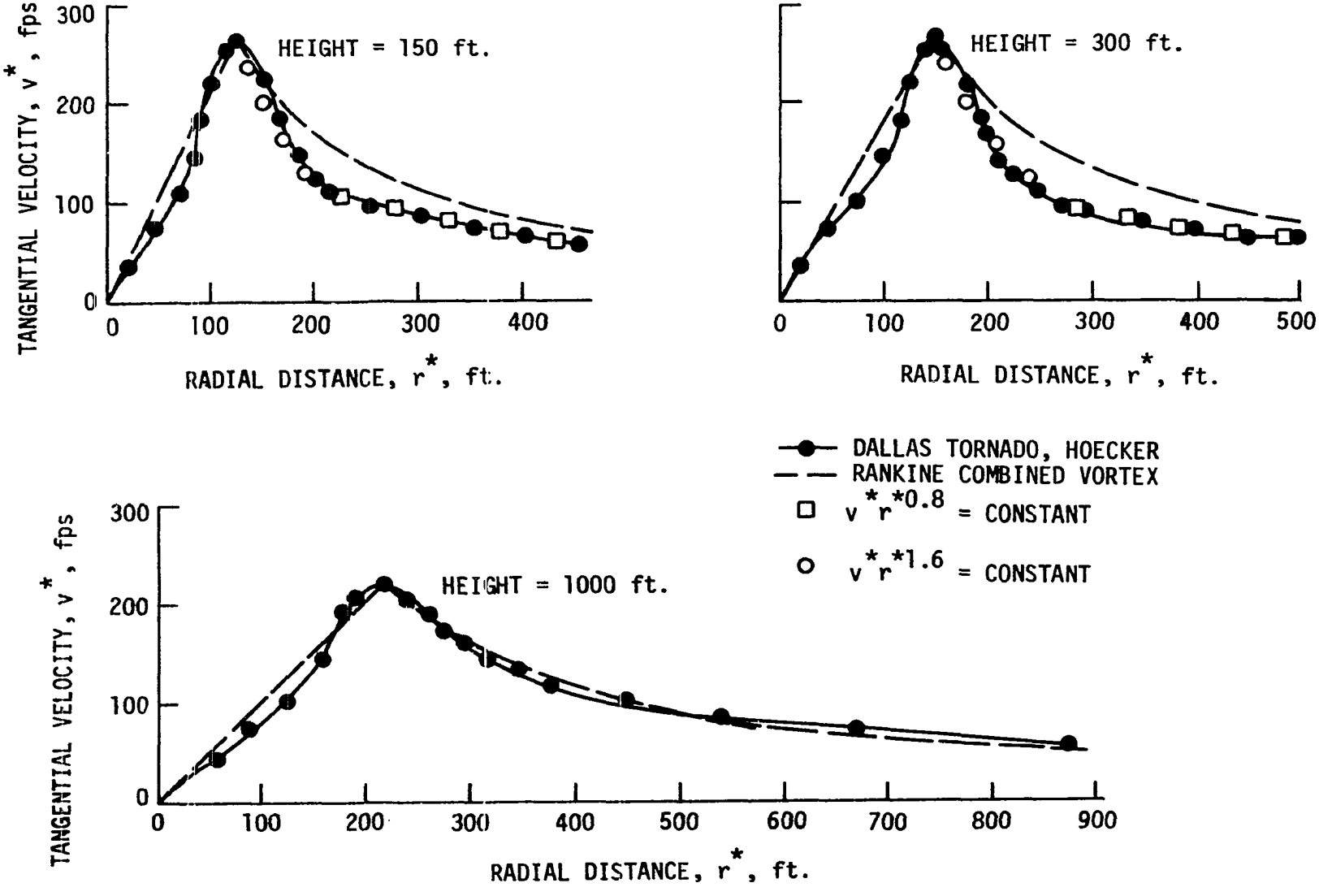
TANGENTIAL VELOCITY, v*, fps
300
200
100
0
HEIGHT = 150 ft.
0
100
200
300
400
RADIAL DISTANCE, r*, ft.
HEIGHT = 300 ft.
0
100
200
300
400
500
RADIAL DISTANCE, r*, ft.
DALLAS TORNADO, HOECKER
RANKINE COMBINED VORTEX
v*r*0.8 = CONSTANT
v*r*1.6 = CONSTANT
TANGENTIAL VELOCITY, v*, fps
300
200
100
0
HEIGHT = 1000 ft.
0
100
200
300
400
500
600
700
800
900
RADIAL DISTANCE, r*, ft.

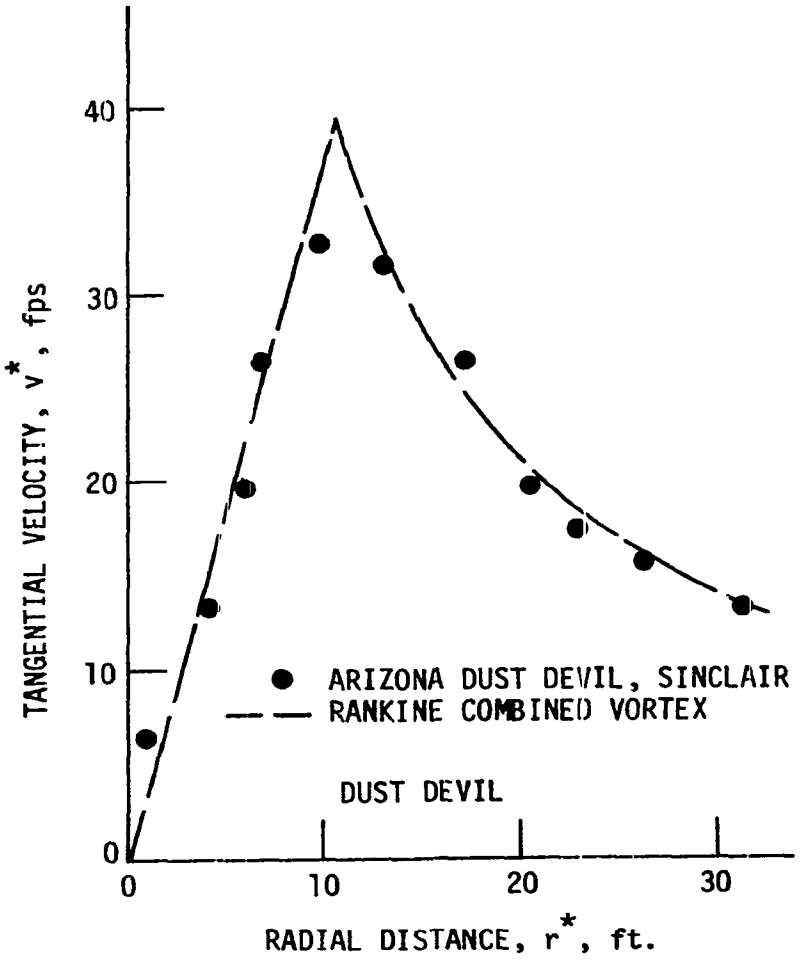

Figure 44. Tangential speed distribution in a dust devil (Sinclair, 1973).

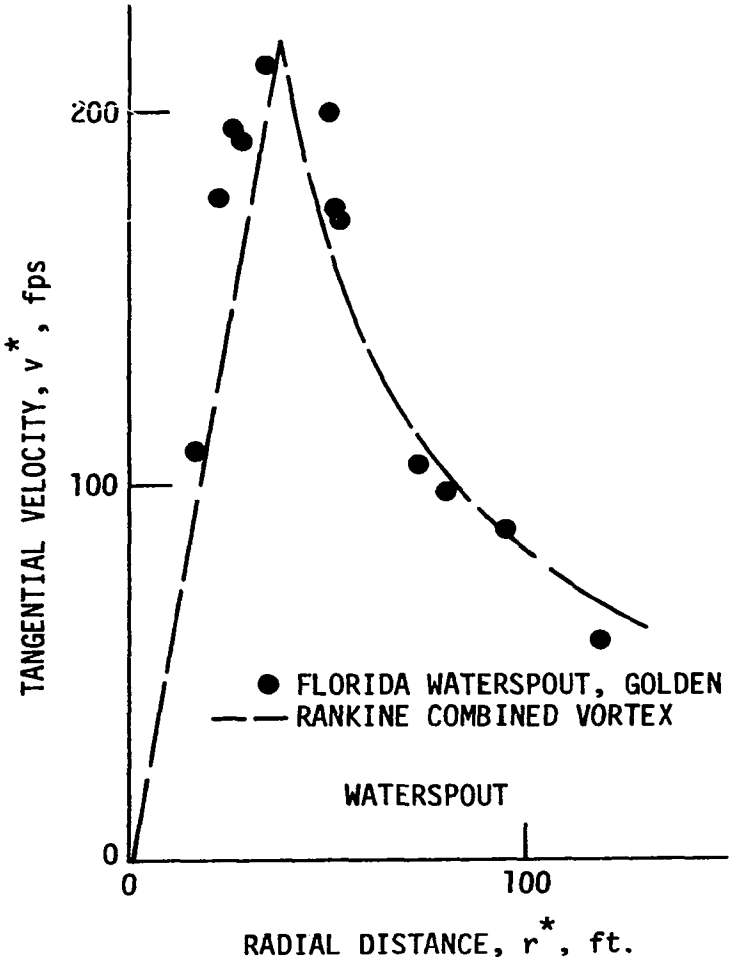

Figure 45. Tangential speed distribution in a waterspout (Golden, 1971).

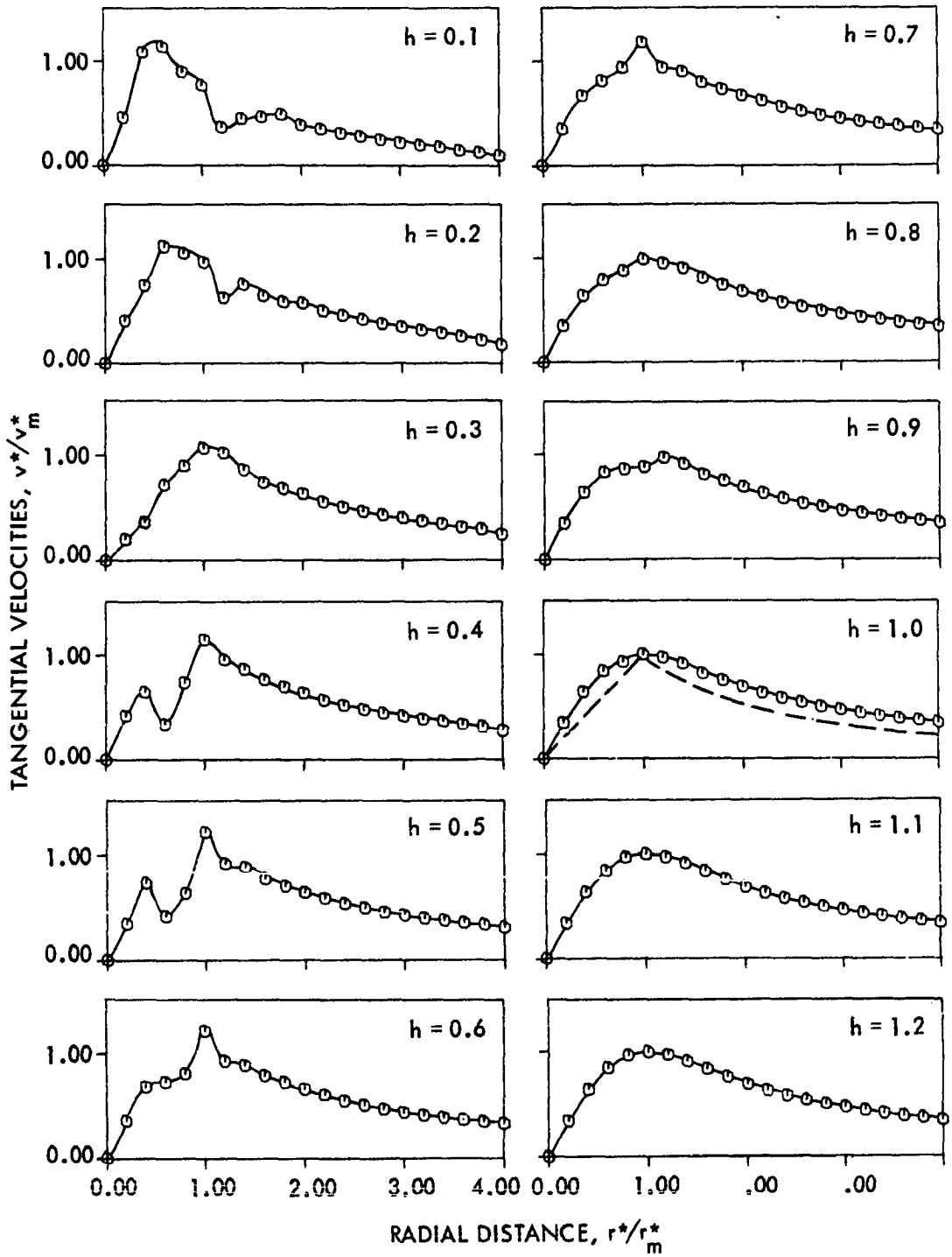

Figure 46. Predicted tangential velocity distribution of a vortex boundary layer flow (Hsu and Tesfamariam, 1975). All quantities are non-dimensionalized. At h = 1.0 the distribution of the imposed vortex is shown where dashed lines indicate a Rankine combined distribution. Note the development of the distribution at lower heights with multiple local maximums.

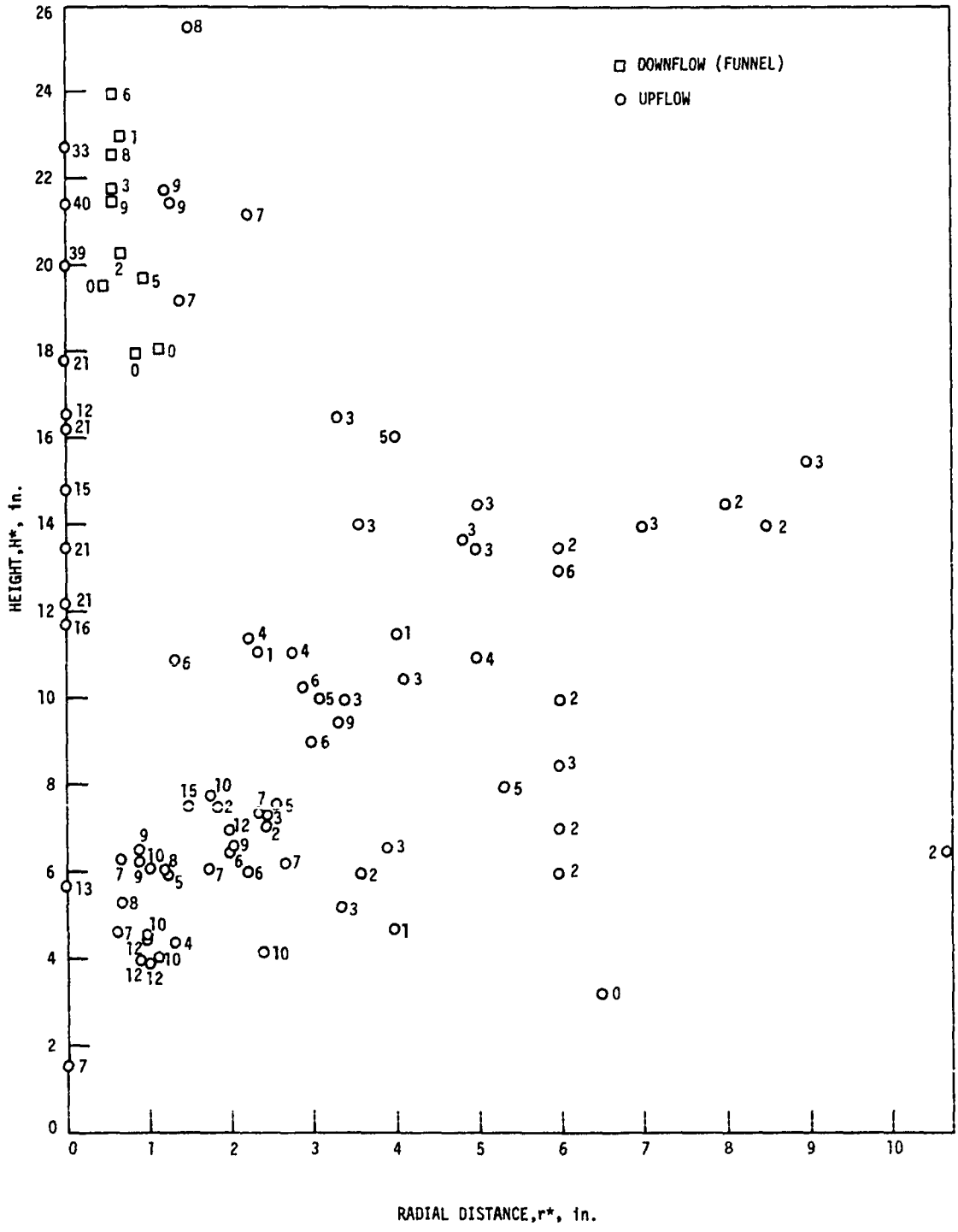

Figure 47. Distribution of measured axial speed in the flow field of the laboratory vortex.

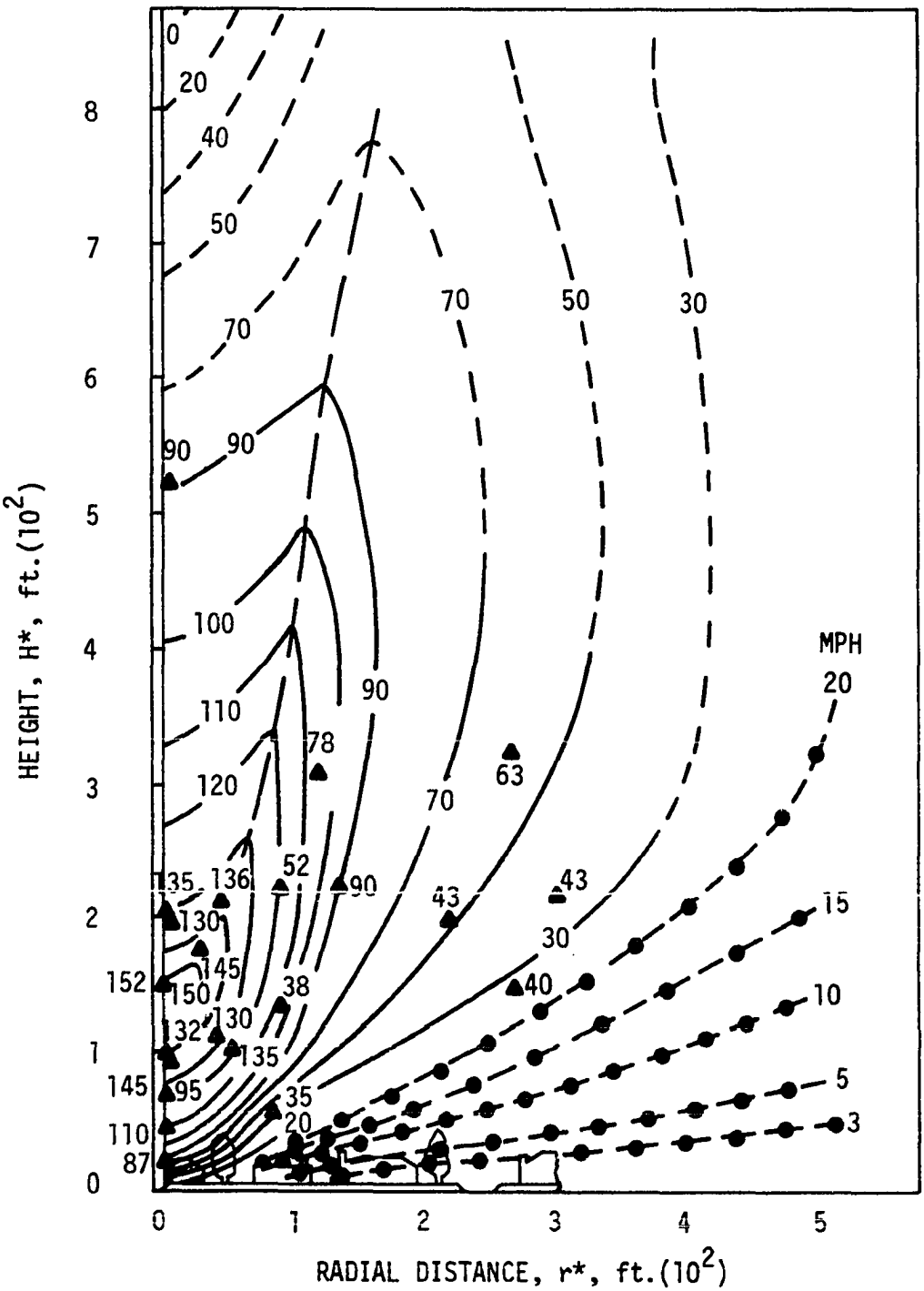

Figure 48. Distribution of derived axial speed from the center of the Dallas Tornado to about 500 ft. in radius and from the ground to about 800 ft. in elevation. Dot-dashed lines are theoretical isotachs computed by Hoecker (1960) by assuming a particular radial speed distribution.

Figure 49. Projected trajectories of the particle of Fig. 27A in the vertical planes of XY and ZY.

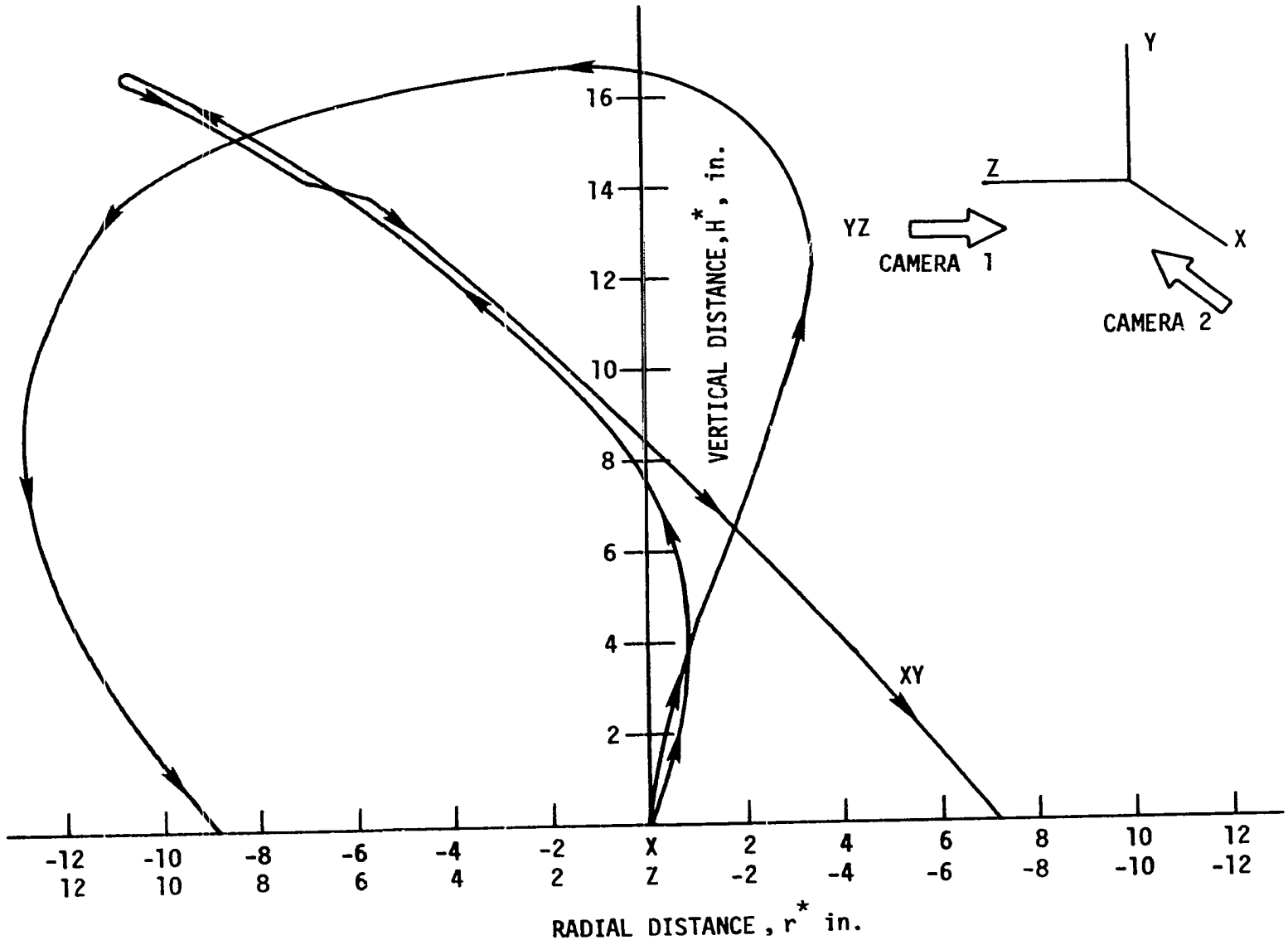
16
14
12
10
8
6
4
2
VERTICAL DISTANCE, H*, in.
XY
-12 12
-10 10
-8 8
-6 6
-4 4
-2 2
X Z
2 -2
4 -4
6 -6
8 -8
10 -10
12 -12
RADIAL DISTANCE, r* in.
Y
Z
X
YZ
CAMERA 1
CAMERA 2

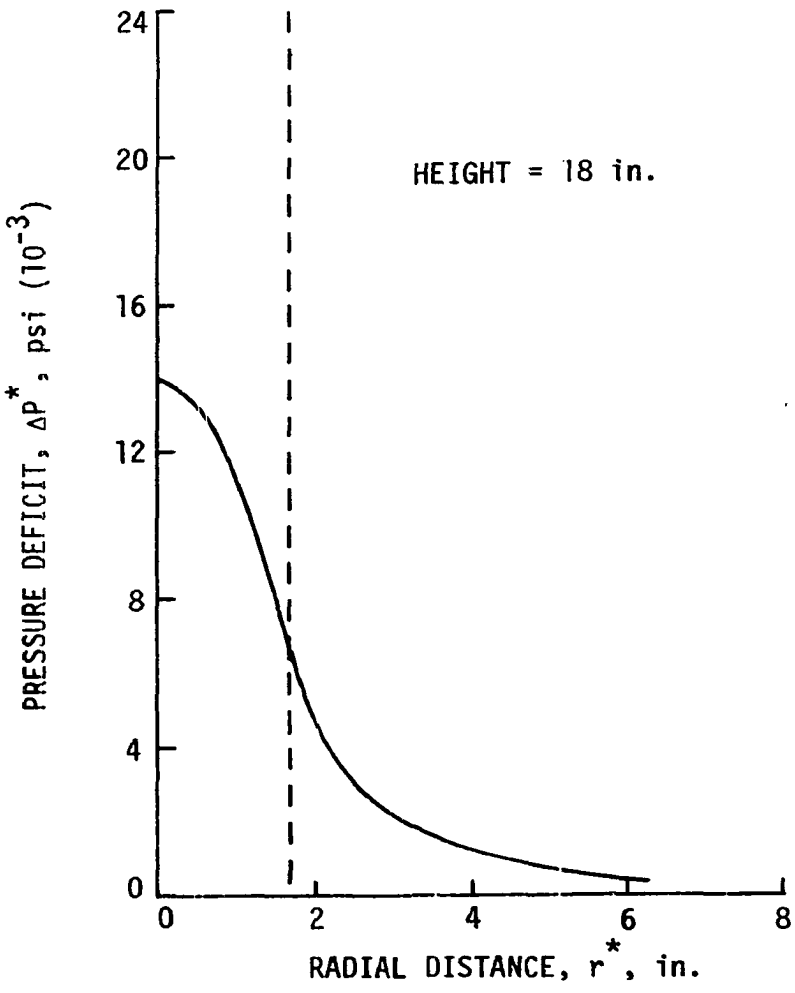

Figure 50. Distribution of derived pressure deficit at $H^* = 18$ in. Dashed line indicates the location of the maximum tangential speed.

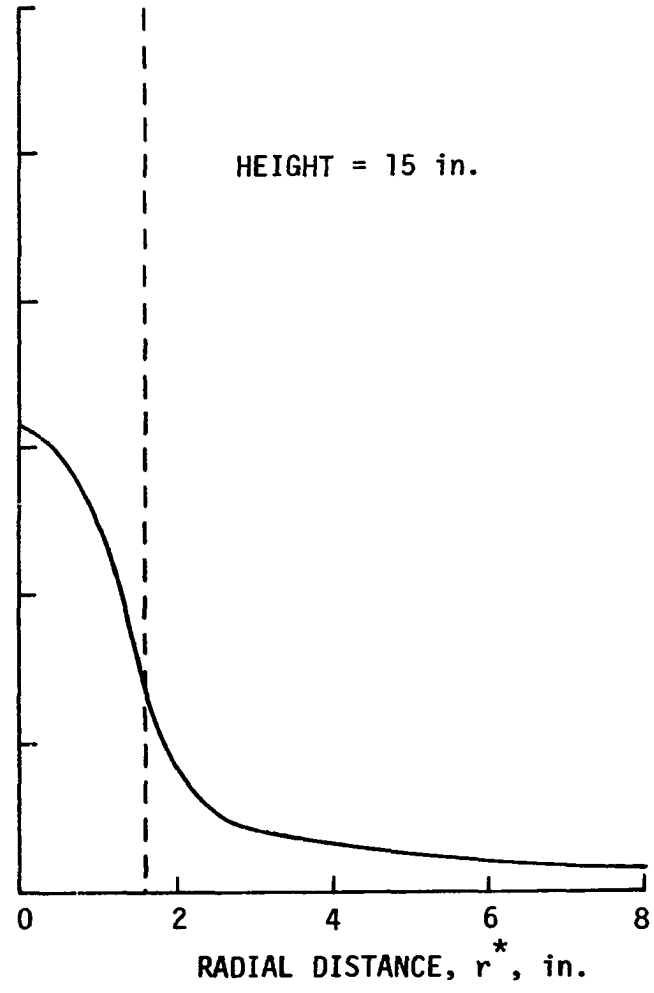

Figure 51. Distribution of derived pressure deficit at $H^* = 15$ in. Dashed line indicates the location of the maximum tangential speed.

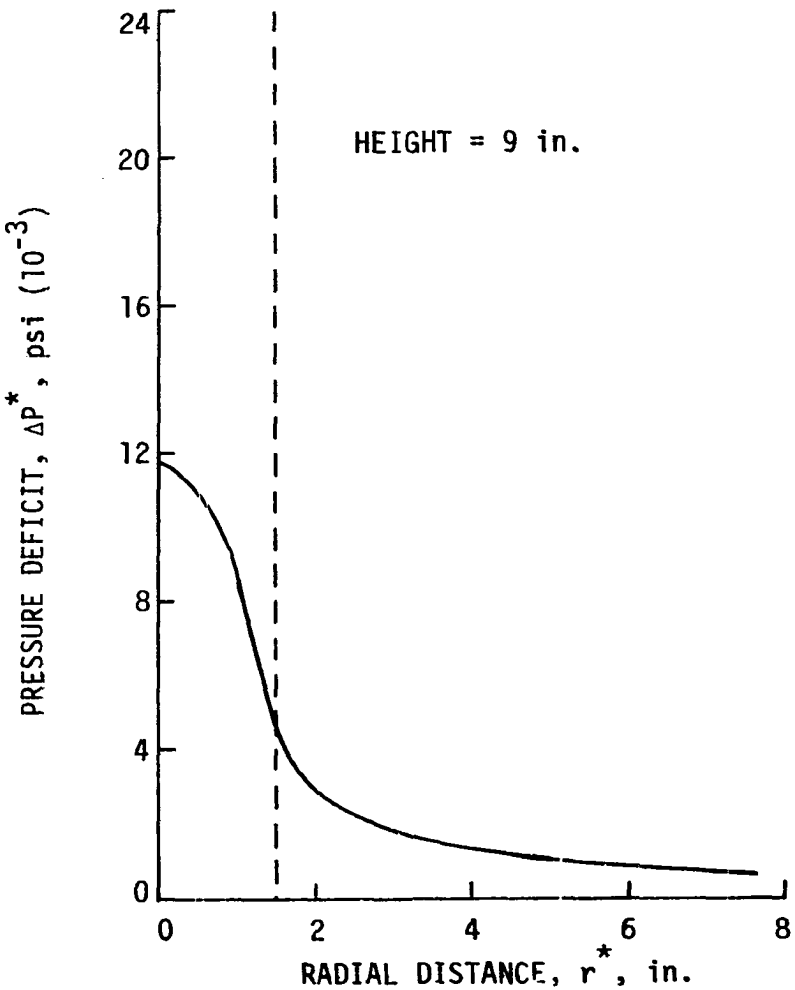

Figure 52. Distribution of derived pressure deficit at H^* = 9 in. Dashed line indicates the location of the maximum tangential speed.

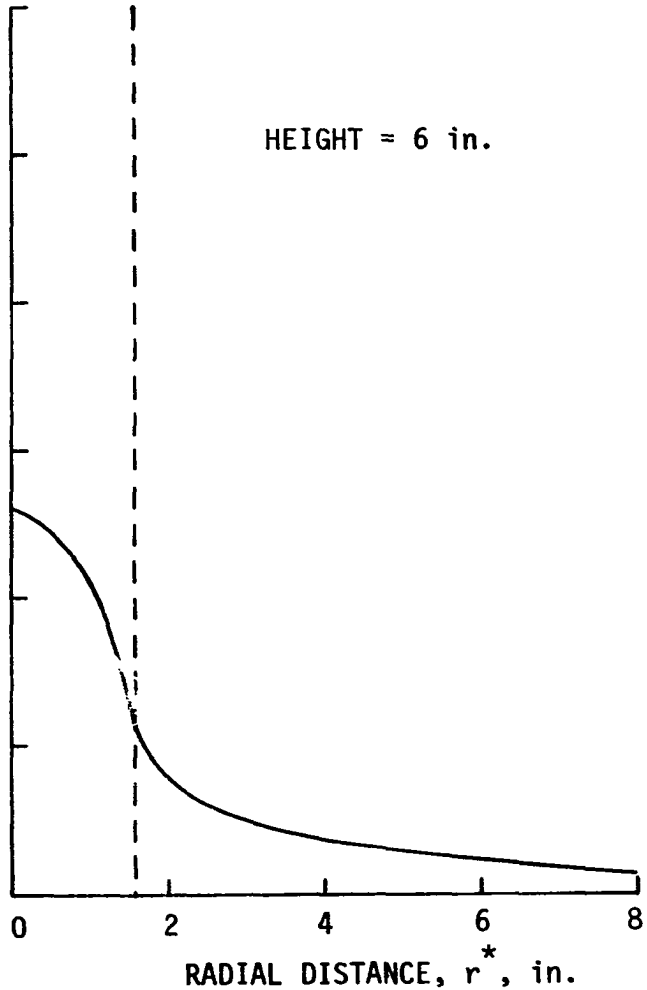

Figure 53. Distribution of derived pressure deficit at H^* = 6 in. Dashed line indicates the location of the maximum tangential speed.

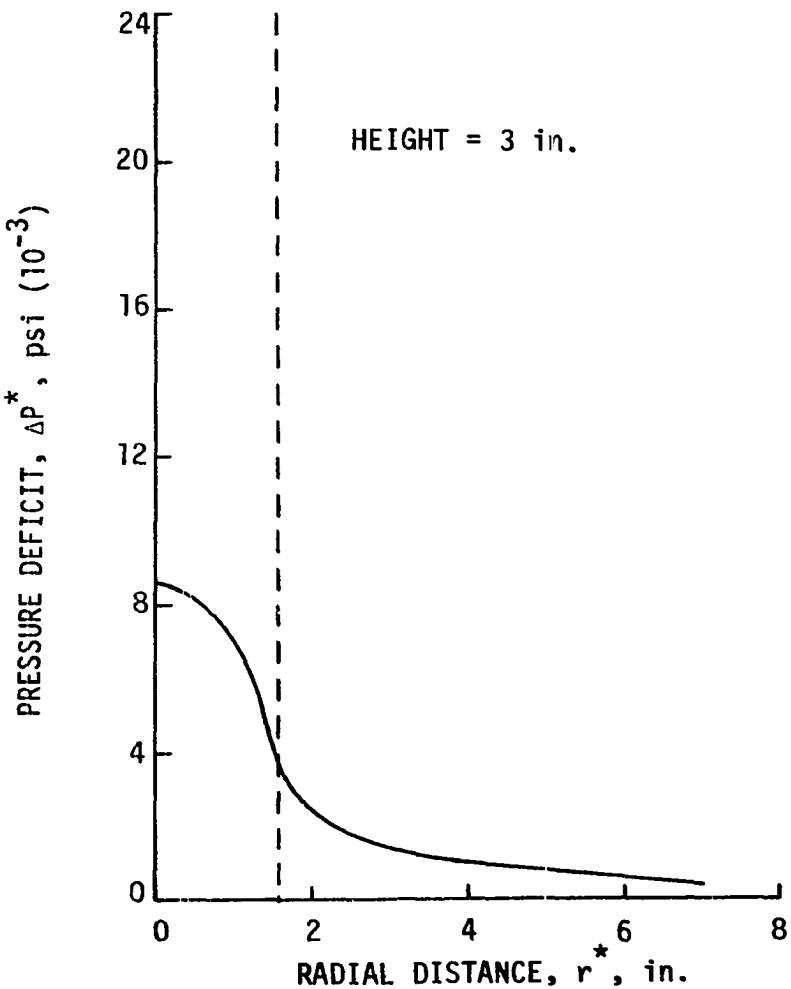

Figure 54. Distribution of derived pressure deficit at H^* = 3 in. Dashed line indicates the location of the maximum tangential speed.

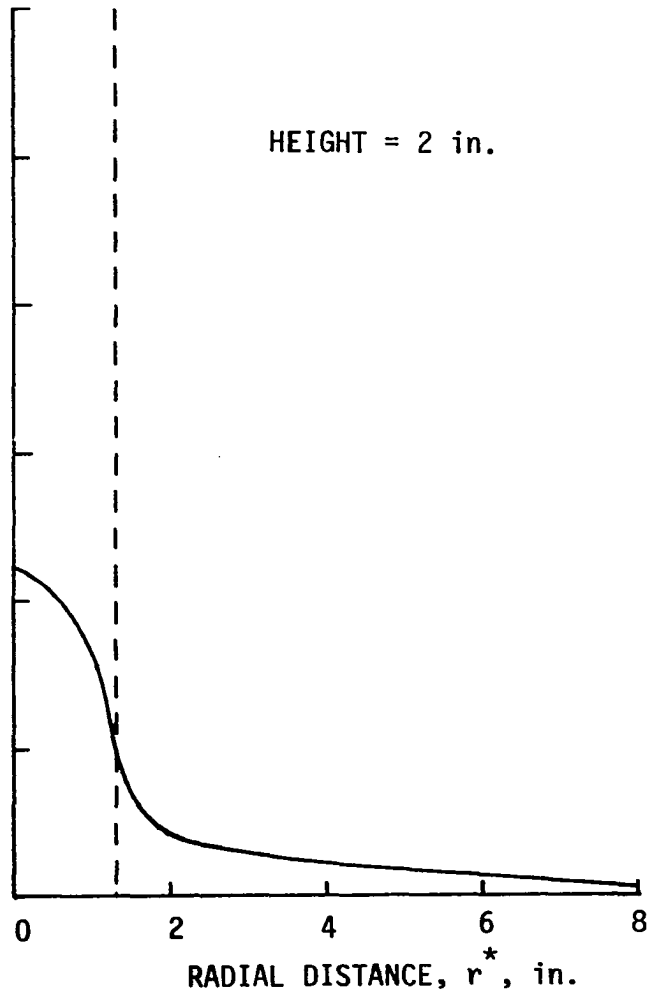

Figure 55. Distribution of derived pressure deficit at H^* = 2 in. Dashed line indicates the location of the maximum tangential speed.

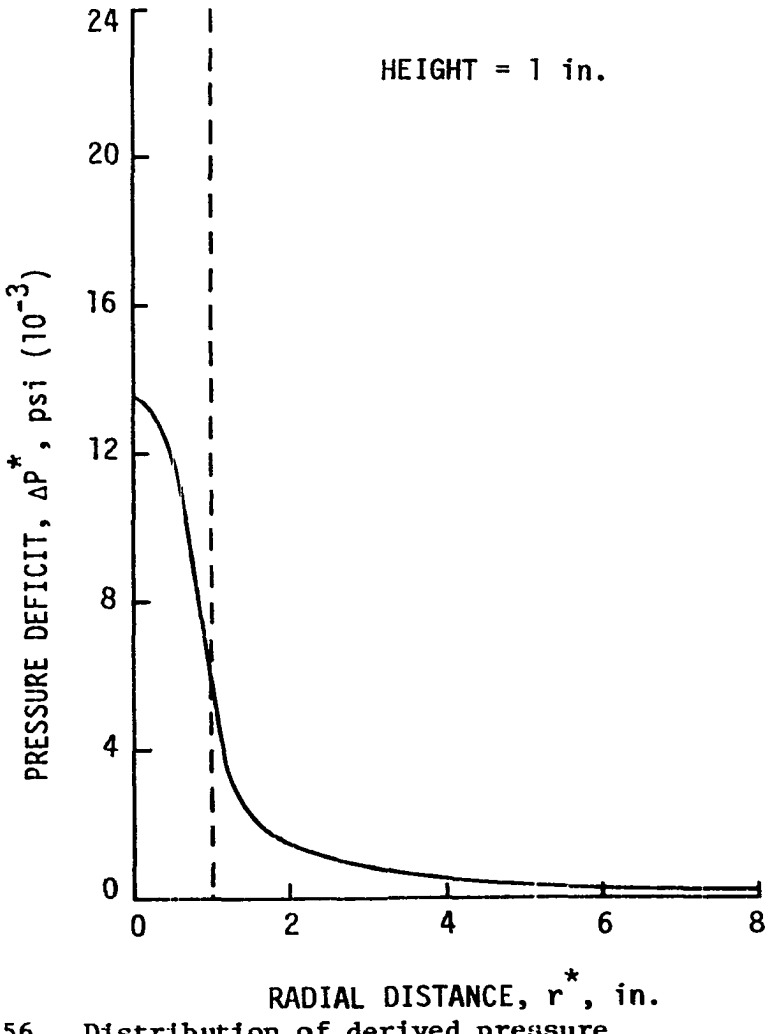

Figure 56. Distribution of derived pressure deficit at $H^* = 1$ in. Dashed line indicates the location of the maximum tangential speed.

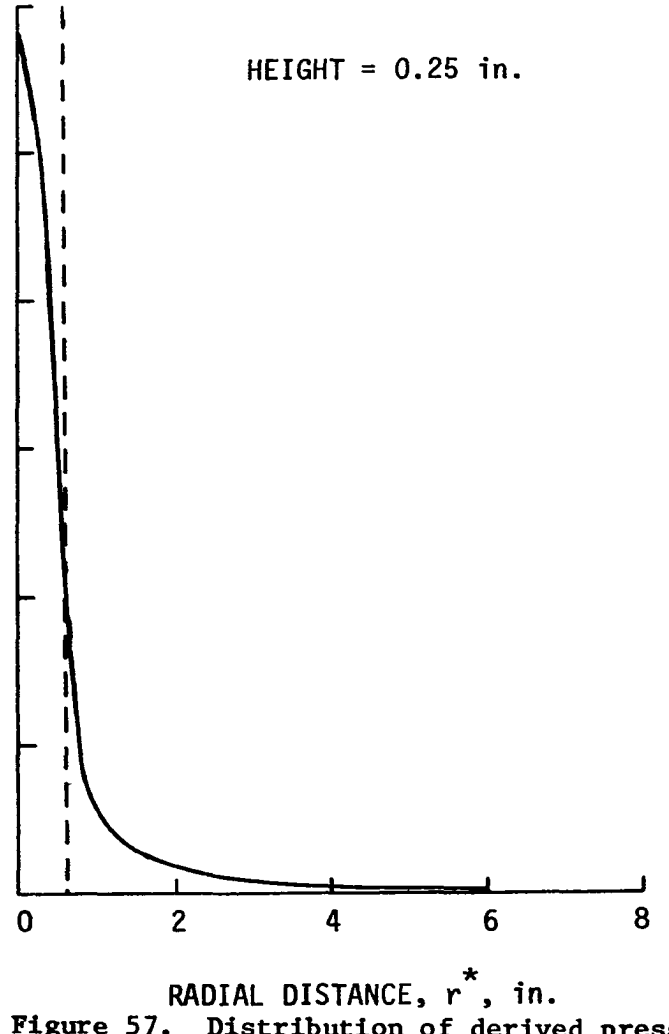

Figure 57. Distribution of derived pressure deficit at $H^* = 0.25$ in. Dashed line indicates the location of the maximum tangential speed.

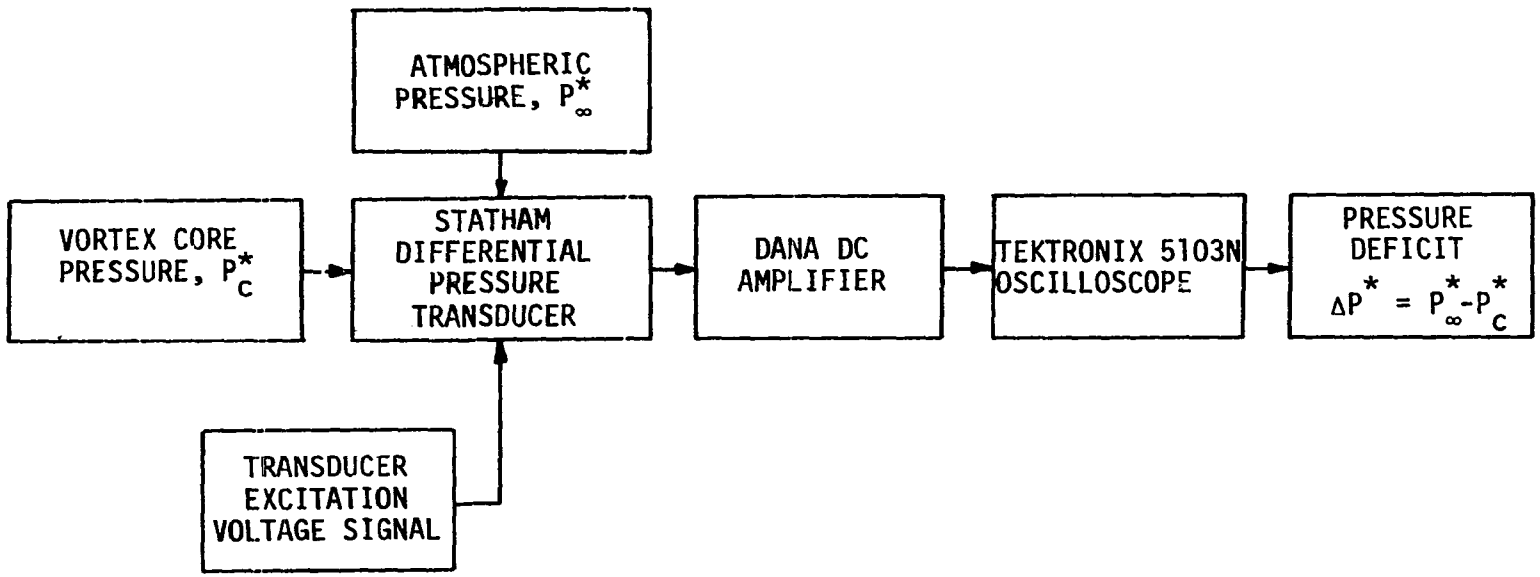

Figure 58. Schematic diagram of data processing and handling systems for measurement of pressure deficit in the vortex core.

Figure 59. Distribution of measured pressure deficit in the vortex core at the ground surface.

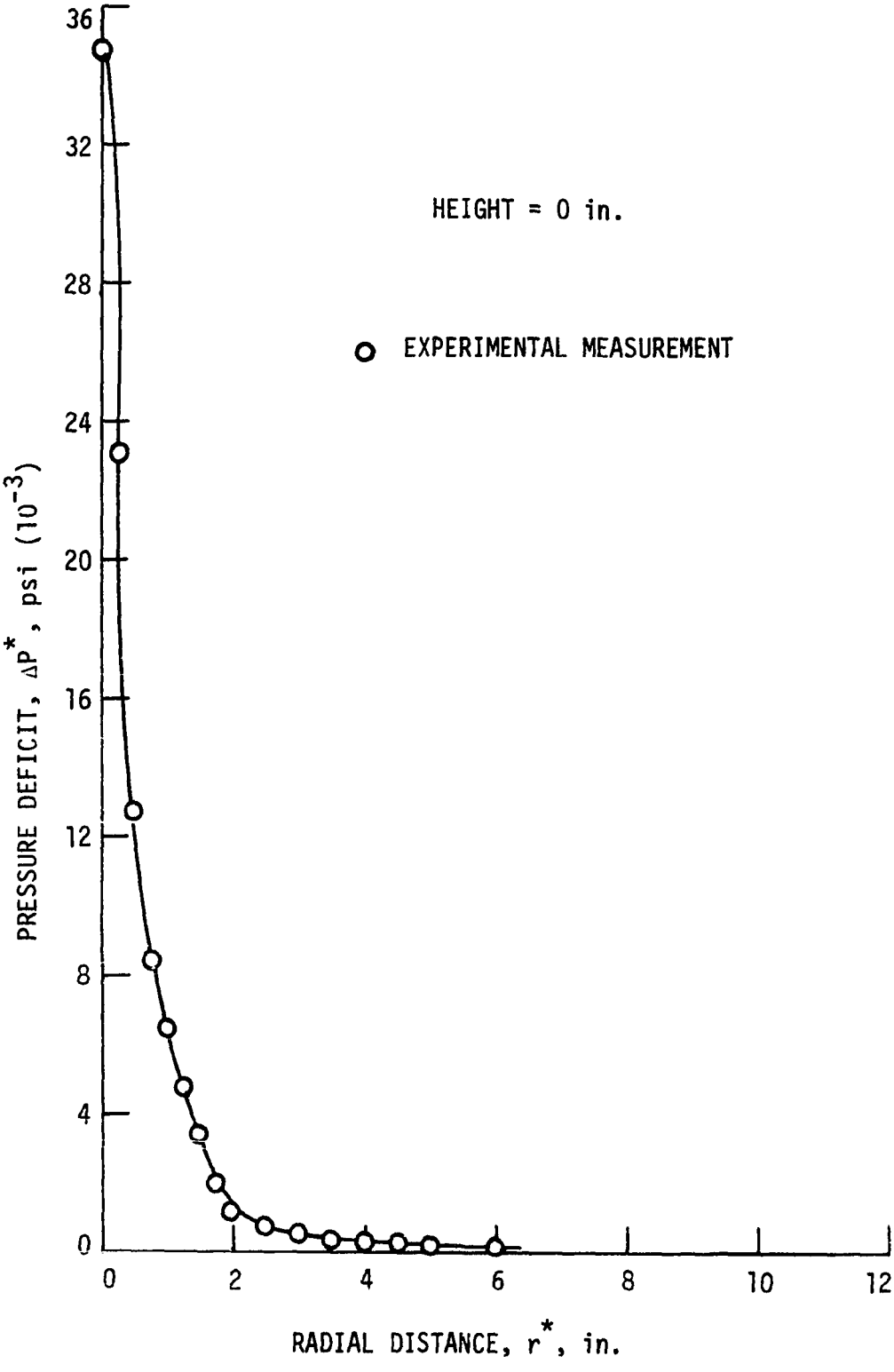
HEIGHT = 0 in.
EXPERIMENTAL MEASUREMENT
PRESSURE DEFICIT, ΔP^*, psi (10^{-3})
RADIAL DISTANCE, r^*, in.
36
32
28
24
20
16
12
8
4
0
0
2
4
6
8
10
12

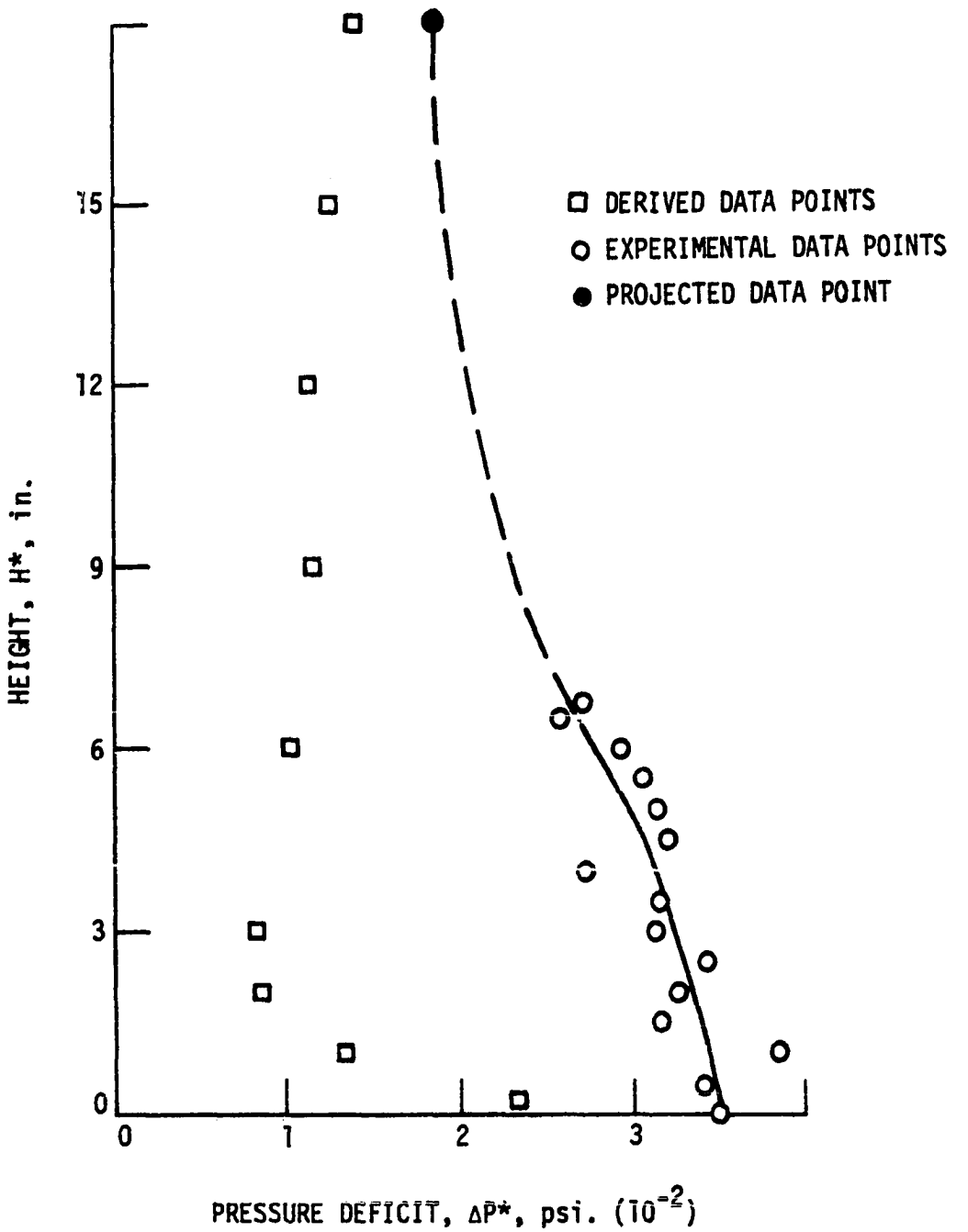

Figure 60. Variation of pressure deficit in the vortex core with height. Derived data points are computed using cyclostrophic assumption.

Figure 61. Variation of the vortex core pressure deficit with angular speed of the rotating honeycomb disk.

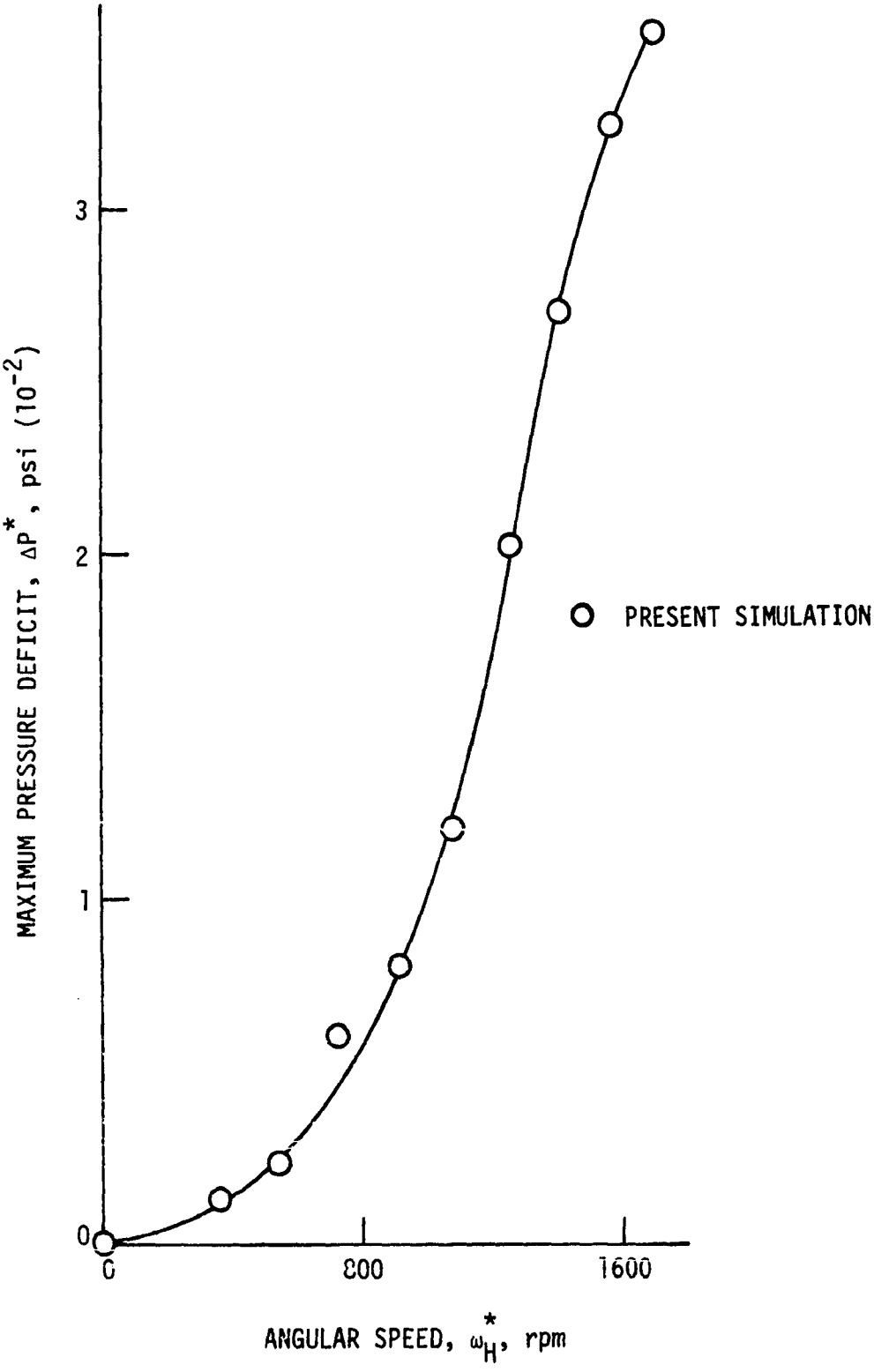
MAXIMUM PRESSURE DEFICIT, ΔP^*, psi (10^{-2})
3
2
1
0
0
800
1600
ANGULAR SPEED, ω_H^*, rpm
PRESENT SIMULATION

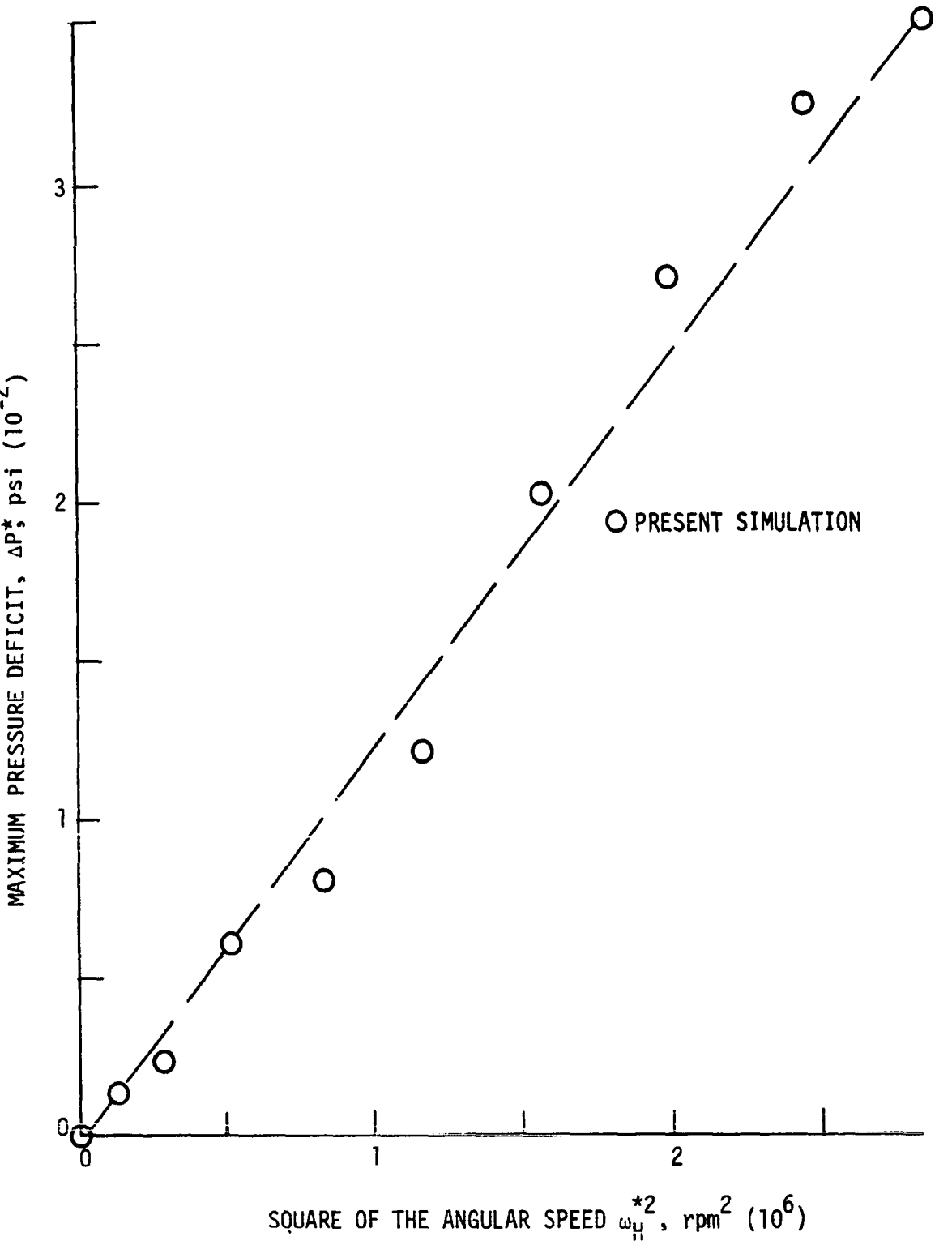

Figure 62. Variation of the vortex core pressure deficit with the square of angular speed of the rotating honeycomb disk.

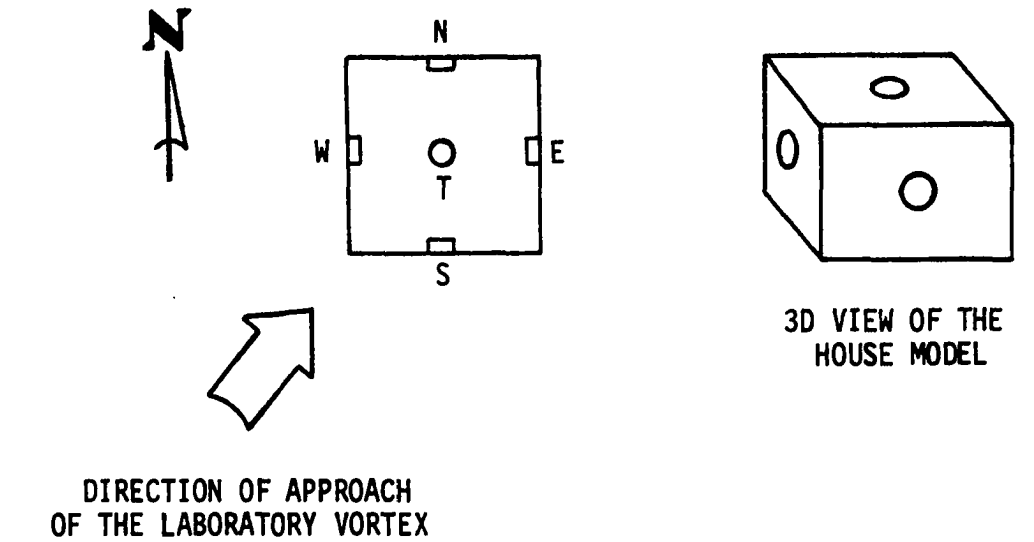

Figure 63. Diagram of the house model and direction of approach of the laboratory vortex.

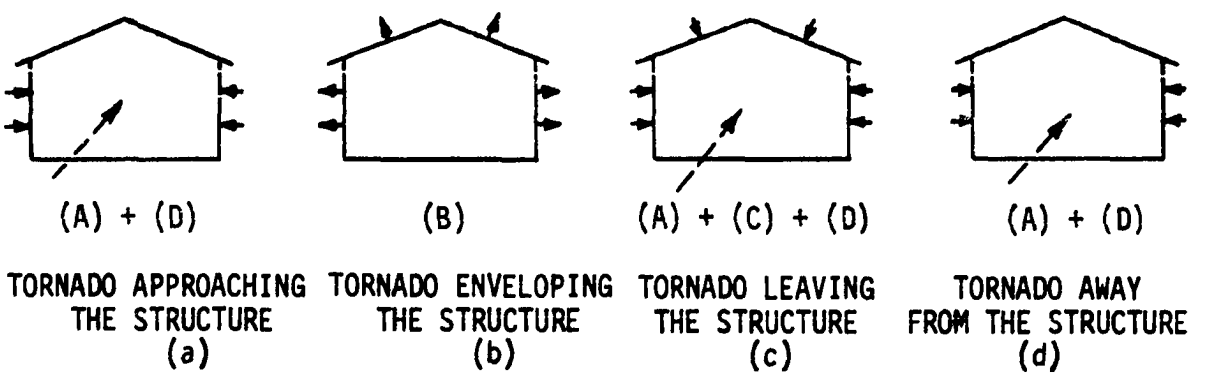

Figure 64. Various loading modes on a structure during tornadic storms. Capital letters in parentheses indicate the loading modes as described in the text.

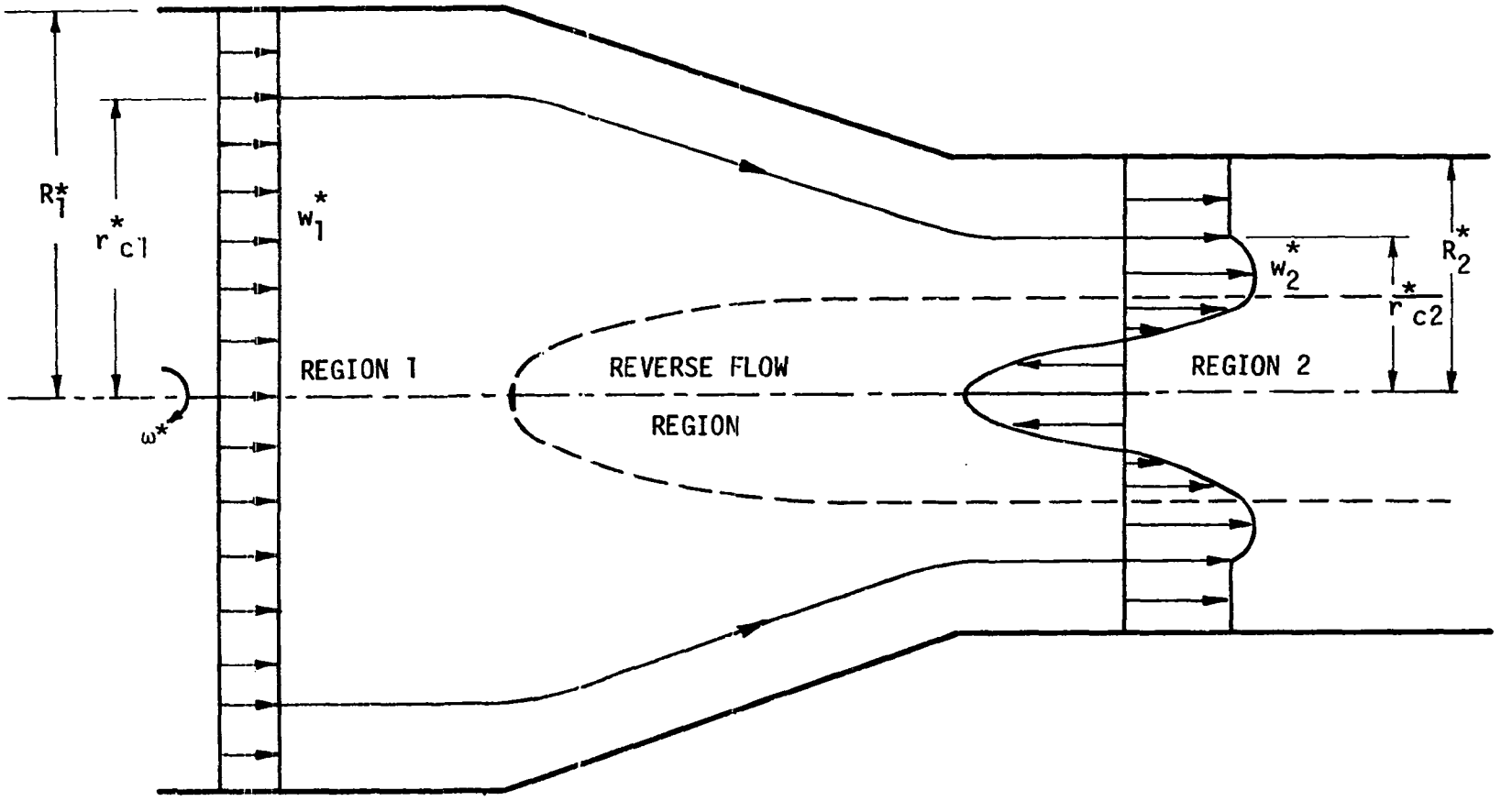

Figure 65. Diagram illustrating the occurrence of axially reversed flow in a varying cross section swirling flow field.

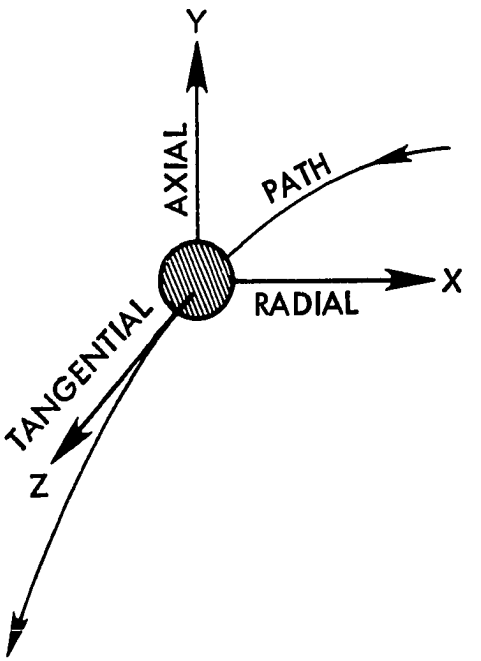

Figure 66. Rectangular coordinate system at a point in the flow field.

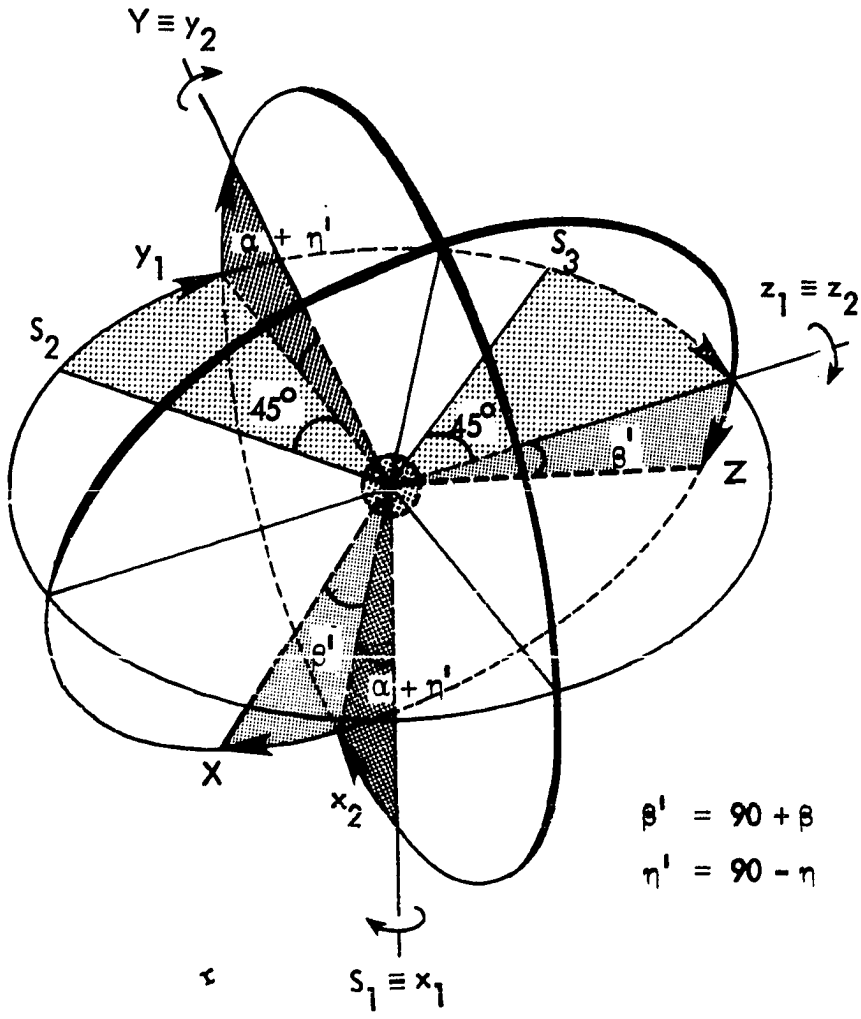

Figure 67. System of rotations leading from the sensor directions to the local horizon.

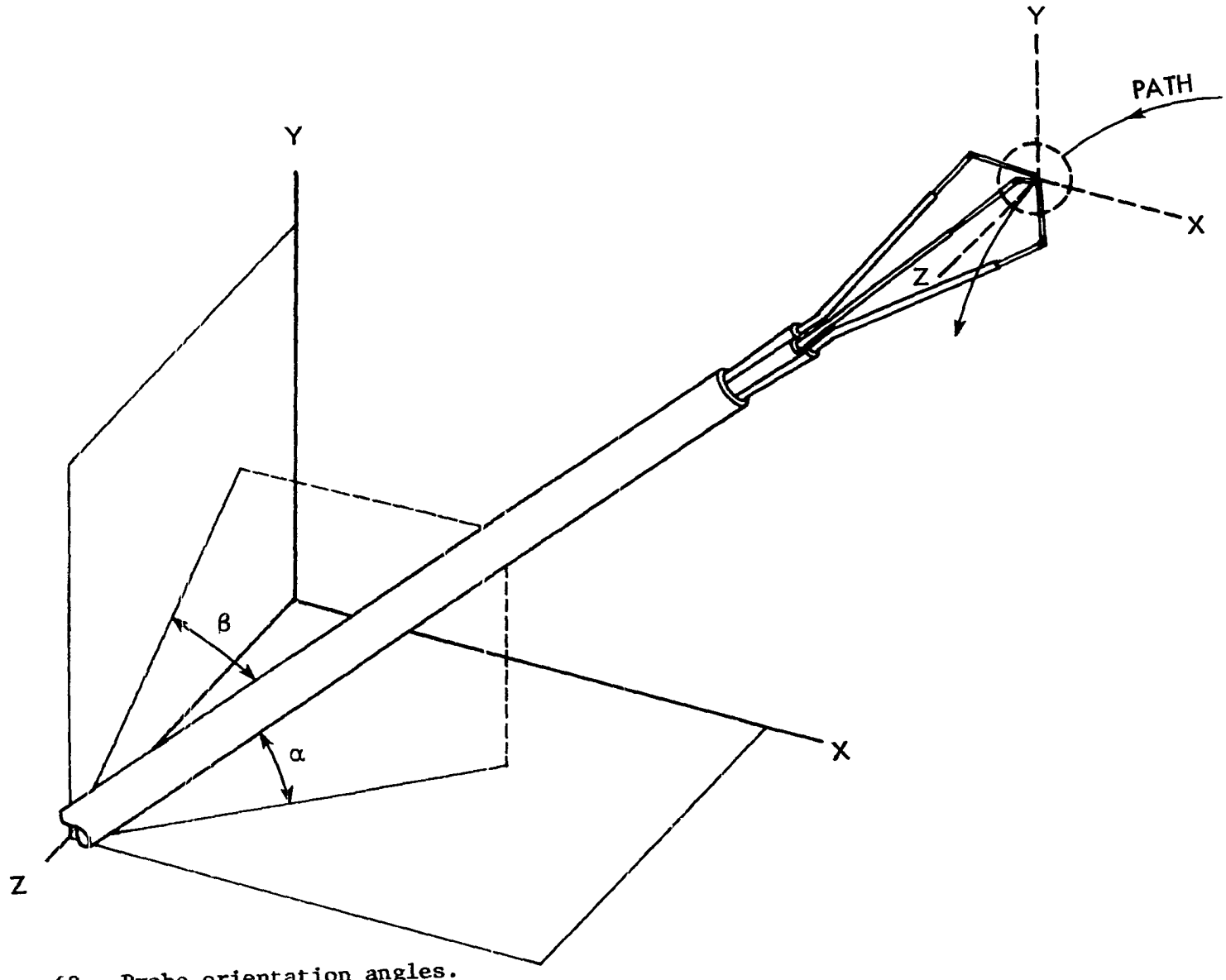

Figure 68. Probe orientation angles.

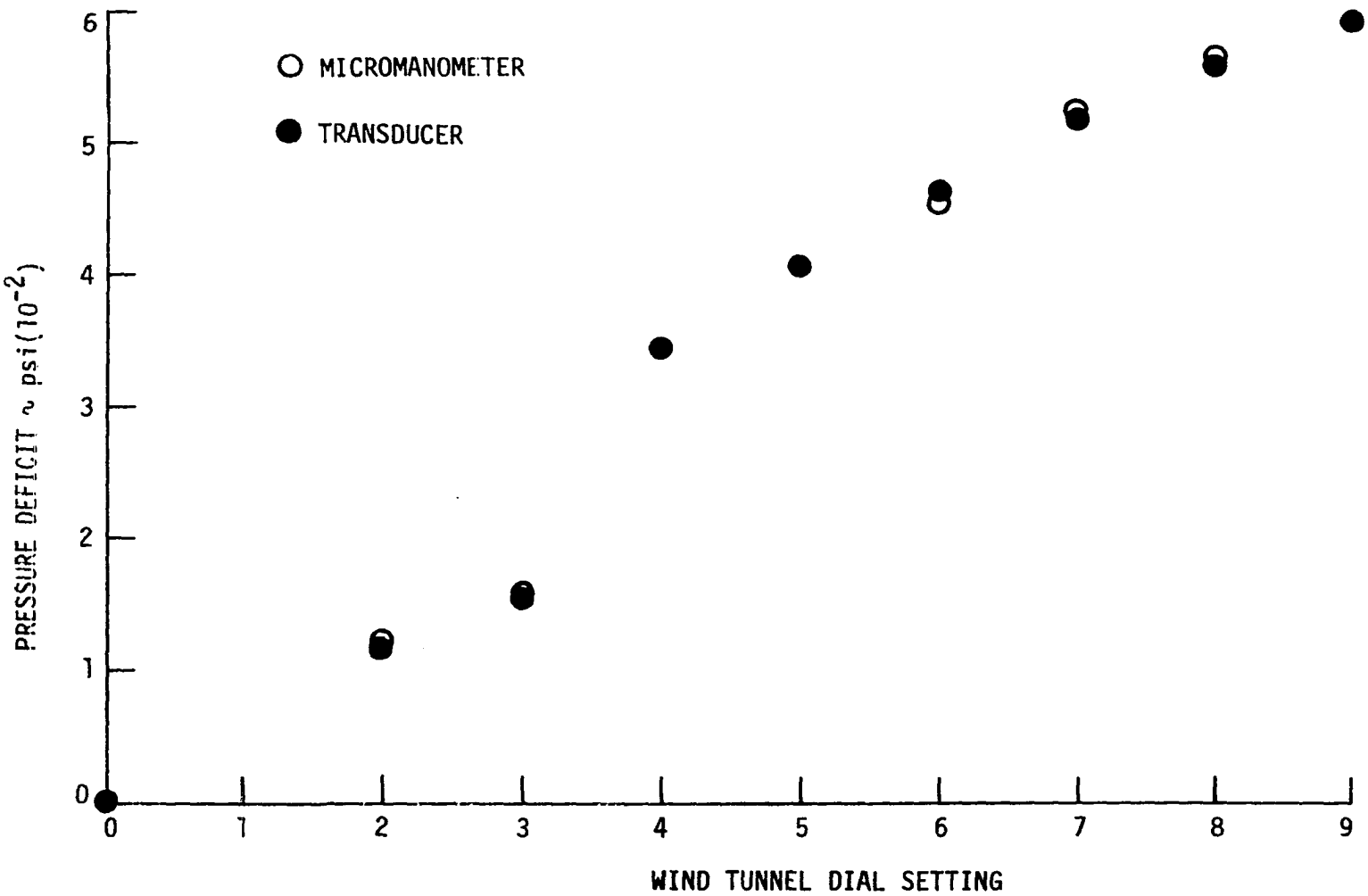

Figure 69. Calibration of the differential pressure transducer with micromanometer in the wind tunnel.

Figure 70. The satellite view of the sequence of formation and dissipation of a macro-circulation.

Figure 71. A typical mesoscale cyclone over the state of Kansas. (Byers, 1948)

Figure 72. The tornado like vortex generator used in the present experimentations.

Figure 73. The dust cloud of the Dallas Tornado over the rough surface of the city landscape. Note the packing of debris at the root of the vortex to form an upflow jet. No funnel is visible. (Hoecker et al., 1960)

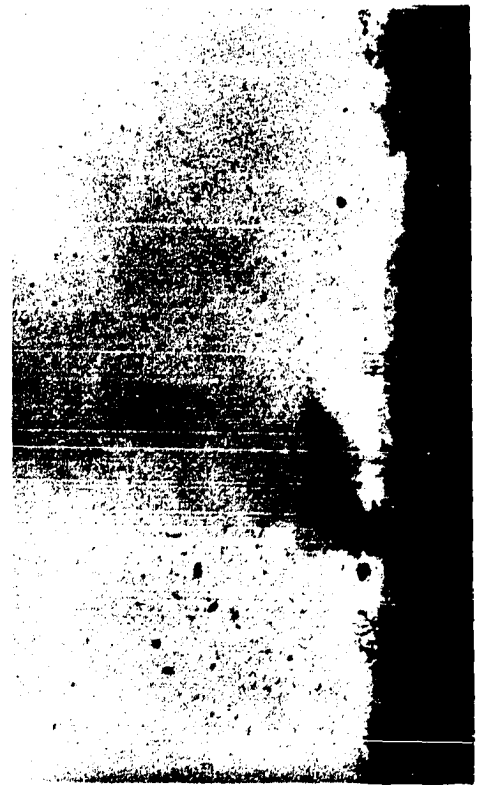


a
b
c
d
e

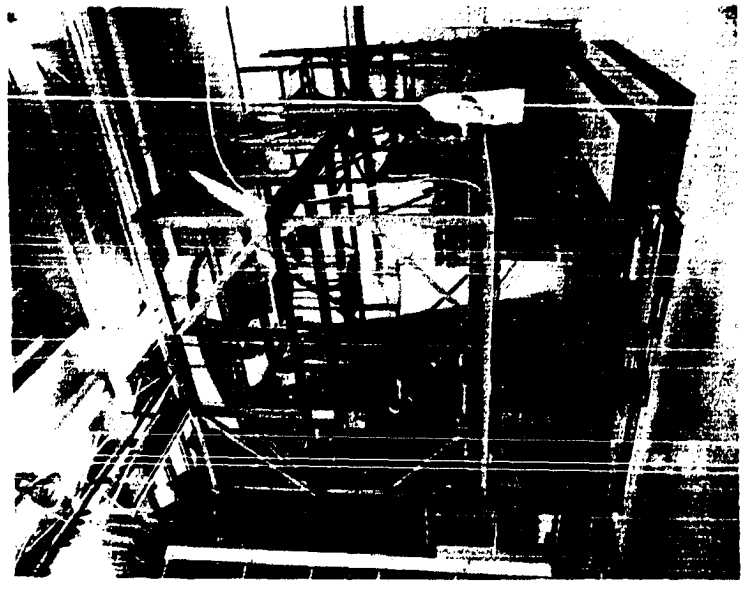

Figure 74. The dust cloud of the Dallas Tornado made up of relatively large debris. No funnel is visible while the explosive effect of the vortical flow near the ground (jet breakdown) is shown. (Hoecker et al., 1960)

Figure 75. The dust cloud of the Dallas Tornado made up of relatively small debris. A funnel is visible. (Hoecker et al., 1960)

Figure 76. The dust cloud of the Dallas Tornado made up of fine debris formed in the open country. (Hoecker et al., 1960)

Figure 77. The dust cloud of the Great Bend (Kansas) Tornado covering the entire subcloud portion of the vortex. (Am. Met. Soc., 1975)

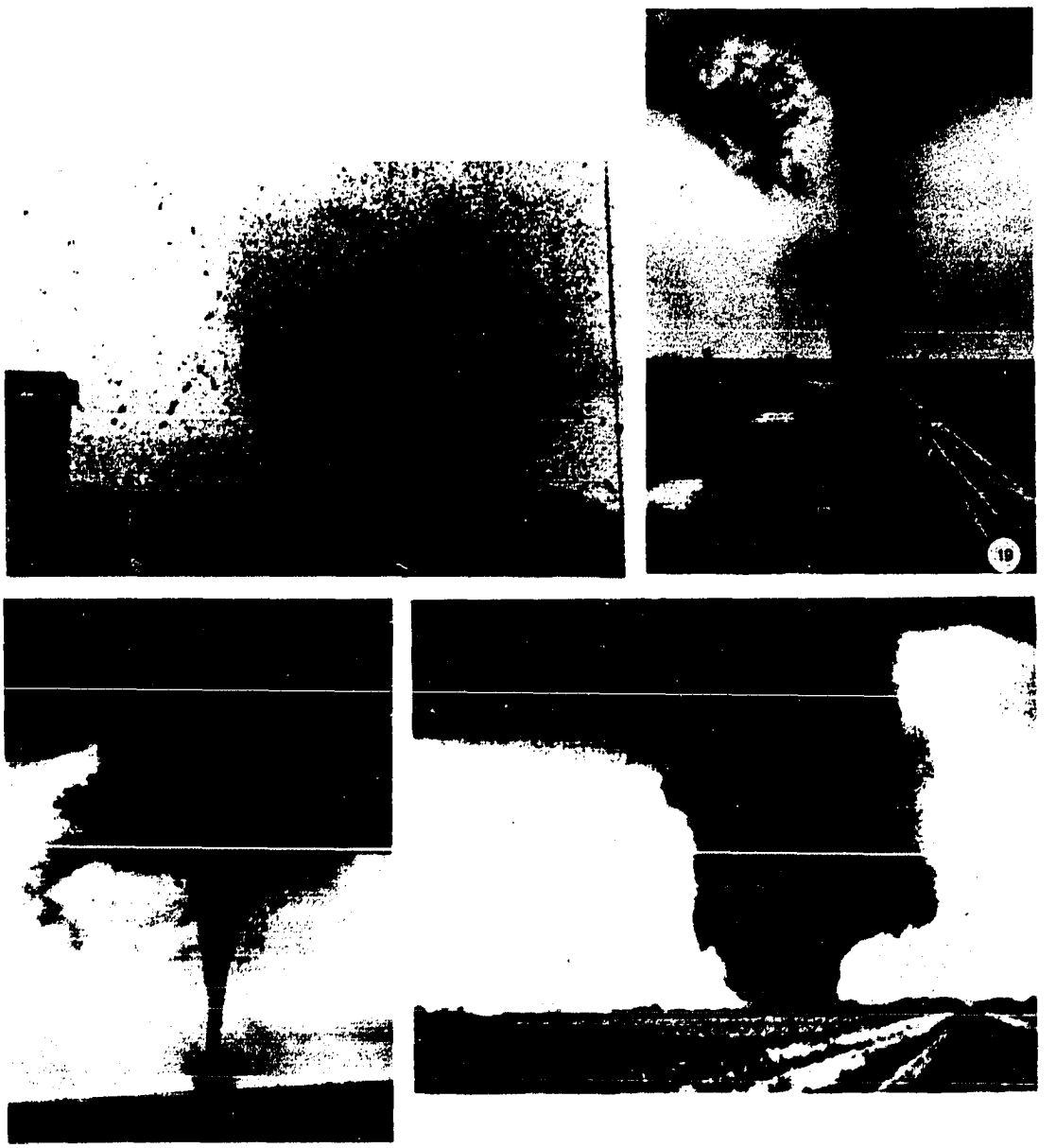
19

Figure 78. The dust cloud of the present laboratory vortex made up of saw dust. Compare to Fig. 73.

Figure 79. The dust cloud of the laboratory vortex made up of saw dust. Compare to Fig. 74.

Figure 80. The dust cloud of the laboratory vortex made up of fine glass particles. Compare to Fig. 76.

Figure 81. The dust cloud of the laboratory vortex made up of flour. Compare to Fig. 77.

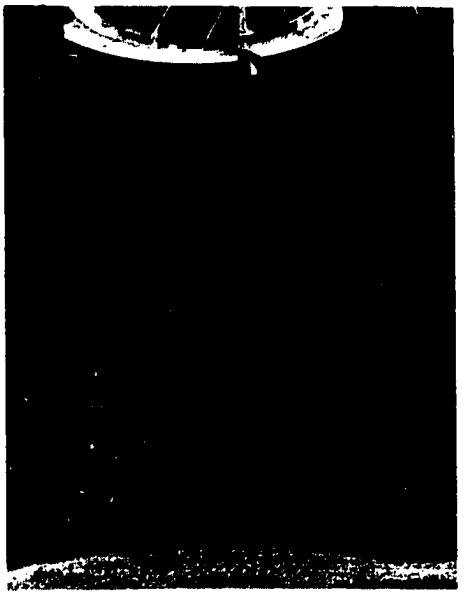

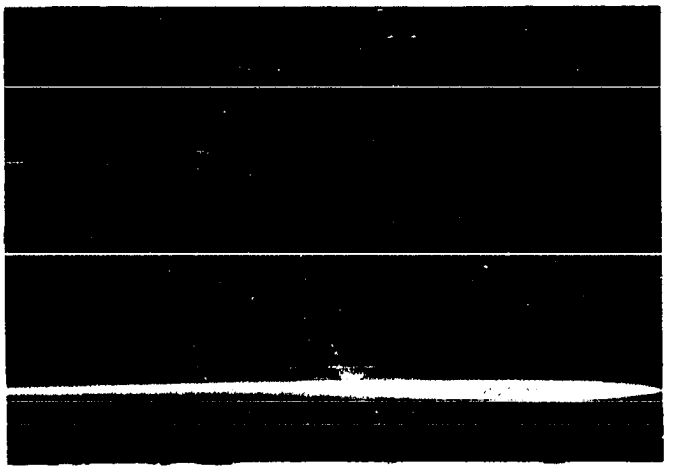

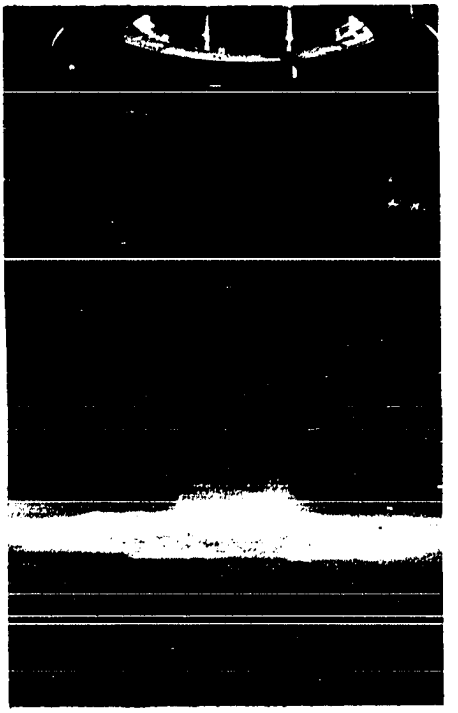

Figure 82. The downward spiral motion along the funnel is clearly shown in this rare photograph. Also visible is the swift upward motion of the center jet into the mouth of the funnel. (Journal of Physics E: Scientific Instruments, 1975)

Figure 83. A typical funnel observed in the laboratory. Compare to Fig. 82.

Figure 84. A tornado funnel near Peshawar, Pakistan, April 5, 1933. Note the visible vortical tube enveloping the funnel. (Flora, 1953).


for measurement of fluid velocity
DISA

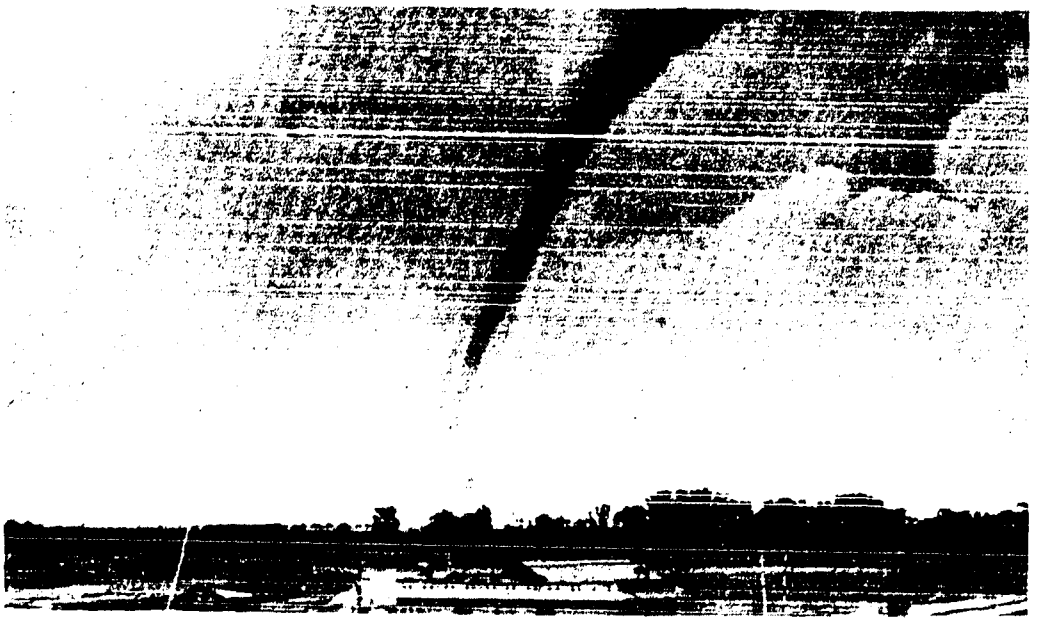

Figure 85. A typical smoke funnel produced in the laboratory showing striking similarity to the funnel of the Peshawar Tornado of Fig. 84.

Figure 86. Enid (Oklahoma) Tornado, 5 June 1966 showing the downmoving funnel and the upmoving vortical tube. Note the helical upflow of the vortical tube which is clearly shown in this rare photograph. (Serrin, 1972)

Figure 87. A laboratory smoke funnel which may be compared to the funnel of Enid Tornado shown in Fig. 86.

Figure 88. The Kingfisher (Oklahoma) Tornado roaring across a wheat field. The visible funnel has a constant diameter. (Roberts, 1972)

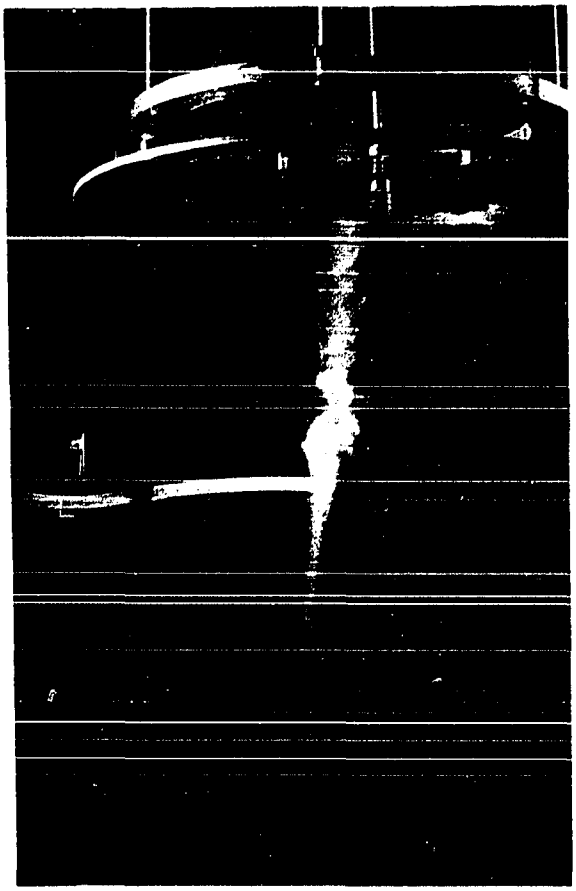

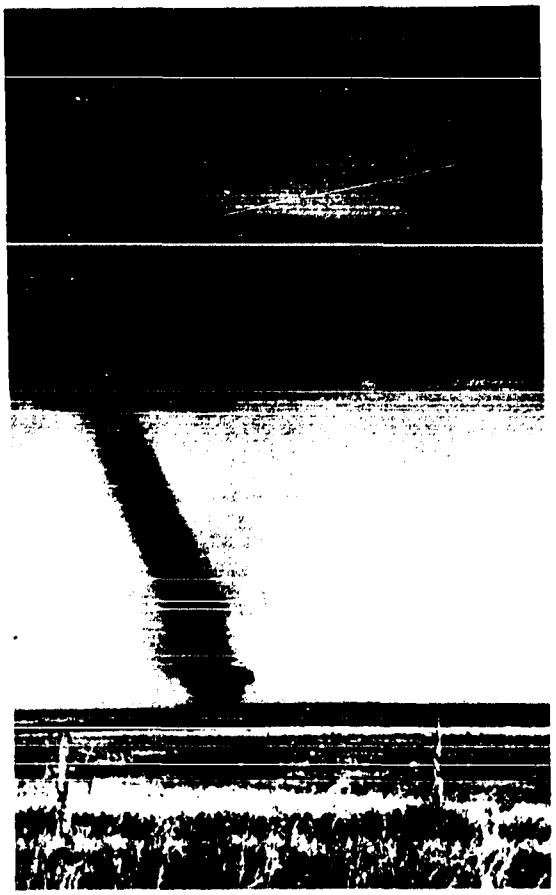

Figure 89. A simulated constant diameter laboratory funnel.

Figure 90. Typical paths of the inflowing particles near the surface are visualized by flour in the laboratory.

Figure 91. The inner vortical tube exhibiting swift axial and tangential motion.

Figure 92. Downward spiral of the funnel into the up-moving vortical tube is visualized by smoke injection into the core of the vortex flow. Also shown is the explosive nature of the flow near the ground surface.

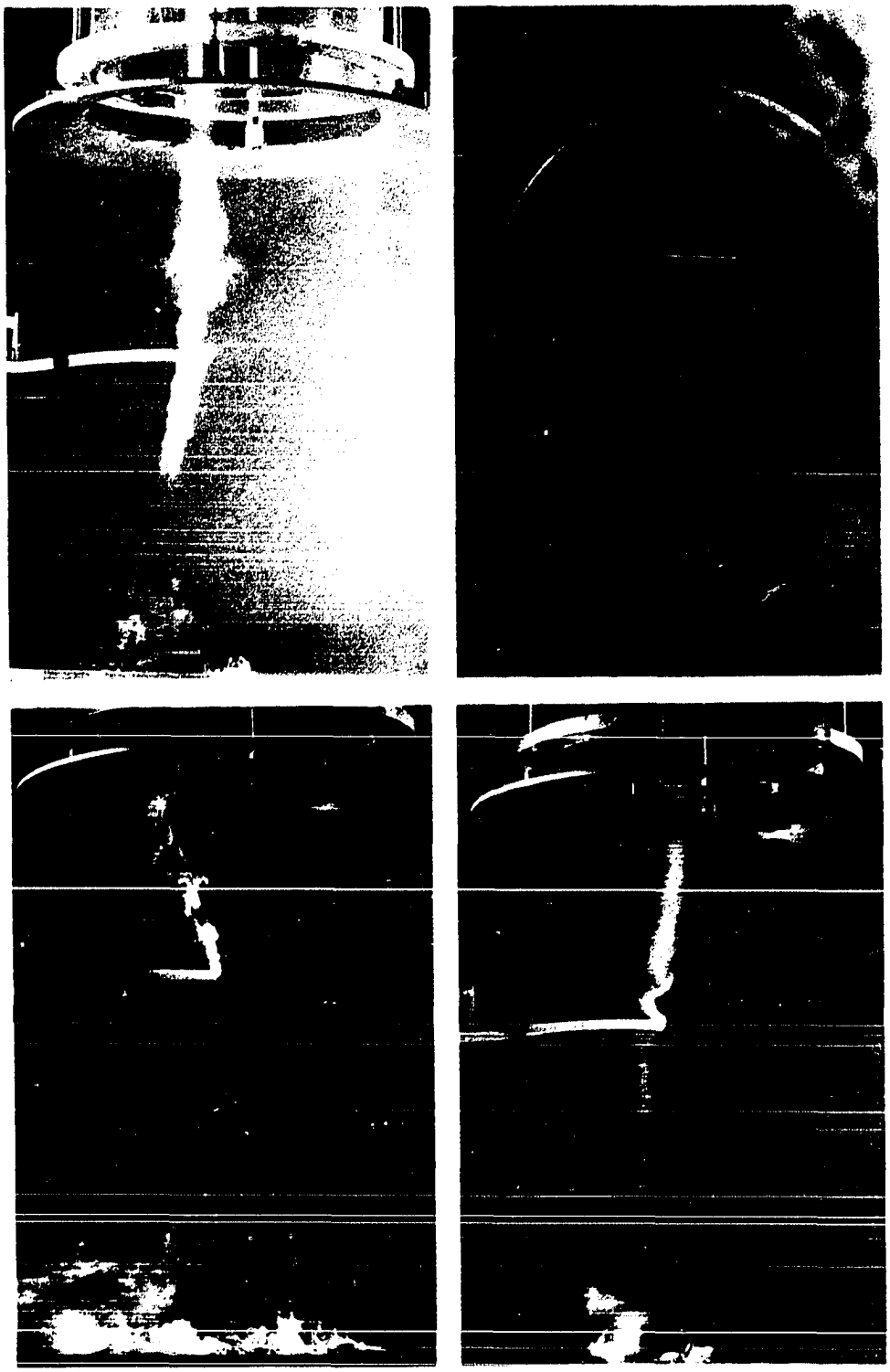

Figure 93. The bottom view of the laboratory smoke funnel showing its hollow structure.

Figure 94. The side view of the laboratory smoke funnel showing its hollow structure.

Figure 95. The upmoving center jet shows the axially dominant motion in the center of the vortex core.

Figure 96. The axially dominant motion of the center jet into the vortical tube is shown. Note the jet breakdown phenomenon just above the ground surface.

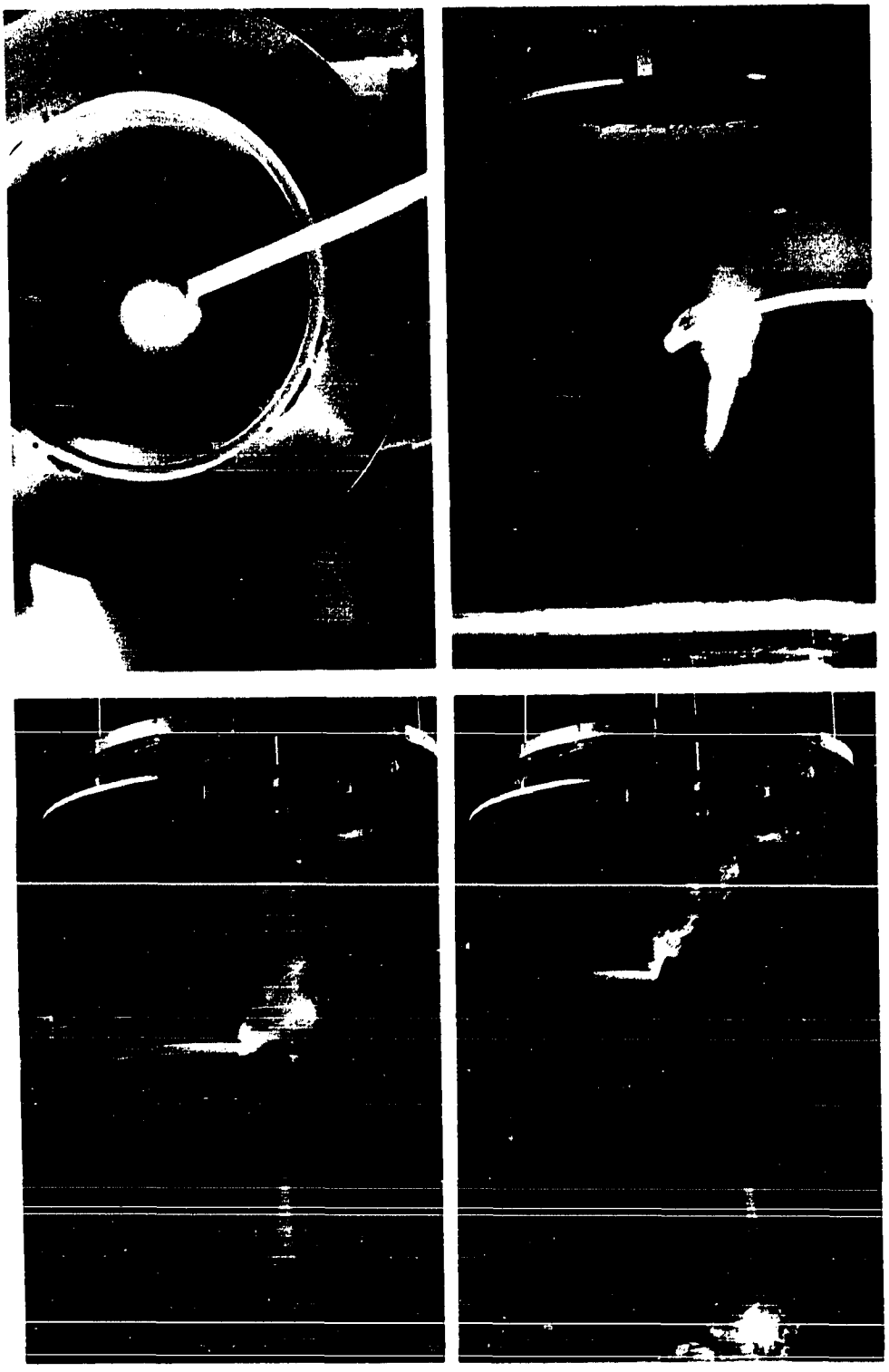

Figure 97. The jet breakdown just above the ground surface exhibiting the explosive nature of the flow in this region. Also shown is a smoke funnel.

Figure 98. The Cheyenne (Wyoming) Tornado, June 2, 1923, showing a possible jet breakdown in a natural tornado. (Flora, 1953)

Figure 99. The inner and outer vortical tubes shown in this photograph are two of the upmoving portions of the complicated flow field. Note the immediate widening of the outer vortical tube just above the surface.

Figure 100. A laboratory smoke funnel is shown to dip down into the outer vortical tube visualized by flour.

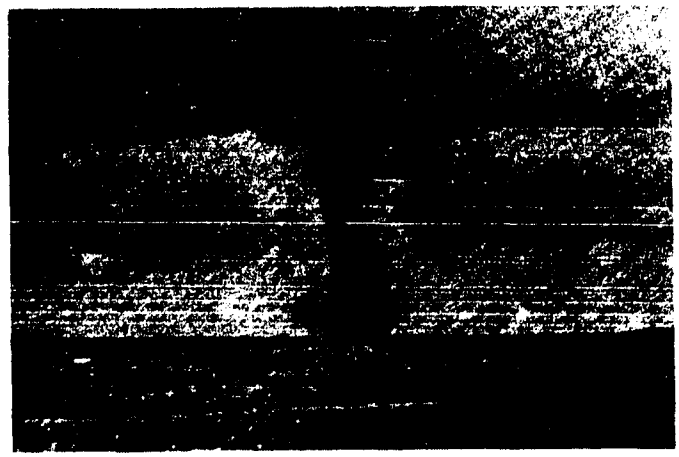

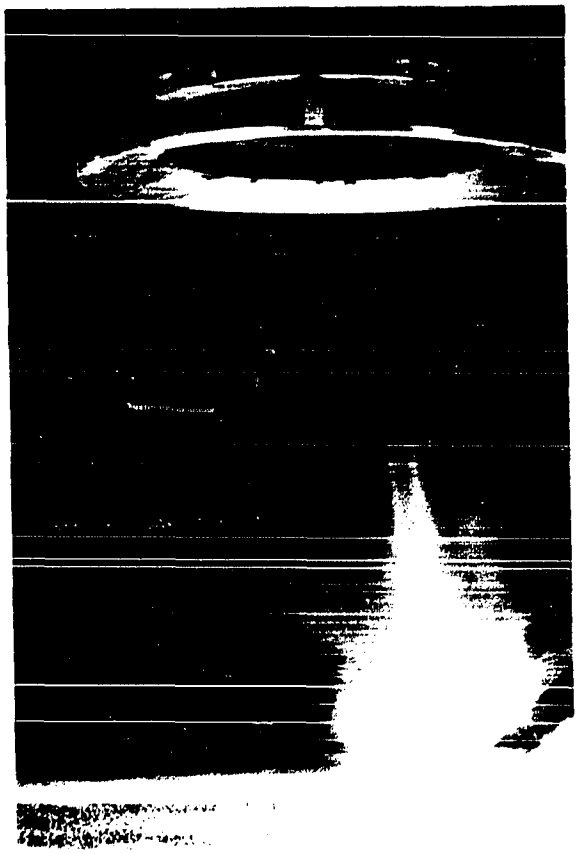

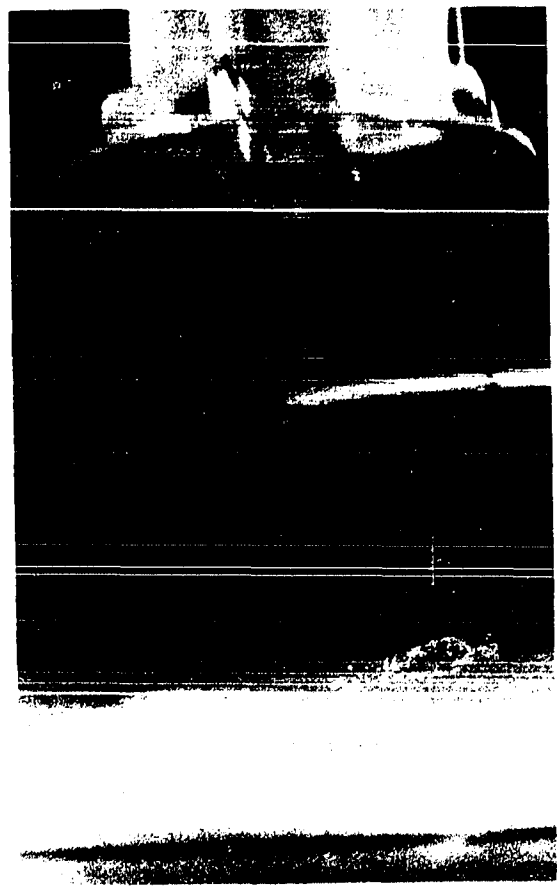

Figure 101. Instant tea is used as a flow visualizing medium to show the two upmoving vortical tubes. The region between the two vertical layers is seen to be dark which probably indicates downward motion. Also shown is the center jet.

Figure 102. The Belleville (Illinois) Tornado, March 15, 1938 was visible below a very low cloud base and was unusually wide. It is possible that the visible portion of this tornado is the second downflow region enveloping the inner vortical tube, funnel and center jet portions of the flow field. (Flora, 1953)

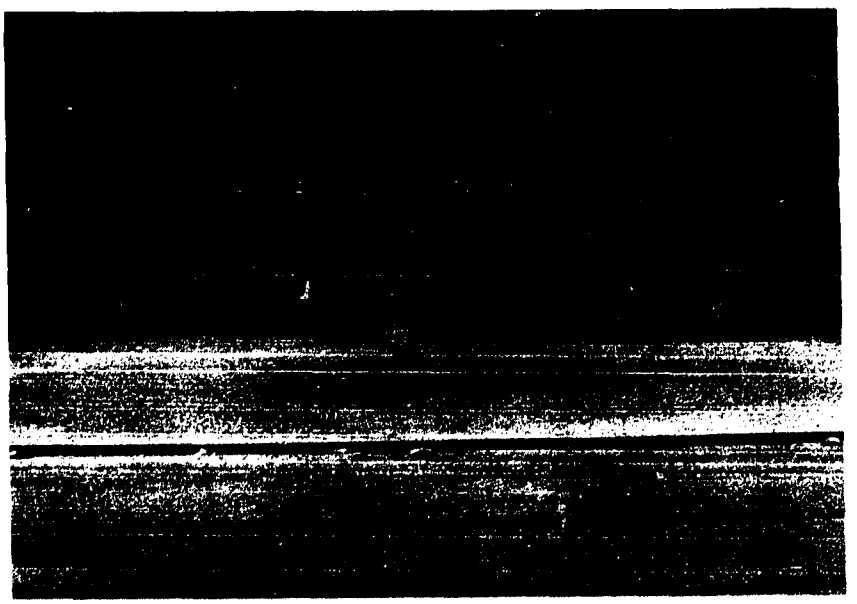

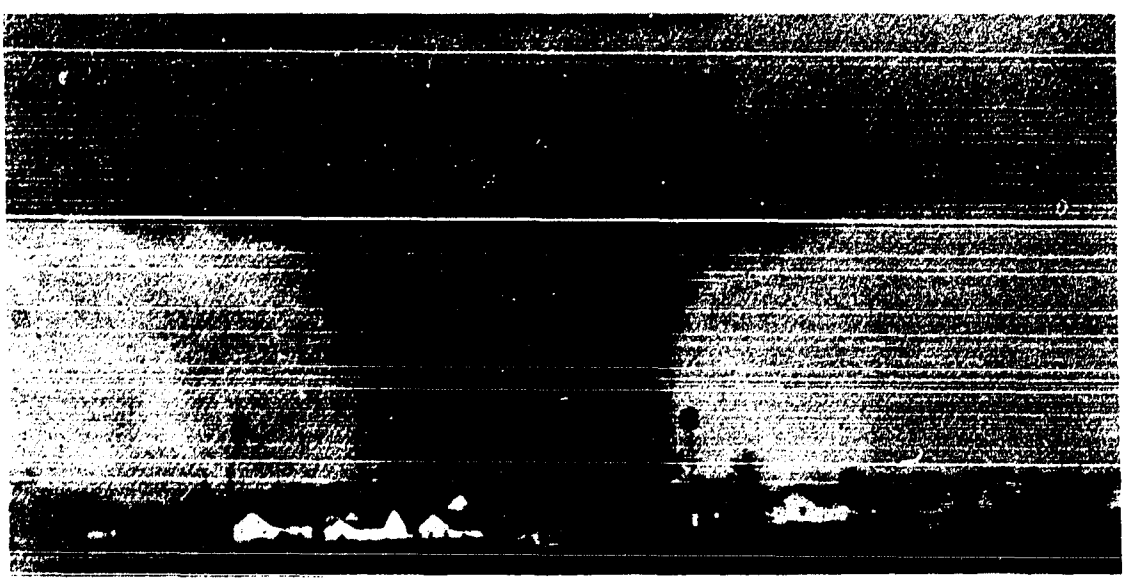

Figure 103. The swift and smooth flow of the vortical tube is shown to be easily disturbed by even small obstacles on the ground surface.

Figure 104. The flow of the vortical tube is severely disrupted when the ground surface becomes rough. This is consistent with the usual disrupted or absence of the funnel of the natural tornadoes when they move over rough landscape of the urban areas.

Figure 105. The vortical tube becomes narrow and curved with increased distance between the ground surface and the source of rotation.

Figure 106. A narrow and long funnel is shown to terminate above the ground surface.

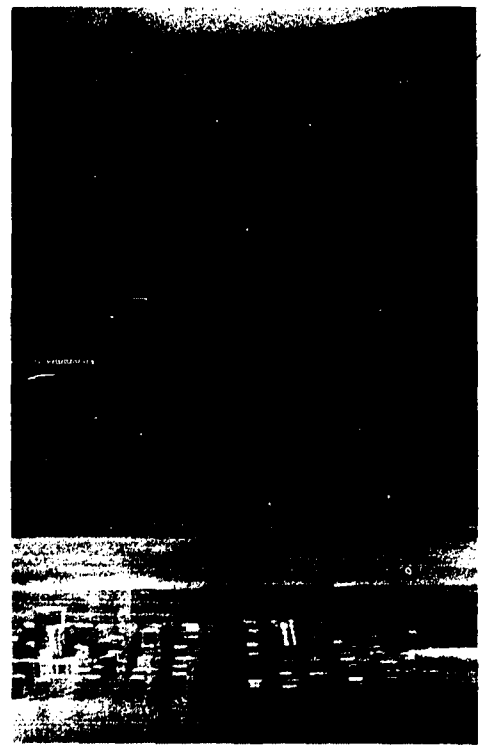

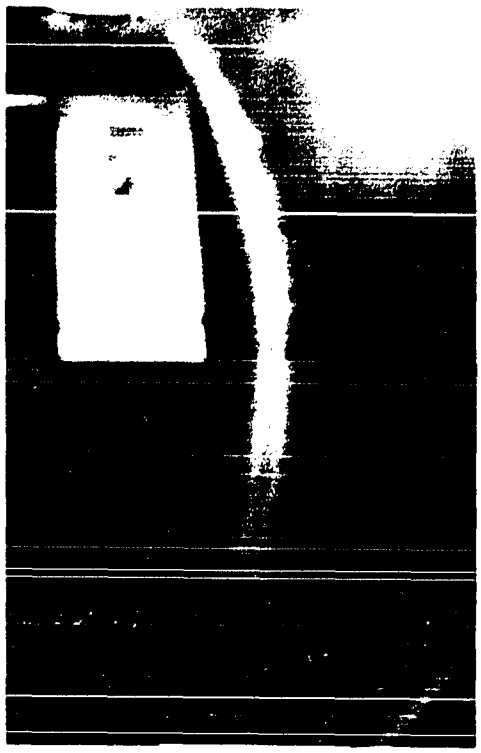

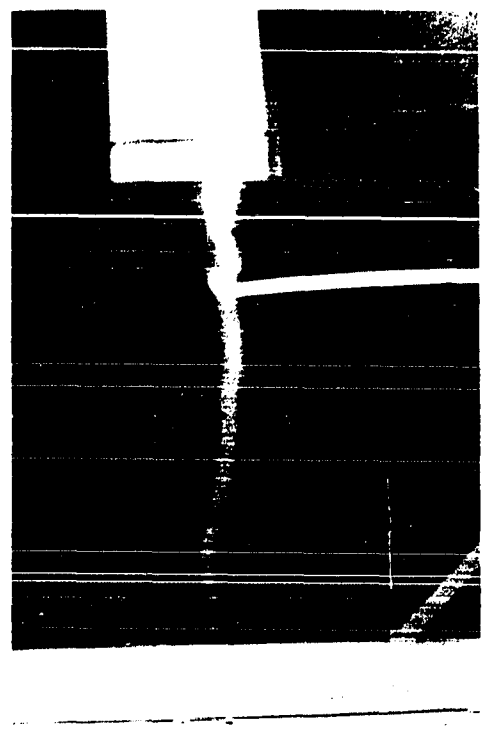

Figure 107. The vortical tube of Fig. 105 is shown to dissipate with a characteristic snake-like motion.

Figure 108. The Jasper (Minnesota) Tornado in its dissipating rope like stages. Also shown are the vortical tube enveloping the funnel and the lower center jet flowing into the mouth of the funnel. (Brooks, 1949)

Figure 109. The "vortex breakdown," a common phenomenon in swirling flows is also encountered in the vortical flow of the present simulation.

Figure 110. The absence of the ground surface prevents the formation of concentrated, vorticity rich tornado like vortices. Only a small upflow motion is observed with negligible rotation.

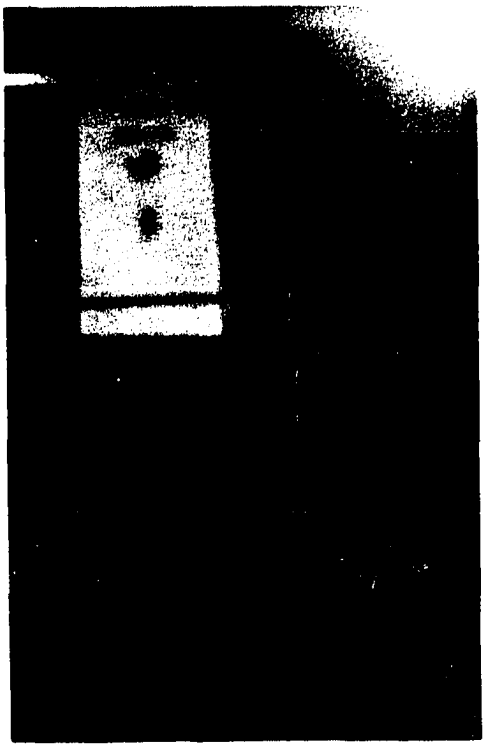

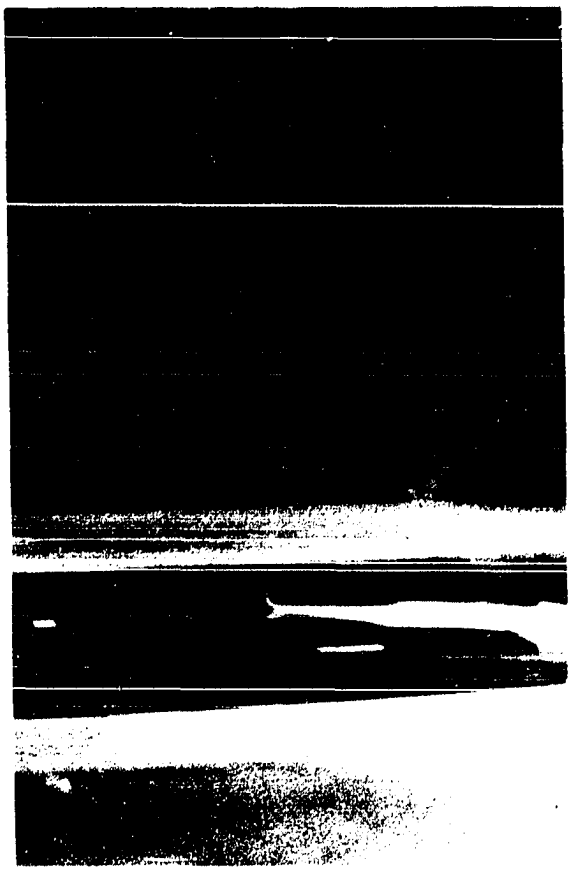

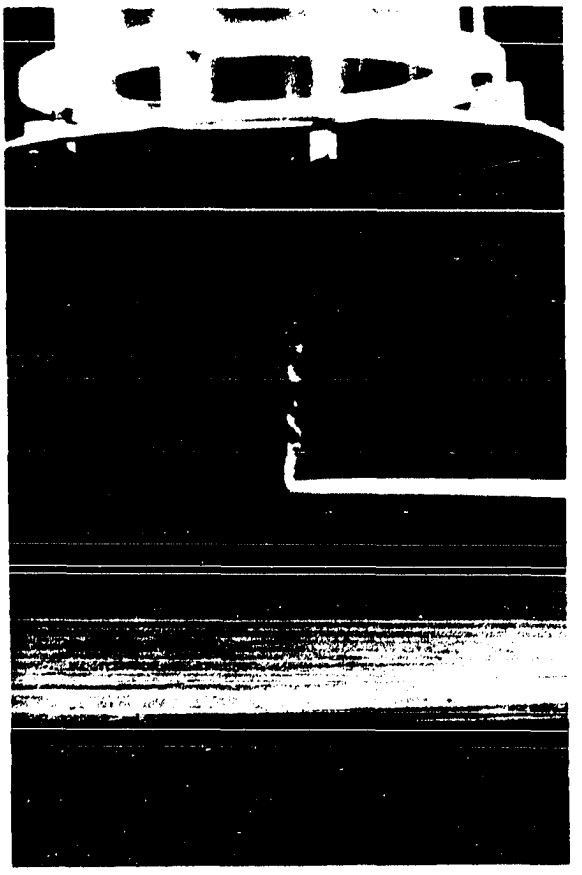

Figure 111. The vortical tube ends normal to the inclined ground surface which is consistent with the Helmholtz theory.

Figure 112. The funnel flow also ends normal to the inclined ground surface. This is observed in all natural tornadic storms.

Figure 113. Multiple tornadoes may form under the same mesoscale circulation. The twin tornadoes of Wamego, Kansas, May 15, 1943, are examples of such occurrences. (Flora, 1953)

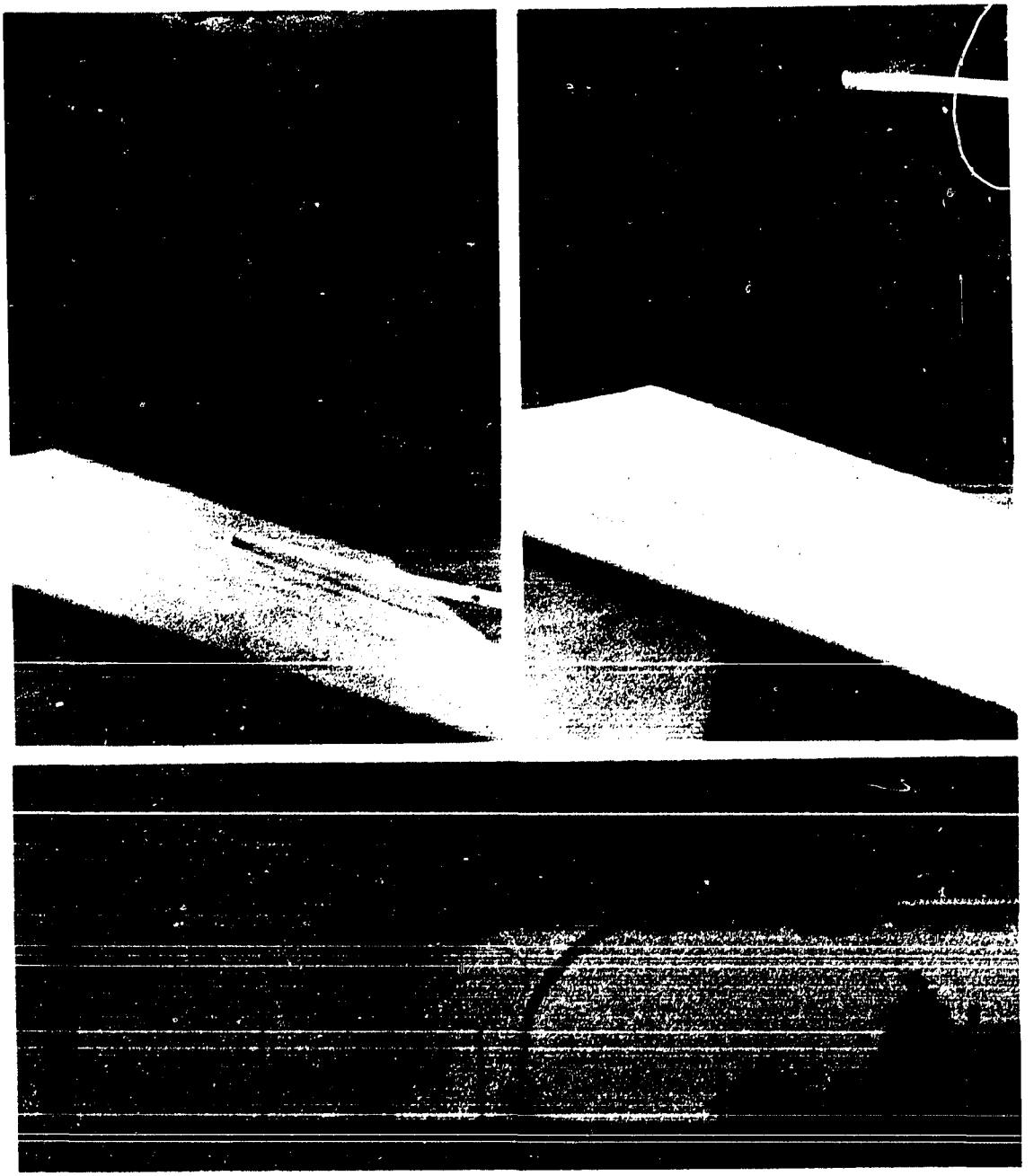

Figure 114. Multiple vortex tornado of Oshkosh (Wisconsin) showed three visible vortices rotating around the core of the larger mother tornado vortex. (Blechman, 1975)

Figure 115. A pair of vortical tubes were visualized using smoke in the laboratory.

Figure 116. The remote control panel for monitoring the flow and measurement of the time averaged velocities of the laboratory vortex.

Figure 117. The specially designed positioning system for the anemometer is shown in the test section of the laboratory vortex generator.

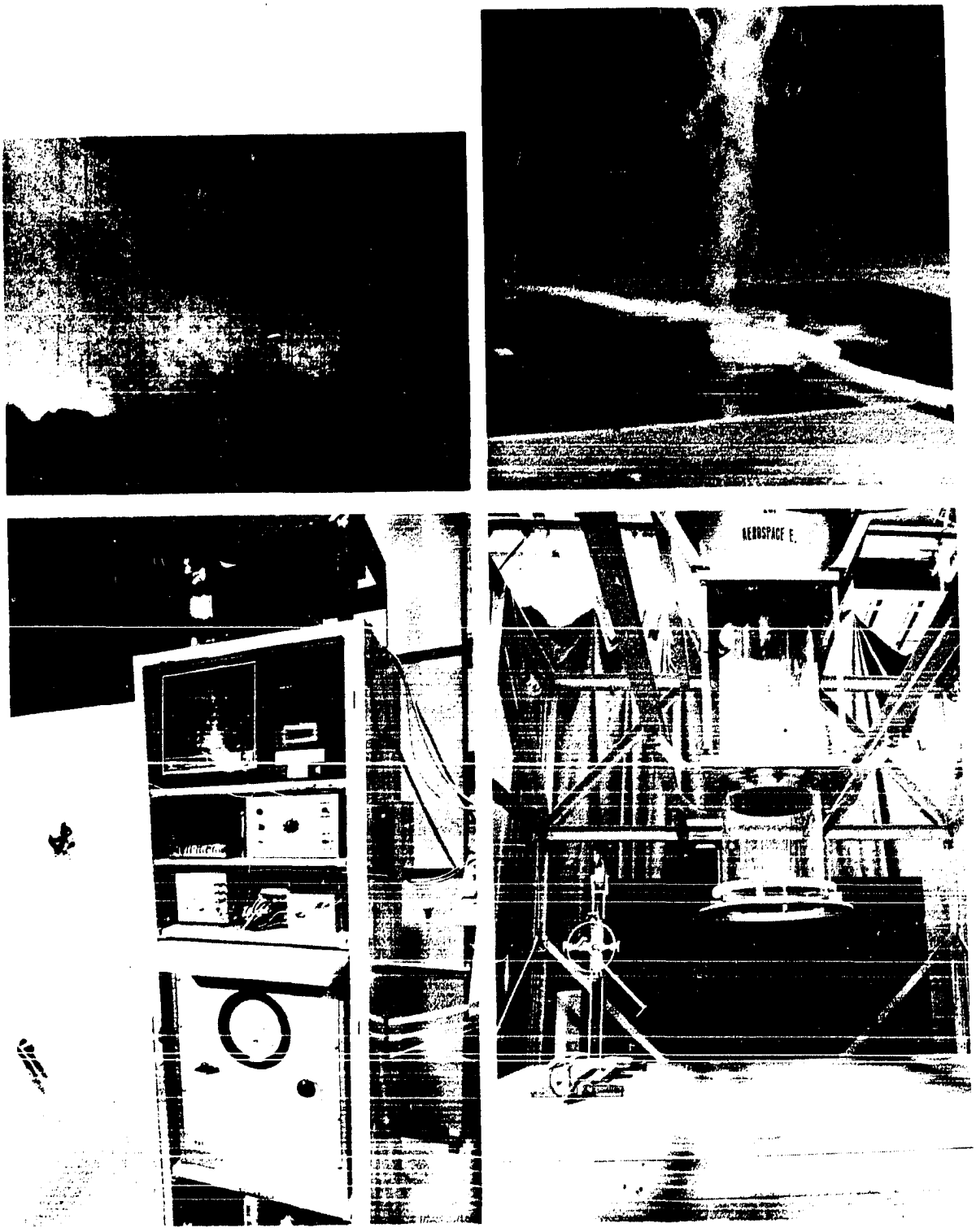
AEROSPACE E.

Figure 118. The penetration of a piece of wood into a 1.5" steel fence pipe indicates the tremendous speeds attained by such flying missiles. (Pearson and Miller, 1971)

Figure 119. Typical damages suffered by different structures are shown in this photograph. The wooden house has twisted off of its foundation while the garage has exploded due to sudden pressure drops experienced near and within the core of tornadic storms. (Weatherwise, 1973)

Figure 120. The house shown in this photograph was crushed due to the implosive loadings of the atmospheric pressure recovery. (Goldman, 1965)